# THESE DE DOCTORAT

pour obtenir le grade de

**DOCTORAT DE L'UNIVERSITE DE LILLE**

*en*

**Sciences agronomiques**

ED SMRE 104
Ecole doctorale Sciences de la Matière, du Rayonnement et de l'Environnement

*par*


# Shehyar IQBAL


Titre de la thèse :

## Nitrogen economy towards ecosystem services: plant key traits and QTL detection in *Miscanthus sinensis*

### Gestion de l'azote en vue de services écosystémiques : traits majeurs de la plante et détection de QTL chez *Miscanthus sinensis*

Thèse présentée et soutenue à Estrées-Mons, le 10 mars 2026

**Composition du jury :**

| | |
|---|---|
| Anne LAPERCHE, Professeure, Agro Rennes-Angers Institute | Présidente |
| Emily HEATON, Professeure, University of Illinois (US) | Rapporteure |
| Jacques LE GOUIS, Directeur de Recherche, INRAE, Clermont-Ferrand | Rapporteur |
| Loïc STRULLU, Ingénieur de Recherche, INRAE, Laon | Examinateur |
| Komlan AVIA, Chargé de Recherche, INRAE, Colmar | Examinateur |
| Emilie SKOWRON, Ingénieure, Novabiom, Champhol | Personne invitée |

| | |
|---|---|
| **Maryse BRANCOURT-HULMEL**, Directrice de Recherche, INRAE, Estrées-Mons | Directrice de thèse |
| **Marion ZAPATER**, Ingénieure de Recherche, INRAE, Estrées-Mons | Co-encadrante |


BioEcoAgro Joint Research Unit, INRAE

2 Chaussée Brunehaut 80200 Estrées-Mons FRANCE

# ACKNOWLEDGEMENTS

As this doctoral journey comes to an end, I realize that a PhD is not only about experiments, results, graphs, and papers. It is also, and maybe mainly, about people. This thesis would simply not exist without the support, patience, and kindness of many individuals who helped me along the way, especially during the moments when I thought the PhD would finish *me* before I finished it.

First and foremost, I would like to express my deepest gratitude to the two super ladies, my supervisors, Dr. Maryse BRANCOURT-HULMEL and Dr. Marion ZAPATER. I feel extremely lucky to have been guided by two inspiring scientists who not only taught me how to think like a researcher, but also helped me grow step by step through this journey. I will truly miss our long meetings and long working sessions where, just when everything seemed blocked, one of you would suddenly pull a trick out of the hat and make the solution look obvious. Of course, it was not magic, it was your experience and your sharp scientific instincts. I hope I was able to pick up a thing or two from the wealth of skills you both have. Thank you for your guidance, your trust, and your support throughout these years. Your encouragement has been one of the key reasons I made it to the finish line, and with *(almost)* all my sanity intact.

I would like to warmly thank Séverine MONNOT and Kristelle LOURGANT for their essential help during different phases of my PhD. Thank you Séverine for your support, your motivation, and the positive energy you always brought when things became difficult. Thank you, Kristelle, for your impressive work and for always taking the time to write clear explanations and little notes for me, which made the more complex parts much easier to understand.

A huge thank you goes to Marie HEUMEZ-LÉVÊQUE for her invaluable support with the experimental work. Your dedication and the way you organized every detail of the field work and sampling campaigns made everything possible, and made the most demanding periods much easier to manage. I would also like to sincerely thank all the people who participated in the experimental work throughout these years, whether as permanent staff, CDD colleagues, interns, or visiting students. Many people came and went, but each contribution played a role in keeping the project moving forward.

I would also like to express my sincere gratitude to my thesis committee members, Véronique JORGE, Manoël COUPRIE, Matthieu REYMOND, Frédéric DUBOIS, and Julie LEROY, for their time, their support, and their guidance throughout the PhD. Their feedback helped me reflect on my work with more perspective and guided me at key moments during the PhD.

I would like to warmly thank the rapporteurs, Professor Emily HEATON and Dr. Jacques LE GOUIS, for agreeing to review my thesis. I also sincerely thank the members of the jury, Professor Anne LAPERCHE, Dr. Loïc STRULLU, Dr. Komlan AVIA, and Emily SKOWRON, for accepting to be part of my thesis defense.

A special thank you also goes to all the amazing people at INRAE who made my daily life easier. I am especially grateful to the administrative staff, whose help and efficiency saved me

more times than I can count, and to the experimental unit teams for their essential work and support.

To my friends and colleagues, Adrien, Julie, Antoine, Manuel, Clotilde and Maëlys, thank you for making these years lighter, funnier, and more human. A special thanks to Adrien, for making my life liveable at Estrées-Mons, and for proving that humour is sometimes as important for survival as coffee. I would also like to thank Jaya, Salman, and Shaban, for simply being there, listening, supporting, and checking in. You helped keep me sane, especially during the moments when I needed it the most.

Finally, I would like to thank my family for their unconditional love and support throughout these years. You have been my strength in more ways than I can fully put into words, especially during the stressful and exhausting phases of the PhD, when the thesis took up far too much space in my mind (and sometimes in my mood as well). A special thank you to my brother Shahzaib, for always being there, checking in, and standing by me. You may not have fully understood what I was working on, but you always understood when I needed encouragement (and food).

To everyone mentioned here, and to those I may have unintentionally forgotten (please blame PhD memory loss), thank you. This thesis carries your support within it, and I will always be grateful.

# Nitrogen economy towards ecosystem services: plant key traits and QTL detection in *Miscanthus sinensis*

**Key-words**: Ecosystem services, Nitrogen economy, Genetic variability, *Miscanthus sinensis*, Proxy traits, Quantitative Trait Loci (QTL) mapping.

**Abstract:** Ecosystem services underpin human well-being, yet agricultural systems can both sustain and degrade them, with water-quality regulation being particularly sensitive to excessive nitrate leaching due to fertilization. Perennial low-input crops such as miscanthus can reconcile biomass production with environmental protection by combining high productivity with low fertilizer requirements further strengthened by efficient internal nitrogen recycling. Nitrogen economy, which characterizes the nitrogen management by the plant through nitrogen uptake, seasonal remobilization and associated nitrogen losses, is therefore central to both biomass productivity and ecosystem service provision. However, in *Miscanthus sinensis*, the internal functioning, genetic variability, predictability, and genetic control of nitrogen economy traits remain poorly understood, limiting their effective mobilization in sustainable agricultural systems.

This thesis aimed to make nitrogen economy traits measurable, predictable, and genetically selectable targets in *M. sinensis* to support the development of cultivars sustaining biomass production while contributing to ecosystem services. Using a segregating diploid progeny of 80 genotypes grown under nitrogen-deficient field conditions, the thesis followed a coherent progression from functional characterization, to predictive modelling, and finally to genetic targeting of nitrogen economy traits.

First, nitrogen economy traits were quantified to characterize functional diversity among genotypes. Substantial inter-genotypic variation was observed, with nitrogen uptake ranging from 5 to 241 kg N $ha^{-1}$, spring remobilization from 0.2 to 85 kg N $ha^{-1}$, and autumn remobilization from 5 to 158 kg N $ha^{-1}$. Hierarchical clustering on principal components based on the nitrogen economy traits revealed three different functional groups of genotypes with contrasting nitrogen-use strategies. Acquisitive genotypes relied primarily on external nitrogen uptake, whereas conservative genotypes relied more on internal recycling, and both strategies sustained high biomass production under nitrogen limitation. Second, these complex nitrogen economy traits, previously accessible only through plant destructive and time-consuming flux measurements, were predicted using easily measurable non-destructive proxy traits, chosen among 35 morphological, phenological and physiological traits. Based on a repeated cross-

validation procedure, Partial Least Squares regression models achieved predictive accuracies of 0.62-0.74 for nitrogen uptake, 0.48-0.63 for autumn remobilization, 0.30-0.46 for spring remobilization, and 0.24-0.39 for nitrogen losses. Reduced, parsimonious models retained similar accuracy, showing that these complex traits can be estimated with simple scalable phenotyping. Finally, QTL mapping translated nitrogen economy traits into genetically defined breeding targets. Nineteen QTLs were detected for nitrogen uptake, remobilization, and losses ($R^2$ = 8.8-37.1% per locus), revealing trait-specific and largely independent genetic architectures. In parallel, 26 proxy traits yielded 85 proxy-trait QTLs ($R^2$ = 0.1-34.0%), with proxy-target co-location limited to two genomic regions for nitrogen uptake and spring remobilization. QTL pyramiding further illustrated how acquisition capacity and nitrogen loss deviation can be jointly combined to design ideotypes aligned with contrasting ecosystem service objectives.

Overall, this thesis moves nitrogen economy traits in *Miscanthus sinensis* from descriptive physiological concepts to operational breeding axes. By integrating functional characterization, non-destructive prediction, and genetic dissection, it provides a coherent framework for developing *M. sinensis* ideotypes that maintain biomass production while supporting ecosystem services, including water-quality regulation, nutrient cycling, and long-term agroecosystem resilience.

# Gestion de l'azote en vue de services écosystémiques : traits majeurs de la plante et détection de QTL chez *Miscanthus sinensis*

**Mots-clés :** Services écosystémiques, gestion de l'azote, variabilité génétique, *Miscanthus sinensis*, caractères proxys, cartographie de régions chromosomiques (QTL).

**Résumé :** Les services écosystémiques sont essentiels au bien-être humain, mais les systèmes agricoles peuvent à la fois les préserver ou les dégrader, tel que le service écosystémique de régulation de la qualité de l'eau qui est sensible au lessivage des nitrates lié à la fertilisation azotée des cultures. Les cultures pérennes à faibles intrants, telles que le miscanthus, peuvent concilier production et protection de l'environnement grâce à une forte productivité et de faibles besoins en fertilisation, renforcés par un recyclage interne efficace de l'azote. La gestion de l'azote par la plante *via* l'absorption de l'azote, sa remobilisation saisonnière et les pertes associées, est ainsi centrale pour ce faire. Mais chez *Miscanthus sinensis*, le fonctionnement, la variabilité inter-génotypique, la prédictibilité et le contrôle génétique de ces caractères, dits traits, restent mal connus.

Cette thèse visait à rendre les traits de gestion de l'azote mesurables, prédictibles et sélectionnables au niveau génétique chez *M. sinensis*, afin de développer des cultivars permettant des services écosystémiques. Une descendance de 80 génotypes diploïdes en ségrégation, cultivée au champ en conditions déficientes en azote, a permis une progression allant de la caractérisation du fonctionnement entre génotypes, à sa prédiction par modélisation statistique jusqu'à des cibles génétiques de sélection.

Les variables relatives à la gestion de l'azote ont d'abord été quantifiées et mis en évidence une forte variation fonctionnelle inter-génotypique, avec une absorption variant de 5 à 241 kg N $ha^{-1}$, une remobilisation printanière de 0,2 à 85 kg N $ha^{-1}$ et une remobilisation automnale de 5 à 158 kg N $ha^{-1}$. Une classification hiérarchique sur composantes principales à partir de ces différents traits a mis en évidence trois groupes fonctionnels avec des stratégies contrastées : des génotypes "extracteurs" reposant surtout sur l'absorption d'azote externe, et des génotypes "recycleurs" reposant davantage sur le recyclage interne de l'azote, ces deux stratégies permettant de maintenir une biomasse élevée en condition limitante en azote. Ces traits complexes, auparavant accessibles seulement *via* des mesures de flux, destructives et chronophages, ont été prédits à partir de 35 variables indicatrices, dites proxys, en lien avec des caractères morphologiques, phénologiques, physiologiques qui sont non destructifs. Sur la base de validations croisées répétées, des modèles de régression par les moindres carrés partiels

(PLS) intégrant ces indicateurs ont atteint des précisions de 0,62-0,74 pour l'absorption, 0,48-0,63 pour la remobilisation automnale, 0,30-0,46 pour la remobilisation printanière et 0,24-0,39 pour les pertes. Des modèles parcimonieux ont conservé des performances similaires, démontrant la faisabilité d'un phénotypage simple et à plus haut débit. Enfin, la cartographie de QTL a permis de traduire ces traits en cibles génétiques. Dix-neuf QTL ont été détectés pour l'absorption, la remobilisation et les pertes ($R^2$ = 8,8-37,1 % par QTL), révélant des architectures génétiques spécifiques et largement indépendantes. En parallèle, 26 indicateurs ont révélé 85 QTL ($R^2$ = 0,1-34,0 %), avec une co-localisation proxy-cible limitée à deux régions pour l'absorption et la remobilisation printanière. Le pyramidage de QTL a montré comment combiner la capacité d'absorption avec la déviation des pertes d'azote pour concevoir des idéotypes répondant à des objectifs contrastés de services écosystémiques.

Cette thèse fait évoluer la gestion d'azote chez *Miscanthus sinensis* de concepts physiologiques descriptifs vers des axes opérationnels de sélection. En combinant caractérisation fonctionnelle, prédiction à l'aide de variables non destructives et dissection génétique, elle propose un cadre cohérent pour développer des idéotypes conciliant la productivité avec la régulation de la qualité de l'eau, le cycle des nutriments et la résilience des agroécosystèmes.

# Une brève synthèse de cette thèse en français

# Introduction

Les services écosystémiques contribuent au bien être humain en reliant le fonctionnement des écosystèmes à des bénéfices tangibles pour la société. Toutefois, les systèmes agricoles occupent une position singulière et souvent contradictoire au sein de ce cadre : ils fournissent des services d'approvisionnement essentiels *via* la production de biomasse, tout en menaçant parfois les services de régulation en raison d'impacts environnementaux négatifs associés à des pratiques agricoles plus ou moins intensives. Parmi ces services, la régulation de la qualité de l'eau (Zheng et al., 2019) apparaît particulièrement vulnérable, car les apports azotés pratiqués en agriculture conduisent fréquemment à la lixiviation des nitrates et à la contamination des eaux de surface et souterraines, notamment dans les aires d'alimentation de captages d'eau potable. Répondre à ce compromis exige des systèmes de culture capables de maintenir la production de biomasse tout en minimisant les impacts environnementaux négatifs.

Les cultures pérennes à bas niveaux d'intrants constituent une voie privilégiée pour atteindre cet équilibre, car elles combinent une couverture durable des sols, une réduction des perturbations et une meilleure rétention des nutriments comparativement aux systèmes de culture annuels. Dans ce contexte, le miscanthus s'est imposé comme une culture pérenne de biomasse particulièrement intéressante, en raison de sa forte productivité, sa résilience et son efficience d'utilisation des ressources (Tavakoli-Hashjini et al., 2020). Un mécanisme clé expliquant ces performances réside dans un recyclage interne efficace de l'azote, au cours duquel l'azote est remobilisé depuis les tiges sénescentes vers les organes souterrains, appelés rhizomes, puis réutilisé lors de la repousse printanière suivante, réduisant ainsi les besoins en fertilisation et améliorant la performance environnementale (Strullu et al., 2011 ; Leroy et al., 2022). A cela s'ajoutent de faibles besoins en azote comparativement à des cultures comme le maïs selon la courbe critique de dilution de l'azote (Zapater et al, 2017).

Malgré ce potentiel, le déploiement actuel du miscanthus repose largement sur un unique clone triploïde stérile de *Miscanthus* × *giganteus*. À l'inverse, *Miscanthus sinensis* présente une diversité génétique intra spécifique importante ainsi qu'un fort potentiel d'adaptation, ce qui en fait une ressource stratégique pour élargir l'offre variétale et concevoir des cultivars conciliant production de biomasse et fourniture de services écosystémiques (Sun et al., 2010 ; Zhao et al., 2013). Atteindre cet objectif nécessite une meilleure compréhension du fonctionnement azoté des plantes, car la gestion de l'azote par la plante est centrale à la fois au niveau de la productivité en biomasse en conditions limitantes en azote et au niveau environnemental. Toutefois chez *M. sinensis*, le fonctionnement interne, la variabilité inter-génotypique, la prédictibilité et le contrôle génétique des principaux caractères de gestion de l'azote par la plante, incluant l'absorption d'azote, la remobilisation saisonnière de l'azote et les pertes d'azote, sont peu décrits dans la littérature.

La valorisation des caractères -également appelés traits- de gestion de l'azote en sélection variétale est actuellement limitée par trois verrous majeurs. Premièrement, bien qu'un recyclage efficace de l'azote ait été rapporté chez le miscanthus, l'ampleur et la structure de la variabilité inter-génotypique au sein de *M. sinensis* restent largement méconnues, au-delà d'observations réalisées sur un nombre restreint de génotypes (Leroy et al., 2022). Deuxièmement, la quantification directe des traits de gestion de l'azote repose sur des mesures de flux qui sont destructives et chronophages, limitant fortement le débit de leur phénotypage (Beale & Long, 1997 ; Himken et al., 1997 ; Strullu et al., 2011 ; Dierking et al., 2017). Troisièmement, bien que des études génétiques aient caractérisé chez *M. sinensis* des traits de biomasse, morphologiques et phénologiques (Atienza et al., 2003 ; Slavov et al., 2014 ; van der Weijde et

al., 2017 ; Hou et al., 2022), les bases génétiques des traits de gestion de l'azote demeurent largement inexplorées.

L'objectif général de cette thèse a donc été d'établir les traits de gestion de l'azote comme des cibles mesurables, prédictibles et sélectionnables au niveau génétique, afin d'améliorer la sélection de cultivars de *M. sinensis* capables de maintenir la production de biomasse tout en contribuant à des services écosystémiques, comme la régulation de la qualité de l'eau. Le chapitre 1 a caractérisé la variation inter-génotypique des traits de gestion de l'azote en conditions limitantes en azote. Le chapitre 2 a développé des modèles statistiques à partir de proxys, variables simples et non destructives, dans l'objectif de prédire ces traits complexes. Le chapitre 3 a identifié des QTL contrôlant les traits de gestion de l'azote et de leurs proxys, et évalué le rôle des relations entre ces caractères cibles et leurs proxys au niveau génétique. L'ensemble de ces chapitres propose un cadre intégré, fonctionnel, prédictif et génétique, visant à valoriser les traits de gestion de l'azote dans l'amélioration génétique du miscanthus.

## Cadre expérimental

L'étude a été conduite sur une descendance diploïde de plein-frères de *Miscanthus sinensis* (2n = 2x = 38), comprenant 80 génotypes issus d'un croisement contrôlé entre les cultivars parentaux « Malepartus » (MAL) et « Herman Mussel » (HER). Cette descendance, appelée SiB, constitue une population en ségrégation adaptée à l'évaluation de la diversité intraspécifique des traits de gestion de l'azote, ainsi qu'aux analyses génétiques chez cette espèce. L'expérimentation au champ a été implantée en 2018 sur l'unité expérimentale INRAE d'Estrées Mons (GCIE, Hauts de France, France). Les plantes ont été cultivées à une densité de 1 plante $m^{-2}$ selon un dispositif en blocs incomplets comprenant quatre blocs. L'essai a été conduit sans apport de fertilisation azotée, avec une irrigation appliquée afin d'éviter tout stress hydrique. La carence azotée de l'essai a été diagnostiquée par le suivi de l'azote minéral du sol et par le diagnostic du statut azoté des cultures au moyen de l'Indice de Nutrition Azotée (INN), basé sur la courbe critique de dilution de l'azote développée sur miscanthus (Zapater et al., 2017).

Les traits de gestion de l'azote ont été quantifiés sur un cycle annuel complet, de février 2023 à février 2024, dans l'essai de la descendance SiB. Quatre campagnes d'échantillonnage destructif ont été réalisées à des stades physiologiques clés du cycle de la plante. Ces dates correspondaient à :

- février 2023, correspondant à la dormance hivernale et représentant la quantité maximale d'azote dans les organes souterrains (Date 0) ;
- juillet 2023, correspondant à la quantité minimale d'azote dans les organes souterrains après la remobilisation printanière (Date 1) ;
- septembre 2023, correspondant à la quantité maximale d'azote dans les organes aériens en phase de croissance active (Date 2) ;
- février 2024, correspondant à la fin du cycle après sénescence complète des parties aériennes de la plante (Date 3).

Des calculs de flux d'azote, entre dates et parties aériennes et souterraines de la plante, ont permis d'estimer la remobilisation printanière (SR), l'absorption d'azote, la remobilisation automnale et les pertes d'azote (définitions des traits et calculs détaillés au chapitre 1). En parallèle des prélèvements destructifs, un phénotypage non destructif a été réalisé tout au long de la saison de croissance afin d'établir un ensemble de proxys pour prédire les traits de gestion de l'azote. Au total, 35 caractères proxys ont été mesurés et concernaient la morphologie des plantes, l'architecture du couvert, la phénologie et le statut azoté des plantes.

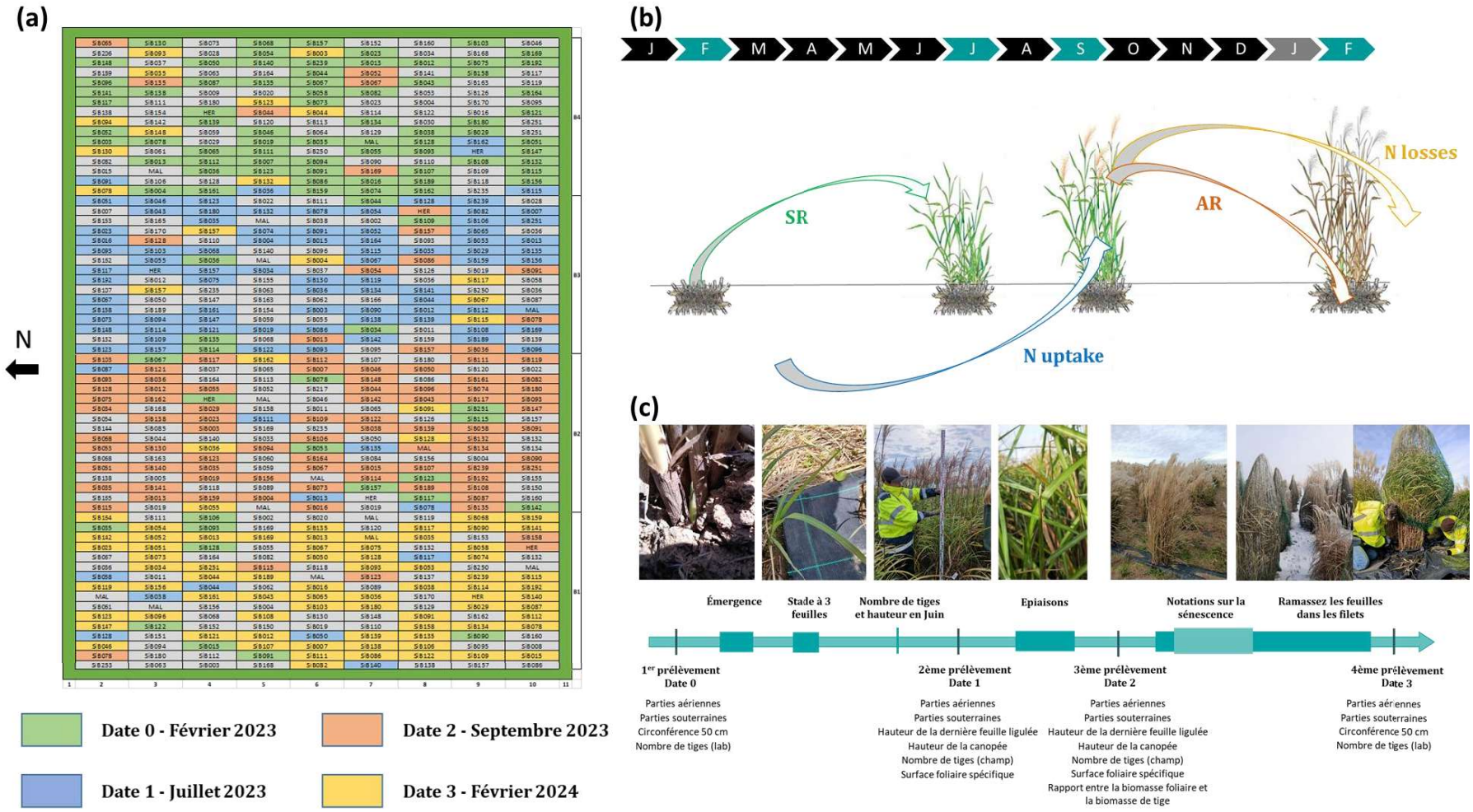


**Figure S1.** Plan du dispositif au champ de l'essai de descendance diploïde plein-frères de *Miscanthus sinensis* à Estrées-Mons, montrant la position des plantes, le dispositif en quatre blocs incomplets et l'attribution des plantes prélevées aux quatre dates d'échantillonnage (a). Représentation des flux saisonniers d'azote chez *M. sinensis*, incluant la remobilisation printanière (SR), l'absorption d'azote (nitrogen uptake), la remobilisation automnale (AR) et les pertes d'azote (nitrogen losses) (b). Vue d'ensemble des mesures saisonnières depuis la reprise de croissance jusqu'à la sénescence complète des parties aériennes de la plante, incluant le phénotypage à chaque date d'échantillonnage ainsi que la mesure non destructive de 35 caractères proxys (proxy traits) (c).

Ces caractères ont été choisis car ils sont simples, facilement mesurables et compatibles avec un phénotypage à plus haut débit dans des contextes de sélection, tout en capturant une variabilité biologiquement pertinente liée aux traits de gestion de l'azote par la plante. Les caractères proxys ont été évalués comme prédicteurs des traits de gestion de l'azote au moyen de corrélations par paires et d'une modélisation statistique multivariée de régression par les moindres carrés partiels (PLS), une méthode adaptée aux ensembles de prédicteurs colinéaires. Des régressions PLS ont été développées à partir des 35 indicateurs pour prédire chaque trait de gestion de l'azote. Les performances des modèles ont été évaluées au moyen de procédures de validations croisées répétées, et des ensembles réduits de prédicteurs ont été identifiés à l'aide du paramètre statistique d'Importance de la Variable dans la Projection (VIP) afin d'obtenir des modèles parcimonieux compatibles avec les contraintes de la sélection variétale (méthodologie complète et évaluation des modèles détaillées au chapitre 2).

Afin d'étudier le contrôle génétique des traits de gestion de l'azote, la descendance et les parents ont été génotypés à l'aide de marqueurs moléculaires SNP, et une carte génétique a été construite selon 19 groupes de liaison, alignés sur le génome de référence de *Miscanthus sinensis* (Mitros et al, 2020). Elle a servi de base à la détection de QTL pour les caractères cibles de gestion de l'azote et leurs proxys (carte génétique et pipeline de détection de QTL détaillés au chapitre 3). Les analyses QTL ont été réalisées à l'aide d'une cartographie par intervalle composite, adaptée aux populations de plein-frères. La détection des QTL a ciblé l'absorption d'azote, les traits de remobilisation saisonnière (SR, ARa, ARb), les pertes d'azote et la déviation des pertes d'azote (cf détail du calcul de cette déviation en chapitre 3). Les proxys ont été cartographiés en parallèle afin de tester si les relations phénotypiques entre proxy et caractère cible montraient des régions génomiques communes. La colocalisation des QTL a été évaluée à l'aide d'intervalles de confiance et les effets alléliques ont été estimés afin d'évaluer l'intérêt des marqueurs détectés pour la sélection. Enfin, le pyramidage de QTL a été exploré afin d'évaluer dans quelle mesure des combinaisons de plusieurs marqueurs associés à des caractères de gestion de l'azote peuvent permettre de concevoir des idéotypes assurant une diversité de services écosystémiques (Chapitre 3).

## Résultats et discussion

### Chapitre 1 : Les stratégies de gestion de l'azote définissent des groupes fonctionnels distincts de génotypes dans une descendance de *Miscanthus sinensis*

La diversité fonctionnelle de gestion de l'azote a été caractérisée au sein de cette même descendance SiB, en quantifiant la variation inter-génotypique des traits de gestion de l'azote et en testant si cette variation reflète des stratégies structurées plutôt qu'une variabilité aléatoire (Iqbal et al., 2026). La descendance a exprimé une forte diversité phénotypique au cours du cycle de la plante sur la période 2023 à 2024. La biomasse aérienne variait de 5 à 60 t $ha^{-1}$, avec les valeurs les plus élevées observées en septembre, tandis que la biomasse souterraine variait de 5 à 40 t $ha^{-1}$ sans tendance saisonnière nette (Figure S2). La biomasse aérienne et la biomasse souterraine étaient fortement corrélées aux quatre dates d'échantillonnage ($r = 0,73$ à $0,85$), ce qui indique que les génotypes présentant un fort potentiel de rendement au niveau aérien étaient également caractérisés par une biomasse souterraine élevée (Iqbal et al., 2026).

En parallèle, les traits de gestion de l'azote présentaient une variation inter-génotypique importante, soutenant l'hypothèse d'une forte variabilité intraspécifique des capacités d'absorption, de recyclage et de pertes d'azote (Leroy et al., 2022 ; Iqbal et al., 2026). La remobilisation printanière (SR) variait de 0,2 à 85 kg N $ha^{-1}$, traduisant de fortes différences entre génotypes quant à la capacité à mobiliser l'azote stocké pour accompagner la croissance

des nouvelles tiges. La remobilisation automnale quantifiée selon la méthode de flux au niveau des parties aériennes de la plante (ARa) variait de 5 à 158 kg N $ha^{-1}$, tandis que la remobilisation automnale quantifiée selon la méthode de flux au niveau des parties souterraines *via* le rhizome (ARb) variait de 0 à 73 kg N $ha^{-1}$. Cet écart entre les deux méthodes de calcul indique que l'azote issu des parties aériennes sénescentes ne se retrouvait pas complètement dans le rhizome, ce qui suggérait l'existence de pertes d'azote par la plante (Iqbal et al., 2026). L'absorption d'azote variait de 5 à 241 kg N $ha^{-1}$, révélant une forte variabilité de la capacité d'acquisition en condition de carence azotée. Les pertes d'azote variaient de 2 à 143 kg N $ha^{-1}$, les feuilles tombées représentant 1 à 27 % des pertes selon le génotype, ce qui indique des niveaux de pertes contrastés (Iqbal et al., 2026).

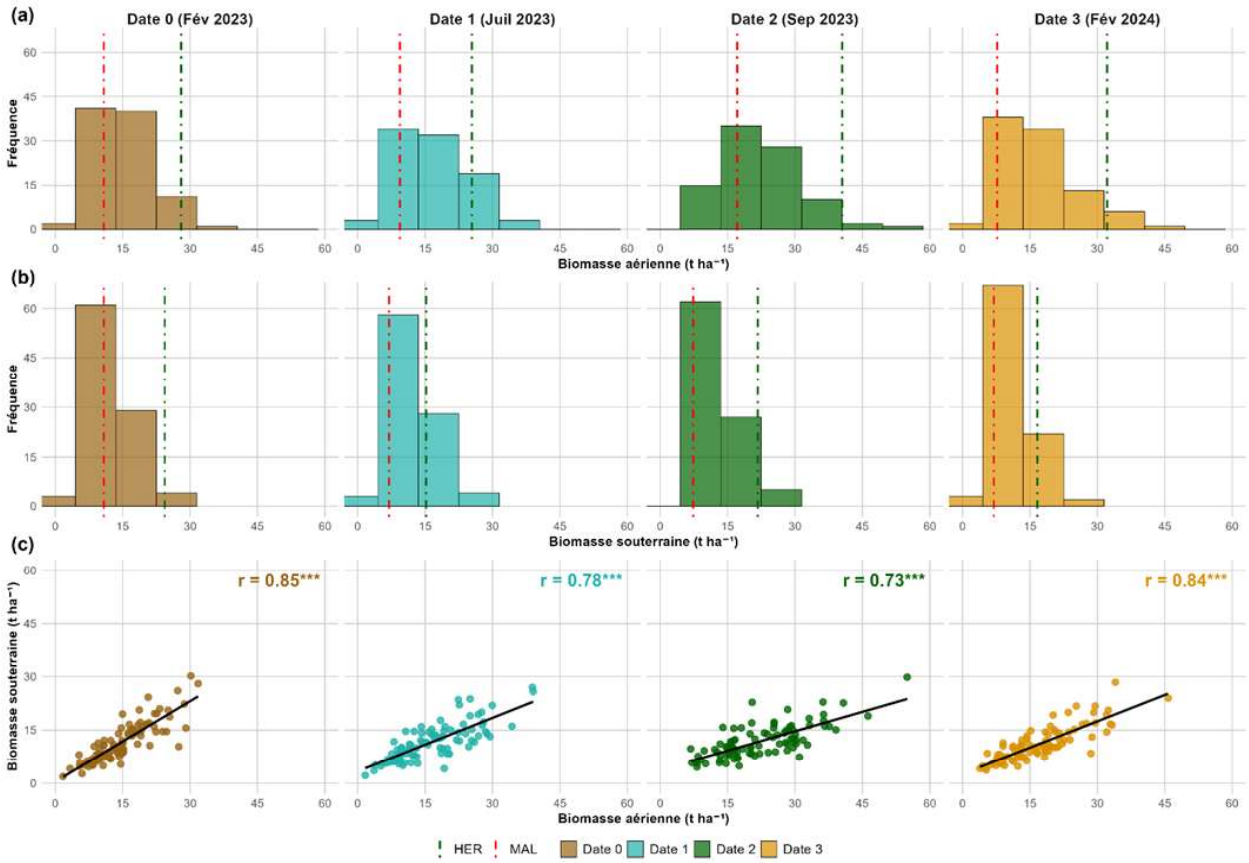


**Figure S2.** Distribution de la biomasse aérienne et souterraine (graphiques a et b) et leur corrélation (graphique c) aux quatre dates d'échantillonnage au cours du cycle végétatif 2023 à 2024. À la date 0, la biomasse aérienne correspond à la fin du cycle végétatif précédent, tandis que la biomasse souterraine correspond à la fois à la fin du cycle précédent et au début du nouveau cycle. Les lignes pointillées vertes et rouges indiquent respectivement les génotypes parentaux HER et MAL.

Les traits de gestion de l'azote ont été analysés au moyen d'une analyse en composantes principales (ACP), suivie d'une classification hiérarchique sur les composantes principales obtenues, révélant que cette diversité s'organisait selon trois groupes fonctionnels différents de génotypes, associés à des stratégies contrastées d'utilisation de l'azote (Figure S3). Le premier groupe rassemblait des génotypes suivant une stratégie de génotypes "extracteurs", caractérisés par une absorption d'azote élevée, des valeurs de remobilisation automnale (ARa), des pertes d'azote et un rendement en biomasse également élevés. Le deuxième groupe rassemblait des génotypes suivant une stratégie de génotypes "recycleurs", caractérisés par une absorption et des pertes en azote plus faibles, mais par des valeurs de recyclage souterrain plus élevées, en particulier SR et ARb, ce qui traduit une dépendance accrue au recyclage interne et aux dynamiques de stockage. Il est important de souligner que ces deux stratégies étaient toutes

deux associées à la capacité de maintenir une production de biomasse élevée en conditions de carence azotée au champ, ce qui montre que des stratégies contrastées d'utilisation de l'azote peuvent contribuer à la production de biomasse (Iqbal et al., 2026). Le troisième groupe rassemblait principalement des génotypes déficients en azote, caractérisés par une absorption et des flux de remobilisation faibles, conduisant à une production de biomasse réduite. Les génotypes parentaux se positionnaient dans des groupes contrastés, illustrant la manière dont le contraste entre les deux parents a structuré les stratégies de gestion de l'azote au sein de la descendance (Iqbal et al., 2026). Dans l'ensemble, ces résultats montrent que ces traits chez *M. sinensis* présentent une forte variabilité inter-génotypique et se distribuent selon des stratégies cohérentes d'utilisation de l'azote qui définissent des groupes fonctionnels différents.

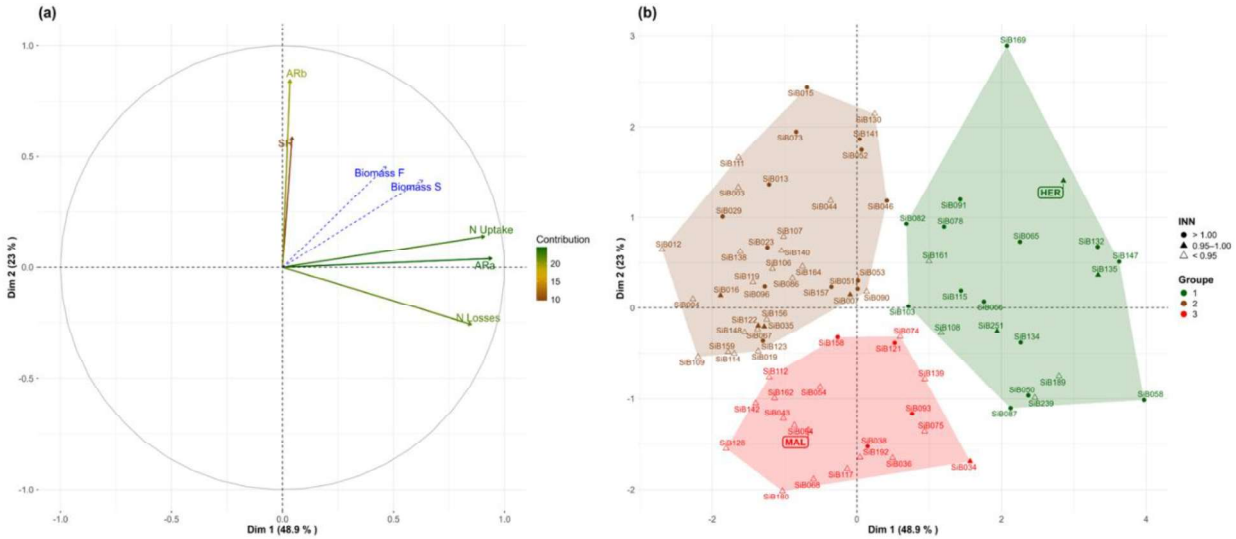


**Figure S3.** Analyse en composantes principales basée sur les caractères de gestion de l'azote (ACP) et classification hiérarchique basées sur les cinq composantes principales obtenues. Représentation des variables de l'ACP (graphique a) et représentation correspondante de la classification hiérarchique des génotypes (graphique b), avec le rendement en biomasse comme variable quantitative supplémentaire et le statut azoté comme variable qualitative supplémentaire. Le codage des variables est identique à celui présenté dans le tableau des abréviations (xviii).

## Chapitre 2 : Les caractères proxys permettent aux sélectionneurs de prédire des traits complexes de gestion de l'azote chez *Miscanthus sinensis*

Une approche non destructive et transposable à plus grande échelle a été développée afin d'estimer les traits de gestion de l'azote dans la descendance SiB, à partir de caractères de la plante qui soient simples et mesurables (Chapitre 2). Un ensemble de 35 caractères morphologiques, phénologiques et physiologiques a été évalué comme proxys candidats pour prédire l'absorption d'azote, la remobilisation printanière, la remobilisation automnale et les pertes d'azote. Les analyses de corrélations par paires ont montré que les relations entre chaque caractère proxy et les traits de gestion de l'azote étaient généralement faibles à modérées (Figure S4). Ce résultat indique qu'aucun caractère ne peut servir de substitut fiable à lui seul à des caractères complexes basés sur des flux, mais que la réunion de plusieurs caractères proxys contient une information prédictive pertinente pour estimer la gestion de l'azote par la plante (Chapitre 2).

Sur la base d'une procédure de validations croisées répétées, des modèles de régression par les moindres carrés partiels intégrant des combinaisons variées de caractères proxys ont permis d'obtenir une précision de prédiction spécifique à chaque caractère pour l'ensemble des composantes de gestion de l'azote. Les précisions de prédiction variaient de 0,62 à 0,74 pour l'absorption d'azote, de 0,48 à 0,63 pour la remobilisation automnale estimée par la méthode

aérienne, de 0,49 à 0,51 pour la remobilisation automnale estimée par la méthode souterraine, de 0,30 à 0,46 pour la remobilisation printanière, et de 0,24 à 0,39 pour les pertes d'azote (Figure S5). Ces résultats montrent que des caractères proxys non destructifs au niveau de la plante peuvent prédire des traits de gestion de l'azote qui nécessitent habituellement des mesures saisonnières destructives, l'absorption d'azote constituant la composante la mieux prédictible, tandis que les pertes d'azote sont les plus difficiles à appréhender à partir d'informations proxys (Chapitre 2).

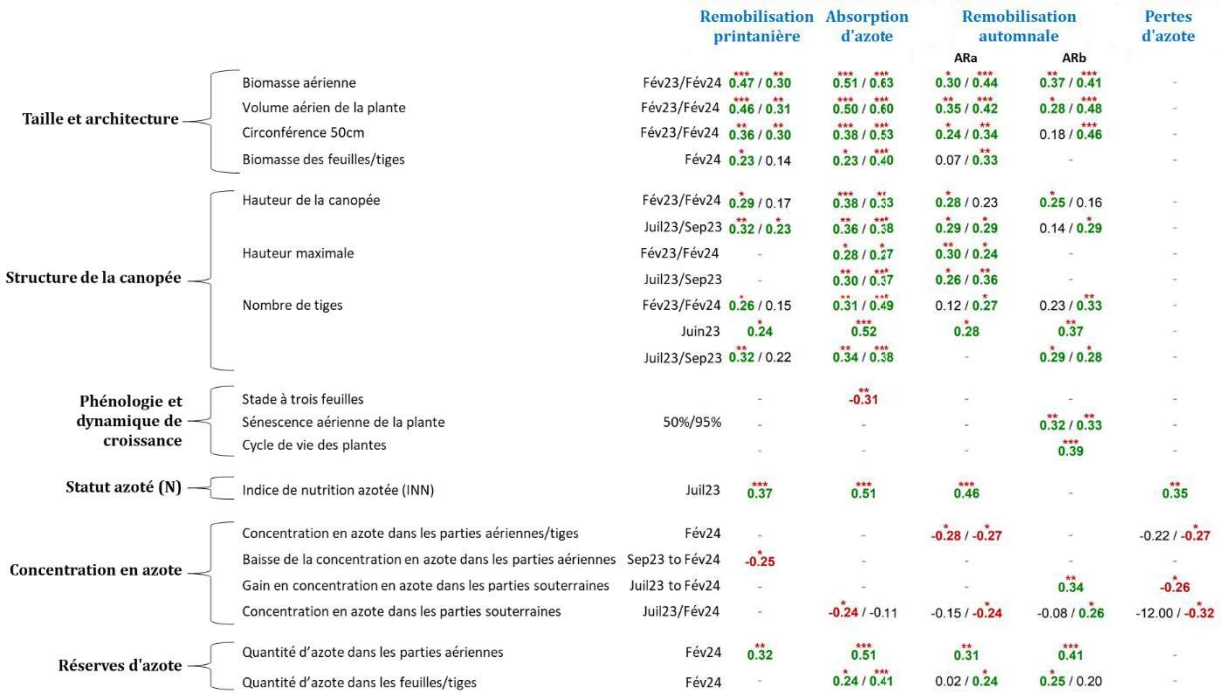


**Figure S4.** Valeurs des coefficients de corrélations de Pearson entre les traits de gestion de l'azote (SR, ARa, ARb, N Uptake et N Losses) et les proxys candidats, les niveaux de significativité étant indiqués (*** p < 0,001, ** p < 0,01, * p < 0,05). Les corrélations positives significatives sont indiquées en vert et les corrélations négatives significatives en rouge. Pour les proxys mesurés à plusieurs dates, les valeurs de corrélation sont présentées sur une même ligne (par exemple Feb23/Feb24).

Les analyses des statistiques d'Importance de la Variable dans la Projection (VIP) ont permis d'identifier les traits contribuant le plus fortement à la prédiction, ce qui a rendu possible le développement de modèles plus réduits et par conséquent parcimonieux. De manière déterminante, les modèles parcimonieux ont conservé des performances de prédiction comparables à celles du modèle complet incluant les 35 proxys, ce qui démontre que la prédiction peut être obtenue avec un nombre plus faible de caractères, plus simples à mesurer, tout en restant compatibles avec des applications en sélection. Au-delà des performances des modèles, ce chapitre a apporté un résultat opérationnel : les modèles fondés sur des proxys ont permis une sélection et une contre sélection efficaces, les modèles parcimonieux permettant de retomber sur 75 à 95 % des génotypes qui auraient été sélectionnés ou écartés à partir de l'ensemble complet de prédicteurs (Chapitre 2). Dans l'ensemble, ces résultats démontrent que des traits de gestion de l'azote, habituellement mesurables uniquement par des approches destructives de la plante, peuvent désormais être approchées à l'aide d'un petit nombre de proxys non destructifs, ce qui permet ainsi un phénotypage à plus haut débit pour ces traits complexes.

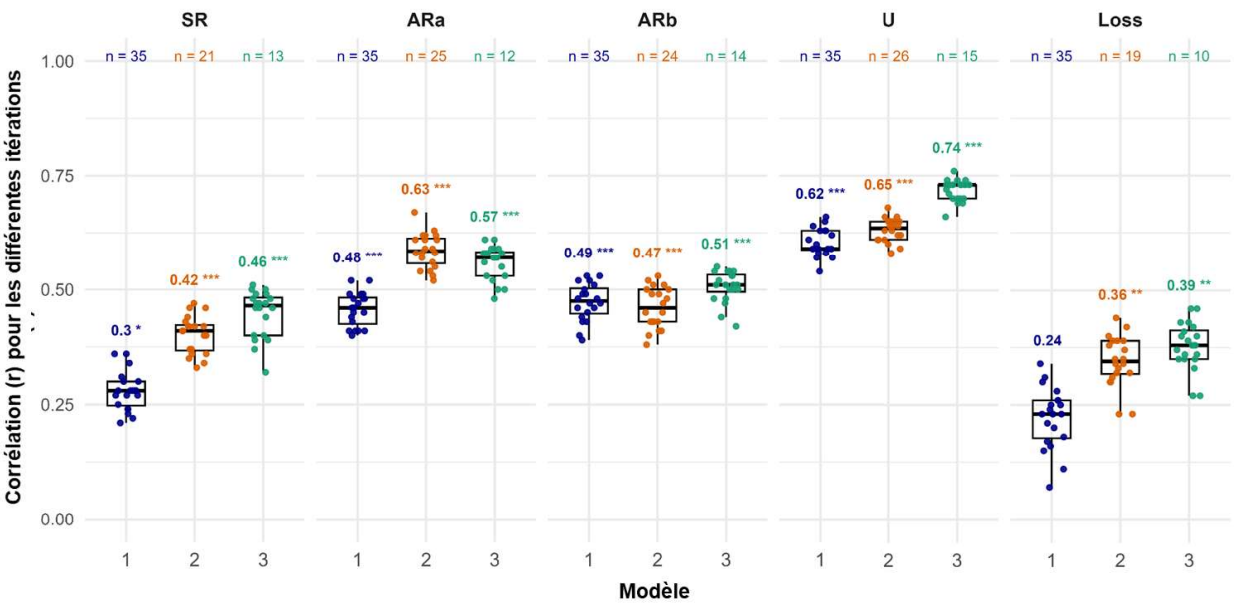


**Figure S5.** Précision de prédiction des trois modèles (Modèle 1, Modèle 2 et Modèle 3) pour chaque trait de gestion de l'azote (SR, ARa, ARb, absorption de l'azote (U) et pertes d'azote). Les boîtes à moustaches représentent la distribution des coefficients de corrélation de Pearson entre les valeurs prédites et observées pour les différentes itérations de validation croisée. Le nombre de prédicteurs (n) inclus dans chaque modèle est indiqué au-dessus de chaque boîte. Définition des modèles : le Modèle 1 inclut l'ensemble des 35 traits proxys ; le Modèle 2 inclut les prédicteurs avec VIP ≥ 0,8 et le Modèle 3 inclut les prédicteurs avec VIP ≥ 1,0.

## Chapitre 3 : La cartographie de QTL identifie des régions génomiques associées aux traits de gestion de l'azote dans une descendance plein-frères de *Miscanthus sinensis*

Les traits de gestion de l'azote ont été traduits en cibles de sélection définies au niveau génétique en disséquant leur contrôle génétique dans la descendance SiB, et en évaluant dans quelle mesure l'information génétique peut contribuer à des stratégies de sélection cohérentes avec des services écosystémiques (Chapitre 3). À partir d'une carte génétique comprenant 19 groupes de liaison, la cartographie de QTL a mis en évidence des régions génomiques impliquées dans l'absorption d'azote, la remobilisation automnale estimée par la méthode aérienne (ARa) et les pertes d'azote (Figure S6). Des QTL ont également été détectés pour la remobilisation printanière (SR), la remobilisation automnale estimée par la méthode souterraine (ARb) et la déviation des pertes d'azote (données non présentées). Au total, 19 QTL ont été détectés pour les traits de gestion de l'azote, avec des effets spécifiques des QTL expliquant entre 8,8 et 37,1 % de la variance phénotypique.

Les architectures génétiques étaient spécifiques à chaque caractère, et aucun chevauchement des intervalles de confiance n'a été observé entre les QTL contrôlant l'absorption, la remobilisation et les pertes d'azote. Cette quasi absence de colocalisation indique un contrôle génomique largement indépendant des principales composantes de gestion de l'azote, ce qui offre la possibilité de dissocier génétiquement les processus d'absorption, de recyclage et de pertes d'azote pour une sélection ciblée de ces caractères.

Afin d'évaluer si les relations qui avaient été établies entre proxy et caractère cible de gestion de l'azote (Chapitre 2) reposaient sur une base génétique, les caractères proxys ont été cartographiés en parallèle. Parmi les 26 proxys fortement impliqués, 85 QTL de proxys ont été identifiés, avec des QTL individuels expliquant jusqu'à 34,0 % de la variance phénotypique.

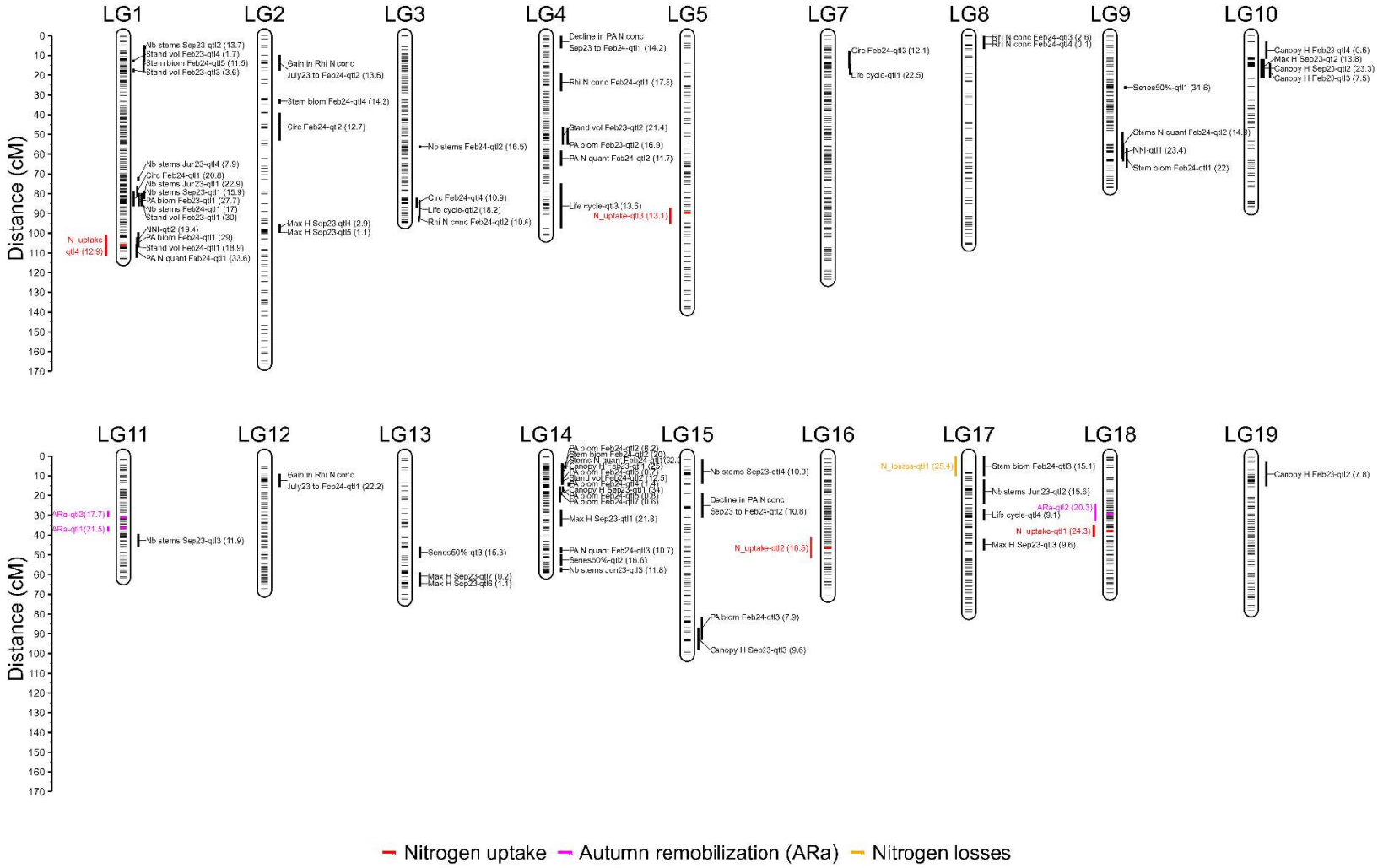


**Figure S6.** Carte génétique intégrée présentant les QTLs associés à la dynamique de l'azote de l'été à l'automne, incluant l'absorption de l'azote (Nitrogen uptake ; en rouge), la remobilisation automnale de l'azote *via* la méthode "aérienne" (ARa ; en violet) et les pertes en azote (Nitrogen losses ; en orange), ainsi que leurs proxys fortement impliqués (VIP > 1). Les positions des QTLs sont indiquées pour chaque groupe de liaison avec leurs intervalles de confiance correspondants. Les valeurs entre parenthèses indiquent la proportion de variance phénotypique expliquée ($R^2$) par chaque QTL. Le codage des variables est identique à celui présenté dans le tableau des abréviations (xviii).

La colocalisation de QTL entre proxys et traits de gestion de l'azote a été limitée à deux endroits, l'une associée à l'absorption d'azote et l'autre à la remobilisation printanière SR. De manière importante, ces colocalisations ont concerné spécifiquement les caractères proxys présentant les corrélations phénotypiques les plus fortes avec les traits correspondants de gestion de l'azote. Cette situation suggère que le contrôle génétique partagé n'apparaît que lorsque les relations proxy - trait cible de gestion de l'azote sont les plus robustes, tandis que l'absence de colocalisation plus fréquente pour les autres composantes de gestion de l'azote est cohérente avec des architectures génétiques spécifiques aux traits (Chapitre 3).

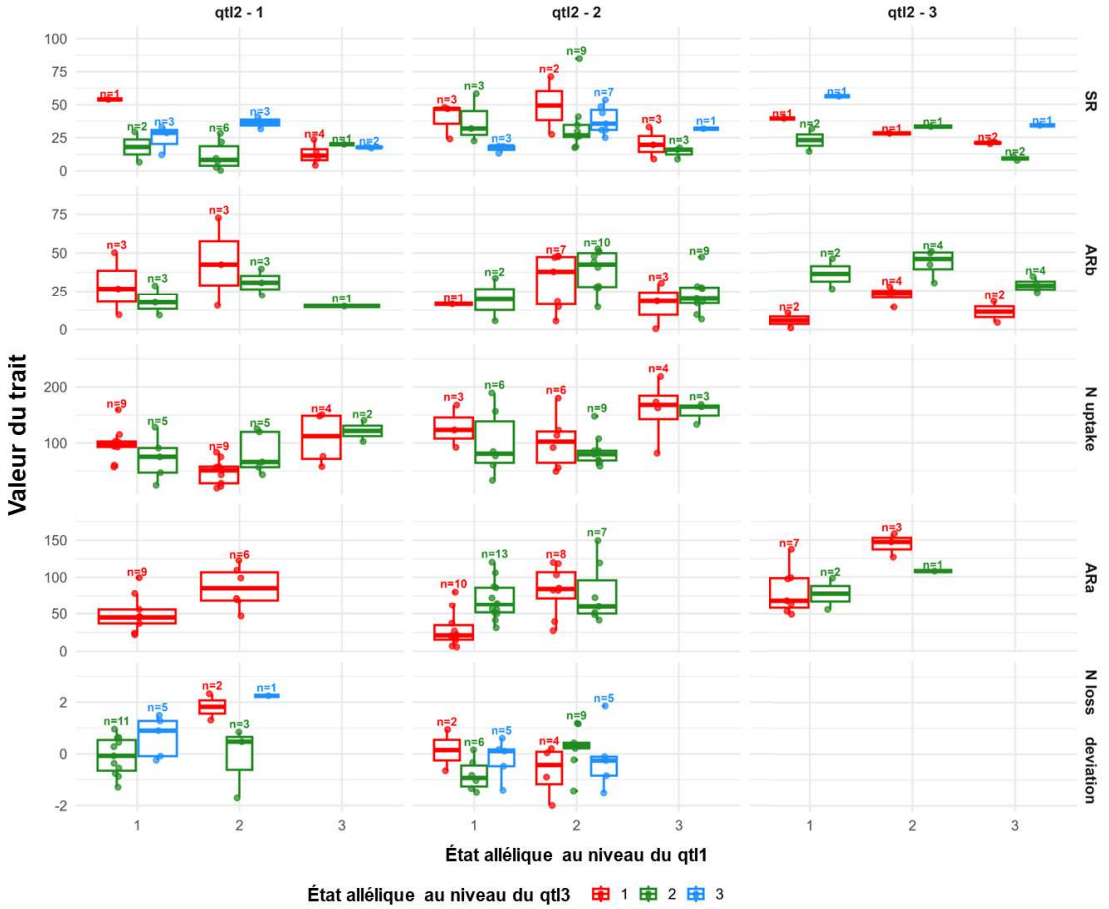


**Figure S7.** Effets de pyramidage de QTL sur les traits de gestion de l'azote pour la population SiB. Les valeurs des traits de gestion de l'azote sont présentées pour des combinaisons d'états alléliques aux trois principaux QTLs (qtl1, qtl2 et qtl3). Les classes alléliques sont définies par la combinaison des états alléliques au qtl1 (représentés sur l'axe des x), qtl2 (représentés selon les colonnes des facettes) et qtl3 (symbolisés par des couleurs différentes). Les valeurs des traits sont exprimées en kg N $ha^{-1}$ pour l'absorption de l'azote, SR, ARa et ARb. La lettre « n » au-dessus des boîtes à moustaches indique le nombre de génotypes par classe allélique. Par exemple, la boîte à moustaches verte située en bas à gauche pour la déviation des pertes d'azote correspond à la classe allélique 1-1-2, indiquant l'état allélique 1 au qtl1, l'état allélique 1 au qtl2 et l'état allélique 2 au qtl3.

Enfin, l'intérêt pour la sélection des QTL en lien avec la gestion de l'azote par la plante a été exploré par l'estimation des effets alléliques et par le pyramidage de QTL. En plus des QTL contrôlant l'absorption d'azote et la remobilisation, trois QTL ont été identifiés pour

la déviation des pertes d'azote, un trait décrivant la variation des pertes d'azote en fonction de l'absorption d'azote. Ce caractère basé sur la déviation constitue un levier génétique pour gérer la relation positive indésirable entre l'absorption d'azote et les pertes d'azote, de fortes pertes d'azote par la plante n'étant pas un atout, en distinguant des génotypes combinant une absorption élevée avec des pertes inférieures à celles attendues. Le pyramidage de QTL a montré que la combinaison d'états alléliques sur plusieurs QTL génère des classes multi loci contrastées pour l'absorption d'azote et la déviation des pertes d'azote, ce qui permet de sélectionner et contre-sélectionner des génotypes présentant une absorption élevée et des pertes plus faibles qu'attendues (Figure S7). Ces résultats ont fourni la première dissection génétique basée sur des QTL des traits de gestion de l'azote chez *M. sinensis* à l'échelle d'une descendance, en traduisant les processus d'absorption, de recyclage et de pertes en cibles génétiques directement valorisables pour la sélection.

## Conclusion et perspectives

Cette thèse montre que les traits de gestion de l'azote chez *Miscanthus sinensis* peuvent être transformés, à partir de processus physiologiques complexes, en cibles opérationnelles de sélection capables de contribuer à la fois à la production de biomasse et à la fourniture en services écosystémiques tels que les services de régulation. En conditions de carence azotée au champ, l'absorption d'azote, la remobilisation saisonnière et les pertes d'azote sont apparues comme des composantes centrales et fortement variables du fonctionnement entre génotypes, révélant une forte diversité intraspécifique dans la manière dont les génotypes acquièrent, recyclent et retiennent l'azote. De manière importante, cette diversité n'était pas distribuée aléatoirement, mais structurée en stratégies cohérentes d'utilisation de l'azote, incluant des profils "extracteurs" reposant plus fortement sur l'absorption d'azote du sol et des profils "recycleurs" reposant davantage sur le recyclage interne de l'azote. Les deux stratégies se sont révélées capables de maintenir la production de biomasse sous une disponibilité limitante en azote.

Un autre résultat majeur de ce travail est la possibilité d'intégrer ces traits complexes de gestion de l'azote dans des pipelines de sélection transposables à plus grande échelle. Les modèles statistiques de prédiction par PLS intégrant des proxys ont montré que des combinaisons de caractères, simples et non destructifs au niveau de la plante, permettent d'approcher de manière assez fiable les composantes de gestion de l'azote, lesquelles nécessitent habituellement des campagnes saisonnières d'échantillonnage destructif. Par ailleurs, des modèles statistiques parcimonieux ont conservé des performances de prédiction élevées avec un nombre réduit de prédicteurs plus simples, rendant possible un phénotypage opérationnel à l'échelle de populations plus grandes. En parallèle, la cartographie de QTL a établi que l'absorption d'azote, la remobilisation et les pertes en azote sont chacune contrôlées par plusieurs régions génomiques, avec des architectures spécifiques aux traits, tandis que les relations proxy - caractère cible de gestion de l'azote n'étaient étayées génétiquement qu'au niveau de régions chromosomiques spécifiques, là où les corrélations phénotypiques étaient les plus fortes. L'ensemble de ces résultats fournit un cadre fonctionnel, prédictif et génétique cohérent, ce qui montre que les traits de gestion de l'azote peuvent être mesurés, prédits et ciblés au niveau génétique avec un niveau de précision compatible avec celui de la sélection.

Dans une perspective de déploiement, les résultats obtenus définissent des priorités claires en matière de validation. Les stratégies d'utilisation de l'azote identifiées devront être testées dans le futur sur plusieurs années, dans différents environnements et sous diverses conditions de conduite, incluant des disponibilités contrastées en azote et en eau, afin de déterminer leur stabilité et leur pertinence dans des contextes agronomiques plus larges. De même, les QTL et les modèles statistiques de prédiction par PLS intégrant des proxys nécessitent désormais une validation sur des données indépendantes afin de distinguer les effets génétiques stables des effets dépendant d'un contexte donné, et de consolider les ensembles de marqueurs et de traits prédicteurs qui pourront être valorisés dans des programmes de sélection. Enfin, ces résultats obtenus sur fond diploïde impliqueront leur transfert vers des fonds triploïdes stériles qui soient agronomiquement utilisables. Ce transfert devra s'accompagner d'une évaluation de leurs performances non seulement pour leur rendement de biomasse, mais également en termes de performance à l'échelle du système -telles que l'extraction de nitrates présents en excès dans les sols des zones vulnérables et qui sont issus du lessivage de nitrates dus aux précédents culturaux-, la conservation des nutriments et la résilience à long terme des agroécosystèmes.

# TABLE OF CONTENTS

# TABLE OF ABBREVIATIONS

*This table lists the abbreviations used throughout the thesis. Abbreviations are introduced as they appear in the different results chapters.*

## Chapter 1 - Abbreviations

### *Genotypes and Trials*

| | |
|---|---|
| Cfb | Marine west-coast climate |
| DOY | Day of Year |
| HER | *Miscanthus sinensis* 'Herman Mussel' |
| INRAE | French National Research Institute for Agriculture, Food and Environment |
| MAL | *Miscanthus sinensis* 'Malepartus' |
| UAN | Urea-ammonium-nitrate solution (applied at 120 kg N ha−1) |
| UE GCIE | Unité Expérimentale Grandes Cultures Innovation Environnement |

### *Organs, Biomass, and Sampling Dates*

| | |
|---|---|
| AP | Aboveground parts (stems and leaves) |
| Biomass F | Aboveground biomass in February 2024 (t ha−1) |
| Biomass S | Aboveground biomass in September 2023 (t ha−1) |
| BP | Belowground parts (rhizomes and roots) |
| Date 0 | February 2023 (dormancy; maximum N quantity in BP) |
| Date 1 | July 2023 (minimum N quantity in BP) |
| Date 2 | September 2023 (maximum N quantity in AP) |
| Date 3 | February 2024 (after full senescence; harvest) |
| W | Aboveground dry biomass (t ha−1) in the critical nitrogen dilution curve equation |
| WA | Biomass of aboveground parts (t ha−1) |
| WA3 | Aboveground biomass in February 2024 (t ha−1) |
| WAmax | Maximum aboveground biomass accumulated in September (t ha−1 |
| WB | Biomass of belowground parts (t ha−1) |

### *Nitrogen Pools, Concentrations, and Quantities*

| | |
|---|---|
| N | Nitrogen |

| | |
|---|---|
| Na | Actual nitrogen concentration in aboveground vegetative parts (for NNI) |
| Nc | Critical nitrogen concentration from the critical nitrogen dilution curve |
| [NA] | Nitrogen concentration of aboveground parts (g N kg−1 DM) |
| [NB] | Nitrogen concentration of belowground parts (g N kg−1 DM) |
| NA | Nitrogen quantity in aboveground parts (kg N ha−1) |
| NA2 | Nitrogen quantity of aboveground parts at Date 2 (September 2023) |
| NA3 | Nitrogen quantity of aboveground parts at Date 3 (February 2024) |
| NB | Nitrogen quantity in belowground parts (kg N ha−1) |
| NB0 | Nitrogen quantity in belowground parts before spring remobilization (February 2023) |
| NB1 | Nitrogen quantity in belowground parts after spring remobilization (July 2023) |
| NB2 | Nitrogen quantity in belowground parts when aboveground N is maximal (September 2023) |
| NB3 | Nitrogen quantity in belowground parts after full senescence (February 2024) |
| NT | Total nitrogen quantity in the whole plant (kg N ha−1) |
| NT2 | Total N quantity at peak growth (September 2023) |
| NT3 | Total N quantity at the end of the cycle (February 2024) |
| NNI | Nitrogen Nutrition Index (=Na/Nc) |

***Nitrogen Fluxes and Efficiencies***

| | |
|---|---|
| SR | Spring remobilization (kg N ha−1) |
| SRE | Spring remobilization efficiency (%) |
| ARa | Autumn remobilization *via* aboveground method (kg N ha−1) |
| ARaE | Autumn remobilization efficiency using the aboveground method (%) |
| ARb | Autumn remobilization via belowground method (kg N ha−1) |
| ARbE | Autumn remobilization efficiency using the belowground method (%) |

| | |
|---|---|
| N uptake | Nitrogen uptake (kg N ha−1) |
| N uptake E | Nitrogen uptake efficiency (%), proportion of aboveground N derived from uptake |
| N losses | Nitrogen losses (kg N ha−1) |
| NUE | Nitrogen use efficiency (kg DM kg−1 N) |
| NUE1 | WAmax/NA2 (aboveground biomass produced using spring-remobilized and absorbed N) |
| NUE2 | WA3/NA3 (aboveground biomass harvested per unit of N exported at end of cycle) |

***Statistical and Multivariate Analyses***

| | |
|---|---|
| ANOVA | Analysis of variance |
| HCPC | Hierarchical clustering on principal components |
| PCA | Principal Component Analysis |
| LSD | Least Significant Difference test (post hoc) |
| *r* | Pearson correlation coefficient |
| *p* | Probability value (significance thresholds *, **, ***, NS) |
| NS | Not significant ($p \geq 0.05$) |
| v- test | Statistic indicating variable contributions in clusters |

***Units and Derived Quantities***

| | |
|---|---|
| DM | Dry matter (e.g., kg DM kg−1 N in NUE units) |
| g N kg−1 DM | Grams of nitrogen per kilogram of dry matter |
| kg N ha−1 | Kilograms nitrogen per hectare |
| t ha−1 | Tons per hectare |

## Chapter 2 - Abbreviations

***Prediction and Modelling***

| | |
|---|---|
| PLS | Partial Least Squares |
| VIP | Variable Importance in Projection |
| CV | Cross-validation |
| $R^2$ | Coefficient of determination |
| $\sqrt{R^2}$_cal | Square root of the coefficient of determination of the calibration set |
| $\sqrt{R^2}$_val | Square root of the coefficient of determination of the validation set |
| RMSE | Root Mean Square Error |

| | |
|---|---|
| RMSE_cal | Root mean squared error of the calibration set |
| RMSE_val | Root mean squared error of the validation set |
| se_RMSE_val | standard error of RMSE in validation set |
| Model 1 | Model with full set of proxy traits (n =35) |
| Model 2 | Model with set of proxy traits with VIP ≥ 0.8 |
| Model 3 | Model with set of proxy traits with VIP ≥ 1.0 |
| M1 | Model 1 |
| M2 | Model 2 |
| M3 | Model 3 |
| $r_{(cal)}$ | Pearson correlation coefficient in the calibration set |
| $r_{(val)}$ | Pearson correlation coefficient in the validation set |
| Predictors | Proxy traits |

## Chapter 3 - Abbreviations

***Genetic Mapping and QTL Analysis***

| | |
|---|---|
| QTL | Quantitative Trait Locus / Loci |
| LG | Linkage Group |
| cM | Centimorgan |
| LOD | Logarithm of odds |
| CI | Confidence interval |
| SNP | Single Nucleotide Polymorphism |
| GBS | Genotyping-by-sequencing |
| CIM | Composite Interval Mapping |
| BLUP | Best Linear Unbiased Predictor |
| BLUE | Best linear unbiased estimates |
| $R^2$ | Proportion of variance explained |
| -log10(pval) | *Negative base-10 logarithm of the p-value* |
| Peak | QTL peak position |
| Pos (cM) | QTL peak position in centiMorgans |
| alpha 'Mal' | Additive effect of the Malepartus parental allele |
| LOD H1 | LOD score testing the additive effect of the Malepartus allele |
| alpha 'Her' | Additive effect of the Herman Mussel parental allele |
| LOD H2 | LOD score testing the additive effect of the Herman Mussel allele |
| delta 'Mal × Her' | Dominance effect arising from the interaction between Malepartus and Herman Mussel alleles |

| | |
|---|---|
| LOD H3 | LOD score testing the dominance effect (interaction between parental alleles) |
| $H^2$ | Broad-sense heritability |
| N loss dev | Nitrogen loss deviation |

***Marker Nomenclature***

| | |
|---|---|
| Bri | Bridge marker (heterozygous in both parents) |
| Mal | Marker heterozygous in Malepartus |
| Her | Marker heterozygous in Herman Mussel |

***Proxy traits for qtl mapping***

| | |
|---|---|
| PA biom | Aboveground biomass |
| Stand vol | Stand volume |
| Leaves biom | Leaves biomass |
| Stem biom | Stems biomass |
| Circ | Circumference (50 cm) |
| Canopy H | Canopy height |
| Max H | Maximum height |
| Nb stems | Number of stems |
| 3-leaf stage | Three-leaf stage |
| Senes50% | Senescence 50% |
| Senes95% | Senescence 95% |
| Life cycle | Plant life cycle |
| NNI | Nitrogen nutrition index |
| PA N conc | Aboveground N concentration |
| Stems N conc | Stems N concentration |
| Decline in PA N conc | Decline in aboveground N concentration |
| Gain in Rhi N conc | Gain in belowground N concentration |
| Rhi N conc | Belowground N concentration |
| PA N quant | Aboveground N quantity |
| Leaves N quant | Leaves N quantity |
| Stems N quant | Stems N quantity |

# LIST OF FIGURES

*Note: Some titles are summarized in this list; more details are available in the main text of the legend related to each figure and table.*

# LIST OF TABLES

# General Introduction

# 1. Conceptual foundations of ecosystem services

## 1.1 Historical development of the ecosystem services concept

The concept of ecosystem services provides a framework to conceptualize and assess the relationship between nature and society (Lele et al., 2013). However, the definitions and conceptual foundations of ecosystem services have evolved over time. Historically, the first scientific studies addressing this notion emerged in the late 1970s, primarily with the aim of raising public awareness about biodiversity conservation. The beneficial functions of ecosystems were then described as "services" (Westman, 1977; Ehrlich and Ehrlich, 1981; de Groot, 1987). These early contributions highlighted the dependence of human societies on ecological processes and began to formalize the idea that ecosystems deliver functions that are useful to humans.

In 1997, Daily defined ecosystem services as "the conditions and processes through which natural ecosystems, and the species that make them up, sustain and fulfill human life." Beyond this definition, several key characteristics of ecosystem services were highlighted. First, ecosystem services contribute to the maintenance of biodiversity and the production of ecosystem goods, such as seafood, timber, biomass fuels, natural fibers, and numerous pharmaceutical and industrial products. Second, they encompass essential life-support functions, including natural processes such as cleansing, recycling, and renewal. These functions include, for example, air and water purification, waste detoxification and decomposition, and the mitigation of floods and droughts. Third, ecosystem services arise from complex natural cycles driven by solar energy, which underpin the fundamental functioning of the biosphere. Fourth, the concept extends beyond material needs to include intangible aesthetic, cultural, and intellectual benefits that contribute to human well-being and spiritual enrichment. Finally, Daily emphasized the irreplaceability of ecosystem services, arguing that while technological solutions may temporarily mask their degradation, they are unlikely to compensate in the long-term for large-scale losses of productive land or biodiversity.

To illustrate the necessity of ecosystem services, Daily proposed a thought experiment involving the establishment of a human colony on the Moon. While attention would initially focus on transporting organisms for food production, such a colony would actually require a large "spaceship" containing a diversity of species capable of performing all the essential but

often overlooked life-support functions such as pollination, nutrient cycling, and decomposition that are usually taken for granted on Earth.

In the same year, Costanza et al. (1997) characterized ecosystem services as the benefits that human populations derive, directly or indirectly, from ecosystem functions. They conceptualized these services as flows of materials, energy, and information generated by stocks of natural capital. Costanza et al. (1997) also explored methodologies for estimating the economic value of ecosystem services.

By 2002, de Groot et al. (2002) further emphasized the anthropocentric dimension of the concept, arguing that ecosystem functions, defined as the capacity of natural processes and components to satisfy human needs, are only "reconceptualized" as goods or services when human values are explicitly accounted for. This reinforced the idea that ecosystem services are located at the interface between ecological functioning and human valuation.

## 1.2 Classification and assessment frameworks

A major milestone in the development of the ecosystem services concept was reached with the Millennium Ecosystem Assessment (MEA, 2005), which provided an internationally recognized synthesis. The MEA defined ecosystem services (ES) as the "benefits people obtain from ecosystems" and proposed a classification into four categories: provisioning, regulating, supporting, and cultural services (Figure 1). This classification also highlighted the links between ecosystem services and human well-being, including security, basic material needs, health, and social relations.

However, in order to support the assessment, standardization, and integration of ecosystem services into environmental accounting frameworks, the European Environment Agency introduced the Common International Classification of Ecosystem Services (CICES) in 2013 (Haines-Young and Potschin, 2013). A key feature of this classification is its focus on final ecosystem services. Supporting services, such as primary production, nutrient cycling, or soil formation, are no longer treated as a separate category, in order to avoid double counting in economic valuation exercises.

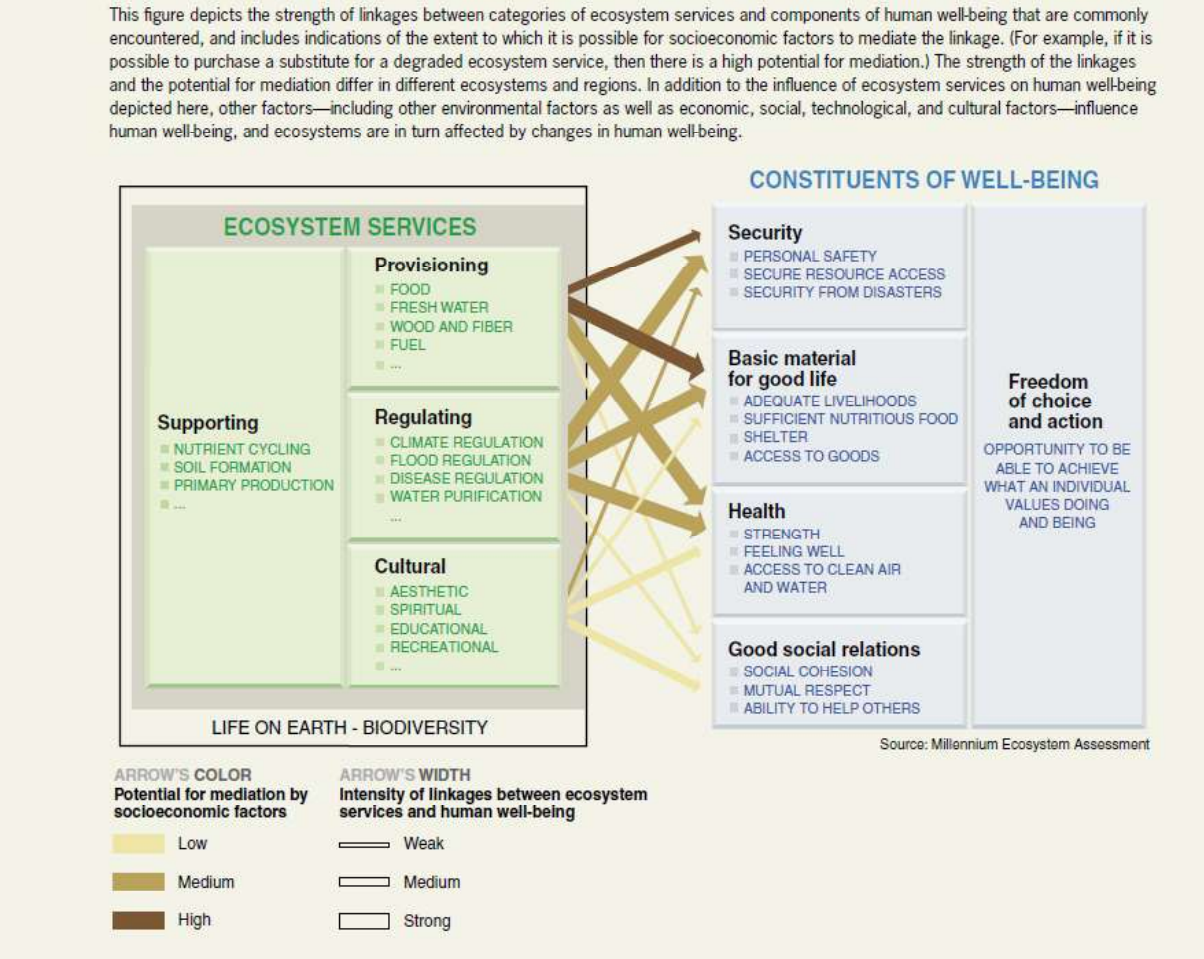


**Figure 1:** Illustration of linkages between Ecosystem Services and human well-being (Millenium Ecosystem assessment, 2005).

CICES version 4.3 was updated in 2018 with the release of CICES 5.1 (Haines-Young and Potschin, 2018), with the objective of improving scientific rigor and enhancing accessibility for non-expert users. This revision also expanded the definition of ecosystem services to include abiotic services. The classification is structured around a cascade model distinguishing: (i) ecological structures and functions, describing what ecosystems do, such as growth processes, nutrient uptake, and photosynthesis; (ii) final services, representing the direct contributions provided by ecosystems, such as standing timber volume; and (iii) benefits and well-being outcomes, such as processed wood products or recreational enjoyment (Figure 2).

More recently, in 2023, CICES was further updated to version 5.2 (Haines-Young, 2023), incorporating feedback from applications since 2018 and aligning more closely with international environmental accounting standards, particularly the United Nations System of Environmental-Economic Accounting - Ecosystem Accounting (SEEA EA), which serves as the United Nations counterpart to CICES. In this updated framework, services previously

referred to as “biotic” are now termed biophysical ecosystem services, reflecting their dependence on interactions between biotic and abiotic processes. Similarly, outputs previously described as “abiotic” are now classified as geophysical services (e.g., wind, minerals, solar energy).

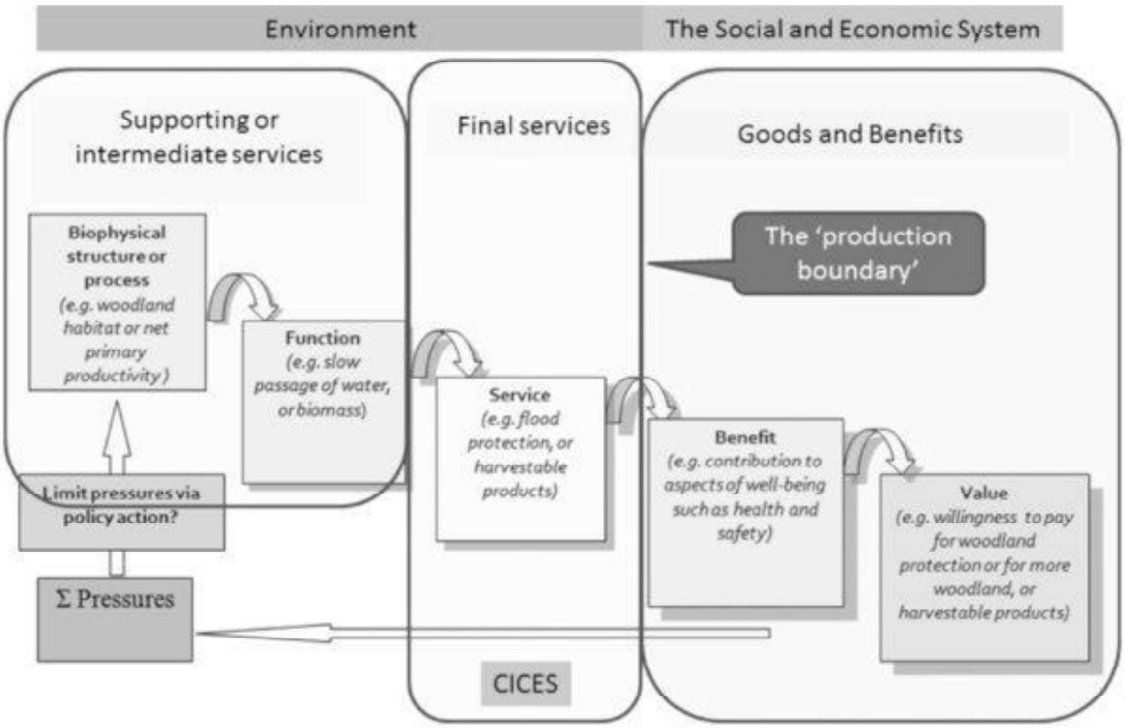


**Figure 2:** The cascade model for structuration of ecosystem services (Haines-Young and Potschin, 2018).

More recently, in 2023, CICES was further updated to version 5.2 (Haines-Young, 2023), incorporating feedback from applications since 2018 and aligning more closely with international environmental accounting standards, particularly the United Nations System of Environmental-Economic Accounting - Ecosystem Accounting (SEEA EA), which serves as the United Nations counterpart to CICES. In this updated framework, services previously referred to as “biotic” are now termed biophysical ecosystem services, reflecting their dependence on interactions between biotic and abiotic processes. Similarly, outputs previously described as “abiotic” are now classified as geophysical services (e.g., wind, minerals, solar energy).

Within this framework, ecosystem services are defined as the contributions that ecosystems make to human well-being, as distinct from the goods and benefits that people subsequently derive. In other words, the service corresponds to the active contribution of nature, whereas the benefit represents the value, often expressed in monetary or health terms, generated once

humans have interacted with or transformed that service. Examples of ecosystem services within this framework are presented in Table 1.

**Table 1:** Example of ecosystem services, by service type (from Haines-Young and Potschin, 2018).

| Service Type | Examples of Final Ecosystem Services |
|---|---|
| Provisioning | Cultivated terrestrial plants (including fungi, algae) grown for nutritional purposes. |
| | Fibers and other materials from cultivated plants, fungi, algae, and bacteria. |
| | Cultivated plants (including miscanthus) grown as a source of energy. |
| | Reared animals and their outputs providing nutrition. |
| | Wild animals (terrestrial and aquatic) harvested for nutrition. |
| | Genetic material from all biota harvested for breeding or biotechnology. |
| | Surface and ground water used for drinking. |
| | Surface water used for navigation, transportation, or as a material. |
| | Use of ice or snow as a means of transport. |
| Regulation & Maintenance | Bio-remediation of wastes or toxic substances by microorganisms, algae, or plants. |
| | Filtration, sequestration, or storage of pollutants by living systems. |
| | Mediation of smell, noise, or visual impacts through vegetation structure. |
| | Control of water erosion rates and stabilization of soils by root systems. |
| | Control of wind erosion rates by vegetation. |
| | Hydrological cycle and water flow regulation, including natural drainage. |
| | Surge and flood wave mitigation provided by living structures (*e.g.*, mangroves). |
| | Pollination of crops and wild plant species. |
| | Seed dispersal by animal agents or wind. |
| | Maintaining or regulating nursery populations and habitats. |
| | Maintaining or regulating refuge habitats or feeding grounds. |
| | Natural pest control and reduction of diseases through biological interactions. |
| | Maintenance of soil structure and resistance to compaction by biological agents. |
| | Regulation of the chemical composition of the atmosphere (including greenhouse gases). |
| | Local regulation of temperature and humidity through ventilation and transpiration. |
| Cultural | Active or immersive physical interactions with nature (*e.g.*, hiking, angling). |
| | Passive or observational interactions allowing enjoyment of scenery. |
| | Characteristics of living systems enabling scientific investigation. |
| | Elements of nature that support the creation of traditional ecological knowledge. |
| | Educational opportunities and training provided by environmental settings. |
| | Ecosystem features with cultural or heritage resonance. |
| | Aesthetic experiences enabled by specific landscape features. |
| | Elements of living systems that have symbolic meaning or provide a sense of place. |
| | Elements of nature that have sacred or religious meaning. |

| | |
|---|---|
| | Characteristics of species or ecosystems used for entertainment or representation.<br>Features of living systems valued for their contemporary existence.<br>Features of nature valued for preservation for future generations (bequest value). |

# 2. Ecosystem services in agricultural systems

## 2.1 Provisioning and regulating services in agriculture

Ecosystem services associated with agricultural systems hold particular importance because agriculture represents one of the dominant global land uses, currently occupying close to 40 percent of the Earth's terrestrial surface (FAO, 2025). As such, agriculture plays a central role in the supply of provisioning ecosystem services, most notably through the production of cultivated biomass for human food, animal feed, fiber, bioenergy, and a variety of pharmaceutical and industrial products (Power, 2010; Gaba et al., 2015; Huang et al., 2015). Beyond these material outputs, agricultural ecosystems contribute substantially to regulating and supporting (maintenance) services (Power, 2010), which are fundamental for both environmental sustainability and the long-term functioning of agricultural production itself.

Among these regulating services, the regulation of water quality is particularly critical. Agricultural systems influence the attenuation of diffuse pollution originating from nutrients, sediments, and pesticides, thereby affecting downstream aquatic ecosystems, drinking water security, and human health. Other essential regulating services include erosion control through soil stabilization and carbon sequestration, thereby contributing to climate regulation *via* increases in soil organic matter and crop photosynthesis (Power, 2010). Supporting services, such as soil fertility and the preservation of soil structure, are equally fundamental, as they underpin nutrient uptake by crops and water retention within agroecosystems (Power, 2010). Thus, agricultural landscapes are not only sites of biomass production but are also multifunctional ecosystems whose management strongly determines their capacity to support broader environmental and societal benefits.

## 2.2 Water catchment areas as an example of endangered environments

Water catchment areas illustrate particularly well how agricultural systems can endanger or preserve essential ecosystem services. In France, drinking water catchment zones have been increasingly affected by nitrate and pesticide contamination, leading to the closure of 7,716

catchments between 1994 and 2013, with 39 percent of closures directly attributed to these pollutants (https://aires-captages.fr/livre-enrichi). Because identifying new uncontaminated groundwater resources is increasingly difficult, France has designated "priority water catchment areas" where water quality is already degraded and requires urgent protection (Grenelle de l'Environnement, 2009; Environmental Conference, 2013).

To address this challenge, a range of Best Management Practices (BMPs) have been implemented worldwide and nationally, including improved nitrogen fertilization management, establishment of cover crops, vegetative buffer strips, adjusted crop rotations, and in some contexts reforestation (López-Ballesteros et al., 2023). Studies in northern France demonstrated that organic systems applied 12 percent less nitrogen compared with conventional systems (Anglade et al., 2015), while combined fertilization management and catch crop use contributed to reduced nitrate concentrations at the catchment scale (Beaudoin et al., 2021). However, BMP efficiency is often scale-dependent and influenced by soil type, hydrology, tile drainage, and interannual climate variability (Merriman et al., 2018), which can limit the consistency of nitrate reduction outcomes across sites.

In this context, perennial crops such as miscanthus have recently been proposed as an additional BMP option for water protection areas (Weik et al., 2022). Their potential contribution to reducing diffuse pollution and mitigating pressures on drinking water resources makes them particularly relevant in priority catchments, where there is a need to combine agricultural production with long-term protection of water quality.

## 2.3 Trade-offs and synergies among ecosystem services

Analyses of ecosystem service provision in agricultural landscapes consistently reveal trade-offs among services. In their review, Zheng et al. (2019) showed that in 80% of the 70 case studies analyzed, trade-offs occurred primarily between provisioning services and regulating or biodiversity-related services. The underlying mechanisms identified include land-use change (particularly conversion to cropland), increasing pressure to maximize resource extraction (*e.g.*, food, timber, biofuels), and management practices, such as fertilizer application, which enhance yields but degrade water quality.

Similarly, the study by Syswerda and Robertson (2014), conducted in Michigan (USA), examined how agricultural management intensity influences the provision of multiple

ecosystem services. Using a management gradient ranging from intensively managed annual crops to perennial systems and unmanaged forest communities, the authors assessed eight ecosystem service indicators spanning provisioning and regulating services. Their results revealed, for example, a clear trade-off between crop yield and nitrate leaching, with conventional cropping systems exhibiting nitrate leaching rates nearly 600 times higher than those observed in poplar plantations (62 vs. 0.1 kg N $ha^{-1}$ $yr^{-1}$).

Such evidence confirms that achieving food and biomass provision often incurs environmental costs, and that agricultural management choices largely determine whether landscapes generate trade-offs or synergies. However, appropriately designed systems can create synergies, particularly when perennial crops, reduced-input management, or diversified systems are implemented. Identifying production systems capable of maintaining yields while protecting water and soil therefore represents a key strategic objective for sustainable agriculture, particularly in environmentally sensitive areas such as water catchments.

## 2.4 Perennial biomass crops as an option for balancing production with other ecosystem services

In this context, perennial biomass crops have attracted increasing interest as promising systems capable of reconciling production with environmental sustainability. Among these, miscanthus has received particular attention. Tavakoli-Hashjini et al. (2020) compared miscanthus with maize and demonstrated that miscanthus maintained or exceeded biomass production while supporting multiple ecosystem services, including greenhouse gas regulation through carbon sequestration, improved water quality due to its deep root system, support for biodiversity, and socio-economic benefits linked to low labor requirements (Figure 3).

These characteristics position perennial biomass crops, particularly miscanthus, as strategic options for regions where both production and environmental regulation must be ensured. Their demonstrated potential to support water quality protection, climate mitigation, and soil sustainability strengthens their relevance in landscapes where ecosystem services must be restored without compromising agricultural productivity.

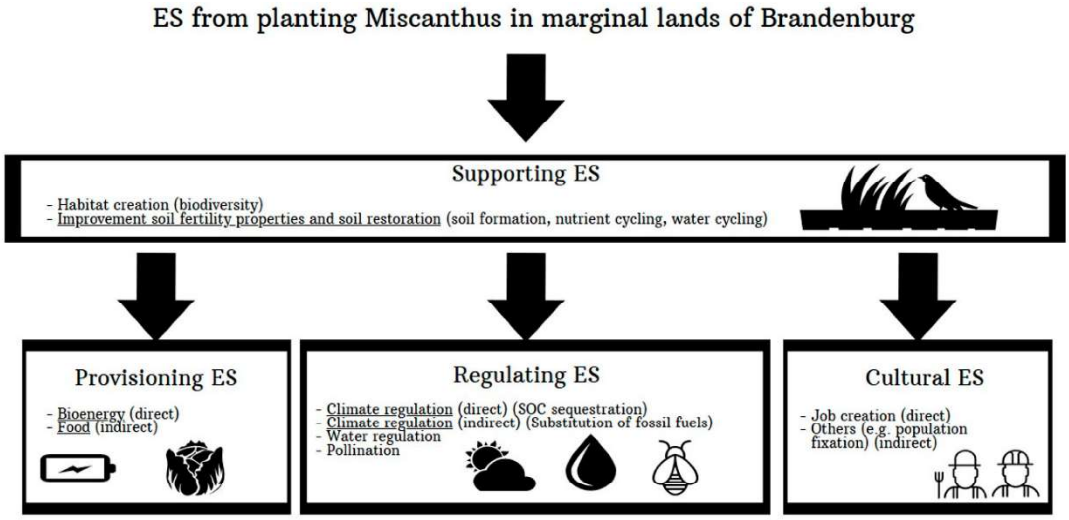


**Figure 3:** Scheme of the ecosystem services delivered after planting miscanthus for bioenergy in marginal lands in Brandenburg (Tavakoli-Hashjini et al., 2020). Underlined ecosystem services refer to those that were specifically estimated in their study, whereas non-underlined services correspond to services identified but not quantified because of insufficient scientific knowledge or because they were outside the study scope.

# 3. Miscanthus: a perennial crop as a solution

## 3.1 General presentation

Miscanthus has emerged over recent decades as one of the most promising biomass crops due to its rapid growth, high productivity, resilience, and adaptability. The *Miscanthus* genus consists of C4 perennial rhizomatous grasses native to tropical and subtropical regions of East Asia (Lewandowski et al., 2000; Hastings et al., 2009). Although its origin lies in East Asia, the development of miscanthus as an energy crop progressed earlier and more extensively in Europe and the United States. To date, a single sterile clone of *Miscanthus* × *giganteus*, a natural hybrid between *M. sacchariflorus* and *M. sinensis*, remains the most widely cultivated material (Clifton-brown et al., 2004). This hybrid, originally introduced to Europe from Japan in 1935 for ornamental purposes (Linde-Laursen, 1993), rapidly attracted agronomic interest due to its high yield potential, low fertilizer requirement, and capacity to contribute to carbon sequestration (Lewandowski et al., 2003).

Miscanthus is a perennial crop established for long-term cultivation (Gauder et al., 2012) and characterized by a rhizome system that stores nutrients (Beale & Long, 1997). The crop is generally harvested once a year in late winter, after senescence, which facilitates nutrient translocation from aboveground parts to belowground parts and supports spring regrowth. The plant nitrogen economy, defined by the internal cycling of nitrogen and uptake of nitrogen from

the soil together (Leroy et al., 2022), is central to sustaining biomass production while reducing environmental impacts in miscanthus systems.

The cultivation system associated with miscanthus further enhances its ecosystem relevance. As a perennial crop, it requires minimal soil disturbance and maintains continuous soil cover, while long-term cultivation promotes organic matter accumulation through sustained increases in soil organic carbon stocks (Ferchaud et al., 2025). These characteristics explain why miscanthus has increasingly been evaluated not only for biomass supply but also for its potential to contribute to climate regulation, water quality protection, erosion control, and biodiversity support (McCalmont et al., 2017; Tavakoli-Hashjini et al., 2020).

## 3.2 Strength of miscanthus crop

Miscanthus exhibits several agronomic and environmental strengths that explain its status as a key bioenergy crop.

**High biomass productivity**

Miscanthus can produce large quantities of lignocellulosic biomass under temperate conditions (Lewandowski et al., 2000; Arnoult & Brancourt-Hulmel, 2015; Lesur-Dumoulin et al., 2016). The exceptional productivity of *M.* × *giganteus* is largely attributed to its efficient use of radiation, water, and nitrogen for biomass production, supported by its C4 photosynthetic pathway and perennial rhizome system as reviewed by (Zub & Brancourt-Hulmel, 2010).

**Low nitrogen requirements and efficient internal nitrogen recycling**

Miscanthus has low nitrogen fertilizer requirements, reflecting both intrinsically low nitrogen needs and an efficient internal nitrogen recycling. At the physiological level, its nitrogen demand is lower than that of annual crops, as shown by a critical nitrogen dilution curve that lies below that of maize, indicating that less nitrogen is required to produce a given amount of biomass (Zapater et al., 2017). In addition, miscanthus is characterized by an efficient internal nitrogen recycling system. The rhizome serves as a perennial storage organ, and nitrogen present in aboveground parts during autumn is remobilized to belowground parts and subsequently remobilized again in spring to support new growth (Beale & Long, 1997; Himken et al., 1997; Strullu et al., 2011; Leroy et al., 2022).

This internal nitrogen economy has direct environmental implications. Under miscanthus, nitrate leaching is significantly lower than under annual crops, with residual soil nitrate at the end of winter often below 20 kg N $ha^{-1}$, compared with much higher values recorded under triticale, sorghum, or fescue (Ferchaud & Mary, 2016). Furthermore, nitrous oxide emissions are reported to be 5 to 100 times lower than those from intensive cropping systems (McCalmont et al., 2017). Miscanthus also contributes to carbon sequestration, with reported increases between 0.4 and 3.8 t C $ha^{-1}$ $yr^{-1}$ depending on site and methodology (Poeplau & Don, 2014; Ferchaud & Mary, 2016; McCalmont et al., 2017; Ferchaud et al., 2025).

**Provision of multiple regulating services**

Beyond nutrient cycling, miscanthus supports a wide range of regulating ecosystem services. Permanent soil cover and dense root systems play a key role in preventing soil erosion and enhancing soil structure (Saunier et al., 2013, Saunier et al., 2018; Holder et al., 2019; Von Cossel et al., 2020; Mazur & Kowalczyk-Juśko, 2021). Improved soil structure also contributes to better hydrological regulation at the scale of water bodies and catchments (Saunier et al., 2018; Holder et al., 2019). Water quality protection is further enhanced through reduced fertilizer requirements, enhanced nitrogen capture and reduced nitrate leaching (Lesur et al., 2014; Ferchaud & Mary, 2016; Holder et al., 2019; Von Cossel et al., 2019; Von Cossel et al., 2020; Weik et al., 2022). Miscanthus also contributes to the maintenance of soil quality, through limited nutrient export, stimulation of soil biological activity, and reduced machinery traffic, which limits compaction (Fernando et al., 2010; Dufosse et al., 2014; Lovett et al., 2015; McCalmont et al., 2017; Von Cossel et al., 2019; Tavakoli-Hashjini et al., 2020). Climate regulation benefits arise from leaf litter return and carbon accumulation within the rhizosphere, which contributes to long-term storage (Dufossé et al., 2014; Lovett et al., 2015; Von Cossel et al., 2019; Weik et al., 2022).

**Biodiversity support and landscape functions**

Miscanthus fields provide habitat opportunities due to the absence of tillage, limited machinery traffic, and low pesticide use (Dauber & Miyake, 2016; Brami et al., 2020; Lask et al., 2020). They also offer refuge and resources for beneficial organisms involved in pest and disease regulation, while the permanent canopy can act as a physical barrier between neighboring fields (Fernando et al., 2010; Lovett et al., 2015; Lask et al., 2020). The crop structure can further function as a windbreak (Littlejohn et al., 2019; Von Cossel et al., 2020).

**Cultural ecosystem services**

Miscanthus landscapes can also contribute to cultural services, including aesthetic appreciation and recreational value associated with tall perennial vegetation structures (Von Cossel et al., 2020).

**Phytoremediation potential**

Miscanthus can additionally participate in the stabilization of contaminants, particularly trace metals in polluted soils (Fernando et al., 2010; Laval-Gilly et al., 2017; Brami et al., 2020). Although biomass yield may decline under such conditions, stabilization and limitation of pollutant dispersion represent valuable ecosystem services. As noted by Fradj et al. (2020), ecosystems cannot maximize all ecosystem services simultaneously, and trade-offs must be recognized.

Altogether, these attributes position miscanthus as a perennial crop capable of simultaneously supplying biomass while supporting key regulating ecosystem services, particularly when nitrogen recycling and low-input management are central objectives.

## 3.3 Current deployment and strategic target areas for miscanthus

The recent expansion of miscanthus cultivation illustrates its growing importance as a biomass crop delivering both production and environmental services. In France, cultivated areas have increased rapidly in recent years, reaching approximately 11,459 ha in 2024, with the national area having doubled since 2017 (France Miscanthus, 2024). As shown in Figure 4, nearly 85 percent of miscanthus fields are located in the northern half of the country, particularly in Pays de la Loire (2,665 ha), Normandy (1,523 ha), Centre-Val de Loire (1,305 ha), and Hauts-de-France (1,360 ha) (France Miscanthus, 2024). This pattern reflects both favorable agronomic conditions and the growing interest of local authorities and farmers in low-input perennial crops.

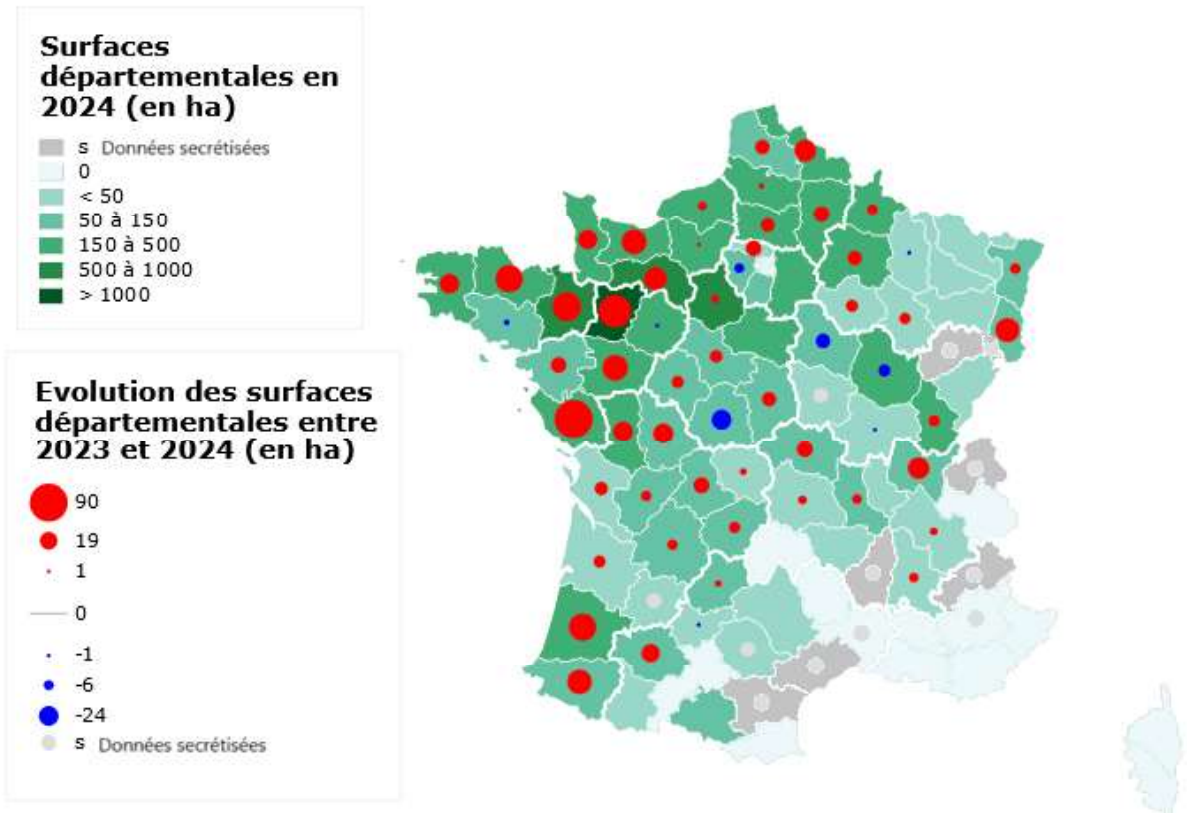


**Figure 4.** Departmental distribution and evolution of miscanthus cultivation areas in France in 2024 (Source: France Miscanthus, 2024).

Beyond its national expansion, miscanthus is increasingly considered as a targeted option for environmentally sensitive territories, particularly water catchment areas. Within the French MisTigation project (Brancourt-Hulmel et al., 2026), 74 percent of agricultural soils in Hauts-de-France were identified as favorable to miscanthus cultivation (Figure 5), representing approximately 1,784,000 ha. Among water catchment recharge areas, 47 percent of the total surface and 58 percent of priority catchments correspond to soils highly suitable for miscanthus, *i.e.* 217,378 ha of favorable soils in priority protection zones. On the most vulnerable soils of these surfaces, miscanthus can simultaneously deliver two key ecosystem services: protection of drinking water quality and biomass production, making it a particularly relevant option where production and regulation objectives must be combined.

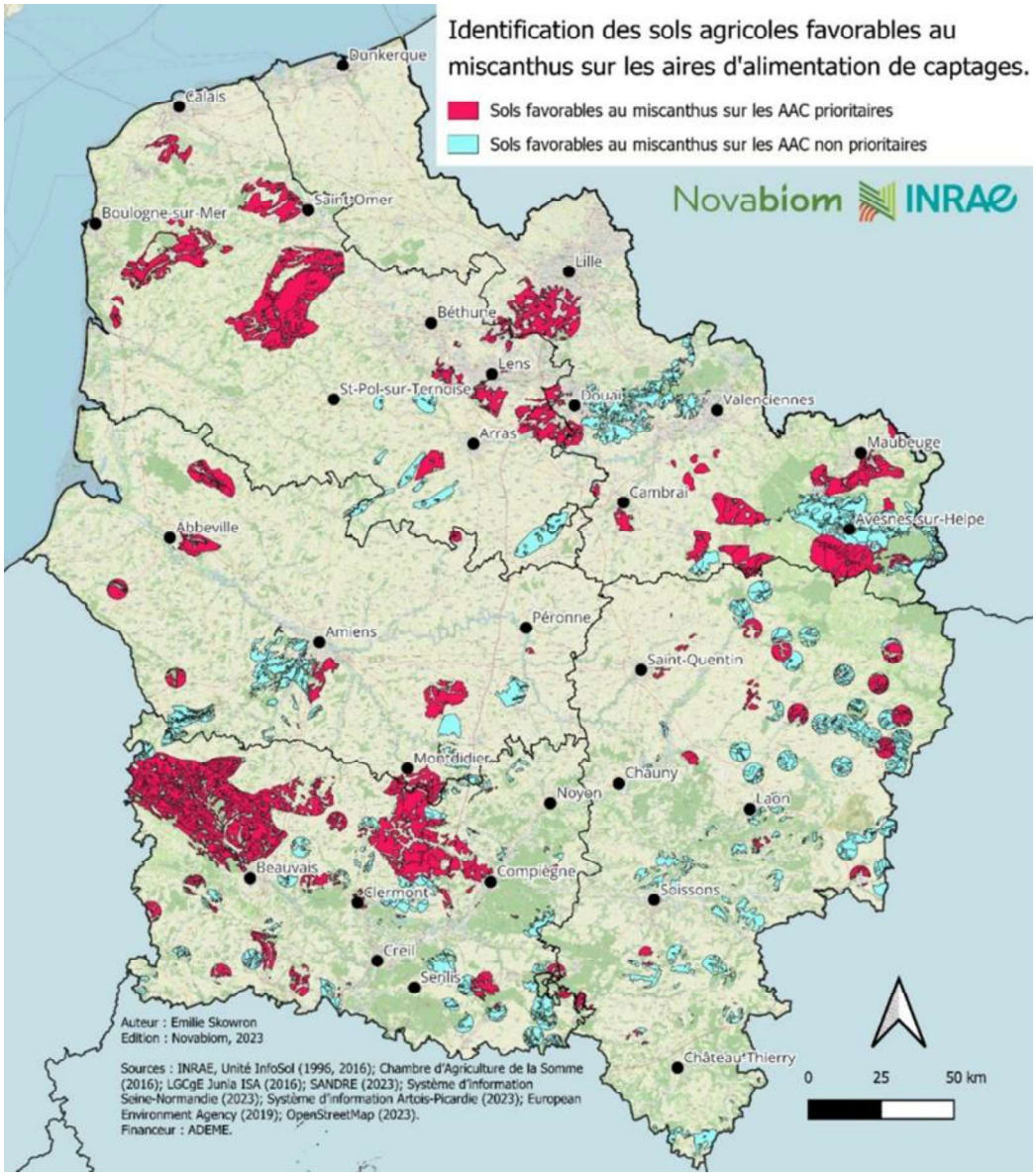


**Figure 5.** Identification of agricultural soils suitable for miscanthus within water catchment recharge areas in Hauts-de-France in the frame of the MisTigation project (from Skowron in Brancourt-Hulmel et al., 2026; ADEME project page: https://recherche.ademe.fr/mistigation-miscanthus-et-services-ecosystemiques-pour-les-collectivites-locales).

At present, however, field deployment relies almost exclusively on a single sterile triploid clone of *Miscanthus* × *giganteus* (Clifton-brown et al., 2004; Brancourt-Hulmel & Höfte, 2022). As cultivation continues to expand and as miscanthus is increasingly promoted in environmental strategic areas such as water catchments, there is a growing need to broaden the varietal offer, in order to secure long-term resilience and better adapt the crop to diverse environments and uses. In this context, broadening the varietal offer becomes essential, and *Miscanthus sinensis* represents a particularly promising source of genetic diversity.

# 4. Miscanthus genetic diversity and traits studied in genetics

## 4.1 *M. sinensis* is the preferred solution for expanding genetic diversity

The reliance of the miscanthus crop on a single genetic background causes several weaknesses: (1) due to the lack of genetic diversity, an increase of the risk of susceptibility to pests and diseases (Greef et al., 1997; Zub and Brancourt-Hulmel, 2010) and a limitation to meet the requirements of different end-uses due to a unique quality (Clifton-Brown et al., 2001; Arnoult and Brancourt-Hulmel, 2015); (2) a low tolerance of the rhizome to frost, leading sometimes to plant death during the first winter after establishment, as well as low biomass yields in cool climates (Jones and Walsh, 2001; Zub et al., 2012); (3) high costs for vegetative propagation and establishment of the crop compared with seed propagation (Clifton-Brown and Lewandowski, 2002). To face this problem, the genetic diversity can be broadened by crossing different *M. sacchariflorus* and *M. sinensis* or by collecting allotriploid seeds from parental sympatric populations (Glowacka et al., 2015; Uwatoko et al., 2016). Breeding within the species *M. sinensis* and *M. sacchariflorus* is also a solution for broadening the genetic base of these parents, which would be beneficial for the offspring of *M.* × *giganteus* (Glowacka, 2011).

In the coming years, more *M.* × *giganteus* cultivars will be made available to farmers: either sterile triploid clones propagated vegetatively to avoid any risk of invasiveness, or diploid or tetraploid seed-propagated cultivars, with late flowering to reduce seed dispersal into the environment. Such late fertile genotypes are favored in Wales while infertile hybrids are preferred in the United States (Clifton-Brown et al., 2018). Sterility is also favored for creating new varieties in France (Brancourt-Hulmel, 2022), due to strong social demand to prevent invasive species.

However, it is difficult to synchronize flowering between the two species: *M. sinensis* is fairly neutral in terms of day length and generally flowers in Northern Europe (Głowacka, 2011; Jensen et al., 2011), while *M. sacchariflorus* is sensitive to day length and requires warmer climates to flower before winter (Głowacka, 2011; Jensen et al., 2013). As a result, very few accessions of *M. sacchariflorus* flower, even in heated greenhouses (Clifton-Brown et al., 2018), which explains why European programs in the UK, the Netherlands, and France have mainly carried out (intraspecific) hybridizations of *M. sinensis* (Clifton-Brown et al., 2018). The domestication of *M. sinensis* as a crop is therefore fairly recent.

## 4.2 Genetic diversity of *Miscanthus sinensis*

*M. sinensis* exhibits very high natural genetic diversity compared to *M.* × *giganteus* (Greef et al., 1997; Glowacka et al., 2015). Wild populations are mainly found in China, Japan, and Korea and show diverse characteristics in terms of phenological, morphological, and agronomic traits (Sun et al., 2010; Xu et al., 2013; Anzoua et al., 2015).

From Asia, miscanthus migrated to other parts of the world as evidenced by Clark et al. (2014). They studied 767 accessions, including 617 *Miscanthus sinensis* from most of its native range in China, Japan and South Korea, 77 ornamental cultivars and 43 naturalized individuals from the USA. They detected six genetic groups from geographically distinct regions of Asia. Their genetic data evidence that southeastern China is the origin of the *M. sinensis* diversity found in eastern Asia. *M. sinensis* migrated directly from this original point to Japan, Korea and other similar latitudes in China. Then, ornamental *M. sinensis* cultivars were derived from a population located in South Japan and naturalized populations in the United States derive from a subset of ornamental cultivars (Clark et al., 2014).

In China, Zhao et al. (2013) collected 459 *M. sinensis* accessions, from the wide geographical distribution regions of the country and highlighted the genetic differentiation in the *M. sinensis* germplasm into five groups. They also observed significant genetic variation among subpopulations, indicating clear genetic differentiation within the collections, but within-subpopulation variation (83%) was substantially greater than the between-subpopulation variation (17%). This phenomenon appears to be common, as wild populations of *M. sinensis* from southwestern China studied by Xu et al. (2013) also revealed greater genetic diversity within each population than between populations.

## 4.3 Phenotypic and genotypic variability of traits of interest

The study of phenotypic and genotypic variability related to traits of interest is very important for determining the degree of variability available in the species evaluated (Arnoult and Brancourt-Hulmel, 2015). The traits related to biomass production, phenological traits, and traits related to composition are the most studied. Bringing together global references, the review by Arnoult and Brancourt-Hulmel (2015) shows high genotypic and environmental variability for traits related to the aboveground biomass production and composition of miscanthus biomass. While aboveground biomass production has been extensively studied,

phenotypic variability has rarely been documented for belowground biomass production. Leroy et al. (2022) are an exception, but with a limited number of genotypes. This lack of knowledge may be due to the complexity of the phenotyping: traits related to the belowground and nitrogen fluxes between the above and the belowground parts of the plants are not easy to measure.

## 4.4 Genetic determinism: heritability and QTL

A variety of studies have estimated broad-sense heritability of *Miscanthus sinensis* for a diversity of traits as shown by Table 2. Broad-sense heritability defines the proportion of the phenotypic variance of a trait that is due to genetic factors, *i.e.* genetic variance (Falconer, 1981). These traits are related to aboveground biomass production (Slavov et al., 2013; Gifford et al., 2015; Clark et al., 2016; Nie et al., 2016; Dong et al., 2018; Clark et al., 2019; Raverdy et al., 2022), its composition or quality (Slavov et al., 2013; Van der Weijde et al., 2017; Raverdy et al., 2022) as well as flowering time (Hou et al., 2022). These studies are fairly recent, highlighting the recent domestication of miscanthus.

This Table 2 clearly illustrates the lack of knowledge about belowground biomass as well as traits related to the nitrogen economy, such as nitrogen uptake, and spring and autumn remobilizations. Nitrogen quantities and concentrations have not yet been studied either.

At the chromosome level, the basic chromosome number of miscanthus is 19 and almost double that of sorghum, which is 10. The *Miscanthus sinensis* genome sequence has been released (Mitros et al. 2020) and represents a powerful tool for comparative genomics. Comparative analysis of the sequenced genomes of *M. sinensis* and sorghum shows that each chromosome of sorghum aligns with a pair of chromosomes of *M. sinensis*, with the exception of one chromosome of miscanthus, which corresponds to the fusion of two chromosomes of sorghum (Mitros et al., 2020). This reference genome is also an interesting tool for aligning genetic maps, as done by Raverdy et al. (2022) and Hou et al. (2022) while earlier studies aligned their map on the reference genome of sorghum.

Regarding QTL detection, all the previous studies have also enabled the detection of QTLs (Table 3), which can be very numerous for certain traits: 20 to 288 for traits related to aboveground biomass production (Slavov et al, 2013; Gifford et al, 2015; Nie et al, 2016; Clark et al, 2016; Dong et al, 2018; Clark et al, 2019 and Raverdy et al, 2022), less than 10 to 283 for traits related to composition and quality (Atienza et al, 2003a,b,c,d; Van der Weijde et al, 2017;

Raverdy et al; 2022) and 24 to 59 QTL for traits related to the flowering time (Jensen et al, 2020; Hou et al, 2022).

**Table 2:** Summary of the studies that estimated broad-sense heritability values of miscanthus biomass production or composition traits (adapted and updated from Raverdy, 2021).

| Publication | Genetic material | Species | Number of locations | Number of Years | Biomass trait type |
|---|---|---|---|---|---|
| Slavov et al (2013a; 2013b) | 244 genotypes *(including a population of 145 M. sinensis)* | *M. sinensis* *M. sacchariflorus* *M. × giganteus* | 1 (Wales) | 3 (2-4 yrs after establisment) | **Aboveground production** Composition |
| Gifford et al (2015) | 221 F1 progenies | *M. sinensis* | 1 (USA) | 2 (yrs 2 and 3 after establishment) | **Aboveground production** |
| Nie et al (2016) | 138 individuals (accessions) | *M. sinensis* | 1 (China) *Individuals collected in Southwest China* | 3 (2-4 yrs after establishment) | **Aboveground production** |
| Clark et al (2016) | 174 clonal germplasm accessions | *M. sacchariflorus* *M. sinensis* | 47 collection sites (eastern Russia) | 1 | **Aboveground production** |
| Van der Weijde et al (2017c) | 182 F1 progenies | *M. sinensis* | 1 (Netherlands) | 2 (yrs 2 and 3 after establishment) | Composition and quality |
| Dong et al (2018) | 3 F1 populations: 281, 243 and 128 progenies | *M. sinensis* *M. sacchariflorus* | 1 (USA) | 2 (yrs 2 and 3 after establishment) | **Aboveground production** |
| Clark et al (2019) | 589 accessions | *M. sinensis* *M. sacchariflorus* *M. × giganteus* | 6 (China, Japan, Canada, USA, South Korea) | 2 (yrs 2 and 3 after establishment) | **Aboveground production** |
| Hou et al (2022) | 159 F1 progeny | *M. sinensis* | 1 (France) | 2 + 2 (staggered-start design / yrs 4 to 5 after establishment) | Flowering time |
| Raverdy et al (2022) | 159 F1 progeny | *M. sinensis* | 2 (France) | 4 + 3 (staggered-start design / yrs 1 to 4 after establishment) | **Aboveground production** Composition |

As with heritability, belowground biomass and nitrogen-related traits have not yet been studied for QTL detection.

**Table 3:** Summary of the studies that carried out QTL mapping for miscanthus aboveground biomass production or composition traits, from biparental populations (adapted and updated from Raverdy et al, 2021). *SIN: M. sinensis; SACC: M. sacchariflorus; FLO: M. floridulus.*

| Publication | Genetic material | Number of locations | Number of Years | Genetic map used | Number of QTL and trait related-type |
|---|---|---|---|---|---|
| Atienza et al (2003 a,b,c,d) | 89 F1 SIN | 1 (Spain) | 2 | Atienza et al. (2002) | 20, 11, 9, 6 QTL: 2 papers for **Aboveground production** + 2 papers for **Combustion quality** |
| Gifford et al (2015) | 221 F1 SIN | 1 (USA) | 2 (yrs 2 to 3 after establishment) | Swaminathan et al. (2012) | 72 QTL **Aboveground production** |
| Van der Weijde et al (2017c) | 182 F1 SIN | 1 (Netherlands) | 2 (yrs 2 to 3 after establishment) | Van der Weijde et al. (2017c) | 86 QTL Composition and quality |
| Dong et al. (2018) | 3 F1 populations: 281 (SIN x SACC), 243 (SIN) and 128 (SIN) | 1 (USA) | 2 (yrs 2 to 3 after establishment) | Dong et al. (2018) | 288, 264, 133 and 109 QTL – 4 methods **Aboveground production** |
| Ge et al (2018) | 116 F1 (FLO x SACC) | 1 (China) | 4 (yrs 2 to 5 after establishment) | Ge et al. (2018) | 66 QTL **Plant height**, Heading time and Flowering time |
| Jensen et al (2020) | 216 F1 SIN | 1 (Wales, UK) | 3 (yrs 2 to 4 after establishment) | (Ma et al., 2012) | 24 QTL Flowering time |
| Hou et al (2022) | 159 F1 SIN | 1 (France) | 2 + 2 (staggered-start design / yrs 1 to 5 after establishment) | Raverdy et al (2022) | 59 QTL Flowering time |
| Raverdy et al (2022) | 159 F1 SIN | 2 (France) | 4 + 3 (staggered-start design / yrs 1 to 5 after establishment) | Map from the current paper | 260 QTL **Aboveground production** 283 QTL Composition |

## 5. Objectives of the thesis

Nitrogen economy is central to both biomass productivity and environmental performance in perennial grasses. However, in *Miscanthus sinensis*, the internal functioning, variability, predictability, and genetic control of key nitrogen processes, including nitrogen uptake, seasonal nitrogen remobilization, and nitrogen losses, have remained largely unresolved. The overarching objective of this thesis was therefore to establish nitrogen economy traits as measurable, predictable, and genetically selectable targets, in order to support the development of *M. sinensis* cultivars capable of sustaining biomass production while contributing to ecosystem service provision.

To address this overarching objective, the thesis was structured around one general experimental chapter and three interconnected results chapters, which together followed a logical progression from functional characterization among genotypes, through predictive application in breeding, to genetic targeting of nitrogen economy traits. The thesis concludes with a general discussion that integrates the main findings across chapters to further reflect on some of the key emerging questions, followed by the overall conclusion and perspectives. The specific aims of each results chapter are outlined below.

### Chapter 1 - Nitrogen Economy Strategies Define Distinct Functional Groups of Genotypes in a *Miscanthus sinensis* Progeny

The objective of chapter 1 was to characterize the functional diversity of nitrogen economy within a segregating diploid *M. sinensis* progeny grown under nitrogen-deficient field conditions. This chapter aimed to:

- quantify inter-genotypic variation in nitrogen uptake, spring and autumn remobilization, nitrogen losses and their efficiencies;
- determine whether this diversity reflects structured nitrogen-use strategies rather than random variability;
- evaluate whether genotypes segregate into different functional groups differing in their reliance on internal nitrogen recycling versus continuous nitrogen uptake.

Based on previous evidence of nitrogen recycling differences between genotypes (Leroy et al., 2022), we hypothesized that substantial intra-specific variation exists in nitrogen economy

traits and that this variation would organize into coherent nitrogen-use strategies. This chapter therefore provided the first intra-specific demonstration that nitrogen economy traits define different functional groups of genotypes in *M. sinensis*, laying the biological foundation for predictive and genetic analyses.

## Chapter 2 - Proxy Traits Help Breeders Predict Complex Nitrogen Economy Traits in a *Miscanthus sinensis* progeny

The objective of chapter 2 was to develop a non-destructive, scalable framework to estimate the complex nitrogen economy traits using simple measurable plant traits. This chapter aimed to:

- identify morphological, phenological and physiological traits capable of acting as proxies for nitrogen uptake, spring and autumn remobilization;
- evaluate whether statistical multivariate modelling, in particular Partial Least Squares regression (PLS), improves predictive accuracy compared with single-trait approaches;
- determine whether reduced, parsimonious predictor sets selected using Variable Importance in Projection (VIP) can retain high predictive power while simplifying phenotyping effort;
- assess how proxy-based models can support breeding decisions, particularly for counter-selection of poorly performing genotypes.

We hypothesized that accessible traits would show interpretable associations with nitrogen economy traits, that multivariate proxies would better capture their complexity than individual descriptors, and that simplified models would remain sufficiently predictive for breeder use. This chapter therefore established the first operational framework for predicting nitrogen economy traits in *M. sinensis* without plant destructive samplings.

## Chapter 3 - QTL Mapping Identifies Genomic Regions for Nitrogen Economy Traits in a Full-sib *Miscanthus sinensis* Progeny

The objective of chapter 3 was to translate nitrogen economy traits from physiological and predictive frameworks into genetically defined breeding targets. This chapter aimed to:

- identify QTLs controlling nitrogen uptake, spring and autumn remobilization traits, and nitrogen losses, thereby characterizing the genetic architecture of nitrogen economy traits;
- determine whether the proxy-nitrogen relationships highlighted in chapter 2 are genetically grounded through QTL co-location analyses;
- evaluate the breeding relevance of detected loci by quantifying allelic effects and exploring how QTL pyramiding could support the design of targeted ideotypes.

Based on the strong phenotypic variability observed and the structured relationships established in the previous chapters, we hypothesized that nitrogen economy traits would be controlled by multiple genomic regions rather than by single major loci. We further hypothesized that part of the proxy-target relationships identified in chapter 2 would reflect shared genomic determinism, meaning that at least some predictive traits and nitrogen economy traits would be influenced by overlapping QTL regions. By establishing these links, this chapter aimed to provide a genetically grounded framework supporting both the selection of targeted nitrogen-economy ideotypes and the potential combination of acquisition and recycling capacities through QTL pyramiding.

*Together, the three chapters establish a coherent progression: they first characterize how nitrogen economy traits vary and combine into different nitrogen-use strategies within a Miscanthus sinensis progeny, then develop predictive approaches using simple proxy traits to estimate these processes without plant destructive measurements, and finally identify the genomic regions involved in their control through QTL analyses. Taken together, this progression provides a functional, predictive, and genetic framework for mobilizing nitrogen economy traits in breeding, with the longer-term objective of developing M. sinensis cultivars capable of maintaining biomass production while contributing to the provision of other ecosystem services. The overall logic, structure, and complementarity of the chapters are synthesized in Figure 6.*

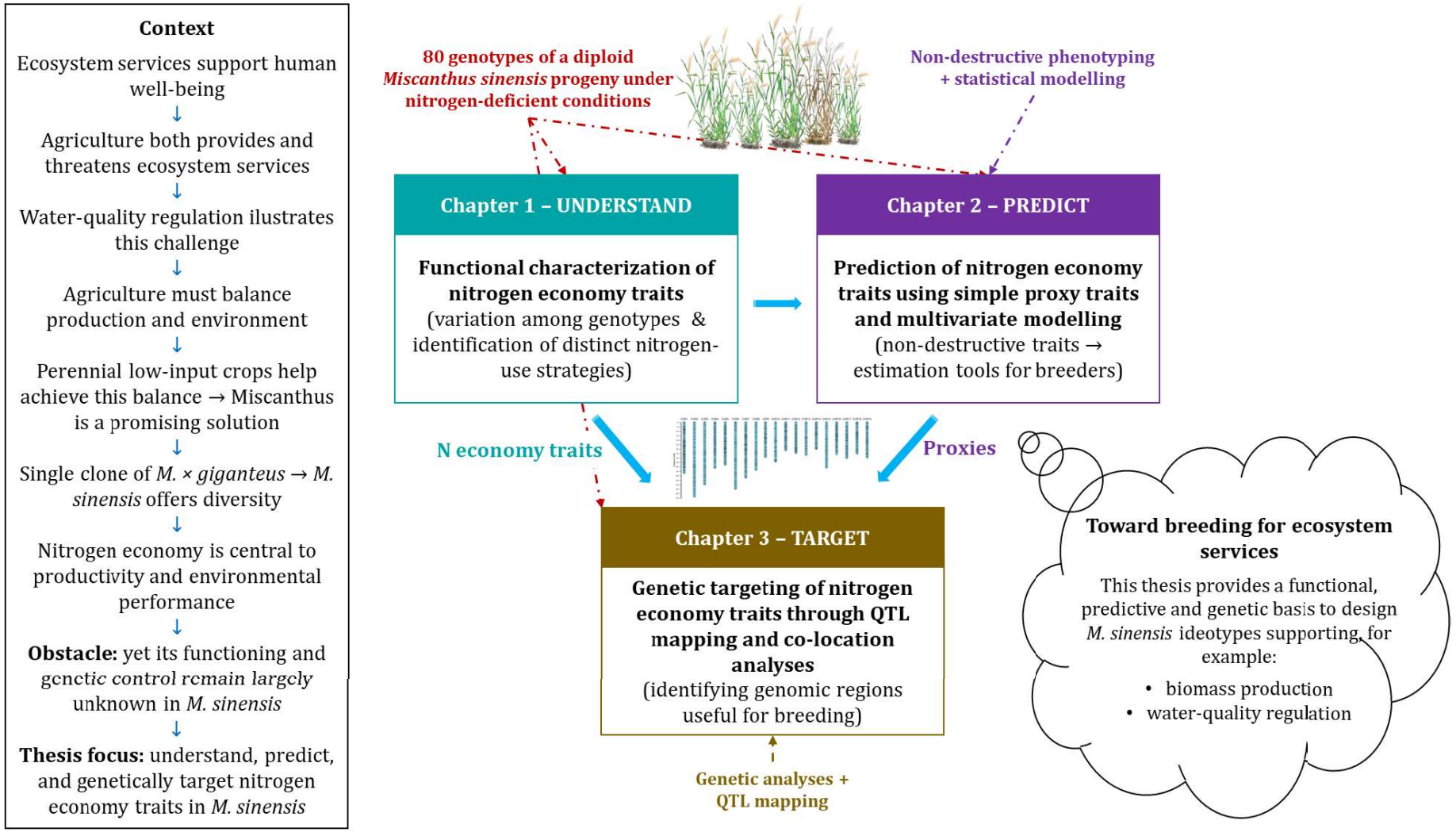


**Figure 6.** Overview diagram of the thesis structure. The diagram summarizes the scientific context, objectives, and organization of the three results chapters, illustrating how their components are interconnected within the overall thesis framework. Color coding indicates the elements associated with each results chapter.

## References

Anglade, J., Billen, G., Garnier, J., Makridis, T., Puech, T., & Tittel, C. (2015). Nitrogen soil surface balance of organic vs conventional cash crop farming in the Seine watershed. Agricultural Systems, 139, 82-92.

Anzoua, K.G., Suzuki, K., Fujita, S., Toma, Y., Yamada, T. (2015). Evaluation of morphological traits, winter survival and biomass potential in wild Japanese *Miscanthus sinensis* Anderss. populations in northern Japan. Grassland Science 61, 83–91. https://doi.org/10.1111/grs.12085

Arnoult, S., & Brancourt-Hulmel, M. (2015). A Review on Miscanthus Biomass Production and Composition for Bioenergy Use: Genotypic and Environmental Variability and Implications for Breeding. BioEnergy Research, 8(2), 502-526. https://doi.org/10.1007/s12155-014-9524-7

Beale, C., & Long, S. (1997). Seasonal dynamics of nutrient accumulation and partitioning in the perennial C4-grasses *Miscanthus* × *giganteus* and *Spartina cynosuroides*. Biomass and Bioenergy, 12(6), 419-428.

Beaudoin, N., Venet, E., Maucorps, J., Vandenberghe, C., Pugeaux, N., Viennot, P., Gourcy, L., Brayer, C., Machet, J.-M., & Couturier, A. (2021). Long term response of water and nitrogen fluxes to Good Agricultural Practices at field and catchment scales. Science of the Total Environment, 776, 145954.

Brami, C., Lowe, C. N., Menasseri, S., Jacquet, T., & Peres, G. (2020). Multi-parameter assessment of soil quality under *Miscanthus x giganteus* crop at marginal sites in Île-de-France. Biomass and bioenergy, 142, 105793.

Brancourt-Hulmel, M., & Höfte, H. (2022). Biomass for the Future: Miscanthus and Sorghum for New End-Uses in France. BioEnergy Research, 15(2), 669-671.

Brancourt-Hulmel, M. (2022). Miscanthus : une culture nouvelle en France. Les mots de l'agronomie - Histoire et critique, sous la direction de P. Morlon, INRAe-ACT.

Brancourt-Hulmel, M., Andre, A., Couprie, M., Desmyttere, H., Dutay, A., Griveau, Y., Heumez, M., Iqbal, S., Leemans, V., Longdoz, B., Monnot, S., Skowron, E., Wathy, C., & Zapater, M. (2025). Projet Mistigation: le miscanthus pour ses services écosystémiques à destination des collectivités locales. Rapport final. 52 pages.

Clifton-brown, J. C., Stampfl, P. F., & Jones, M. B. (2004). Miscanthus biomass production for energy in Europe and its potential contribution to decreasing fossil fuel carbon emissions. Global change biology, 10(4), 509-518.

Clifton-Brown, J., Harfouche, A., Casler, M.D., Dylan Jones, H., Macalpine, W.J., Murphy-Bokern, D., Smart, L.B., Adler, A., Ashman, C., Awty-Carroll, D., Bastien, C., Bopper,

S., Botnari, V., Brancourt-Hulmel, M., Chen, Z., Clark, L.V., Cosentino, S., Dalton, S., Davey, C., Dolstra, O., Donnison, I., Flavell, R., Greef, J., Hanley, S., Hastings, A., Hertzberg, M., Hsu, T.W., Huang, L.S., Iurato, A., Jensen, E., Jin, X., Jørgensen, U., Kiesel, A., Kim, D.S., Liu, J., McCalmont, J.P., McMahon, B.G., Mos, M., Robson, P., Sacks, E.J., Sandu, A., Scalici, G., Schwarz, K., Scordia, D., Shafiei, R., Shield, I., Slavov, G., Stanton, B.J., Swaminathan, K., Taylor, G., Torres, A.F., Trindade, L.M., Tschaplinski, T., Tuskan, G.A., Yamada, T., Yeon Yu, C., Zalesny, R.S., Zong, J., Lewandowski, I., (2018). Breeding progress and preparedness for mass-scale deployment of perennial lignocellulosic biomass crops switchgrass, miscanthus, willow and poplar. GCB Bioenergy 118–151. https://doi.org/10.1111/gcbb.12566

Clifton-Brown, J.C., Lewandowski, I., (2002). Screening miscanthus genotypes in field trials to optimise biomass yield and quality in southern germany. European Journal of Agronomy 16, 97–110. https://doi.org/10.1016/S1161-0301(01)00120-4

Clifton-Brown, J.C., Lewandowski, I., Andersson, B., Basch, G., Christian, D.G., Kjeldsen, J.B., Jørgensen, U., Mortensen, J.V., Riche, A.B., Schwarz, K.-U., Tayebi, K., Teixeira, F., (2001). Performance of 15 Miscanthus genotypes at five sites in Europe. Agronomy Journal 93, 1013–1019.

Clifton-Brown, J., Hastings, A., Von Cossel, M., Murphy-Bokern, D., McCalmont, J., Whitaker, J., Alexopoulou, E., Amaducci, S., Andronic, L., Ashman, C., Awty-Carroll, D., Bhatia, R., Breuer, L., Cosentino, S., Cracroft-Eley, W., Donnison, I., Elbersen, B., Ferrarini, A., Ford, J., Greef, J., Ingram, J., Lewandowski, I., Magenau, E., Mos, M., Petrick, M., Pogrzeba, M., Robson, P., Rowe, R.L., Sandu, A., Schwarz, K., Scordia, D., Scurlock, J., Shepherd, A., Thornton, J., Trindade, L.M., Vetter, S., Wagner, M., Wu, P., Yamada, T., Kiesel, A., (2023). Perennial biomass cropping and use: Shaping the policy ecosystem in European countries. GCB Bioenergy 15, 538–558. https://doi.org/10.1111/gcbb.13038

Costanza, R., Limburg, K., Naeem, S., O'Neill, R.V., Paruelo, J., Raskin, R.G., Sutton, P., (1997). The value of the world's ecosystem services and natural capital 387.

Clark, L.V., Brummer, J.E., Glowacka, K., Hall, M.C., Heo, K., Peng, J., Yamada, T., Yoo, J.H., Yu, C.Y., Zhao, H., Long, S.P., Sacks, E.J., (2014). A footprint of past climate change on the diversity and population structure of *Miscanthus sinensis*. Annals of Botany 114, 97–107. https://doi.org/10.1093/aob/mcu084

Clark, L.V., Dwiyanti, M.S., Anzoua, K.G., Brummer, J.E., Ghimire, B.K., Glowacka, K., Hall, M., Heo, K., Jin, X., Lipka, A.E., Peng, J., Yamada, T., Yoo, J.H., Yu, C.Y., Zhao, H., Long, S.P., Sacks, E.J., (2019). Genome-wide association and genomic prediction for biomass yield in a genetically diverse *Miscanthus sinensis* germplasm panel phenotyped at five locations in Asia and North America. GCB Bioenergy 988–1007. https://doi.org/10.1111/gcbb.12620

Clark, L.V., Dzyubenko, E., Dzyubenko, N., Bagmet, L., Sabitov, A., Chebukin, P., Johnson, D.A., Kjeldsen, J.B., Petersen, K.K., Jørgensen, U., Yoo, J.H., Heo, K., Yu, C.Y., Zhao, H., Jin, X., Peng, J., Yamada, T., (2016). Ecological characteristics and in situ genetic associations for yield-component traits of wild Miscanthus from eastern Russia. Annals of Botany 941–955. https://doi.org/10.1093/aob/mcw137

Dauber, J., & Miyake, S. (2016). To integrate or to segregate food crop and energy crop cultivation at the landscape scale? Perspectives on biodiversity conservation in agriculture in Europe. Energy, Sustainability and Society, 6(1), 25.

Daily, G.C., (1997). Introduction: What Are Ecosystem Services, in: Natures's Services Societal Dependence on Natural Ecosystems. Island Press, Washington DC, Covelo, California, pp. 1–19.

De Groot, R.S., Wilson, M.A., Boumans, R.M.J., (2002). A typology for the classification, description and valuation of ecosystem functions, goods and services. Ecological Economics 41, 393–408. https://doi.org/10.1016/S0921-8009(02)00089-7

Dong, H., Liu, S., Clark, L.V., Sharma, S., Gifford, J.M., Juvik, J.A., Lipka, A.E., Sacks, E.J., (2018). Genetic mapping of biomass yield in three interconnected Miscanthus populations. GCB Bioenergy 10, 165–185. https://doi.org/10.1111/gcbb.12472

Dufosse, K., Drewer, J., Gabrielle, B., & Drouet, J.-L. (2014). Effects of a 20-year old *Miscanthus* × *giganteus* stand and its removal on soil characteristics and greenhouse gas emissions. Biomass and bioenergy, 69, 198-210.

Falconer, D.S., (1981). Introduction to Quantitative Genetics. Ronald Press New York.

FAO. 2025. La Situation mondiale de l'alimentation et de l'agriculture (2025). Lutter contre la dégradation des terres à toutes les échelles d'exploitation. Rome. https://doi.org/10.4060/cd7067fr

Ferchaud, F., Marsac, S., & Mary, B. (2025). Conversion of arable land to perennial bioenergy crops increases soil organic carbon stocks on the long term. Agriculture, Ecosystems & Environment, 388, 109637. https://doi.org/https://doi.org/10.1016/j.agee.2025.109637

Ferchaud, F., & Mary, B. (2016). Drainage and nitrate leaching assessed during 7 years under perennial and annual bioenergy crops. BioEnergy Research, 9(2), 656-670.

Fernando, A. L., Duarte, M. P., Almeida, J., Boléo, S., & Mendes, B. (2010). Environmental impact assessment of energy crops cultivation in Europe. Biofuels, Bioproducts and Biorefining, 4(6), 594-604.

Fradj, N. B., Rozakis, S., Borzęcka, M., & Matyka, M. (2020). Miscanthus in the European bio-economy: A network analysis. Industrial Crops and Products, 148, 112281.

Gauder, M., Graeff-Hönninger, S., Lewandowski, I., & Claupein, W. (2012). Long-term yield and performance of 15 different Miscanthus genotypes in southwest Germany. Annals of Applied Biology, 160(2), 126-136. https://doi.org/https://doi.org/10.1111/j.1744-7348.2011.00526.x

Gaba, S., Lescourret, F., Boudsocq, S., Enjalbert, J., Hinsinger, P., Journet, E.-P., Navas, M.-L., Wery, J., Louarn, G., Malézieux, E., Pelzer, E., Prudent, M., Ozier-Lafontaine, H., (2015). Multiple cropping systems as drivers for providing multiple ecosystem services: from concepts to design. Agron. Sustain. Dev. 35, 607–623. https://doi.org/10.1007/s13593-014-0272-z

Greef, J.M., Deuter, M., Jung, C., Schondelmaier, J., (1997). Genetic diversity of European Miscanthus species revealed by AFLP fingerprinting. Genetic Resources and Crop Evolution 44, 185–195. https://doi.org/10.1023/A:1008693214629

Gifford, J.M., Chae, W.B., Swaminathan, K., Moose, S.P., Juvik, J.A., (2015). Mapping the genome of Miscanthus *sinensis* for QTL associated with biomass productivity. GCB Bioenergy 7, 797–810. https://doi.org/10.1111/gcbb.12201

Glowacka, K., (2011). A review of the genetic study of the energy crop Miscanthus. Biomass and Bioenergy 35, 2445–2454. https://doi.org/10.1016/j.biombioe.2011.01.041

Glowacka, K., Clark, L.V., Adhikari, S., Peng, J., Stewart, J.R., Nishiwaki, A., Yamada, T., Jørgensen, U., Hodkinson, T.R., Gifford, J., Juvik, J.A., Sacks, E.J., (2015). Genetic variation in *Miscanthus* × *giganteus* and the importance of estimating genetic distance thresholds for differentiating clones. GCB Bioenergy 7, 386–404. https://doi.org/10.1111/gcbb.12166

Hastings, A., Clifton-Brown, J., Wattenbach, M., Mitchell, C. P., & Smith, P. (2009). The development of MISCANFOR, a new Miscanthus crop growth model: towards more robust yield predictions under different climatic and soil conditions. Gcb Bioenergy, 1(2), 154-170.

Haines-Yong, R. and Potschin, M. (2013): CICES V4.3 – Revised report prepared following consultation on CICES Version 4, August-December 2012. EEA Framework Contract No EEA/IEA/09/003

Haines-Young, R. and M.B. Potschin (2018): Common International Classification of Ecosystem Services (CICES) V5.1 and Guidance on the Application of the Revised Structure. Available from www.cices.eu

Haines-Young, R. (2023): Common International Classification of Ecosystem Services (CICES) V5.2 and Guidance on the Application of the Revised Structure. [Available from www.cices.eu]

Himken, M., Lammel, J., Neukirchen, D., Czypionka-Krause, U., & Olfs, H.-W. (1997). Cultivation of Miscanthus under West European conditions: Seasonal changes in dry matter production, nutrient uptake and remobilization. Plant and soil, 189(1), 117-126.

Holder, A. J., Rowe, R., McNamara, N. P., Donnison, I. S., & McCalmont, J. P. (2019). Soil & Water Assessment Tool (SWAT) simulated hydrological impacts of land use change from temperate grassland to energy crops: A case study in western UK. Gcb Bioenergy, 11(11), 1298-1317.

Hou, W., Raverdy, R., Lourgant, K., Mignot, E., Arnoult, S., Giauffret, C., Brancourt-Hulmel, M., (2022). QTL Detection for Flowering-Time Related Traits in *Miscanthus sinensis* Using a Staggered-Start Design. BIOENERGY RESEARCH 15, 718–733. https://doi.org/10.1007/s12155-021-10386-x

Huang, J., Tichit, M., Poulot, M., Darly, S., Li, S., Petit, C., Aubry, C., (2015). Comparative review of multifunctionality and ecosystem services in sustainable agriculture. Journal of Environmental Management 149, 138–147. https://doi.org/10.1016/j.jenvman.2014.10.020

Jensen, E., Farrar, K., Thomas-Jones, S., Hastings, A., Donnison, I., Clifton-Brown, J., (2011). Characterization of flowering time diversity in Miscanthus species. GCB Bioenergy 3, 387–400. https://doi.org/10.1111/j.1757-1707.2011.01097.x

Jensen, E., Robson, P., Norris, J., Cookson, A., Farrar, K., Iain, D., Clifton-Brown, J., (2013). Flowering induction in the bioenergy grass *Miscanthus sacchariflorus* is a quantitative short-day response, whilst delayed flowering under long days increases biomass accumulation. Journal of Experimental Botany 64, 541–552.

Jones, M., Walsh, M., (2001). Miscanthus for Energy and Fibre. James & James (Science Publishers) Ltd., London.

Lask, J., Magenau, E., Ferrarini, A., Kiesel, A., Wagner, M., & Lewandowski, I. (2020). Perennial rhizomatous grasses: Can they really increase species richness and abundance in arable land? A meta-analysis. GCB Bioenergy, 12(11), 968-978.

Laval-Gilly, P., Henry, S., Mazziotti, M., Bonnefoy, A., Comel, A., & Falla, J. (2017). *Miscanthus x giganteus* composition in metals and potassium after culture on polluted soil and its use as biofuel. BioEnergy Research, 10(3), 846-852.

Leroy, J., Ferchaud, F., Giauffret, C., Mary, B., Fingar, L., Mignot, E., Arnoult, S., Lenoir, S., Martin, D., & Brancourt-Hulmel, M. (2022). *Miscanthus sinensis* is as efficient as *Miscanthus× giganteus* for nitrogen recycling in spite of smaller nitrogen fluxes. Bioenergy Research, 15(2), 686-702.

Lesur-Dumoulin, C., Lorin, M., Bazot, M., Jeuffroy, M. H., & Loyce, C. (2016). Analysis of young Miscanthus× *giganteus* yield variability: a survey of farmers' fields in east central France. Gcb Bioenergy, 8(1), 122-135.

Lesur, C., Bazot, M., Bio-Beri, F., Mary, B., Jeuffroy, M. H., & Loyce, C. (2014). Assessing nitrate leaching during the three-first years of *Miscanthus× giganteus* from on-farm measurements and modeling. Gcb Bioenergy, 6(4), 439-449.

Lewandowski, I., Clifton-Brown, J., Scurlock, J., & Huisman, W. (2000). Miscanthus: European experience with a novel energy crop. Biomass and Bioenergy, 19(4), 209-227.

Lewandowski, I., Scurlock, J. M., Lindvall, E., & Christou, M. (2003). The development and current status of perennial rhizomatous grasses as energy crops in the US and Europe. Biomass and Bioenergy, 25(4), 335-361.

Lele, S., Springate-Baginski, O., Lakerveld, R., Deb, D., Dash, P., (2013). Ecosystem Services: Origins, Contributions, Pitfalls, and Alternatives. Conservat Soc 11, 343. https://doi.org/10.4103/0972-4923.125752

Linde-Laursen, I. (1993). Cytogenetic analysis of Miscanthus' Giganteus', an interspecific hybrid.

Littlejohn, C. P., Hofmann, R. W., & Wratten, S. D. (2019). Delivery of multiple ecosystem services in pasture by shelter created from the hybrid sterile bioenergy grass *Miscanthus x giganteus.* Scientific reports, 9(1), 5575.

López-Ballesteros, A., Trolle, D., Srinivasan, R., & Senent-Aparicio, J. (2023). Assessing the effectiveness of potential best management practices for science-informed decision support at the watershed scale: The case of the Mar Menor coastal lagoon, Spain. Science of the Total Environment, 859, 160144.

Lovett, A., Dockerty, T., Papathanasopoulou, E., Beaumont, N., & Smith, P. (2015). A framework for assessing the impacts on ecosystem services of energy provision in the UK: an example relating to the production and combustion life cycle of UK produced biomass crops (short rotation coppice and Miscanthus). Biomass and bioenergy, 83, 311-321.

Mazur, A., & Kowalczyk-Juśko, A. (2021). The assessment of the usefulness of *Miscanthus x giganteus* to water and soil protection against erosive degradation. Resources, 10(7), 66.

McCalmont, J. P., Hastings, A., McNamara, N. P., Richter, G. M., Robson, P., Donnison, I. S., & Clifton-Brown, J. (2017). Environmental costs and benefits of growing Miscanthus for bioenergy in the UK. Glob Change Biol Bioenergy, 9(3), 489-507. https://doi.org/10.1111/gcbb.12294

Merriman, K. R., Russell, A. M., Rachol, C. M., Daggupati, P., Srinivasan, R., Hayhurst, B. A., & Stuntebeck, T. D. (2018). Calibration of a field-scale Soil and Water Assessment Tool (SWAT) model with field placement of best management practices in Alger Creek, Michigan. Sustainability, 10(3), 851.

Millennium Ecosystem Assessment, (2005). Ecosystems and Human Well-being: Synthesis. Island Press, Washington, DC.

Mitros, T., Session, A.M., James, B.T., Wu, G.A., Belaffif, M.B., Clark, L.V., Shu, S., Dong, H., Barling, A., Holmes, J.R., Mattick, J.E., Bredeson, J.V., Liu, S., Farrar, K., Glowacka, K., Jezowski, S., Barry, K., Chae, W.B., Juvik, J.A., Gifford, J., Oladeinde, A., Yamada, T., Grimwood, J., Putnam, N.H., Vega, J.D., Barth, S., Klaas, M., Hodkinson, T., Li, L., Jin, X., Peng, J., Yu, C.Y., Heo, K., Yoo, J.H., Ghimire, B.K., Donnison, I.S., Schmutz, J., Hudson, M.E., Sacks, E.J., Moose, S.P., Swaminathan, K., Rokhsar, D.S., (2020). Genome biology of the paleotetraploid perennial biomass crop Miscanthus. Nature Communications 1–11. https://doi.org/10.1038/s41467-020-18923-6

Nie, G., Huang, L., Zhang, X., Taylor, M., Jiang, Y., Yu, X., (2016). Marker-Trait Association for Biomass Yield of Potential Bio-fuel Feedstock *Miscanthus sinensis* from Southwest. Frontiers in Plant Science 7. https://doi.org/10.3389/fpls.2016.00802

Poeplau, C., & Don, A. (2014). Soil carbon changes under Miscanthus driven by C4 accumulation and C3 decompostion–toward a default sequestration function. Gcb Bioenergy, 6(4), 327-338.

Raverdy, R., (2021). Study of the genetic determinism related to biomass production and composition traits in Miscanthus *sinensis*. AgroParisTech, Paris.

Raverdy, R., Lourgant, K., Mignot, E., Arnoult, S., Bodineau, G., Griveau, Y., Taniguti, C.H., Brancourt-Hulmel, M., (2022). Linkage Mapping of Biomass Production and Composition Traits in a *Miscanthus sinensis* Population. Bioenergy Research. https://doi.org/10.1007/s12155-022-10402-8

Power, A.G., (2010). Ecosystem services and agriculture: tradeoffs and synergies. Phil. Trans. R. Soc. B 365, 2959–2971. https://doi.org/10.1098/rstb.2010.0143

Saunier, M., Ouvry, J. F., & Richet, J. B. (2013). Programme de recherche 2013 sur les bandes ligno-cellulosiques testées par la Chambre d'Agriculture de Seine-Maritime, compte-rendu des mesures de ruissellement réalisées par l'AREAS. https://www.areas-asso.fr/wp-content/uploads/2022/01/blc-infiltration-areas-ca76-def-2013-11-29.pdf

Saunier, M., Ouvry, J. F., & Verger, A. (2018). INNOBIOMA - Programme de recherches sur les Bandes Ligno-Cellulosiques— Capacités d'infiltration et de sédimentation sous saules (TTCR) et sous miscanthus [Rapport d'étude]. https://www.areas asso.fr/ressources/documents/rapport-innobioma-programme-de-recherche-sur-les-

bandes-ligno-cellulosiques-capacites dinfiltration-et-de-sedimentation-sous-saules-ttcr-et-sous-miscanthus-saunier-areas-2018/

Shepherd, A., Thornton, J., Trindade, L.M., Vetter, S., Wagner, M., Wu, P., Yamada, T., Kiesel, A., (2023). Perennial biomass cropping and use: Shaping the policy ecosystem in European countries. GCB Bioenergy 15, 538–558. https://doi.org/10.1111/gcbb.13038

Strullu, L., Cadoux, S., Preudhomme, M., Jeuffroy, M.-H., & Beaudoin, N. (2011). Biomass production and nitrogen accumulation and remobilisation by *Miscanthus* × *giganteus* as influenced by nitrogen stocks in belowground organs. Field Crops Research, 121(3), 381-391.

Slavov, G.T., Nipper, R., Robson, P., Farrar, K., Allison, G.G., Bosch, M., Clifton-brown, J.C., Donnison, I.S., Jensen, E., (2013). Genome-wide association studies and prediction of 17 traits related to phenology, biomass and cell wall composition in the energy grass *Miscanthus sinensis*. New Phytologist.

Sun, Q., Lin, Q., Yi, Z.-L., Yang, Z.-R., Zhou, F.-S., (2010). A taxonomic revision of Miscanthus s.l. (Poaceae) from China. Botanical Journal of the Linnean Society 164, 178–220. https://doi.org/10.1111/j.1095-8339.2010.01082.x

Syswerda, S.P., Robertson, G.P., (2014). Ecosystem services along a management gradient in Michigan (USA) cropping systems. Agriculture, Ecosystems & Environment 189, 28–35. https://doi.org/10.1016/j.agee.2014.03.006

Tavakoli-Hashjini, E., Piorr, A., Müller, K., & Vicente-Vicente, J. L. (2020). Potential bioenergy production from *Miscanthus* × *Giganteus* in Brandenburg: Producing bioenergy and fostering other ecosystem services while ensuring food self-sufficiency in the Berlin-Brandenburg region. Sustainability, 12(18), 7731.

Uwatoko, N., ichi Tamura, K., Yamashita, H., Gau, M., (2016). Naturally occurring triploid hybrids between Miscanthus *sacchariflorus* and *M. sinensis* in Southern Japan, show phenotypic variation in agronomic and morphological traits. Euphytica 212, 355–370. https://doi.org/10.1007/s10681-016-1760-9

Von Cossel, M., Wagner, M., Lask, J., Magenau, E., Bauerle, A., Von Cossel, V., Warrach-Sagi, K., Elbersen, B., Staritsky, I., & Van Eupen, M. (2019). Prospects of bioenergy cropping systems for a more social-ecologically sound bioeconomy. Agronomy, 9(10), 605.

Von Cossel, M., Winkler, B., Mangold, A., Lask, J., Wagner, M., Lewandowski, I., Elbersen, B., van Eupen, M., Mantel, S., & Kiesel, A. (2020). Bridging the gap between biofuels and biodiversity through monetizing environmental services of miscanthus cultivation. Earth's Future, 8(10), e2020EF001478.

Van der Weijde, T., Dolstra, O., Visser, R.G.F., Trindade, L.M., (2017). Stability of cell wall composition and saccharification efficiency in Miscanthus across diverse environments. Frontiers in Plant Science 7, 1–14. https://doi.org/10.3389/fpls.2016.02004

Weik, J., Lask, J., Petig, E., Seeger, S., Marting Vidaurre, N., Wagner, M., Weiler, M., Bahrs, E., Lewandowski, I., & Angenendt, E. (2022). Implications of large-scale miscanthus cultivation in water protection areas: A Life Cycle Assessment with model coupling for improved policy support. Gcb Bioenergy, 14(11), 1162-1182.

Xu, W.Z., Zhang, X.Q., Huang, L.K., Nie, G., Wang, J.P., (2013). Higher genetic diversity and gene flow in wild populations of *Miscanthus sinensis* in southwest China. Biochemical Systematics and Ecology 48, 174–181. https://doi.org/10.1016/j.bse.2012.11.024

Zapater, M., Catterou, M., Mary, B., Ollier, M., Fingar, L., Mignot, E., Ferchaud, F., Strullu, L., Dubois, F., & Brancourt-Hulmel, M. (2017). A single and robust critical nitrogen dilution curve for *Miscanthus* × *giganteus* and *Miscanthus sinensis*. Bioenergy research, 10(1), 115-128.

Zhao, H., Wang, B., He, J., Yang, J., Pan, L., Sun, D., Peng, J., (2013). Genetic Diversity and Population Structure of *Miscanthus sinensis* Germplasm in China. PLoS ONE 8. https://doi.org/10.1371/journal.pone.0075672

Zheng, H., Wang, L., Wu, T., (2019). Coordinating ecosystem service trade-offs to achieve win–win outcomes: A review *of* the approaches. Journal of Environmental Sciences 82, 103–112. https://doi.org/10.1016/j.jes.2019.02.030

Zub, H. W., & Brancourt-Hulmel, M. (2010). Agronomic and physiological performances of different species of Miscanthus, a major energy crop. A review. Agronomy for Sustainable Development, 30(2), 201-214. https://doi.org/10.1051/agro/2009034

Zub, H.W., Arnoult, S., Younous, J., Lejeune-Henaut, I., Brancourt-Hulmel, M., (2012). The frost tolerance of Miscanthus at the juvenile stage: Differences between clones are influenced by leaf-stage and acclimation. EUROPEAN JOURNAL OF AGRONOMY 36, 32–40. https://doi.org/10.1016/j.eja.2011.08.001

# General Experimental Framework

This thesis is based on a common experimental framework designed to characterize, predict, and genetically analyze nitrogen economy traits in a full-sib *Miscanthus sinensis* progeny grown under nitrogen-deficient field conditions. This chapter describes the biological material, field experimental platform, sampling strategy, phenotyping scheme, genotyping procedures, and genetic map construction that are shared across all three results chapters. The aim is to provide a coherent overview of the overall experimental structure within which the different analyses were conducted, while detailed methodological procedures specific to each objective are presented in the corresponding results chapters.

## 1. Population and experimental design

The diploid full-sib *Miscanthus sinensis* population studied in this thesis, hereafter also referred to as SiB, was created from a controlled cross between *M. sinensis* 'Malepartus' (MAL) and *M. sinensis* 'Herman Mussel' (HER), both diploid genotypes (2n = 2x = 38). Crosses were performed in 2014 at the INRAE GCIE experimental unit in Estrées-Mons under controlled pollination conditions. Seeds obtained from this cross were germinated *in vitro*, and 253 seedlings were produced and assigned identifiers from SiB001 to SiB253. Seedlings were subsequently transplanted into pots, acclimated in a glasshouse, and clonally propagated by rhizome division to generate field replicates, although multiplication success varied among genotypes.

A total of 127 genotypes were finally established in 2018 at the INRAE GCIE site of Estrées-Mons in a progeny trial planted at a density of 1 plant $m^{-2}$ in an incomplete block design with four blocks. The field comprised eleven rows of sixty-seven planting positions, with border rows composed of *M. sinensis* 'Malepartus'. Replication per genotype ranged from one to twelve plants depending on the success of clonal propagation, this ability being genotype dependent. The spatial organization of genotypes within the field is shown in Figure 1. The two parents, MAL and HER, were present within the trial and were sampled together with their progeny. Further methodological details concerning the establishment of the progeny trial are presented in Iqbal et al. (2026, Chapter 1).

In parallel with the progeny trial, an independent parental trial composed of MAL and HER was established at the same site with higher replication to characterize the nitrogen status of the trials and seasonal nitrogen dynamics over two growing seasons (2023-2024 and 2024-2025). Both the progeny and parental trials were unfertilized. In addition, data from a previously

studied fertilized miscanthus trial located at the same site, in which 120 kg N $ha^{-1}$ were applied annually as a urea-ammonium-nitrate solution, were used as a nitrogen-sufficient reference for interpreting nitrogen status and comparing soil mineral nitrogen concentrations (Leroy et al., 2022). The parental trial and the fertilized reference trial were used primarily to diagnose and compare the nitrogen status of the trials, whereas the quantification of nitrogen economy traits and all corresponding analyses presented in this thesis were carried out on the progeny trial.

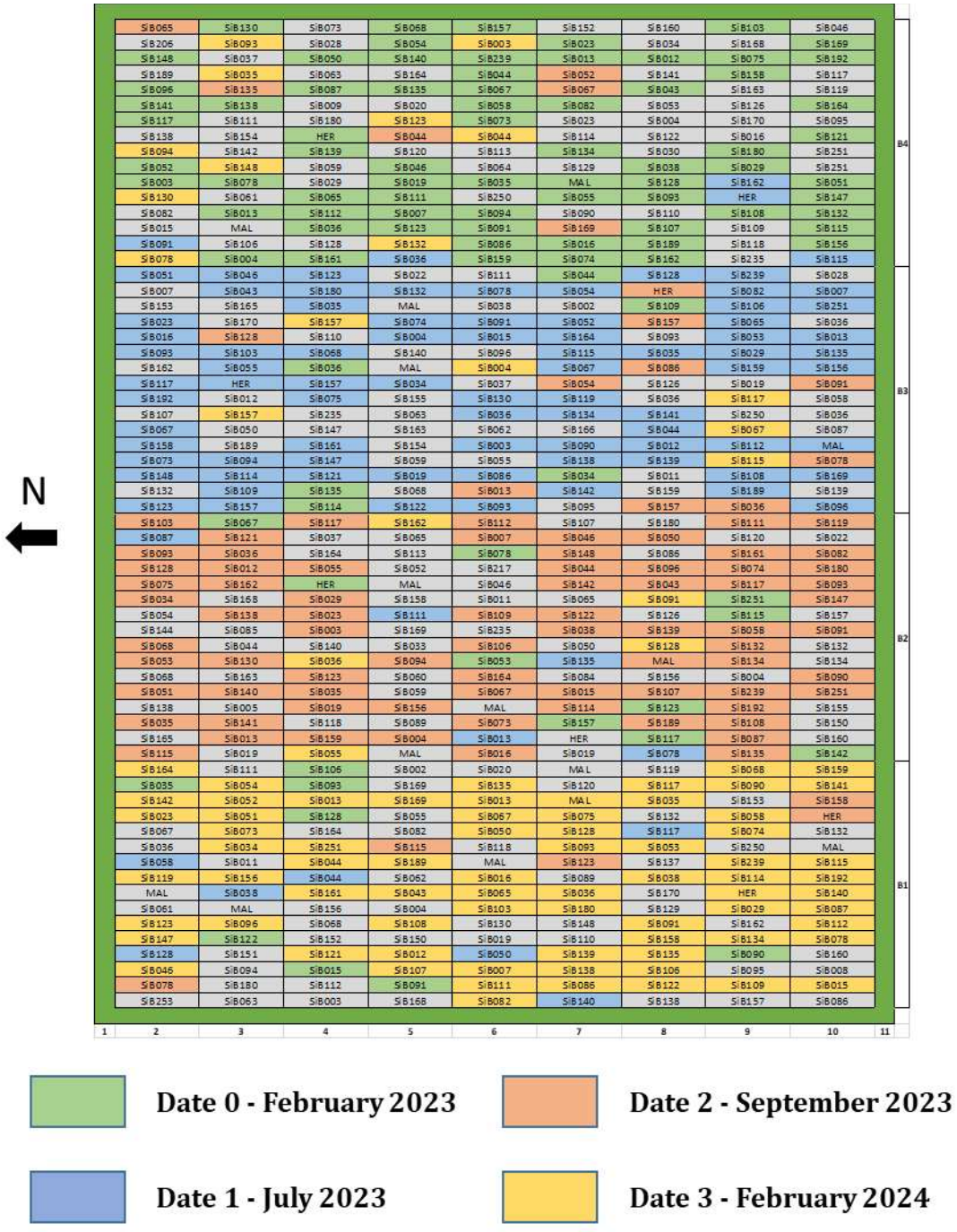


**Figure 1.** Field layout of the *Miscanthus sinensis* progeny trial at Estrées-Mons. Each cell represents an individual plant position within the field. The progeny trial comprised 127 genotypes planted in an incomplete block design with four blocks. Colors indicate the sampling date assigned to each plant during the four sampling campaigns of the 2023-2024 growth cycle.

## 2. Site description and trial management

The progeny and parental trials were conducted at the INRAE GCIE experimental unit of Estrées-Mons in northern France (49°87′ N, 3°01′ E) (Figure 2). The site experiences a marine west coast climate (Cfb), with a mean annual temperature of 11.2°C and an average annual precipitation of 675 mm over the period 2017-2024. During the 2023-2024 growing season considered in this study (February 2023 to February 2024), the mean temperature was 11.4°C and total precipitation reached 925 mm (CLIMATIK platform, 2025). The soils at the Estrées-Mons site are deep silt loams classified as Haplic Luvisols (IUSS Working Group WRB, 2022), with approximately 16.5% clay, 72.7% silt and 7.8% fine sand, a near-neutral pH (7.9), a high cation exchange capacity (96.8 meq 100 $g^{-1}$) and a moderate organic carbon content (11.4 g $kg^{-1}$; C/N = 10.6). These physicochemical characteristics were determined in 2017 and are considered representative of the site's baseline status.

**Figure 2.** Photograph of the *Miscanthus sinensis* progeny trial at the INRAE GCIE experimental site of Estrées-Mons.

Both the progeny and parental trials were unfertilized and irrigated throughout the years of cultivation to ensure non-limiting water conditions. Recorded irrigation volumes for the progeny trial were 36, 926 and 393 $m^3$ in 2021, 2022 and 2023, respectively (Iqbal et al., 2026, Chapter 1). From establishment in 2018 until the beginning of the measurement period, management consisted of standard agronomic practices, including manual weed control, with

no chemical inputs applied, and plantations were harvested each year in February. Leaf litter and other plant residues senesced naturally during autumn and winter. They were left on the soil surface.

Soil mineral nitrogen concentrations were measured in both the progeny and parental trials over the 0-150 cm depth in early spring. In March 2023, mean soil mineral N concentrations were 20 kg N $ha^{-1}$ in the progeny trial and 13 kg N $ha^{-1}$ in the parental trial. In March 2024, these values increased to 29 kg N $ha^{-1}$ and 25 kg N $ha^{-1}$, respectively. During each plant sampling campaign, soil mineral nitrogen concentrations were also measured in the 0-30 cm horizon, where most root activity occurs, and remained low across sampling dates in both trials (Iqbal et al., 2026, Chapter 1).

Nitrogen status of the unfertilized trials was diagnosed using the nitrogen nutrition index (NNI), with *Miscanthus sinensis* 'Malepartus' (MAL) used as a probe genotype, following the probe-genotype approach described by Brancourt-Hulmel (1999) and applied for trial-level nitrogen diagnosis as in Laperche et al. (2008). NNI was calculated using the critical nitrogen dilution curve established for *M. sinensis* by Zapater et al. (2017), as the ratio between the actual nitrogen concentration in aboveground vegetative parts and the critical nitrogen concentration required to achieve maximum biomass production. Aboveground biomass and nitrogen concentration data for MAL measured in July were compared between the unfertilized progeny and parental trials and the fertilized reference trial, as shown in Figure 1 of Chapter 1 (Iqbal et al., 2026). In that figure, MAL data from the fertilized trial were positioned close to or above the critical nitrogen dilution curve and corresponded to a non-deficient nitrogen status, whereas all MAL data points from the progeny and parental trials fell consistently below the curve, which corresponded to deficient nitrogen status. Based on this NNI diagnosis, both the progeny and parental trials were classified as nitrogen-deficient during the study period.

## 3. Sampling, plant effect correction and nitrogen economy traits

Nitrogen economy traits were quantified over a full annual growth cycle from February 2023 to February 2024 in the *Miscanthus sinensis* progeny trial. Four destructive sampling campaigns were carried out at key physiological stages of the plant cycle, following the framework presented in Iqbal et al. (2026, Chapter 1). These dates corresponded to:

i. February 2023, corresponding to winter dormancy and representing the maximum nitrogen quantity in belowground parts (Date 0);

ii. July 2023, corresponding to the minimum nitrogen quantity in belowground parts after spring remobilization (Date 1);
iii. September 2023, corresponding to the maximum nitrogen quantity in aboveground parts during active growth (Date 2);
iv. February 2024, corresponding to the end of the cycle after complete senescence (Date 3).

On each sampling date, aboveground and belowground plant parts were collected, biomass and nitrogen concentrations were measured, and nitrogen quantities and fluxes were calculated as described in Iqbal et al. (2026, Chapter 1). Because calculation of fluxes depends on differences in nitrogen pool quantities between two dates, and because the sampling are destructive, different plants of the same genotype were sampled at each of the four time points. This introduced a potential plant effect due to plant-to-plant variability for each genotype, which could bias nitrogen flux calculations due to a confounding effect between plants and dates.

Regarding the plant effect, several approaches have been proposed in the literature to account for plant-to-plant variability introduced by destructive sampling, including mathematical smoothing of biomass dynamics (Beale & Long, 1997), stem density normalization (Strullu et al., 2011), and the selection of representative median plants (Leroy et al., 2022). These methods aim to reduce variability between sampled plants, but no single approach fully eliminates this effect. In the present study, the plant effect was taken into account to adjust biomass and these corrected data were used instead of raw biomass data before calculating nitrogen quantities and fluxes. The correction was applied consistently across sampling dates.

The plant effect was taken into account using the aboveground biomass and its correlation with its belowground part.

Firstly, the correction of the aboveground part was based on a four step-approach based on data from preceding years:

1. The mean aboveground biomass per genotype was calculated using all available plants from the two preceding years. It can be noted that for each genotype, four plants were at least available for this trait during the preceding years.
2. For each individual plant, the mean aboveground biomass was calculated across the two years.

3. A correction percentage was computed for each plant as:

   Correction % = (Mean aboveground biomass per plant for two years / Mean aboveground biomass per genotype) × 100

   This percentage represents how much each plant deviates from the genotype mean.

4. The correction percentage was then applied to adjust the raw biomass values obtained during the 2023-2024 plant cycle:

   Adjusted value = (Raw value / Correction %) × 100

   This adjustment rescales each sampled plant relative to the mean biomass of its genotype, reducing differences due to plant size.

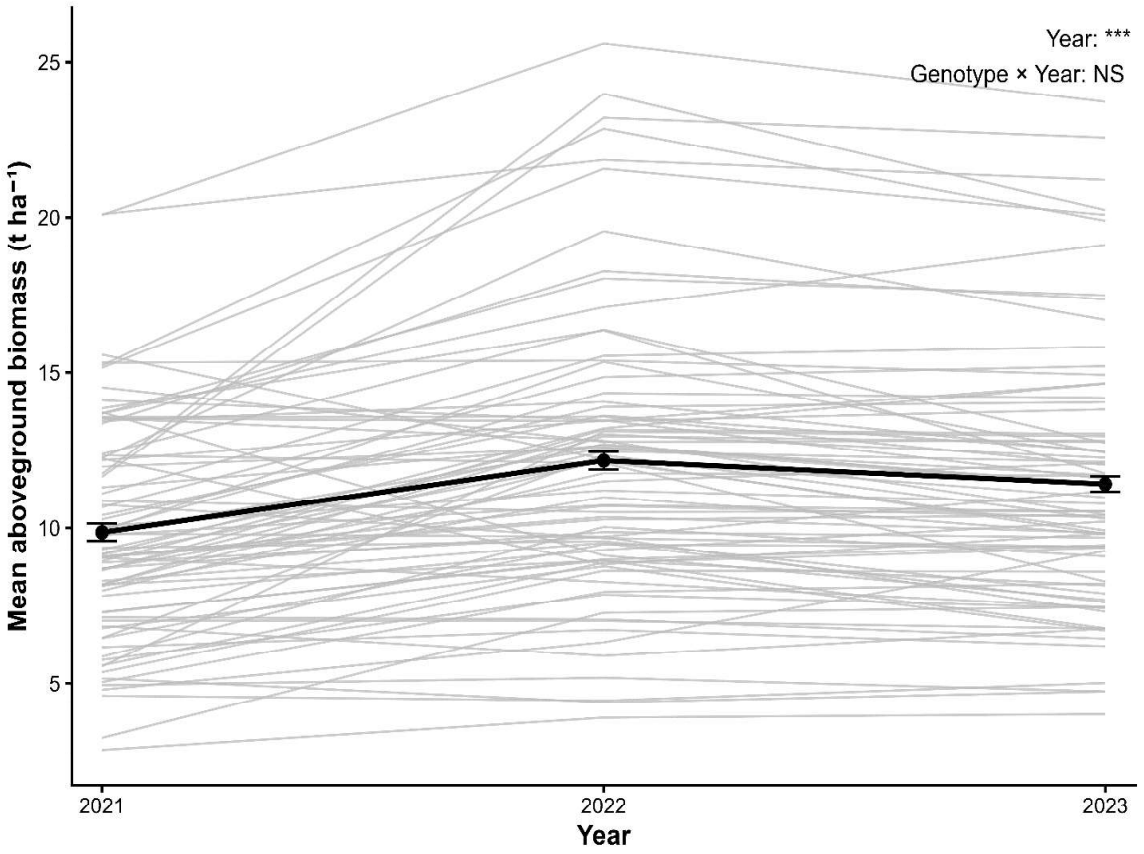


**Figure 3.** Aboveground biomass of the progeny measured in February 2021-2023 (grey lines represent individual genotypes; black line shows the general mean ± standard error) and corresponding year and genotype x year significance in the ANOVA table.

Before the plant effect correction, we verified that aboveground biomass was a reliable reference trait for plant effect correction, by testing year and genotype x year effects on aboveground biomass during the preceding years: these data corresponded to February 2021, 2022, and 2023 (Figure 3). A year effect was observed, but the genotype x year interaction was

non-significant, indicating that genotype rankings remained consistent across years. In particular, aboveground biomass of the genotypes was more stable between 2022 and 2023. These two years were chosen for the data correction. Together, these results supported the use of aboveground biomass as a reliable reference trait for plant effect correction.

To illustrate this correction, an example for one genotype (MAL) is provided in Table 1. The mean of this genotype was based on eight individual values corresponding to four plants observed during two years (step 1 column). The four individual plants showed differences in biomass across the two reference years, resulting in different mean biomass values per plant (step 2 column). These differences led to different correction percentages for each plant relative to the genotype mean (step 3 column). Plants with higher-than-average biomass (correction percentage > 100) were scaled down, whereas plants with lower-than-average biomass (correction percentage < 100) were scaled up. In this way, all plants were adjusted relative to the same genotype-level reference, making them more comparable.

**Table 1.** Example of aboveground biomass-based plant effect correction for one genotype

| Genotype | Plant | Aboveground biomass Feb 2023 (g) | Aboveground biomass Feb 2022 (g) | Step 1: Mean aboveground biomass per genotype (g) | Step 2: Mean aboveground biomass per plant for two years (g) | Step 3: Correction percentage (%) |
|---|---|---|---|---|---|---|
| MAL | 1 | 898.8 | 1235.0 | 1028.9 | 1066.9 | 103.7 |
| MAL | 2 | 976.1 | 1405.0 | 1028.9 | 1190.5 | 115.7 |
| MAL | 3 | 726.0 | 1288.9 | 1028.9 | 1007.5 | 97.9 |
| MAL | 4 | 713.0 | 988.4 | 1028.9 | 850.7 | 82.7 |

Secondly, the same correction was applied to belowground biomass. This was supported by the strong correlation between aboveground and belowground biomass observed in February 2023 ($r = 0.85$) and February 2024 ($r = 0.84$), indicating that plant size differences were consistently reflected across plant compartments. Therefore, the correction percentage calculated from aboveground biomass was also used to adjust belowground biomass.

By reducing plant-to-plant variability introduced by plant destructive sampling, this correction improved the comparability of biomass values across sampling dates and allowed nitrogen quantities and fluxes to be estimated more reliably.

Sampling was performed on a subset of 80 genotypes that provided the required number of repetitions for the evaluation of the nitrogen-related traits within the population. Among these, 65 genotypes had at least four replicates, allowing one plant per genotype to be sampled at each date, while 15 genotypes had at least eight replicates, permitting two plants per genotype to be sampled per date. This structure allowed the four sampling dates to be covered consistently for each genotype included in the nitrogen economy analyses. The parental genotypes MAL and HER were sampled in parallel.

Within this temporal framework, four nitrogen economy traits were quantified (Figure 4). Spring remobilization (SR) corresponds to the nitrogen mobilized from belowground parts to support regrowth after winter. Nitrogen uptake represents the nitrogen acquired from the soil during the growing season. Autumn remobilization (AR) corresponds to nitrogen transferred from senescing aboveground parts to belowground parts from autumn to winter. Nitrogen losses correspond to the nitrogen that is not retained in the plant at the end of the annual cycle. The definitions, calculations and full methodological procedures used to derive these traits are presented within the flux-based framework in Iqbal et al. (2026, Chapter 1).

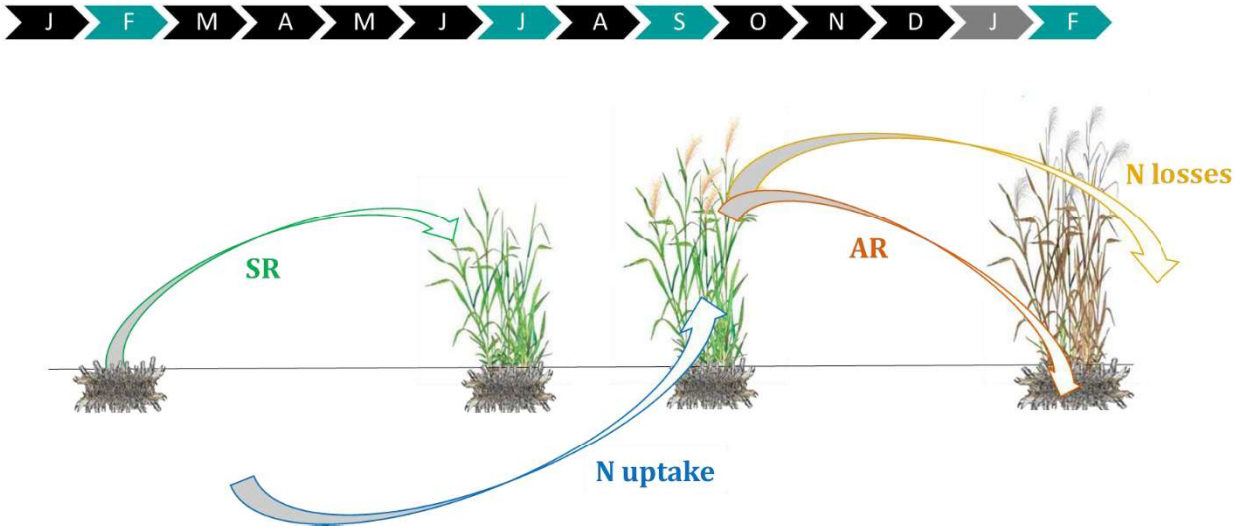


**Figure 4.** Representation of seasonal nitrogen fluxes in *Miscanthus sinensis*. Spring remobilization (SR) corresponds to nitrogen mobilized from belowground parts to support regrowth; nitrogen uptake corresponds to nitrogen acquired from the soil during the growing season; autumn remobilization (AR) corresponds to nitrogen transferred from senescing aboveground parts to belowground parts; nitrogen losses represent nitrogen not retained in the plant after complete senescence.

## 4. Seasonal phenotyping and proxy trait measurements

In parallel with plant destructive sampling for nitrogen economy traits, 35 proxy traits related to plant size and architecture, canopy structure, phenology and growth dynamics, nitrogen

status, nitrogen concentration and nitrogen pools were measured non-destructively throughout the 2023-2024 growth cycle on the same plants used for nitrogen flux calculations (Table 2). These traits were selected because they can be measured during the season without plant destructive sampling, making them suitable candidates for predicting nitrogen economy traits derived from plant destructive harvests, as developed in detail in Chapter 2. Measurements followed the plant life cycle from early regrowth to complete senescence (Figure 5), and the detailed description of their measurement protocols is provided in Chapter 2.

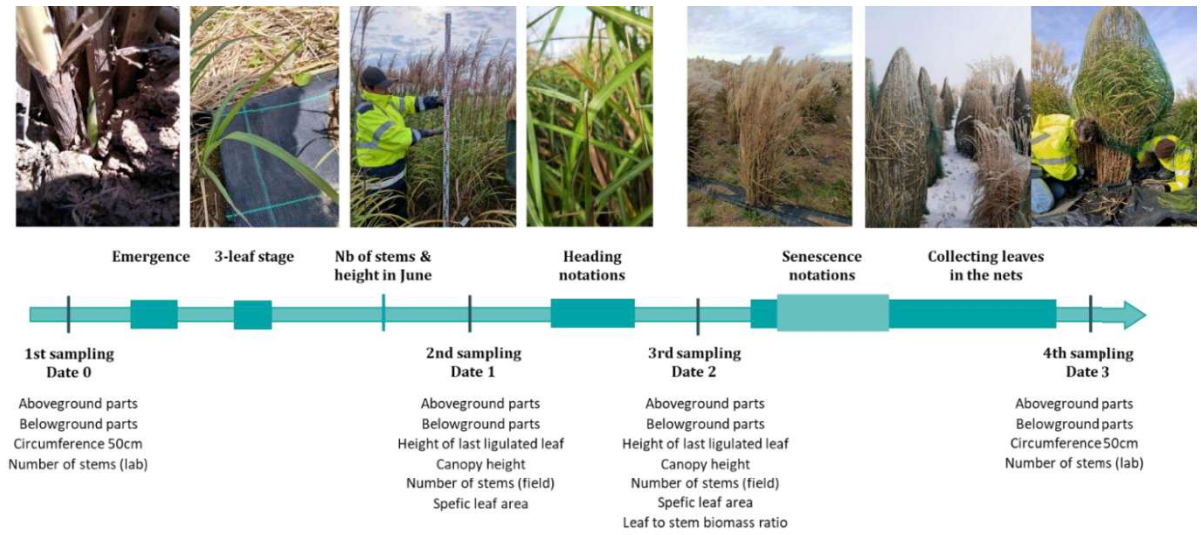


**Figure 5.** Overview of seasonal measurements conducted in the progeny trial. Illustration of field operations and seasonal measurements carried out from early regrowth to complete senescence, including plant phenotyping and leaf litter collection using nets, positioned along the annual crop cycle.

**Traits related to plant size and architecture** included plant height, maximum canopy height, stem number, stem circumference and stand volume. These variables described plant structure, overall plant dimension and canopy occupation and were measured during the growing season and/or at destructive harvests.

**Phenology and growth dynamics traits** were monitored through repeated field observations. These included emergence, progression of plant development, onset and progression of senescence and key phenological timings characterizing the duration and dynamics of the growth cycle.

**Nitrogen status** was assessed using the nitrogen nutrition index, calculated following the framework described in Iqbal et al. (2026, Chapter 1).

**Physiological proxy traits based on nitrogen concentration and nitrogen pools** were obtained by measuring nitrogen concentration in different plant parts and combining these

values with corresponding biomass data to estimate nitrogen quantities, as presented methodologically in Chapter 2. In addition, leaf litter was collected using nets during senescence to quantify nitrogen present in fallen leaves (Figure 5).

These seasonal measurements were synchronized with the destructive sampling campaigns used to quantify nitrogen quantities and fluxes. Initial pairwise relationships between proxy traits and nitrogen economy traits were explored to assess their direct associations, and this dataset then served as the basis for statistical multivariate prediction analyses.

**Table 2.** Nitrogen economy traits and non-destructive proxy traits measured in the *Miscanthus sinensis* progeny trial.

| Category | Trait | Sampling period / timing |
|---|---|---|
| **Nitrogen economy traits** | | |
| | Spring remobilization | Feb23 → Jul23 |
| | Nitrogen uptake | Feb23 → Sep23 |
| | Autumn remobilization (ARa) | Sep23 → Feb24 |
| | Autumn remobilization (ARb) | Sep23 → Feb24 |
| | Nitrogen losses | Sep23 → Feb24 |
| **Proxy traits** | | |
| **Size & architecture** | Aboveground biomass | Feb23 / Feb24 |
| | Stand volume | Feb23 / Feb24 |
| | Leaves biomass | Feb24 |
| | Stems biomass | Feb24 |
| | Circumference (50 cm) | Feb23 / Feb24 |
| **Canopy structure** | Canopy height | Feb23 / Jul23 / Sep23 / Feb24 |
| | Maximum height | Feb23 / Jul23 / Sep23 / Feb24 |
| | Number of stems | Feb23 / Jun23 / Jul23 / Sep23 / Feb24 |
| **Phenology & growth dynamics** | Three-leaf stage | May23 |
| | Senescence 50% / 95% | Sep23 → Feb24 |
| | Plant life cycle | Full growth cycle |
| **Nitrogen status** | Nitrogen nutrition index | Jul23 |
| **Nitrogen concentration** | Aboveground N concentration | Feb24 |
| | Stems N concentration | Feb24 |
| | Decline in aboveground N concentration | Sep23 → Feb24 |
| | Gain in belowground N concentration | Jul23 → Feb24 |
| | Belowground N concentration | Jul23 / Feb24 |
| **Nitrogen pools** | Aboveground N quantity | Feb24 |
| | Leaves N quantity | Feb24 |
| | Stems N quantity | Feb24 |

## 5. Multivariate modelling framework for predicting nitrogen economy traits

Nitrogen economy traits result from plant destructive sampling and multi-step nitrogen flux calculations, and their complexity could not be adequately represented by single proxy traits or simple pairwise correlations. Because these traits arise from multiple, interdependent processes and the proxy traits are often correlated, a multivariate modelling approach was required to integrate several predictors simultaneously. This motivated the use of Partial Least Squares regression to evaluate whether nitrogen uptake, spring and autumn remobilization and nitrogen losses could be predicted from proxy traits that are easier to measure.

Partial Least Squares regression (PLS1) was used to build predictive models for each nitrogen economy trait using the complete set of non-destructive proxy traits as predictors. PLS1 was selected because it is well suited for datasets with many correlated predictors, summarizing them into latent components that maximize their covariance with the target trait. Model construction, data standardization, cross-validation procedure, component selection strategy and model evaluation criteria are fully described in Chapter 2.

Models were first fitted using the full proxy dataset to assess predictive capacity. Variable Importance in Projection (VIP) scores were then used to identify informative predictors and construct reduced, parsimonious models. Full and reduced models were re-evaluated under the same validation framework to compare predictive performance. Details of VIP thresholds, model reconstruction and comparative assessment are presented in Chapter 2.

This framework provided the methodological link between seasonal phenotyping and nitrogen flux measurements by testing whether nitrogen economy traits derived from plant destructive sampling could be approached using non-destructive, scalable field traits.

## 6. Calculation of nitrogen loss deviation

Nitrogen uptake and nitrogen losses were strongly and positively related across genotypes in the population. To identify genotypes combining high nitrogen uptake with contrasting nitrogen losses independently of this overall relationship, nitrogen loss deviation was calculated following the deviation-based framework proposed by Oury and Godin (2007) for grain protein deviation.

Nitrogen losses were regressed against nitrogen uptake using a linear model fitted across all progeny (Figure 6). For each genotype, nitrogen loss deviation was defined as the standardized difference between observed nitrogen losses and the nitrogen losses expected from the regression line at the same level of uptake. Negative deviation values indicate genotypes exhibiting lower nitrogen losses than expected for their uptake level (in green on Figure 6), whereas positive deviation values indicate higher losses than expected (in red on Figure 6). The negative deviations are desirable in contrast to the non-desirable positive ones. This approach allows nitrogen losses to be interpreted independently of uptake and was used in Chapter 3 to identify genotypes that deviate from the positive uptake-loss relationship, following the deviation-based framework of Oury and Godin (2007). Full methodological details of deviation computation and its genetic analysis are provided in Chapter 3.

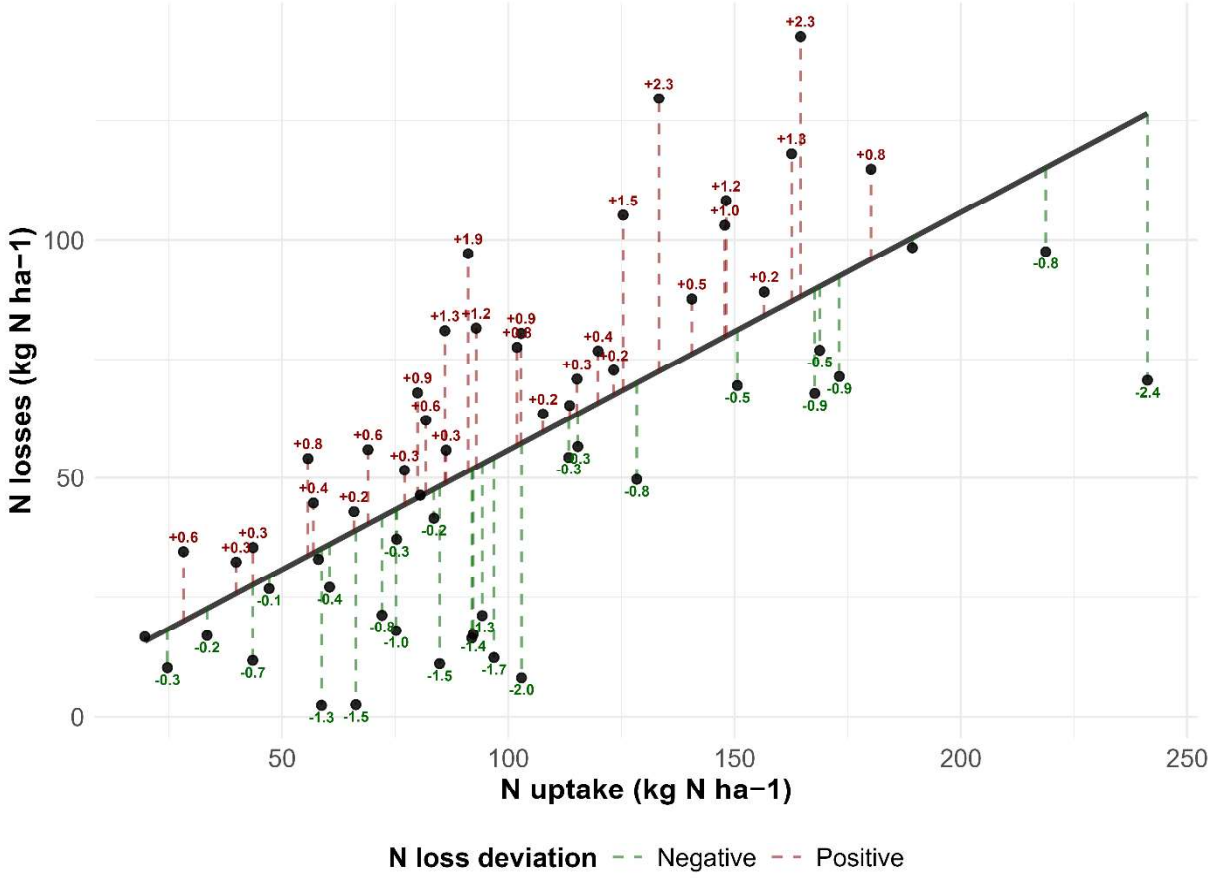


**Figure 6.** Illustration of a nitrogen deviation calculation from the relationship between genotypic nitrogen uptake (kg N ha$^{-1}$) and nitrogen losses (kg N ha$^{-1}$) across the progeny. Dashed red and green lines indicate non-desirable positive and desirable negative deviations from the regression line, respectively.

## 7. Genotyping

The two parents, *M. sinensis* 'Malepartus' (MAL) and *M. sinensis* 'Herman Mussel' (HER), together with 129 progeny genotypes, were genotyped using genotyping-by-sequencing (GBS). For that purpose, leaf samples from plants of the same genotype were pooled, frozen and used for DNA extraction. DNA extraction and library preparation were performed at the INRAE Gentyane Genomic Services platform (Clermont-Ferrand, France) using the sbeadex™ livestock kit (LGC Group, United Kingdom). GBS was then carried out at the CIRAD GPTR genotyping platform (Montpellier, France) following the protocol of Elshire et al. (2011) and Cormier et al. (2019). 96-plex libraries were constructed using the restriction enzyme PstI, and single-end sequencing was performed at the GenoToul GeT platform (Auzeville, France) on an Illumina HiSeq™ 3000 sequencer.

SNP discovery and genotypic data processing was carried out at the BioEcoAgro research unit (Kristelle Lourgant) following the procedure described by Raverdy et al. (2022) for *Miscanthus sinensis*. Sequence reads were aligned to the *M. sinensis* reference genome released by Mitros et al. (2020). SNP markers were filtered based on missing data and minor allele frequency prior to genetic map construction. The retained SNPs segregated according to segregation types expected in outcrossing full-sib populations (Wu et al., 2002).

Three marker classes were kept:

- Bridge markers (Bri): heterozygous in both parents (ab × ab), segregating 1:2:1
- Mal markers: heterozygous in MAL and homozygous in HER (ab × aa), segregating 1:1
- Her markers: homozygous in MAL and heterozygous in HER (aa × ab), segregating 1:1

Marker nomenclature followed Wu et al. (2002), with Bri, Mal and Her markers coded as B3.7, D1.10 and D2.15, respectively.

## 8. Genetic map construction

Once the desired SNPs had been obtained, the genetic map construction followed the methodological framework described by Raverdy et al. (2022) for *M. sinensis*, using the OneMap R package (Margarido et al., 2007; 2020). A schematic summary of the full pipeline is presented in Figure 7.

Redundant markers were first identified and removed. Remaining markers were tested for deviation from expected Mendelian segregation ratios using chi-square tests with multiple-testing correction. Pairwise recombination fractions were estimated using two-point methods for outcrossing species (Wu et al., 2002).

Markers were grouped into linkage groups (LGs) using recombination information in combination with correspondence to the *M. sinensis* reference genome. Grouping thresholds were defined by a maximum recombination fraction of 0.35 and an adapted LOD score suited to the dataset, resulting in 19 linkage groups, consistent with the base chromosome number of miscanthus (x = 19). Segregation-distorted markers were retained during grouping but removed prior to marker ordering and QTL detection.

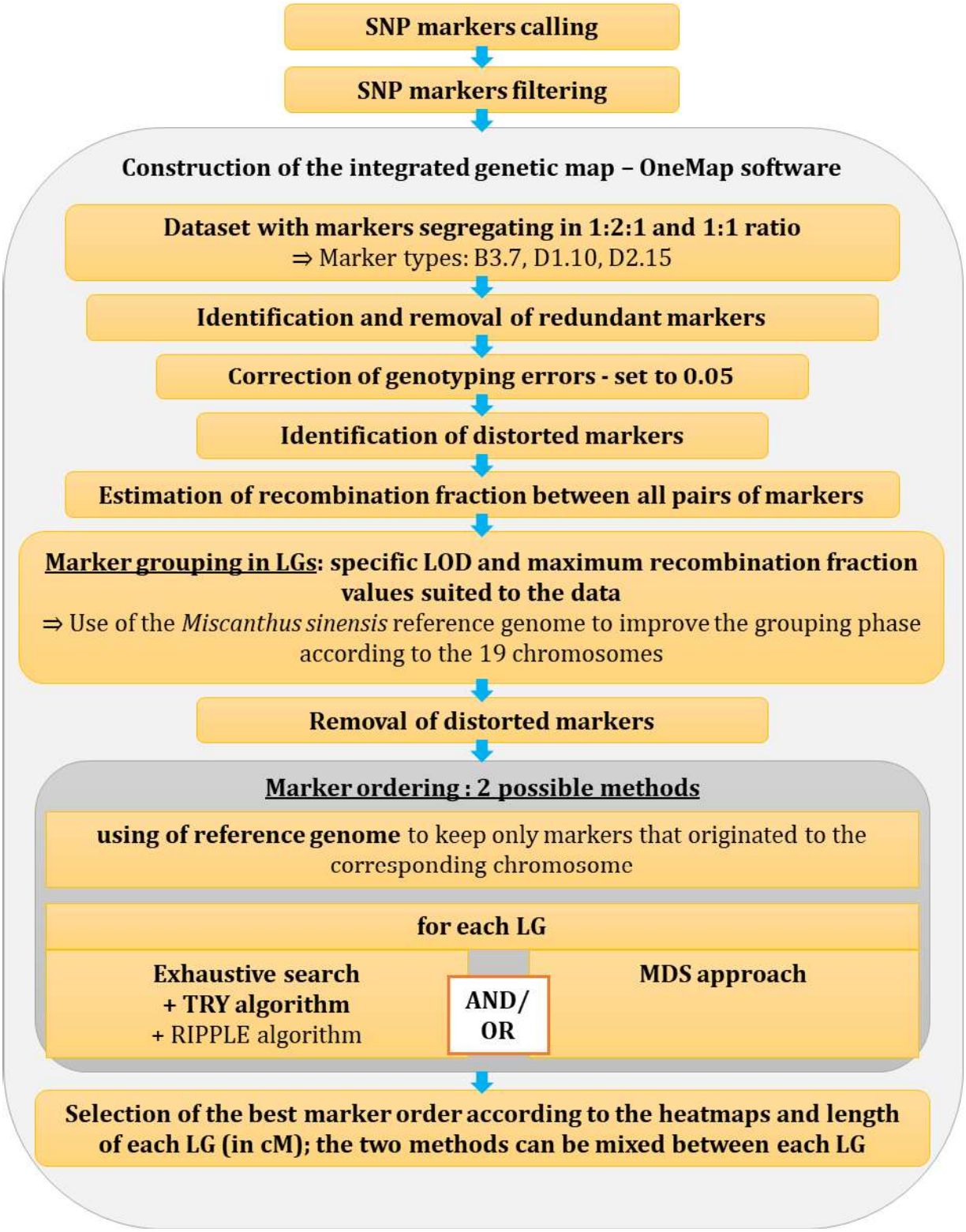


**Figure 7.** Schematic overview of the genetic map construction pipeline. Step-by-step workflow from SNP calling and filtering to marker grouping, ordering and final consensus map construction (Raphaël Raverdy, Kristelle Lourgant).

Marker ordering and estimation of genetic distances were performed using multipoint hidden Markov model approaches adapted for outcrossing species (Wu et al., 2002) and implemented in OneMap. Genetic distances were computed using the Kosambi mapping function (Kosambi, 1943). A genotyping error probability of 0.05 was specified in the hidden Markov model to account for uncertainty between observed and estimated genotypes (Taniguti et al., 2023).

The only methodological difference compared with Raverdy et al. (2022) concerns marker ordering: in the present study, marker order was inferred from recombination information and multipoint likelihoods rather than imposed primarily by physical genome position.

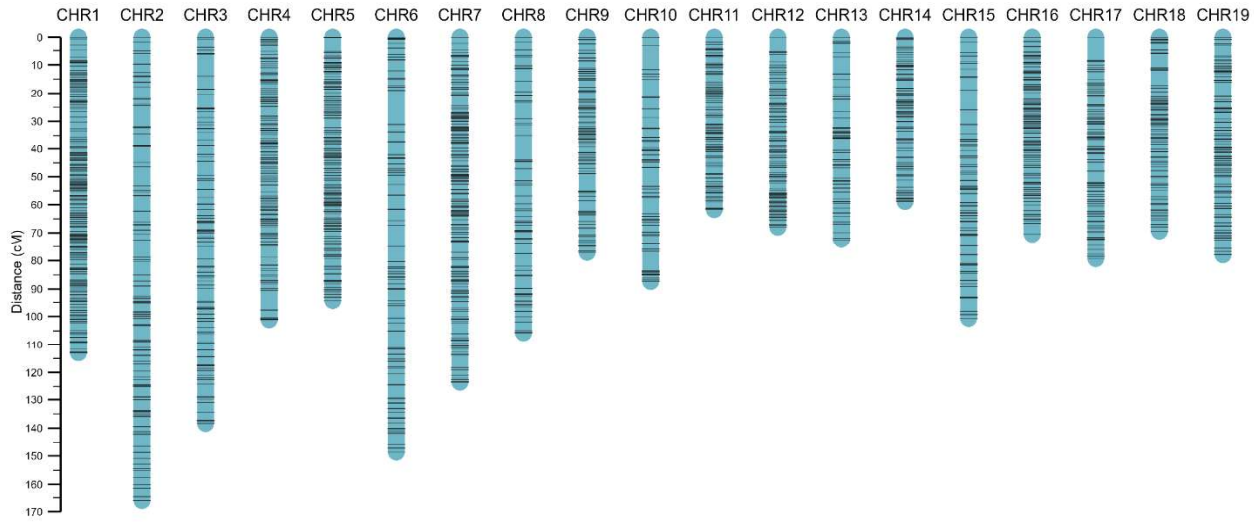


**Figure 8.** Integrated genetic map of the *Miscanthus sinensis* progeny. Consensus linkage map showing the 19 linkage groups with ordered SNP markers and genetic distances (cM) (Kristelle Lourgant).

The resulting integrated genetic map of the *Miscanthus sinensis* progeny provided the genetic framework for subsequent QTL analyses and is presented in Figure 8.

## 9. QTL detection framework

QTL detection for nitrogen economy traits and associated proxy traits was conducted using the integrated genetic map described above. QTL analyses were performed within a composite interval mapping (CIM) framework specifically adapted to full-sib outcrossing populations, which is detailed in Chapter 3. Genotypic values were used as phenotypic inputs for genome scans.

For each trait, genome-wide scans were carried out along the 19 linkage groups to identify genomic regions associated with variation in nitrogen uptake, spring and autumn

remobilization, nitrogen losses and their related proxy traits. Genome-wide significance thresholds were defined by permutation testing, and confidence intervals were determined using the LOD profile along the linkage groups. Detailed parameter settings, threshold definition procedures, and trait-by-trait results are fully presented in Chapter 3.

QTL co-location analyses were then performed to evaluate whether nitrogen economy traits and predictive proxy traits shared common genomic regions. Co-location was assessed based on positional overlap between QTL confidence intervals using the same genetic-map reference scale to ensure direct comparability. This analysis was used to evaluate whether relationships between proxy traits and nitrogen economy traits reflected shared genetic determinism, with detailed analyses provided in Chapter 3.

Finally, the potential for QTL mapping related to plant nitrogen management was explored through the estimation of allelic effects and QTL pyramiding, combining up to three QTLs.

*Altogether, this integrated experimental design connects field experimentation, physiological quantification, predictive phenotyping and genetic analysis within a single population. It provides the basis on which the subsequent results chapters are structured: the characterization of nitrogen economy diversity in the progeny, the development of proxy-based prediction tools, and the identification of genomic regions associated with nitrogen economy traits. Building on this common framework, the following chapters successively present these results, moving from phenotypic characterization to predictive modelling and genetic analysis.*

## References

Beale, C., & Long, S. (1997). Seasonal dynamics of nutrient accumulation and partitioning in the perennial C4-grasses *Miscanthus* × *giganteus* and *Spartina cynosuroides*. *Biomass and Bioenergy*, *12*(6), 419–428.

Brancourt-Hulmel, M. (1999). Crop diagnosis and probe genotypes for interpreting genotype × environment interaction in winter wheat trials. *Theoretical and Applied Genetics*, *99*, 1018–1030.

Cormier, F., Throude, M., Ravel, C., Le Gouis, J., & Praud, S. (2019). Development of a cost-effective SNP genotyping array for wheat and its application in genetic studies. *Ecology and Evolution*, *9*(11), 6205–6216. https://doi.org/10.1002/ece3.5141

Elshire, R. J., Glaubitz, J. C., Sun, Q., Poland, J. A., Kawamoto, K., Buckler, E. S., & Mitchell, S. E. (2011). A robust, simple genotyping-by-sequencing (GBS) approach for high diversity species. *PLoS One*, *6*(5), e19379. https://doi.org/10.1371/journal.pone.0019379

Iqbal, S., Brancourt-Hulmel, M., & Zapater, M. (2026). Nitrogen economy strategies define distinct functional groups of genotypes in a *Miscanthus sinensis* progeny. *GCB Bioenergy*, *18*(1), e70096. https://doi.org/10.1111/gcbb.70096

Kosambi, D. D. (1943). The estimation of map distances from recombination values. *Annals of Eugenics*, *12*(1), 172–175. https://doi.org/10.1111/j.1469-1809.1943.tb02321.x

Laperche, A., Le Gouis, J., Hanocq, E., & Brancourt-Hulmel, M. (2008). Modelling nitrogen stress with probe genotypes to assess genetic parameters and genetic determinism of winter wheat tolerance to nitrogen constraint. *Euphytica*, *161*(1), 259–271.

Leroy, J., Ferchaud, F., Giauffret, C., Mary, B., Fingar, L., Mignot, E., Arnoult, S., Lenoir, S., Martin, D., & Brancourt-Hulmel, M. (2022). *Miscanthus sinensis* is as efficient as *Miscanthus* × *giganteus* for nitrogen recycling in spite of smaller nitrogen fluxes. *BioEnergy Research*, *15*(2), 686–702.

Margarido, G. R., Souza, A. P., & Garcia, A. A. F. (2007). OneMap: Software for genetic mapping in outcrossing species. *Hereditas*, *144*(3), 78–79.

Mitros, T., Session, A. M., James, B. T., Wu, G. A., Belaffif, M. B., Clark, L. V., Shu, S., Dong, H., Barling, A., Holmes, J. R., Mattick, J. E., Bredeson, J. V., Liu, S., Farrar, K., Głowacka, K., Jeżowski, S., Barry, K., Chae, W. B., Juvik, J. A., Gifford, J., Oladeinde, A., Yamada, T., Grimwood, J., Putnam, N. H., Vega, J. J. D., Barth, S., Klaas, M., Hodkinson, T., Li, L., Jin, X., Peng, J., Yu, C. Y., Heo, K., Yoo, J. H., Ghimire, B. K., Donnison, I. S., Schmutz, J., Hudson, M. E., Sacks, E. J., Moose, S. P., Swaminathan, K., & Rokhsar, D. S. (2020). Genome biology of the paleotetraploid perennial biomass crop *Miscanthus*. *Nature Communications*, *11*, 5442. https://doi.org/10.1038/s41467-020-18923-6

Oury, F.-X., & Godin, C. (2007). Yield and grain protein concentration in bread wheat: How to use the negative relationship between the two characters to identify favourable genotypes? *Euphytica*, *157*(1), 45–57.

Raverdy, R., Lourgant, K., Mignot, E., Arnoult, S., Bodineau, G., Griveau, Y., Taniguti, C. H., & Brancourt-Hulmel, M. (2022). Linkage mapping of biomass production and composition traits in a *Miscanthus sinensis* population. *BioEnergy Research*. https://doi.org/10.1007/s12155-022-10402-8

Strullu, L., Cadoux, S., Preudhomme, M., Jeuffroy, M.-H., & Beaudoin, N. (2011). Biomass production and nitrogen accumulation and remobilisation by *Miscanthus* × *giganteus* as influenced by nitrogen stocks in belowground organs. *Field Crops Research*, *121*(3), 381–391.

Taniguti, C. H., Taniguti, L. M., Amadeu, R. R., Lau, J., Gesteira, G. S., Oliveira, T. P., Ferreira, G. C., Pereira, G. S., Byrne, D., & Mollinari, M. (2023). Developing best practices for genotyping-by-sequencing analysis in the construction of linkage maps. *GigaScience*, *12*, giad092.

Wu, R., Ma, C.-X., Painter, I., & Zeng, Z.-B. (2002). Simultaneous maximum likelihood estimation of linkage and linkage phases in outcrossing species. *Theoretical Population Biology*, *61*(3), 349–363.

Zapater, M., Catterou, M., Mary, B., et al. (2017). A single and robust critical nitrogen dilution curve for *Miscanthus* × *giganteus* and *Miscanthus sinensis*. *BioEnergy Research*, *10*(1), 115–128. https://doi.org/10.1007/s12155-016-9781-8

# Chapter 1

***Chapter 1 objectives and methodology within the overall thesis framework.***

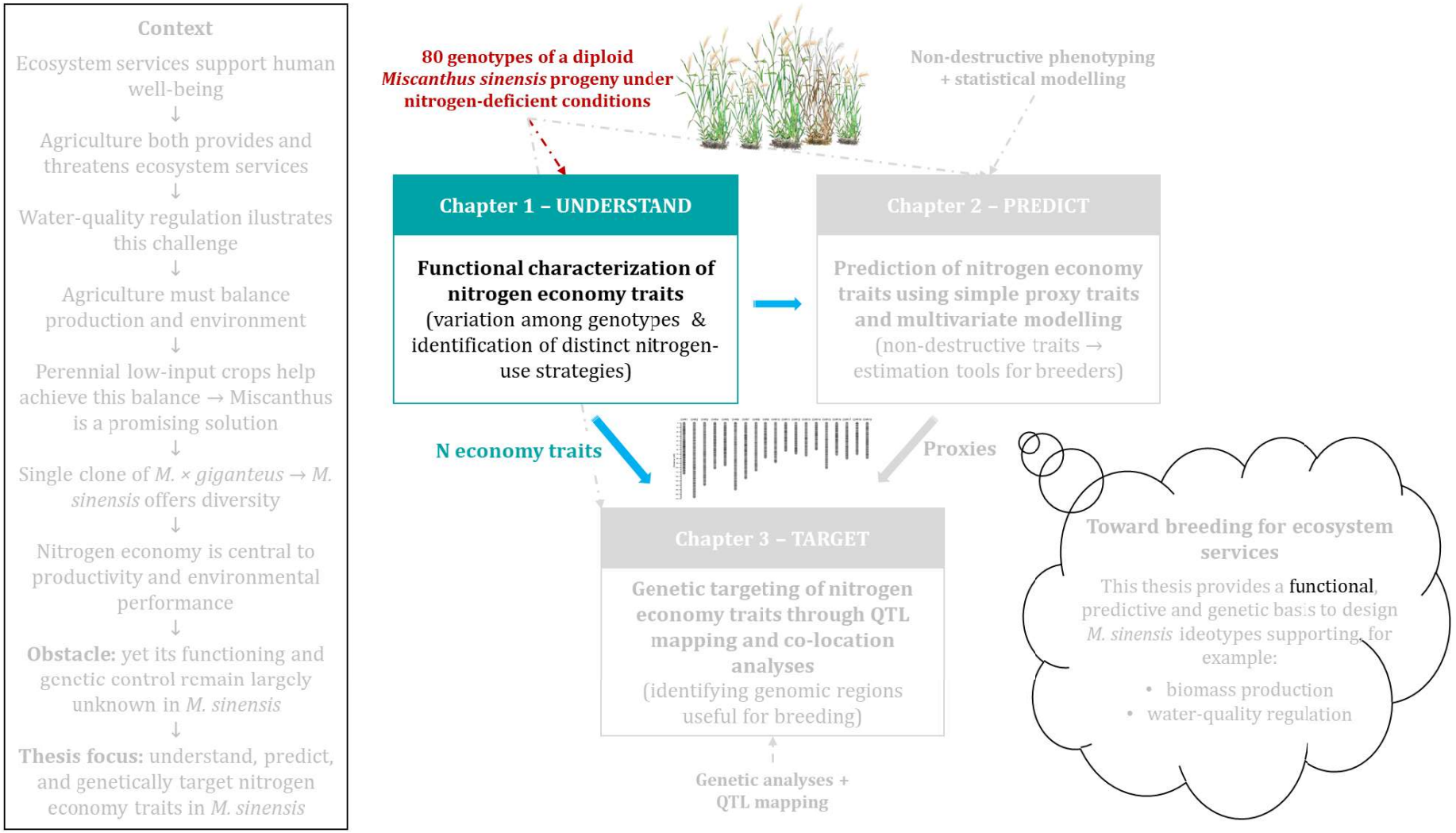

*GCB Bioenergy*

WILEY

Global Change Biology Bioenergy
BIOPRODUCTS FOR A SUSTAINABLE BIOECONOMY

RESEARCH ARTICLE OPEN ACCESS

# Nitrogen Economy Strategies Define Distinct Functional Groups of Genotypes in a *Miscanthus sinensis* Progeny

Shehyar Iqbal | Maryse Brancourt-Hulmel | Marion Zapater

BioEcoAgro Joint Research Unit, INRAE, Univ de Liege, Univ Lille, Univ Picardie Jules Verne, Chaussée Brunehaut, Entrées-Mons, France

**Correspondence:** Maryse Brancourt-Hulmel (maryse.hulmel@inrae.fr)

**Received:** 7 July 2025 | **Revised:** 4 November 2025 | **Accepted:** 18 November 2025

**Keywords:** bioenergy | ecosystem services | functional groups | intra-specific variability | nitrogen economy | nitrogen fluxes | nitrogen recycling | nitrogen uptake | perennial crop

## ABSTRACT

Understanding nitrogen-use strategies in *Miscanthus sinensis* is essential for optimizing biomass production while minimizing environmental impact, and providing sustainable bioenergy and ecosystem services. Nitrogen recycling in *M. sinensis* is known to be efficient, but the extent of intra-specific variability and its translation into distinct functional strategies remain unknown to date. Our objective was to assess the intergenotypic variation in nitrogen uptake and recycling and their relation to biomass yield in a diploid *M. sinensis* progeny. Endogenous remobilization fluxes were calculated for 80 genotypes from seasonal nitrogen dynamics under nitrogen deficient conditions, showing substantial intergenotypic variation, ranging from 0.2 to 85 kg N $ha^{-1}$ in spring and 5 to 158 kg N $ha^{-1}$ in autumn. Recycling efficiency, defined as the remobilized nitrogen relative to maximum nitrogen quantity, did not correlate with biomass yield, indicating that nitrogen recycling was independent of plant size. Exogenous nitrogen uptake varied widely (5–241 kg N $ha^{-1}$) and was strongly correlated with biomass yield ($r = 0.72$), making it the dominant factor influencing productivity, while principal component analysis highlighted the contribution of nitrogen recycling traits. Three functional groups emerged from hierarchical clustering on the principal components. The first group comprised nitrogen-acquisitive genotypes with high uptake and productivity, suitable for low-input bioenergy systems and potential ecosystem services like nitrate removal in water catchment areas. The second group followed a conservative strategy, with efficient belowground nitrogen storage and endogenous recycling, supporting resilience to environmental stress. The third group comprised nitrogen-deficient genotypes with low uptake, remobilization, and productivity. These findings demonstrate that substantial variation in nitrogen economy traits defined distinct functional groups in *M. sinensis*, providing a framework for breeding ideotypes that sustain biomass under nitrogen-limited conditions through enhanced uptake or remobilization, while delivering ecosystem services through contrasting remobilization strategies that can support nutrient retention, soil nitrogen conservation, and water quality regulation.

## 1 | Introduction

The concept of ecosystem services arises from the observation that by degrading ecosystems, societies compromise their own well-being by losing the benefits provided by nature (Barnaud and Muradian 2024). A crop like miscanthus can play a role in such a context, as Tavakoli-Hashjini et al. (2020) identified it as a multifunctional crop providing provisioning services (energy), supporting services (soil formation, nutrient cycling, water holding capacity, and biodiversity), regulating services (climate regulation, water regulation, pollination), and cultural and socio-economic services. In particular, the water regulation service is of special interest in water catchment areas to maintain the quality of drinking water. For instance, Weik et al. (2022)

have proposed the cultivation of miscanthus in water catchment areas in some German regions as a contribution to mitigating the negative impacts of increasing nitrate levels in the soil. Such ecosystem benefits are further supported by miscanthus's ability to reduce nitrate leaching (Cibin et al. 2016; Ferrarini et al. 2017), manage inorganic and organic contaminated land, and restore ecosystem services (Nsanganwimana et al. 2014).

In this context, the cultivation of miscanthus, based on the interspecific hybrid *Miscanthus* × *giganteus*, is interesting, as this rhizomatous perennial grass is highly productive and can remobilize nitrogen (N) from aboveground to belowground organs in autumn so that the stems harvested in winter have a low mineral nutrient quantity (Beale and Long 1997; Strullu et al. 2011; Magenau et al. 2022). The nitrogen stored in the rhizomes is then available for the following year of growth thanks to its remobilization during spring regrowth, which reduces the need for exogenous nitrogen inputs (Strullu et al. 2011). These two processes are known as autumn and spring remobilization, respectively. Harvest can be carried out every year, mainly at the end of winter, when the stems are senescent, to maintain the sustainability of the crop, as early harvesting depletes belowground nitrogen stocks and therefore increases the need for exogenous nitrogen inputs (Strullu et al. 2011). In addition to high amounts of biomass, it has several environmentally favorable traits, such as low nitrate losses (Lesur et al. 2014), high water-use efficiency (Ferchaud and Mary 2016), and low nitrogen input needs as defined by its critical nitrogen dilution curve (Zapater et al. 2017). In their review, Cadoux et al. (2012) link these low requirements to (1) high nutrient uptake, (2) high absorbed nutrient efficiency, (3) significant spring nutrient remobilization, (4) efficient autumn nutrient remobilization, which is an important trait linked to the perennial nature of the crop, and lastly (5) a potential contribution of nitrogen fixation by bacteria. Moreover, it has demonstrated potential for phytostabilization on trace element-contaminated soils (Nsanganwimana et al. 2021).

Despite these favorable characteristics, a single sterile triploid clone of *Miscanthus* × *giganteus* (Greef et al. 1997; Głowacka et al. 2015) is currently grown commercially for biomass production (Ben Fradj et al. 2020; Kumari et al. 2024), which is risky in the case of new environmental pressures (climate, pathogens) and is even more serious as it is a perennial crop. *Miscanthus sinensis* is targeted for the development of new varieties because it can offer good performance in terms of biomass production (Arnoult and Brancourt-Hulmel 2015) and a composition suitable for new markets (Belmokhtar et al. 2017; Codina Gironès et al. 2017). It also shows good tolerance to frost (Farrell et al. 2006; Zub et al. 2012), water deficit conditions, including drought (van der Weijde et al. 2017; Nie et al. 2017; Stavridou et al. 2019; Weng et al. 2022), and flooding stress (De Vega et al. 2021), as well as salt stress (Chen et al. 2017; van der Cruijsen et al. 2024). In addition, it also has good capacity for carbon sequestration (Briones et al. 2023) and phytoremediation (Zheng et al. 2022). It exhibits high intra-specific genetic variability (Sun et al. 2010; Zhao et al. 2013), which could help secure and expand the production area while maintaining decent yields. Like *M.* × *giganteus*, *M. sinensis* also exhibits nitrogen recycling capacities by efficiently remobilizing nitrogen during spring and autumn (Leroy et al. 2022), allowing nutrient-depleted stems at harvest and supporting growth under nitrogen-poor conditions (Lewin et al. 2024).

However, while the existence of nitrogen recycling in *M. sinensis* is established, the extent of its variability within the species remains poorly documented. Leroy et al. (2022) report variability in nitrogen recycling between two *M. sinensis* genotypes, suggesting that such variability may be widespread. Yet, beyond these isolated comparisons, no systematic evaluation has been carried out to characterize intra-specific diversity in nitrogen recycling. Whether this diversity leads to distinct nitrogen-use or nitrogen-economy strategies within *M. sinensis* is still an open question. Functional groups are often used to classify genotypes based on shared physiological traits, enabling researchers to identify plant types with distinct resource-use patterns (Byun et al. 2013; Fry et al. 2014). Yet, no such studies have been conducted to date for nitrogen-economy-related traits in *M. sinensis*, underlining the need to better understand how this variability may translate into functional differences among genotypes.

This study aimed to evaluate the intergenotypic diversity in nitrogen economy in a progeny of *M. sinensis* through the ability to reuse nitrogen stored in belowground parts. We hypothesized that the progeny would exhibit substantial functional diversity among genotypes, with variability across nitrogen-economy-related traits. Leroy et al. (2022) observed notable differences in nitrogen recycling between two genotypes, suggesting broader variability within the species. Analyzing variation between two parental cultivars and their progeny therefore provides a valuable framework to begin addressing this gap, while also laying the groundwork for broader studies across more genetically diverse accessions. Furthermore, we hypothesized that this diversity would follow structured patterns, leading to the formation of distinct functional groups. Rather than displaying a continuous gradient of nitrogen economy or nitrogen-use-related traits, the *M. sinensis* progeny may segregate into groups where some genotypes rely predominantly on nitrogen remobilization while others depend more on continuous uptake. To our knowledge, this is the first study to evaluate intra-specific variability in nitrogen economy in *M. sinensis* at the progeny scale, addressing a critical gap in understanding the species' nitrogen-use strategies. Furthermore, it pioneers the use of hierarchical clustering on principal components to identify distinct functional groups, providing new insights into how genotypic diversity shapes nitrogen-use strategies with direct implications for breeding and ecosystem service applications.

## 2 | Materials and Methods

### 2.1 | Experimental Site and Trial Design

The field experiment was conducted at the French National Research Institute for Agriculture, Food, and Environment (INRAE) in Estrées-Mons, northern France (49°87′ N, 3°01′ E). The site belonged to the UE GCIE, Unité Expérimentale Grandes Cultures Innovation Environnement (doi: 10.15454/1.5572425838988464E12). Regarding climatic data, the site experienced a marine west coast climate (Cfb). Over the last 8 years (2017–2024), the experimental site was characterized by a mean annual temperate of 11.2°C and an average annual

precipitation of 675 mm. During the growing season of the study (February 2023 to February 2024), the mean temperature was 11.4°C, and the mean precipitation was 925 mm.

The study was carried out over the 2023–2024 growing season and included two complementary field trials: the progeny trial and the parental trial. The progeny trial comprised 127 *Miscanthus sinensis* genotypes derived from a diploid cross between *M. sinensis* 'Malepartus' (MAL) and 'Herman Mussel' (HER). Seeds resulting from the cross were germinated in vitro in 2014. The resulting seedlings were planted in a greenhouse in 2015 and then transferred to Orléans in 2016, where the plants were clonally propagated by dividing rhizomes in 2017. The trial at Estrées-Mons was established in 2018 using an incomplete block design with four blocks and a planting density of 1 plant $m^{-2}$. A subset of 80 genotypes was selected for detailed analysis of nitrogen uptake and remobilization. Each genotype was represented by at least one replicate in each block. The parental trial, established with the two parental genotypes (MAL and HER), included increased replications with 15 plants per genotype at each sampling date (60 replications per genotype per season) and extended sampling over two growing seasons (2023–2024 and 2024–2025) to support the characterization of nitrogen status in the progeny trial. In the progeny trial, plant emergence occurred between March 24 and April 11, 2023. The duration of the growing season, defined as the time from emergence to complete senescence (95% of the aboveground part senesced by visual scoring) ranged from 201 to 270 days across genotypes. On average, 50% senescence was reached on Day of Year (DOY) 304, while 95% senescence occurred around DOY 333. Both the progeny and parental trials were unfertilized and irrigated throughout the 5 years of cultivation to ensure non-limiting water conditions. Recorded irrigation volumes for the years 2021 to 2023 amounted to 36, 926, and 393 $m^3$ in the progeny trial, and 140, 738, and 521 $m^3$ in the parental trial, respectively.

From establishment in 2018 until 2023, management primarily consisted of standard agronomic practices, including manual weed control, with no chemical inputs applied, and the plants were harvested each year in February. Leaf litter and other plant residues senesced naturally during autumn to winter and were left on the soil surface. During the 2023–2024 measurement cycle, however, fallen leaves from plants designated for the fourth (February 2024) sampling were systematically collected. Nets were installed over these plants throughout the senescence period, and leaves were gathered at regular intervals to quantify nitrogen losses through fallen leaves.

The soils at the Estrées-Mons site are deep silt loam, classified as Haplic Luvisols (IUSS Working Group WRB 2022). Soil texture was approximately 16.5% clay, 72.7% silt, and 7.8% fine sand, with a near-neutral pH (7.9), a high cation exchange capacity (96.8 meq 100 $g^{-1}$), and a moderate organic carbon content (11.4 g $kg^{-1}$; C/N = 10.6). These physicochemical characteristics were determined in 2017 and are considered representative of the site's baseline fertility. Soil mineral nitrogen concentrations were measured in both the progeny and parental trials over the 0–150 cm depth in early spring. In March 2023, the mean soil mineral N concentrations were 20 kg N $ha^{-1}$ in the progeny trial and 13 kg N $ha^{-1}$ in the parental trial. In March 2024, these values increased to 29 kg N $ha^{-1}$ and 25 kg N $ha^{-1}$, respectively. These levels were markedly lower than those recorded in a previously studied, fertilized trial, located at the same site, in which 120 kg N $ha^{-1}$ was applied as a urea-ammonium-nitrate solution in May. In which the soil mineral N concentrations measured in March or April over the 0–150 cm profile were 85, 85, 53, and 54 kg N $ha^{-1}$ in 2014, 2015, 2016, and 2017, respectively (Leroy et al. 2022).

During each plant sampling campaign, soil N concentrations were also measured in the 0–30 cm horizon, where most root activity occurs. In the progeny trial, mean values were 8 kg N $ha^{-1}$ in March 2023, 11 kg N $ha^{-1}$ in July 2023, 12 kg N $ha^{-1}$ in September 2023, and 19 kg N $ha^{-1}$ in March 2024. In the parental trial, corresponding values were 5 kg N $ha^{-1}$ in March 2023, 8 kg N $ha^{-1}$ in August 2023, 10 kg N $ha^{-1}$ in September 2023, 15 kg N $ha^{-1}$ in March 2024, 16 kg N $ha^{-1}$ in July 2024, and 15 kg N $ha^{-1}$ in September 2024.

The nitrogen status of the progeny trial was assessed using the genotype *Miscanthus sinensis* 'Malepartus' (MAL), which served as a probe genotype. A probe genotype, as defined by Brancourt-Hulmel (1999), helps to diagnose nitrogen limitation through the nitrogen nutrition index (NNI) (Justes et al. 1994). MAL was chosen because it is one of the two parents of the progeny and, importantly, was present across all three reference trials: the unfertilized progeny trial, the unfertilized parental trial, and the historical fertilized trial (Leroy 2021). This allowed a direct comparison across nitrogen-limited and nitrogen-sufficient conditions, making it possible to diagnose the nitrogen status of the progeny trial.

The NNI was calculated as the ratio between the actual nitrogen concentration in the aboveground vegetative parts ($N_a$) and the critical nitrogen concentration ($N_c$), defined as the minimum concentration required to achieve maximum biomass production.

$$NNI = \frac{N_a}{N_c}$$

For *M. sinensis*, this critical nitrogen concentration was determined using the nitrogen dilution curve established by Zapater et al. (2017):

$$N_c = 23.4\ W^{-0.42} \text{ when } W > 1 \text{ t ha}^{-1}$$
$$\text{and } N_c = 23.4 \text{ when } W \leq 1 \text{ t ha}^{-1}$$

where $W$ is the aboveground dry biomass (t $ha^{-1}$).

NNI was calculated with aboveground biomass and nitrogen concentration data for MAL, collected in July 2023 from the two previous trials represented by blue and red points, respectively, in Figure 1. These values were compared with historical data from 2016 and 2017 collected in the fertilized trial in July as well (Leroy 2021). In Figure 1, MAL data from the fertilized trial (green triangles) were positioned, as expected, close to or above the critical dilution curve, indicating nitrogen sufficiency or luxury status. In contrast, all MAL data points from the progeny and parental trials, both unfertilized, (red and blue) fell consistently below the curve, indicating nitrogen deficiency in both trials.

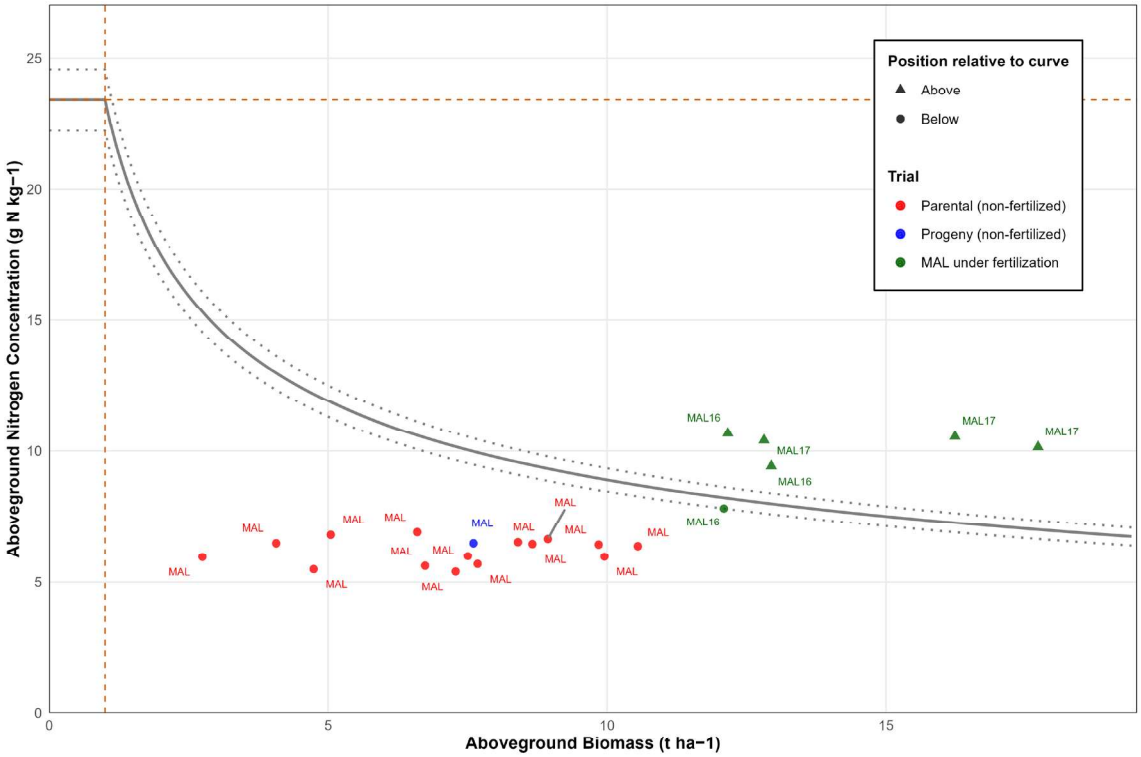


**FIGURE 1** | Relationship between aboveground nitrogen concentration and aboveground biomass of *Miscanthus sinensis* (Malepartus), sampled across three field trials with contrasting soil nitrogen availability. Red and blue points represent samples from two non-fertilized trials (parental and progeny) collected in July 2023, while green points represent samples from a fertilized trial (120 kg N $ha^{-1}$ applied as UAN) collected in 2016 and 2017. The black curve depicts the critical nitrogen dilution curve for *M. sinensis*, given by the equation: $Nc = 23.4 \times W^{-0.42}$ for $W > 1$ t $ha^{-1}$, $Nc = 23.4$ for $W \leq 1$ t $ha^{-1}$ (Zapater et al. 2017), where Nc is the critical nitrogen concentration (g N $kg^{-1}$) and W is the aboveground biomass (t $ha^{-1}$). Dotted lines represent a ±5% confidence interval around the critical nitrogen dilution curve.

This diagnosis confirmed that the studied progeny trial was nitrogen-deficient for the probe genotype, suggesting that nitrogen availability may also be a limiting factor for other genotypes. NNI values calculated across the progeny population showed variation, with some genotypes classified as nitrogen-deficient and others as nitrogen-sufficient (data not shown).

## 2.2 | Plant Sampling

Plant sampling was carried out during four campaigns between February 2023 and February 2024 to assess nitrogen fluxes and remobilization dynamics in the *Miscanthus sinensis* progeny, following a refined protocol based on Leroy et al. (2022) (Figure 2). On each sampling date, both aboveground parts (AP: stems and leaves) and belowground parts (BP: rhizomes and associated roots) were collected to determine nitrogen quantities associated with specific stages of the plant's annual growth cycle. Rhizomes and associated roots were sampled to a maximum depth of approximately 30–40 cm, which corresponded to the maximum rhizome depth.

Each sampling date represented a key period in the annual cycle, characterized by distinct nitrogen stocks in the aboveground and belowground parts of the plants: February 2023 (dormancy, representing maximum nitrogen quantity in belowground parts), July 2023 (minimum nitrogen quantity in belowground parts), September 2023 (maximum nitrogen quantity in aboveground parts during active growth), and February 2024 (end of the growth cycle, when nitrogen had been remobilized to belowground parts for winter dormancy).

The samplings were conducted on 80 genotypes from the progeny trial, along with the two parental genotypes in the parental trial. Of the progeny genotypes, 65 had at least four replicates each, allowing one plant per genotype to be sampled on each of the four sampling dates. The remaining 15 genotypes had at least eight replicates each, which allowed two plants per genotype to be sampled per date, providing within-date replication for the analysis of variance.

## 2.3 | Plant Measurements and Determination of Biomass and Nitrogen Concentration

At each sampling date, the collected aboveground and belowground plant parts were used to assess biomass and nitrogen concentration. Aboveground plant parts were harvested at 7 cm above the soil surface, a commonly used cutting height in miscanthus plot trials (Cadoux et al. 2014; Scordia et al. 2022), consistent with standard mechanical harvesting practices. In our study, aboveground biomass included both the harvested part and the basal stems remaining below the cutting height, which were collected during rhizome excavation to ensure complete accounting of aboveground biomass and better reflect biomass and nitrogen dynamics. Belowground parts were excavated

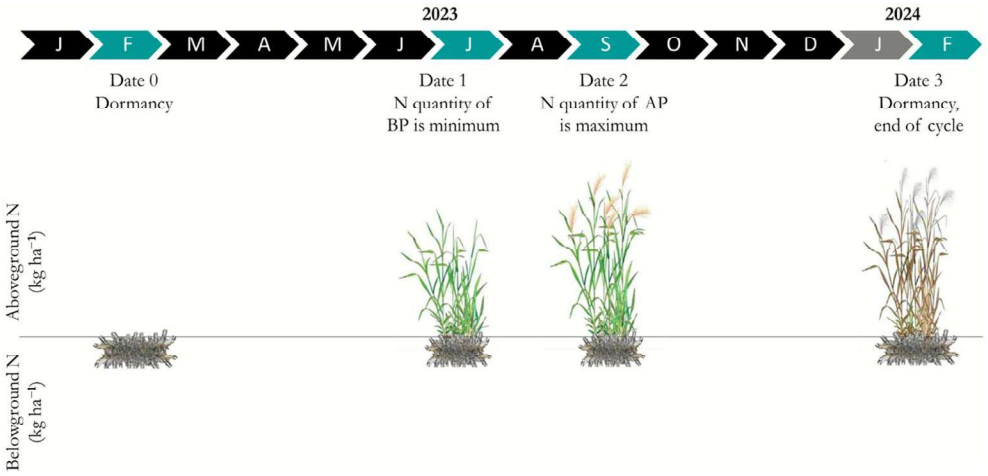


**FIGURE 2** | Seasonal evolution of nitrogen stocks in the aboveground and belowground parts during key periods of nitrogen recycling over the course of 1 year (plant cycle). Adapted from Hou et al. (2022) and Leroy et al. (2022).

as described previously. The collected samples were weighed fresh, and a representative subsample was taken for dry matter determination. The subsample was weighed fresh, dried at 65°C for 96 h until a constant weight had been achieved, and then weighed again to determine dry weight. The dry matter content was calculated as:

$$\text{Dry Matter Content} = \text{Dry weight of subsample} / \text{Fresh weight of subsample}$$

This dry matter content was then used to estimate the dry biomass of the entire sample:

$$\text{Dry Biomass} = \text{Fresh Weight of Entire Plant} \times \text{Dry Matter Content}$$

Biomass yield ($t\,ha^{-1}$) was subsequently determined based on the dry biomass and the planting density.

Corrections of the raw biomass data were made to reduce potential bias due to a plant effect, as sampling belowground biomass is a destructive process. The same plants could not be reused on several sampling dates. As a result, a different plant for each genotype was sampled at each of the four time points, leading to plant-to-plant variability between the four plants sampled. This plant effect introduced potential bias in nitrogen flux calculations due to confounding between the nitrogen fluxes and the plant effect.

To mitigate this bias, the adjustment was based on aboveground biomass, given its strong and stable correlation with belowground biomass ($r = 0.85$ in February 2023; $r = 0.84$ in February 2024, Figure 3). The procedure followed four steps:

Step 1. Calculate the mean aboveground biomass of all plants per genotype sampled in the preceding years (February 2022 and February 2023).

Step 2. Determine the mean aboveground biomass of each individual plant across the two preceding years (February 2022 and February 2023).

Step 3. Compute a correction percentage for each plant:

$$\text{Correction Percentage} = (\text{Mean Biomass per Plant} / \text{Mean Biomass per Genotype}) \times 100$$

Step 4. Apply this correction percentage to both aboveground and belowground biomass values:

$$\text{Adjusted Value} = (\text{Raw Value} / \text{Correction Percentage}) \times 100$$

By applying this correction, the bias introduced by plant-to-plant variability was minimized, allowing for more reliable nitrogen flux calculations between sampling dates.

The nitrogen concentration of each sample was analyzed to quantify nitrogen fluxes and recycling rates across different growth stages.

The total nitrogen quantity of the plant was calculated as follows:

$$NA = WA \times [NA]$$
$$NB = WB \times [NB]$$
$$NT = NA + NB$$

where NA and NB represent the nitrogen quantity ($kg\,N\,ha^{-1}$) in aboveground and belowground compartments, respectively, WA and WB correspond to the dry matter quantity of each compartment ($t\,ha^{-1}$), and [NA] and [NB] are the corresponding nitrogen concentrations ($g\,N\,kg^{-1}$ DM).

## 2.4 | Quantification of Nitrogen Remobilization, Uptake, and Corresponding Use Efficiencies

Nitrogen-economy traits were evaluated, including nitrogen fluxes, uptake, and remobilizations, along with their corresponding efficiencies. Nitrogen remobilization was assessed separately for spring and autumn through two complementary approaches: spring and autumn remobilization.

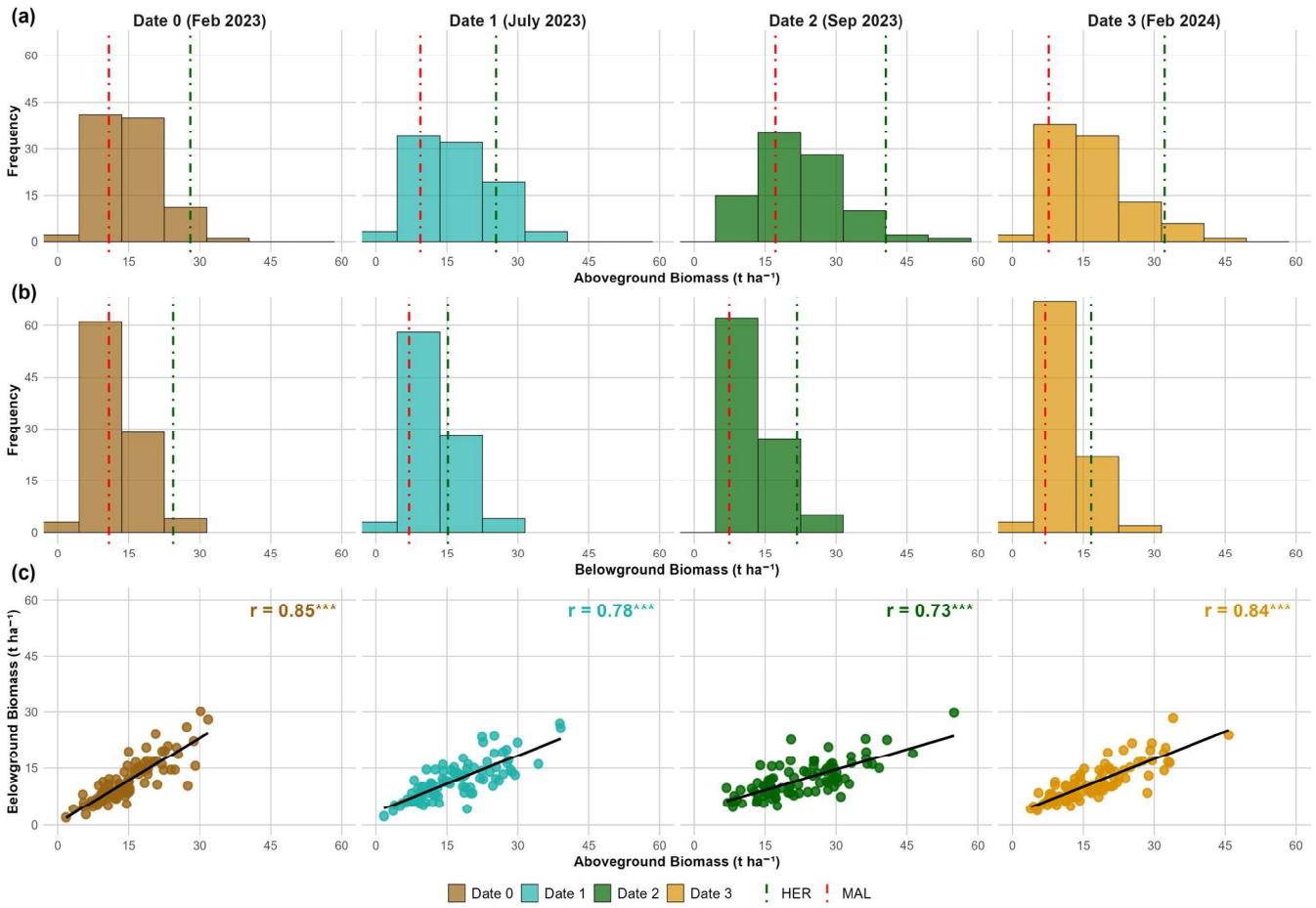


**FIGURE 3** | Distribution of aboveground and belowground biomass (plots a and b) and their correlation (plot c) across four sampling dates during the 2023–2024 plant cycle. At Date 0, aboveground biomass belongs to the end of the previous plant cycle, whereas belowground biomass corresponds to both the end of the previous cycle and the beginning of the new one. The green and red dashed lines indicate the parental genotypes HER and MAL, respectively.

Spring remobilization (SR, kg N ha$^{-1}$), representing the nitrogen translocated from belowground storage organs to support new shoot growth in spring, was calculated following the method of Strullu et al. (2011) as:

$$SR = NB_0 - NB_1$$

where $NB_0$ was the nitrogen quantity in the belowground parts before spring regrowth (February 2023), and $NB_1$ was the nitrogen quantity after spring remobilization (July 2023), during summer.

The corresponding spring remobilization efficiency was calculated relative to maximum aboveground nitrogen quantity ($NA_2$):

$$SRE = \left(SR / NA_2\right) \times 100$$

Autumn remobilization (AR, kg N ha$^{-1}$), defined as the nitrogen withdrawn from senescing aboveground parts and stored in belowground organs before dormancy, was estimated using two methods described by Dierking et al. (2017): via aboveground method (ARa) and via belowground method (ARb).

$$ARa = NA_2 - NA_3$$

where $NA_2$ was the nitrogen quantity in aboveground parts at the start of senescence (September 2023), and $NA_3$ was the nitrogen quantity after full senescence (February 2024). ARa corresponds to the proportion of N in the aboveground part withdrawn during senescence.

$$ARb = NB_3 - NB_2$$

where $NB_3$ was the nitrogen quantity in belowground parts after full senescence (February 2024), and $NB_2$ was the nitrogen quantity in the belowground parts when aboveground nitrogen reached its maximum (September 2023). ARb corresponds to the proportion of N effectively withdrawn from the aboveground part that was finally stored in the rhizome.

As with spring remobilization efficiency, the corresponding autumn remobilization efficiencies were also calculated relative to maximum aboveground nitrogen quantity and were coded as ARaE and ARbE, respectively.

The nitrogen uptake (N Uptake, kg N ha$^{-1}$) represents the maximum nitrogen acquired from the soil during the growing season. It was calculated as:

$$N\ Uptake = NT_2 - NB_0$$

where $NT_2$ was the total nitrogen quantity of the whole plant at date 2 (September 2023), when aboveground biomass reached its peak nitrogen accumulation, and $NB_0$ was the nitrogen quantity in belowground parts before spring regrowth (February 2023). Similar to SRE, the corresponding nitrogen uptake efficiency was calculated relative to the maximum aboveground nitrogen quantity.

The nitrogen losses (N losses, kg N $ha^{-1}$) were calculated following the method of Leroy et al. (2022), considering the difference between total nitrogen at the peak of the growing season and after complete senescence:

$$\text{N losses} = NT_2 - NT_3$$

where $NT_2$ was the total nitrogen quantity at peak growth (September 2023), and $NT_3$ was the total nitrogen quantity at the end of the cycle (February 2024).

The nitrogen use efficiency (NUE, kg DM $kg^{-1}$ N) represents the amount of biomass produced per unit of nitrogen accumulated in the plant. It can be calculated by considering the whole plant, but we chose to consider AP to be able to compare our results with other studies. Following the methodology of Ra et al. (2012); Olson et al. (2013) and Dierking et al. (2016) two NUE calculations were performed at different dates:

1. $NUE_1$: represents the plant's ability to produce aboveground biomass using nitrogen remobilized in spring and absorbed from the soil:

$$NUE_1 = WAmax / NA_2$$

where WAmax was the maximum biomass accumulated in the aboveground parts in September (t $ha^{-1}$), and $NA_2$ was the nitrogen quantity of the aboveground parts at date 2 (September 2023).

2. $NUE_2$: represents the amount of aboveground biomass that was harvested in February per Unit of Nitrogen Exported at the end of the growth cycle

$$NUE_2 = WA_3 / NA_3$$

where $WA_3$ was the aboveground biomass at date 3, and $NA_3$ was the nitrogen quantity of the aboveground parts at date 3 (February 2024).

In order to name all traits in a relevant manner, a *Miscanthus* ontology was developed at the INRAE BioEcoAgro research unit of Estrées-Mons (https://urgi.versailles.inra.fr/ephesis/ephesis/ontologyportal.do) by using the GnpIS multispecies integrative information system from the INRAE-URGI of Versailles (Steinbach et al. 2013). The data that support the findings of this study, along with variable names and alternative trait abbreviations, are openly available in *Recherche Data Gouv* at https://doi.org/10.57745/CEDLW2. (Iqbal et al. 2025).

## 2.5 | Statistical Analyses

All statistical analyses were conducted using R software (version 4.3.2, R Core Team). Data normality was assessed using the Shapiro–Wilk test, and homogeneity of variance was evaluated using Levene's test from the car package (version 3.1.3). When necessary, natural logarithm transformations were applied to nitrogen remobilization traits to meet the assumptions of normality and homoscedasticity required for analysis of variance (ANOVA).

The genotype effect on nitrogen remobilization fluxes, efficiencies, nitrogen uptake, and nitrogen use efficiency was analyzed using ANOVA, applied to the subset of the 15 repeated genotypes from the progeny trial. ANOVA models were fitted using the aov() function, and post hoc comparisons were conducted using the Least Significant Difference (LSD) test from the agricolae package (version 1.3.7). The overall threshold for statistical significance was set at $\alpha = 0.05$, with significance levels denoted as * $p < 0.05$, ** $p < 0.01$, *** $p < 0.001$, and NS for $p \geq 0.05$ in tables and figures. Pearson correlation analysis, based on the complete progeny subset of 80 genotypes, was used to assess pairwise relationships between nitrogen-economy traits and biomass yield.

To identify broader patterns in nitrogen-economy traits and classify genotypes with similar functional characteristics, hierarchical clustering on principal components (HCPC) was performed following the method of Husson et al. (2010). This involved conducting a principal component analysis (PCA) followed by hierarchical clustering using Ward's method with k-means consolidation. PCA was used to improve clustering reliability by retaining the essential variance while minimizing noise.

PCA was performed using the PCA() function from the FactoMineR package (version 2.11), with nitrogen remobilization fluxes including spring remobilization (SR), autumn remobilization via the aboveground method (ARa) and the belowground method (ARb), as well as nitrogen uptake and nitrogen losses, included as active variables. Biomass yields in September 2023 (Biomass S) and February 2024 (Biomass F) were included as quantitative supplementary variables. Nitrogen status, based on the nitrogen nutrition index, was included as a qualitative supplementary variable, distinguishing genotypes as either luxury or deficient.

Hierarchical clustering on all five principal components (explaining 100% of the variance) was performed using the HCPC() function in FactoMineR (version 2.11) to define functional groups of genotypes with similar nitrogen-economy characteristics. The statistical contribution of each variable to the formation of these groups was evaluated using *v*-test values.

In parallel, a second PCA was conducted using nitrogen remobilization efficiencies as active variables, followed by hierarchical clustering on the resulting principal components to evaluate the role of efficiency traits in shaping functional groupings.

# 3 | Results

The progeny exhibited great variability in biomass production in the above and belowground parts during the growing season.

Significant variability was observed in aboveground and belowground biomass of the *Miscanthus sinensis* progeny at the sampling dates during the 2023–2024 plant cycle (Figure 3a,b). Aboveground biomass ranged from 5 to 60 t ha$^{-1}$, with the highest values recorded in September. Belowground biomass showed a similar range, between 5 and 40 t ha$^{-1}$, with no seasonal trend. The parental genotypes HER and MAL, represented by the green and red dashed lines, respectively, were positioned at opposite ends of the distribution for multiple sampling dates, highlighting that the observed variability in the progeny reflects the genetic divergence between the parents (Figure 3a,b). We found a strong correlation between aboveground and belowground biomass at each sampling date in the progeny ($r = 0.85$, 0.78, 0.73, and 0.84 for Date 0, Date 1, Date 2, and Date 3, respectively), indicating that genotypes with high yield potential were also characterized by significant rhizome biomass (Figure 3c).

This observed variability highlighted the genetic diversity in biomass production potential among the progeny. As expected, we also found high variability in nitrogen quantities among the genotypes and across the dates (data not shown). This observed seasonality in nitrogen quantities provided key insights into nitrogen transfer and recycling within genotypes, serving as a basis for subsequent analysis of the nitrogen recycling variability in the progeny.

### 3.1 | Nitrogen Recycling, Assessed Through Remobilization Fluxes and Efficiencies in Autumn and Spring, Exhibited Substantial Variability Among the *M. sinensis* Progeny

Regarding spring remobilization fluxes, a huge variation was observed among the progeny, ranging from 0.2 to 85 kg N ha$^{-1}$, with parental genotypes MAL and HER showing fluxes of 22 kg N ha$^{-1}$ and 10 kg N ha$^{-1}$, respectively (Figure 4a, Table 1). Spring remobilization efficiency (SRE), corresponding to the part of nitrogen in the aboveground part derived from spring remobilization, ranged from 0% to 80%, with parents MAL and HER at 27% and 3%, respectively (Figure 4b). Parental values fell within the broad progeny range, illustrating that variability extended beyond both parents. Differences between genotypes were substantial. The LSD values were 16.7 kg N ha$^{-1}$ for SR and 21.1% for SRE (Figure 4), and when the difference between two genotypes exceeded these values, the genotypes were considered significantly different.

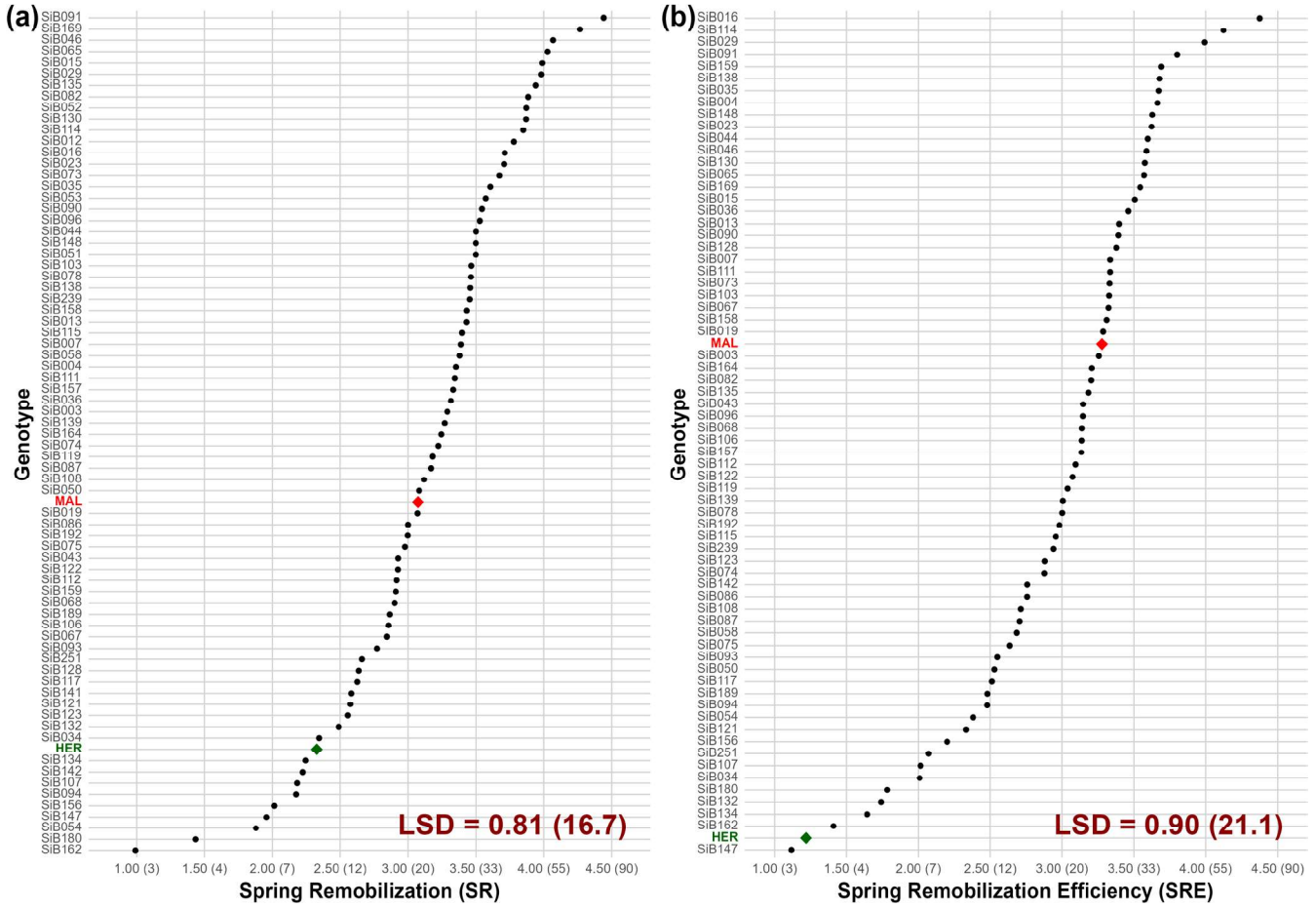


**FIGURE 4** | Spring remobilization flux (SR) (plot a) and spring remobilization efficiency in proportion to maximum aboveground nitrogen (SRE) (plot b) across *Miscanthus sinensis* progeny. The *x*-axis scale shows log-transformed values. The corresponding non-transformed values are given in parentheses with units: Kg N ha$^{-1}$ for (a) and % for (b). Each point represents the mean value. Green and red points highlight the HER and MAL genotypes, respectively. The least significant difference (LSD) is based on the subset of the 15 repeated genotypes to indicate the minimum difference required for statistical significance between genotypes.

**TABLE 1** | Variables related to nitrogen recycling and nitrogen use efficiency in the progeny: Minimum, maximum, and mean values, as well as *F* values, *p* values, significance, and coefficient of variation (CV) of the ANOVA table. ANOVA results are based on the 15 repeated genotypes, and their corresponding minimum, maximum, and mean values are indicated in brackets.

| Variable | Unit | Minimum | Maximum | Mean value | CV | *F* | *p* | Significance |
|---|---|---|---|---|---|---|---|---|
| Spring Remobilization (SR) | kg N ha$^{-1}$ | 0.2 (10.2) | 84.9 (84.9) | 27.0 (29.2) | 37.5 | 8.46 | $7.8\times10^{-8}$ | *** |
| Autumn Remobilization (ARa) | kg N ha$^{-1}$ | 5.6 (26.2) | 158.4 (137.1) | 69.0 (76.2) | 41.8 | 4.07 | $2.0\times10^{-4}$ | *** |
| Autumn Remobilization (ARb) | kg N ha$^{-1}$ | 0.5 (1.1) | 72.8 (59.7) | 28.6 (27.3) | 56.1 | 3.30 | $2.1\times10^{-3}$ | ** |
| Nitrogen Uptake (U) | kg N ha$^{-1}$ | 5.2 (39.9) | 241.2 (241.2) | 93.9 (98.0) | 30.2 | 13.8 | $1.3\times10^{-11}$ | *** |
| Spring Remobilization Efficiency (SRE) | % | 0.2 (3.4) | 79.5 (44.8) | 23.5 (24.8) | 53.0 | 2.03 | $4.2\times10^{-2}$ | * |
| Autumn Remobilization Efficiency (ARaE) | % | 7.0 (35.8) | 86.3 (73.1) | 54.7 (58.3) | 20.5 | 2.56 | $9.5\times10^{-3}$ | ** |
| Autumn Remobilization Efficiency (ARbE) | % | 0.6 (0.8) | 65.4 (50.2) | 26.2 (24.3) | 62.4 | 3.54 | $1.2\times10^{-3}$ | ** |
| $NUE_1$ | kg DM kg$^{-1}$ N | 122.7 (122.7) | 365.3 (268.8) | 195.1 (191.8) | 15.5 | 5.02 | $1.6\times10^{-5}$ | *** |
| $NUE_2$ | kg DM kg$^{-1}$ N | 161.7 (241.4) | 553.2 (424.2) | 328.4 (340.3) | 10.2 | 9.84 | $2.8\times10^{-9}$ | *** |

*Note:* Significance levels: ***$p<0.001$, **$p<0.01$, *$p<0.05$, NS $p\geq0.05$.

Concerning autumn remobilization, fluxes and efficiencies were expressed in terms of above and belowground parts. Fluxes calculated via aboveground (ARa) or belowground (ARb) methods ranged from 5 to 158 kg N ha$^{-1}$ and 0 to 73 kg N ha$^{-1}$, respectively.

Mean value of autumn remobilization fluxes was significantly ($p<0.05$, data not shown) higher when calculated with the aboveground method (69 kg N ha$^{-1}$) than with the belowground method (28.6 kg N ha$^{-1}$) (Table 1), indicating that the quantity of nitrogen withdrawn from the aboveground part in autumn is bigger than the quantity of nitrogen stored in the rhizome in winter. Parental genotypes showed contrasting values, with MAL and HER at 63 kg N ha$^{-1}$ and 114 kg N ha$^{-1}$ for ARa, and 9 kg N ha$^{-1}$ and 60 kg N ha$^{-1}$ for ARb, respectively. Efficiencies, calculated as the proportion of nitrogen in the aboveground part withdrawn towards the rhizome (ARaE), or calculated as the proportion of N effectively withdrawn from the aboveground part that was finally stored in the rhizome (ARbE), also exhibited substantial variability among the progeny. ARaE ranged from 7% to 86%, with MAL and HER at 77% and 43%, respectively, while ARbE ranged from 1% to 65%, with MAL and HER at 11% and 26%, respectively. These parental positions represented different points within the progeny distributions, confirming that variation encompassed both parents (data not shown).

ANOVA based on the repeated genotypes confirmed significant genotype effects for all the preceding variables related to nitrogen recycling and nitrogen use efficiency (Table 1), further underlining the genotypic diversity in the progeny. The range of values for these repeated genotypes (in brackets in Table 1) covered quite well the range observed for the entire progeny. As expected, the coefficients of variation related to the fluxes or efficiencies were relatively high due to the involvement of several variables in their calculations. Nevertheless, highly significant effects were detected, highlighting significant genotype-dependent differences in nitrogen recycling behavior during the late growing season.

### 3.2 | Nitrogen Remobilization Fluxes Were Linked to Remobilization Efficiencies, but Not Between Seasons

Spring remobilization fluxes were strongly correlated with spring remobilization efficiency ($r=0.71$, Figure 5a).

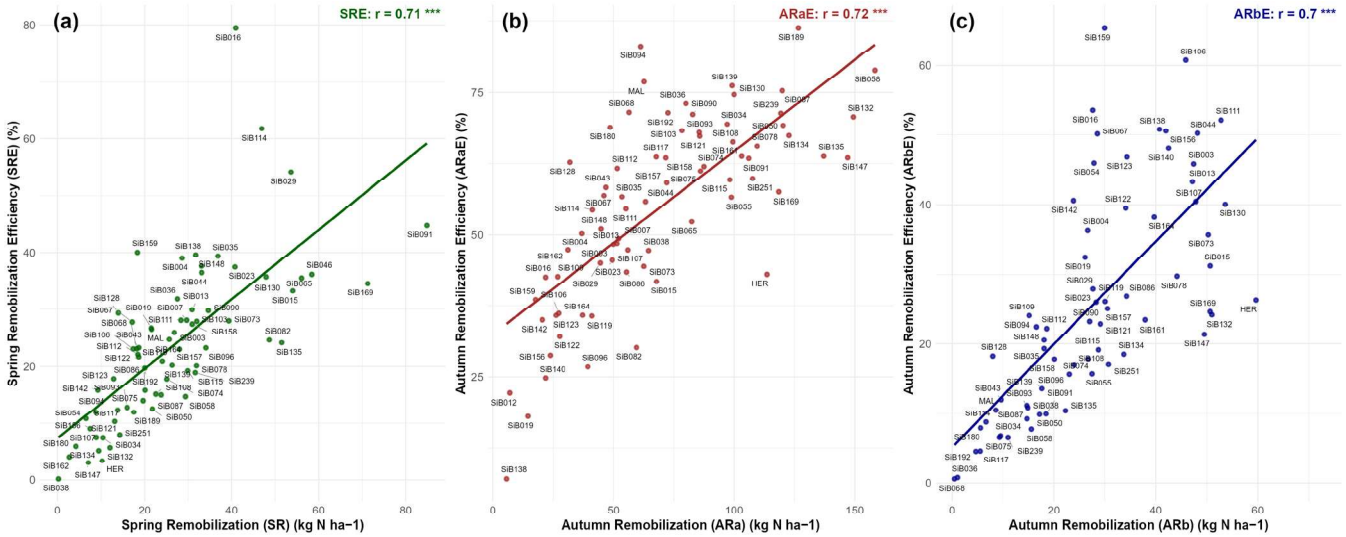


**FIGURE 5** | Correlations in the progeny between spring remobilization, SR, autumn remobilization via aboveground method, ARa, and autumn remobilization via belowground method, ARb, respectively with their corresponding efficiencies SRE (plot a), ARaE (plot b) and ARbE (plot c). The Pearson correlation coefficient ($r$) is shown in the top right corner of each plot, along with its significance level. "***" indicates a highly significant correlation ($p < 0.001$).

Genotypes with higher nitrogen fluxes during the spring demonstrated greater remobilization efficiencies, indicating a consistent relationship between fluxes and efficiencies, which was partly expected given their mathematical dependence. In other words, a larger proportion of the nitrogen present in the aboveground part was derived from spring remobilization when the quantity of remobilized nitrogen in spring was higher.

Similarly, significant positive correlations were observed in autumn. Autumn remobilization fluxes significantly correlated with autumn remobilization efficiency using the aboveground and the belowground methods ($r = 0.72$ and 0.70, respectively, Figure 5b,c). Genotypes with higher nitrogen fluxes in autumn also exhibited greater remobilization efficiencies, whether we examined what was withdrawn from the aboveground part (Figure 5b) or what was finally stored in the belowground part (Figure 5c).

No significant correlations were found between spring and autumn remobilization fluxes (Figure 7). We observed a significant but weak relationship between spring and autumn remobilization efficiencies; however, this was considered to be non-relevant, as it was driven by only three genotypes that exhibited markedly different efficiencies compared to the other 77.

### 3.3 | Endogenous and Exogenous Nitrogen Strongly Influenced Biomass Production in *M. sinensis* Progeny

In perennial plants like miscanthus, the nitrogen accumulated by plants comes from both endogenous (reserve) and exogenous (soil) sources. Nitrogen Use Efficiency (NUE), representing the amount of biomass produced per unit of nitrogen accumulated in the plant, exhibited substantial variability among *M. sinensis* progeny. Throughout the growing season, the range of NUE progressively increased: from 111–195 in July 2023, to 123–365 in September 2023, and 162–553 kg DM $kg^{-1}$ N in February 2024. This progressive increase indicated that nitrogen was utilized more efficiently as plants matured, particularly after the onset of senescence in February 2024.

$NUE_1$, corresponding to the plant's ability to produce aboveground biomass using both nitrogen remobilized in the spring (endogenous nitrogen) and nitrogen absorbed from the soil (exogenous nitrogen uptake), showed a weak but significant correlation with biomass yield in September 2023 and February 2024 ($r = 0.26$ and 0.23, respectively). To further examine how the two nitrogen sources influenced biomass, we investigated the respective effects of endogenous and exogenous nitrogen.

Regarding endogenous nitrogen, both spring and autumn nitrogen remobilization fluxes were positively correlated with biomass yield in February 2024 (brown harvest, Figure 6a, Table 1) as well as in September 2023 (green harvest, Figure 7). Spring remobilization fluxes showed a moderate correlation with biomass yield in September 2023 and February 2024 ($r = 0.34$ and 0.30, respectively). Stronger correlations were observed for autumn remobilization fluxes via aboveground method (ARa: $r = 0.62$ and 0.44, respectively) and via belowground method ($r = 0.31$ and 0.41, respectively), for the same dates (Figures 6a and 7). These results indicated that greater spring remobilization could contribute to increased aboveground biomass, although the moderate correlation suggested that other factors, such as exogenous nitrogen uptake, might also play a role. In turn, larger aboveground biomass in September appeared to support greater autumn remobilization, which contributed more strongly to the biomass yield observed in February.

In contrast, no significant correlations were observed between nitrogen remobilization efficiencies and biomass yield (Figures 6b and 7). In other words, biomass yield, whether at

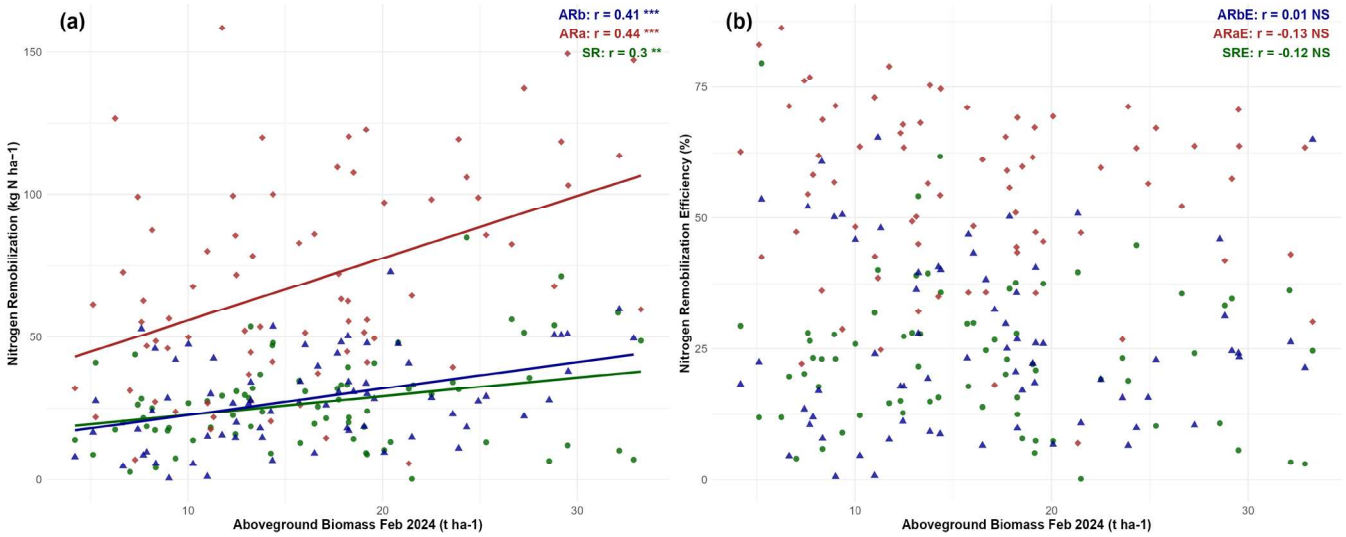


**FIGURE 6** | Correlation between nitrogen remobilization fluxes (plot a) and nitrogen remobilization efficiencies (plot b) with biomass yield. The remobilization quantities are SR in green, ARa (AR calculated via aboveground method) in dark red, and ARb (AR calculated via belowground method) in blue, along with their respective efficiencies in proportion to maximum aboveground nitrogen. Pearson correlation coefficients ($r$) are shown, with *** for $p < 0.001$, ** for $p < 0.01$, and NS for non-significant correlations ($p \geq 0.05$).

the green or brown harvest, was not related to the proportion of nitrogen withdrawn from the aboveground part (ARaE), the proportion ultimately stored in the belowground part (ARbE), or the proportion of aboveground nitrogen derived from spring remobilization (SRE) (Figures 6b and 7). These findings suggested that plant functioning, in terms of nitrogen recycling, operated independently of biomass size across the progeny.

SRE and ARbE were significantly negatively correlated with nitrogen uptake ($r = -0.52$ and $r = -0.35$, respectively; Figure 7), indicating that genotypes with lower endogenous remobilization efficiency tended to rely more on exogenous nitrogen uptake.

Exogenous nitrogen uptake, corresponding to the quantity of nitrogen absorbed from the soil during the growing season, exhibited substantial variability among the *M. sinensis* progeny, ranging from 5 to 241 kg N ha$^{-1}$. The parental genotypes also differed, with MAL showing 56 kg N ha$^{-1}$ and HER 241 kg N ha$^{-1}$, with HER positioned at the upper extreme of the progeny range. A significant positive correlation was observed between nitrogen uptake and aboveground biomass yield at both sampling dates ($r = 0.72$ and 0.63 in September 2023 and February 2024, respectively; Figure 7). Genotypes with higher nitrogen uptake produced greater biomass yields, demonstrating the strong link between nitrogen acquisition and productivity. This reciprocal relationship also reflected the influence of plant size on nitrogen uptake, with larger plants exhibiting greater uptake capacities.

However, nitrogen uptake efficiency, defined as the proportion of aboveground nitrogen derived from nitrogen uptake, was not significantly correlated with biomass yield in September 2023 ($r = 0.22$), and showed only a weak but significant correlation in February 2024 ($r = 0.24$; Figure 7). These results suggested that, while total nitrogen uptake was strongly linked to biomass accumulation, the efficiency with which absorbed nitrogen was converted into aboveground biomass was more variable and less predictive of yield.

Nitrogen uptake showed no significant correlation with spring remobilization fluxes (Figure 7). However, a strong positive correlation was observed between nitrogen uptake and autumn remobilization fluxes, particularly when calculated via the aboveground method ($r = 0.83$), while the belowground method showed no significant correlation (Figure 7). In other words, at the scale of the growing season, plants that absorbed more nitrogen (uptake) also withdrew greater amounts of nitrogen from the aboveground part. However, the result didn't highlight any relationship with the amount of nitrogen ultimately stored in the belowground part. This gap between the nitrogen withdrawn from the aboveground part and the amount finally stored in the belowground part was already highlighted by the comparison of the two methods used to calculate autumn remobilization, and indicated losses of nitrogen during the growing season.

Nitrogen losses were calculated as the difference between the total amount of nitrogen in the plant in September and in the following February, ranging from 2 to 143 kg N ha$^{-1}$ across the progeny, with MAL and HER showing 54 and 71 kg N ha$^{-1}$, respectively. When expressed as a proportion of the total nitrogen quantity in the plant in September, these losses were highly variable, ranging from 2% to 67% (data not shown). These calculations did not take into account abscised fallen leaves prior to the final sampling date in February (Date 3). Between 1% and 27% of these nitrogen losses were accounted for by fallen leaves across the progeny. Nitrogen uptake was significantly correlated with nitrogen losses ($r = 0.70$, Figure 7), suggesting that genotypes absorbing higher amounts of nitrogen not only presented higher ARa (Figure 8) but also experienced greater nitrogen losses.

$NUE_2$ corresponded to the amount of biomass that could be harvested per unit of nitrogen exported at the end of the season (Date 3). It was significantly higher than $NUE_1$. This increase


**FIGURE 7** | Pairwise correlation matrix and scatterplots for nitrogen-related traits and aboveground biomass yield in *Miscanthus sinensis* progeny. Pearson correlation coefficients ($r$) are shown in the upper triangle, with significance levels indicated as follows: *** for $p < 0.001$, ** for $p < 0.01$, * for $p < 0.05$, and non-significant correlations ($p \geq 0.1$). Trait abbreviations are as follows: ARa, autumn remobilization flux calculated via aboveground method (kg N ha$^{-1}$); ARaE, autumn remobilization efficiency using the aboveground method (%); ARb, autumn remobilization flux calculated via belowground method (kg N ha$^{-1}$); ARbE, autumn remobilization efficiency using the belowground method (%); Biomass F, aboveground biomass in February 2024 (t ha$^{-1}$); Biomass S, aboveground biomass in September 2023 (t ha$^{-1}$); N Losses, nitrogen losses (kg N ha$^{-1}$); N uptake E, nitrogen uptake efficiency (%); N Uptake, nitrogen uptake (kg N ha$^{-1}$); NUE1, nitrogen use efficiency calculated in September 2023 (kg DM kg$^{-1}$ N); NUE2, nitrogen use efficiency calculated in February 2024 (kg DM kg$^{-1}$ N); SR, spring remobilization flux (kg N ha$^{-1}$); SRE, spring remobilization efficiency (%).

in $NUE_2$ was attributed to the seasonal decline in aboveground nitrogen quantity during autumn. Despite this higher efficiency, no significant correlations were observed between $NUE_2$ and biomass yield, either in September 2023 or February 2024 (Figure 7). These findings suggested that higher $NUE_2$ did not necessarily translate into greater biomass yield at the intergenotypic level, opening the way for further investigation into genotype classification through functional groups and the assessment of their distinct nitrogen utilization strategies.

Regarding the contribution of remobilization fluxes to nitrogen use efficiency, no significant correlations were observed between spring remobilization fluxes and $NUE_1$ (Figure 7). A weak positive correlation was found between autumn remobilization fluxes,

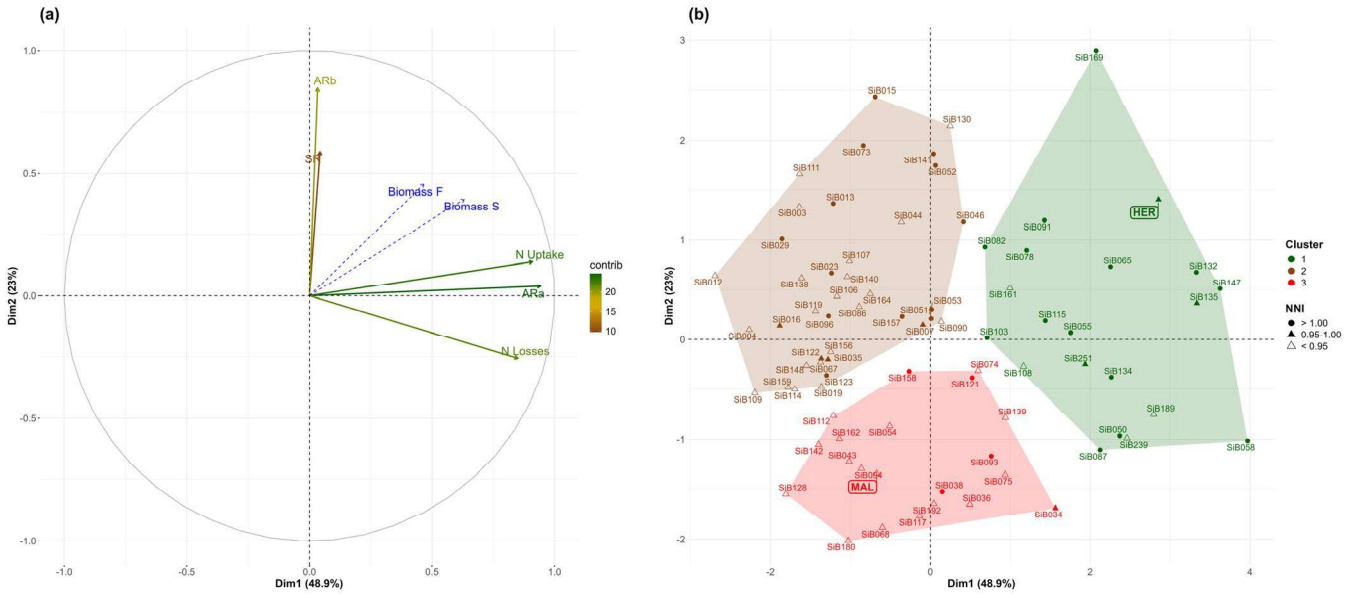


**FIGURE 8** | Principal Component Analysis (PCA) and hierarchical clustering based on all five principal components. PCA biplot (plot a) and corresponding hierarchical clustering plot (plot b) of nitrogen remobilization fluxes, with biomass yield as a quantitative supplementary variable and nitrogen status as a qualitative supplementary variable. The variable coding is the same as in Figure 7.

calculated via the aboveground method, and $NUE_2$ ($r=0.25$), whereas no significant correlation was observed via the belowground method (Figure 7). These results suggested that plants that were more nitrogen-efficient, meaning those producing greater amounts of biomass per unit of nitrogen, tended to transfer larger quantities of nitrogen from the aboveground part toward the belowground part in autumn, even though the final amount of nitrogen stored in the rhizome was not significantly affected.

Significant correlations were found between spring remobilization efficiency and $NUE_1$ ($r=0.32$; Figure 7), indicating that nitrogen recycling during early growth stages contributed to improved nitrogen use efficiency. This suggested that nitrogen derived from spring remobilization formed an important part of the nitrogen sources building aboveground biomass.

In contrast, a significant negative correlation was observed between $NUE_1$ and autumn remobilization efficiency using the aboveground method (ARaE; $r=-0.32$), suggesting that plants with higher nitrogen use efficiency in September had less nitrogen remaining to be withdrawn from the aboveground part in autumn.

A significant positive correlation was also found between autumn remobilization efficiency (ARaE) and $NUE_2$ ($r=0.42$), whereas no such correlation was observed using the belowground method (Figure 7). These results indicated that plants producing more biomass per unit of nitrogen, whether remobilized or uptaken, also tended to remobilize nitrogen more efficiently in autumn.

### 3.4 | Genotypic Differences in Nitrogen Recycling and Uptake in the Progeny Led to the Formation of Functional Groups

The above results related to nitrogen remobilization, uptake, and use efficiency suggested that *M. sinensis* progeny did not follow a uniform nitrogen-use strategy. For example, higher NUE did not necessarily translate into greater biomass production at the intergenotypic level, supporting the existence of functional groups. To investigate these differences among genotypes, a multidimensional analysis was carried out through Principal Component Analysis (PCA), followed by a hierarchical clustering based on all five principal components (HCPC). Such an approach classified genotypes into distinct functional groups based on shared nitrogen economy characteristics.

A first PCA (Figure 8a) was performed using nitrogen remobilization fluxes as active variables. Biomass yield variables (Biomass F and Biomass S) were introduced as supplementary quantitative variables, and their position on the principal component axes allowed for the visualization of their relationship with the set of active nitrogen remobilization flux variables. Nitrogen status was introduced as a supplementary qualitative variable to describe the groups formed after clustering based on principal components. The genotypes were classified as nitrogen-deficient when their NNI was below 1 or nitrogen-sufficient when their NNI was above 1.

The first two principal components explained a substantial portion of the total variance (72%), with the first dimension of the PCA accounting for almost half (49%) and the second for a quarter (23%). The first component was associated with nitrogen uptake, nitrogen losses, and autumn remobilization via the aboveground method (ARa), representing aboveground nitrogen dynamics. The second component was linked to spring remobilization (SR) and autumn remobilization flux via the belowground method (ARb), reflecting belowground nitrogen recycling and early-season nitrogen remobilization processes.

Clustering based on the principal components (Figure 8b) grouped genotypes into three distinct groups (Clusters 1, 2, and 3 in Table 2). Of the 80 genotypes analyzed, Cluster 1 contained 21 genotypes (26%), Cluster 2 contained 38 genotypes (48%), and

**TABLE 2** | Description of the three clusters based on the principal component analysis (PCA) and clustering of *Miscanthus sinensis* genotypes shown in Figure 8.

| | Cluster 1 | | Cluster 2 | | Cluster 3 | |
|---|---|---|---|---|---|---|
| | **category** | ***v*.test** | **category** | ***v*.test** | **category** | ***v*.test** |
| Qualitative Variable | Luxury | 3.17 | Null | | Deficient | 2.39 |
| Quantitative Variables | N. Uptake | 6.69 | ARb | 3.76 | Biomass F | −2.99 |
| | ARa | 6.66 | SR | 2.14 | Biomass S | −3.69 |
| | N. Losses | 6.11 | N. Uptake | −4.76 | SR | −3.92 |
| | Biomass S | 5.36 | ARa | −5.41 | ARb | −5.16 |
| | Biomass F | 3.87 | N. Losses | −5.57 | | |

*Note:* The first line corresponds to the description of the clusters by the qualitative nitrogen status variable (deficient and luxury categories), with the value of the *v*-test corresponding to the magnitude of the variable category (deficient or luxury) involvement. In the second line, the most significant quantitative variables in the formation of each cluster are indicated by the *v*-test, where their signs correspond to positive or negative involvement and values describe their magnitudes; only the strongest (in absolute value) are shown. The coding of these quantitative variables is same as in Figure 7.

Cluster 3 contained 21 genotypes (26%). The supplementary variable about nitrogen status significantly influenced the formation of these three groups ($p = 0.001$; data not shown), highlighting the role of nitrogen availability in shaping genotypic behavior.

1. Cluster 1 consisted mainly of nitrogen-sufficient genotypes (71%), demonstrated higher nitrogen uptake, nitrogen losses, ARa, and biomass yield (Biomass F, Biomass S), reinforcing the positive influence of plant nitrogen status on productivity. This cluster represented high biomass-producing, nitrogen-sufficient genotypes and included 21 out of the 80 genotypes. The parental genotype HER was classified in this group, consistent with its high nitrogen uptake and sufficient nitrogen status (NNI = 0.97).
2. Cluster 2 was characterized by genotypes exhibiting lower nitrogen uptake, nitrogen losses, and ARa but higher belowground nitrogen recycling traits (ARb, SR). This group did not strongly associate with a clear nitrogen status. This cluster included genotypes that could be considered effective nitrogen storers and spring recyclers. It comprised 38 out of the 80 genotypes.
3. Cluster 3 primarily included nitrogen-deficient genotypes (81%), exhibited lower biomass production (Biomass F, Biomass S), lower ARb, and lower SR, reflecting the impact of limited nitrogen availability on these traits. This cluster represented low-biomass-producing, nitrogen-deficient genotypes and also included 21 out of the 80 genotypes. The parental genotype MAL was positioned in this group, reflecting its lower nitrogen uptake and deficient nitrogen status.

The contrasting placement of HER in cluster 1 and MAL in cluster 3 illustrated the divergence between the parents and showed how this divergence structured the functional groups identified in the progeny. Instead of the previously cited fluxes, a second PCA (data not shown) was conducted using nitrogen remobilization efficiencies as active variables, with biomass yield variables introduced as supplementary quantitative variables. The first principal component was primarily associated with nitrogen uptake efficiency and spring remobilization efficiency (SRE), while the second component was related to both spring and autumn remobilization efficiency, particularly ARaE.

However, clustering based on this PCA did not result in functionally distinct groups in relation to nitrogen recycling efficiencies, nitrogen status, or biomass production. In contrast to the first PCA, these results suggested that nitrogen recycling efficiency did not drive genotypic differentiation. Instead, nitrogen fluxes, nitrogen status, and uptake emerged as the dominant factors defining functional groups.

## 4 | Discussion

The results of this study provided clear evidence of substantial variability in the functioning of *M. sinensis* progeny in terms of nitrogen remobilization, uptake, and biomass production. Our first hypothesis proposed that genotypes would exhibit diverse functioning with significant differences in nitrogen recycling and acquisition traits. The second hypothesis predicted that this diversity would not follow a continuous gradient but instead would segregate into distinct functional groups based on shared nitrogen economy, i.e., endogenous and exogenous nitrogen fluxes and nitrogen use linked with biomass production. The discussion therefore focuses on three points: (1) the existence of genotypic diversity in nitrogen remobilization and uptake that highlights functional variability among the genotypes, (2) the existence of functional groups among genotypes regarding nitrogen recycling, and finally (3) the idea that spring remobilization efficiency reduces nitrogen uptake, while higher uptake enhances autumn remobilization and biomass yield.

### 4.1 | Genotypic Diversity in Nitrogen Remobilization and Uptake Highlights Functional Variability Among the Genotypes

Significant genotypic variation was observed across key nitrogen-related traits, including nitrogen remobilization fluxes,

efficiencies, and exogenous nitrogen uptake. These differences reflect not only genetic diversity but also functional variability, referring to differences in how genotypes acquire, recycle, and allocate nitrogen within the plant system. Together, these findings indicate that nitrogen acquisition and recycling were genotype-dependent, reflecting physiological flexibility and genetic control of nitrogen-economy traits within *M. sinensis* progeny.

The association between nitrogen remobilization fluxes and biomass production suggests that efficient endogenous recycling supported growth when exogenous nitrogen was scarce. Genotypes that remobilized larger nitrogen fluxes from storage organs during spring sustained greater aboveground biomass, indicating that remobilized nitrogen substituted for external inputs. Higher autumn remobilization fluxes were also positively correlated with aboveground biomass yield in February (Figure 7) and contributed to greater nitrogen transfer to belowground organs, enhancing nitrogen storage for the subsequent growth cycle. This aligns with findings in *Miscanthus* × *giganteus*, where delaying harvest until after senescence enables nitrogen translocation back to belowground storage organs, reducing external nitrogen requirements while maintaining long-term productivity (Strullu et al. 2011; Lewin et al. 2024). Recent multisite evidence in miscanthus also shows that spring harvest following full senescence is associated with lower tissue nitrogen contents across locations, consistent with nutrient relocation to rhizomes prior to harvest (Magenau et al. 2022). The observed variability in remobilization fluxes across genotypes further underscores the functional diversity in nitrogen allocation strategies within *M. sinensis*.

Nitrogen remobilization efficiencies in both spring and autumn also displayed substantial genotypic variability. Some genotypes were more efficient in recycling internal nitrogen than others, reflecting different physiological strategies for nitrogen use. Such differences may reflect genotypic variation in senescence timing, nitrogen transporter activity, and root–shoot nitrogen partitioning, which together determine how efficiently nitrogen is recycled within the plant.

Exogenous nitrogen uptake also varied considerably across genotypes. Some individuals absorbed more nitrogen from the soil, indicating variation in uptake capacity under low nitrogen conditions. While nitrogen availability in the trial was assumed to be uniform, minor spatial variability likely occurred due to soil heterogeneity and plant competition. Nonetheless, the observed differences suggest genotypic variation in nitrogen acquisition ability. Previous studies have shown that increasing nitrogen availability enhances biomass yield in *Miscanthus* × *giganteus*, although these findings are based on responses observed within a single genotype (Namoi et al. 2024). In the context of our study, we hypothesize that genotypes with low nitrogen uptake were unable to absorb sufficient nitrogen under the low nitrogen conditions of the trial. Their biomass production could therefore have increased if more nitrogen had been available.

The nitrogen status assessment based on Malepartus (Brancourt-Hulmel 1999; see Section 2) confirmed nitrogen-deficient conditions in the trial, which probably magnified differences among genotypes in their ability to compensate for limited soil nitrogen availability. Under such constraints, uptake capacity becomes a decisive component of the nitrogen economy, distinguishing genotypes able to sustain growth from those that rely primarily on remobilized reserves.

Taken together, these results confirm that *M. sinensis* progeny exhibit highly diverse nitrogen-economy traits, thereby validating our first hypothesis. The substantial variation in remobilization and uptake traits indicates that genotypic differences drive nitrogen-economy strategies, highlighting the potential for targeted breeding to optimize nitrogen efficiency in bioenergy crops. Breeding should prioritize genotypes that sustain high biomass and effective remobilization under limiting conditions, while assessing responsiveness under higher nitrogen to identify broadly adapted lines. Previous work indicates that nitrogen management can alter internal storage pools and recycling dynamics (Dierking et al. 2017). Integrating molecular and quantitative-genetic tools, including QTL mapping and genomic prediction (Atienza et al. 2003; Clark et al. 2019), will enable efficient identification of nitrogen-efficient ideotypes in *M. sinensis*.

### 4.2 | Genotypic Variation in Nitrogen Recycling Define Distinct Functional Groups in the Progeny

Three functional groups were identified through a hierarchical clustering on principal components, each group characterized by distinct nitrogen economy traits. Nitrogen status, used as a qualitative variable, significantly influenced the clustering, reinforcing the role of nitrogen availability in shaping genotypic behavior. Moreover, the clustering was structured primarily by nitrogen fluxes rather than remobilization efficiencies, highlighting that genotypic differentiation was driven by the net nitrogen movement rather than by the relative efficiency of recycling.

The first functional group (genotypes from Cluster 1) included nitrogen-sufficient genotypes that exhibited high nitrogen uptake, elevated nitrogen losses, and greater biomass yields, even under the nitrogen-limited conditions experienced in our experiment. These genotypes follow a nitrogen-acquisitive strategy, efficiently absorbing and utilizing available nitrogen to sustain growth and biomass production. Such a strategy, marked by rapid nitrogen uptake and high resource turnover, has also been documented in $C_4$ perennial bioenergy grasses, where it is considered an adaptive trait linked to productivity under variable environmental conditions (Heckman et al. 2024). Although the specific mechanisms were not analyzed in our study, this pattern may reflect greater root activity and transporter expression facilitating sustained nitrogen acquisition under low supply. Their ability to maintain high biomass productivity despite limited soil nitrogen availability suggests that they are well suited for low-input bioenergy systems. High nitrogen uptake capacity has been linked to improved biomass yield in resource-limited environments across perennial grasses (Namoi et al. 2024). Given these parallels, genotypes from this functional group hold potential for sustainable biomass production on degraded or marginal soils, where nitrogen fertilization is not viable or desirable.

The second functional group (genotypes from Cluster 2) was characterized by lower nitrogen uptake, reduced nitrogen losses, and lower aboveground remobilization (ARa) but higher belowground nitrogen recycling fluxes (ARb and SR). These genotypes can be described as effective nitrogen storers and spring recyclers, following a nitrogen-conservative strategy relying more on internal nitrogen recycling than external nitrogen acquisition. This strategy has been identified in perennial grasses and is typically associated with long-term resource conservation and reduced input dependency (Smith 2017). Unlike genotypes in other clusters, this group did not clearly align with nitrogen-deficient or nitrogen-sufficient status, indicating a more balanced or stable nitrogen-use pattern. The ability to store nitrogen efficiently in belowground organs may help these genotypes resume growth quickly after stress events such as late frost or drought. From an ecological standpoint, this behavior corresponds to a Root–Nitrogen–K-conservation (RNK) survival strategy, where plant success is linked to retaining critical resources during unfavorable periods (Chapin 1980). Similar nitrogen-conserving mechanisms have been reported in *Miscanthus* × *giganteus*. In a controlled study by Dierking et al. (2017), two *M.* × *giganteus* genotypes were compared under different nitrogen input levels, and under low nitrogen one genotype increased belowground nitrogen storage without sacrificing biomass yield, a conservative strategy relying on internal recycling rather than continuous external supply. This mirrors the functional characteristics observed in Cluster 2 genotypes of our study. Such traits may also contribute to ecosystem services by supporting long-term nitrogen retention in plant–soil systems, potentially stabilizing nutrient dynamics under low-input or variable environmental conditions.

Lastly, the third functional group (genotypes of Cluster 3) consisted primarily of nitrogen-deficient genotypes, with low nitrogen uptake and low remobilization fluxes, resulting in reduced biomass yield under nitrogen-limited conditions. While less productive, they may suit agroecosystems aiming to preserve soil nitrogen or reduce nutrient competition in mixed cropping. These genotypes may offer valuable traits, such as favorable biomass composition or morphology, making them useful in breeding. Crossing them with high-uptake genotypes might combine improved composition with stronger nutrient acquisition, though this requires experimental confirmation in breeding programs. Overall, they represent a complementary group for systems focused on nutrient stability or specific biomass goals rather than maximum yield.

These findings emphasize the functional diversity present within *M. sinensis* progeny and provide a framework for selecting genotypes tailored to different agroecological contexts. Since these groupings were derived under nitrogen-limited conditions, it remains essential to test their stability under higher nitrogen availability and across diverse environments. Future work should explore the physiological mechanisms behind the contrasting behaviors of Clusters 1 and 3, including root architecture, nitrogen transporter activity, and rhizosphere interactions, to determine how these traits influence acquisition and recycling under variable conditions. Understanding these mechanisms will enhance the targeted use of *M. sinensis* genotypes for both biomass production and ecosystem services.

These results confirm our second hypothesis, demonstrating that nitrogen-economy traits in *M. sinensis* are structured into distinct functional groups rather than distributed along a continuous gradient. This classification represents a novel approach in *Miscanthus* research, providing a functional framework for breeding nitrogen-efficient varieties.

### 4.3 | Endogenous Remobilization Efficiency Reduces Reliance on Nitrogen Uptake, While Higher Uptake Enhances Autumn Remobilization and Biomass Yield

Our study highlighted the central role of nitrogen uptake in driving biomass yield and shaping nitrogen remobilization dynamics in *Miscanthus sinensis*. Nitrogen uptake, defined as the nitrogen absorbed from external sources during the growing season, varied widely among genotypes (5–241 kg N $ha^{-1}$) and showed a strong positive correlation with aboveground biomass yield at both September 2023 and February 2024. This relationship underscores the reciprocal link between plant size and nitrogen uptake, whereby larger plants tend to absorb more nitrogen. However, nitrogen uptake efficiency did not correlate with biomass yield, suggesting that the quantity of nitrogen absorbed, rather than the efficiency of uptake, is the primary driver of biomass production.

In our unfertilized trial, the total aboveground nitrogen quantity measured in September was, on average, composed of 51% from nitrogen uptake, 16% from spring remobilization (SR), and 34% corresponded to other internal nitrogen pools. This distribution contrasts with findings from fertilized *Miscanthus sinensis* trials, where nitrogen uptake accounted for 75%–81% of total plant nitrogen, and spring remobilization contributed only 2%–11% in two genotypes (Leroy et al. 2022). The greater reliance on exogenous nitrogen uptake in fertilized systems highlights how nitrogen availability influences plant nitrogen sourcing strategies. In contrast, in our unfertilized system, the higher contribution of spring remobilization emphasizes the importance of internal nitrogen recycling in sustaining growth under low nitrogen conditions.

Interestingly, nitrogen uptake showed no correlation with spring remobilization fluxes (SR; $r = -0.01$), indicating that plants can have either high or low SR while still exhibiting a wide range of nitrogen uptake capacities. However, nitrogen uptake was significantly negatively correlated with spring remobilization efficiency ($r = -0.52$) and with autumn remobilization efficiency estimated via the belowground method ($r = -0.35$). These results indicate a compensatory trade-off, where genotypes with higher endogenous remobilization efficiency tend to depend less on exogenous nitrogen sources, while those with lower efficiency compensate through increased nitrogen uptake from the soil. To our knowledge, no such relationship has been documented in miscanthus until now, making these findings novel in the context of perennial bioenergy crops.

In contrast to spring remobilization, nitrogen uptake was positively correlated with autumn remobilization fluxes, particularly when calculated via aboveground method (ARa; $r = 0.83$). Higher nitrogen uptake increases the nitrogen reservoir available

for translocation during autumn senescence, a process crucial for storing nitrogen in rhizomes before winter. Autumn remobilization ensures the storage of nitrogen in rhizomes for use in the following growing season, linking current-season nitrogen uptake to long-term productivity (Muhammad et al. 2020). The strong correlation between nitrogen uptake and autumn remobilization underscores the importance of nitrogen uptake not only for current-season biomass production but also for sustaining perennial growth cycles. This relationship indicates that nitrogen acquired late in the growing season contributes to reserve formation in rhizomes, a process well documented in *M.* × *giganteus*, where decreases in shoot nitrogen during autumn coincide with increased rhizome nitrogen that supports regrowth in spring (Strullu et al. 2011; Dierking et al. 2017).

However, while nitrogen uptake and ARa were strongly correlated, no such relationship was observed between uptake and nitrogen ultimately stored belowground (ARb). This discrepancy suggests that not all nitrogen withdrawn from the aboveground parts during senescence was successfully transferred to rhizomes. Instead, part of this nitrogen was lost. It is also highlighted by our comparison of the two methods (ARa vs. ARb), which showed diverging values across genotypes. Nitrogen losses, calculated as the difference between total plant nitrogen in September and February, corresponded to 2%–67% of September nitrogen quantity. Of these losses, only a small fraction (1%–27%) was attributable to leaf abscission, indicating that a significant portion of nitrogen is lost through other physiological processes. Leroy et al. (2022) similarly reported winter nitrogen losses of 42%–56% in *M. sinensis*, of which only a small portion could be explained by fallen leaves. These findings highlight that nitrogen loss is a key yet understudied component of perennial nitrogen cycling.

Nitrogen losses beyond leaf abscission can be explained by several processes. Part of the nitrogen may be stored in deeper roots not captured by our sampling depth, although previous studies indicate that root nitrogen content decreases sharply with depth and is probably low (Neukirchen et al. 1999; Ferchaud et al. 2016). Other pathways include rhizodeposition and root turnover, which transfer organic and inorganic nitrogen from living roots to the soil, where it can be immobilized by microbes rather than recovered in rhizomes (Wichern et al. 2008; Heaton et al. 2010; Hromádko et al. 2010). Further losses may occur through gaseous emissions, including ammonia volatilization from aerial tissues (Schjoerring and Mattsson 2001) and nitrous oxide emissions directly mediated by plants (Pihlatie et al. 2005; Lenhart et al. 2019). The relative contribution of these processes remains uncertain in our trial, yet their combined effect offers a plausible explanation for the substantial nitrogen losses observed.

Together, these results revealed a dual nitrogen-use strategy among genotypes. Those with high nitrogen uptake achieved greater biomass and stronger autumn remobilization, supporting both immediate growth and nitrogen storage for the following season. In contrast, genotypes with high endogenous remobilization efficiency depended less on soil nitrogen, making them well-suited for low-input systems. This functional variation allows the selection of genotypes based on environmental objectives. High-efficiency, low-uptake genotypes may perform better in marginal soils with limited fertilizer availability, while high-uptake genotypes may be effective in nutrient-rich or polluted environments, such as water catchment areas or fields targeted for phytoremediation.

Since endogenous remobilization efficiencies are not correlated with biomass yield, genotypes can be selected for either high or low efficiency without sacrificing productivity. This reinforces the conclusion of the section: nitrogen uptake is the primary driver of both biomass yield and autumn remobilization, but high remobilization efficiency provides an additional pathway to reduce dependence on external nitrogen. Optimizing both traits in combination could enhance nitrogen-use resilience in *M. sinensis*, enabling sustained productivity and improved nutrient retention across contrasting agroecosystems.

## 5 | Conclusion

This study demonstrated substantial genotypic variability in nitrogen remobilization, uptake, and biomass production among *Miscanthus sinensis* progeny grown under nitrogen-deficient field conditions. Nitrogen economy traits, reflecting how plants acquire, redistribute, and use nitrogen, were shown to follow coherent, genotype-dependent strategies, each with distinct implications for productivity and nutrient cycling. The identification of functionally diverse genotypes provided valuable insights for optimizing *M. sinensis* for both bioenergy production and ecosystem services.

The results strongly supported our first hypothesis that *M. sinensis* progeny exhibited functional diversity in nitrogen remobilization and uptake. Spring and autumn nitrogen remobilization fluxes were strongly associated with biomass yield, reinforcing their role as an endogenous nitrogen source contributing to plant growth. However, nitrogen remobilization efficiencies were not correlated with biomass yield, indicating that genotypes with both high and low remobilization efficiencies could still achieve high biomass production. Genotypes with higher spring remobilization efficiency generally showed reduced reliance on nitrogen uptake, suggesting a trade-off between sourcing strategies. Conversely, high nitrogen uptake supported both greater autumn remobilization and biomass yield, making it a primary driver of productivity in low-input systems.

The study also addressed the second hypothesis by showing that *M. sinensis* genotypes grouped into three distinct functional groups, each defined by coherent nitrogen-economy traits: nitrogen-acquisitive genotypes can enhance yield in nutrient-limited systems; conservative types can improve nutrient retention in rotations; and low-uptake genotypes can preserve soil fertility in nitrogen-rich zones. These functional groupings, in particular the nitrogen-acquisitive and conservative types, provide a new framework for breeding nitrogen-efficient *M. sinensis* ideotypes, enabling genotype selection tailored to contrasting agroecosystem goals. Beyond breeding, these findings also hold broader significance for sustainable bioenergy cropping and ecosystem management.

Future studies should evaluate whether these functional groups remain stable across varying nitrogen availability, soil

conditions, and climatic regimes. Multi-environment trials, including contrasting management practices, will help identify genotypes that consistently maintain their nitrogen-acquisitive or conservative strategies across environmental gradients.

Investigating the physiological and molecular traits underpinning these groups, such as root architecture, microbial associations, and nitrogen transport mechanisms, will be key to refining selection criteria for nitrogen-efficient genotypes. From a genetic perspective, this study provides the physiological foundation for further quantitative-genetic dissection of nitrogen-related traits. The next step will be to estimate heritability and genetic correlations for remobilization, uptake, and efficiency traits, and to identify quantitative trait loci (QTLs) and genomic regions linked to nitrogen-economy mechanisms.

Expanding beyond the current parental backgrounds to a broader panel of genetically diverse *M. sinensis* accessions will further enhance understanding of the species' adaptive potential and improve the transferability of these findings to breeding programs across diverse agroecological zones. In summary, integrating multi-environment validation with ongoing QTL mapping and heritability analyses will help to transform this functional framework into a predictive, genetically informed breeding strategy for nitrogen-efficient, high-yielding *M. sinensis* cultivars.

---

**Abbreviations**

**Genotypes, and Trials**

| | |
|---|---|
| Cfb | Marine west-coast climate |
| DOY | Day of Year |
| HER | *Miscanthus sinensis* 'Herman Mussel' |
| INRAE | French National Research Institute for Agriculture, Food and Environment |
| MAL | *Miscanthus sinensis* 'Malepartus' |
| UAN | Urea-ammonium-nitrate solution (applied at 120 kg N $ha^{-1}$) |
| UE GCIE | Unité Expérimentale Grandes Cultures Innovation Environnement |

**Organs, Biomass, and Sampling Dates**

| | |
|---|---|
| AP | Aboveground parts (stems and leaves) |
| Biomass F | Aboveground biomass in February 2024 (t $ha^{-1}$) |
| Biomass S | Aboveground biomass in September 2023 (t $ha^{-1}$) |
| BP | Belowground parts (rhizomes and associated roots) |
| Date 0 | February 2023 (dormancy; maximum N in BP) |
| Date 1 | July 2023 (minimum nitrogen quantity in belowground parts) |
| Date 2 | September 2023 (maximum nitrogen quantity in aboveground parts) |
| Date 3 | February 2024 (after full senescence; harvest) |
| W | Aboveground dry biomass (t $ha^{-1}$) in the critical nitrogen dilution curve equation |
| WA | Biomass of aboveground parts (t $ha^{-1}$) |
| $WA_3$ | Aboveground biomass in February 2024 (t $ha^{-1}$) |
| WAmax | Maximum aboveground biomass accumulated in September (t $ha^{-1}$) |
| WB | Biomass of belowground parts (t $ha^{-1}$) |

**Nitrogen Pools, Concentrations, and Quantities**

| | |
|---|---|
| $N_a$ | Actual nitrogen concentration in aboveground vegetative parts (for NNI) |
| $N_c$ | Critical nitrogen concentration from the critical nitrogen dilution curve |
| [NA] | Nitrogen concentration of aboveground parts (g N $kg^{-1}$ DM) |
| [NB] | Nitrogen concentration of belowground parts (g N $kg^{-1}$ DM) |
| N | Nitrogen |
| NA | Nitrogen quantity in aboveground parts (kg N $ha^{-1}$) |
| $NA_2$ | Nitrogen quantity of aboveground parts at Date 2 (September 2023) |
| $NA_3$ | Nitrogen quantity of aboveground parts at Date 3 (February 2024) |
| NB | Nitrogen quantity in belowground parts (kg N $ha^{-1}$) |
| $NB_0$ | Nitrogen quantity in belowground parts before spring remobilization (February 2023) |
| $NB_1$ | Nitrogen quantity in belowground parts after spring remobilization (July 2023) |
| $NB_2$ | Nitrogen quantity in belowground parts when aboveground N is maximal (September 2023) |
| $NB_3$ | Nitrogen quantity in belowground parts after full senescence (February 2024) |
| NNI | Nitrogen Nutrition Index ($=N_a/N_c$) |
| NT | Total nitrogen quantity in the whole plant (kg N $ha^{-1}$) |
| $NT_2$ | Total N quantity at peak growth (September 2023) |
| $NT_3$ | Total N quantity at the end of the cycle (February 2024) |

**Nitrogen Fluxes and Efficiencies**

| | |
|---|---|
| ARa | Autumn remobilization via aboveground method (kg N $ha^{-1}$) = $NA_2 - NA_3$ |
| ARaE | Autumn remobilization efficiency using the aboveground method (%) |
| ARb | Autumn remobilization via belowground method (kg N $ha^{-1}$) = $NB_3 - NB_2$ |
| ARbE | Autumn remobilization efficiency using the belowground method (%) |
| N Losses | Nitrogen losses (kg N $ha^{-1}$) = $NT_2 - NT_3$ |
| N uptake E | Nitrogen uptake efficiency (%), proportion of aboveground N derived from uptake |
| N Uptake | Nitrogen uptake (kg N $ha^{-1}$) = $NT_2 - NB_0$ |
| NUE | Nitrogen use efficiency (kg DM $kg^{-1}$ N) |
| $NUE_1$ | $WAmax/NA_2$ (aboveground biomass produced using spring-remobilized and absorbed N) |
| $NUE_2$ | $WA_3/NA_3$ (aboveground biomass harvested per unit of N exported at end of cycle) |
| SR | Spring remobilization (kg N $ha^{-1}$) = $NB_0 - NB_1$ |
| SRE | Spring remobilization efficiency (%) = $(SR/NA_2) \times 100$ |

**Statistical and Multivariate Analyses**

| | |
|---|---|
| ANOVA | Analysis of variance |
| HCPC | Hierarchical clustering on principal components |
| LSD | Least Significant Difference test (post hoc) |

| | |
|---|---|
| NS | Not significant ($p \geq 0.05$) |
| $p$ | Probability value (significance thresholds *, **, ***, NS) |
| PCA | Principal component analysis |
| $r$ | Pearson correlation coefficient |
| $v$-test | Statistic indicating variable contributions in clusters |

**Units and Derived Quantities**

| | |
|---|---|
| DM | Dry matter (e.g., kg DM $kg^{-1}$ N in NUE units) |
| g N $kg^{-1}$ DM | Grams of nitrogen per kilogram of dry matter |
| kg N $ha^{-1}$ | Kilogram of nitrogen per hectare |
| t $ha^{-1}$ | Tons per hectare |


## Acknowledgements

This research was conducted as part of the MisTigation project, funded by ADEME (French Environment and Energy Management Agency) through the GRAINE 2022 program. It also benefited from the URGI facilities (https://doi.org/10.15454/1.5572414581735654E12) and was supported by the French government through the National Research Agency (ANR), as part of the France 2030 program for research infrastructure (EQUIPEX+), reference ANR-21-ESRE-0048, as well as Phenome-Emphasis (ANR-11-INBS-0012) and the e-Infrastructure to boost the use of diversified biological resources (reference ANR-22-PEAE-0014). Shehyar Iqbal also received a thesis grant from the Hauts-de-France region and the Biology and Plant Breeding division of INRAE.The authors would like to acknowledge Marie Heumez (GCIE INRAE experimental unit) and all persons who participated in the work.

## Funding

This work was supported by Agence de l'Environnement et de la Maîtrise de l'Energie, MisTigation Project 2203D0151.


## Conflicts of Interest

The authors declare no conflicts of interest.

## Data Availability Statement

The data that support the findings of this study are openly available in Recherche Data Gouv at https://doi.org/10.57745/CEDLW2.

## References


Arnoult, S., and M. Brancourt-Hulmel. 2015. "A Review on *Miscanthus* Biomass Production and Composition for Bioenergy Use: Genotypic and Environmental Variability and Implications for Breeding." *Bioenergy Research* 8, no. 2: 502–526. https://doi.org/10.1007/s12155-014-9524-7.

Atienza, S. G., Z. Satovic, K. K. Petersen, O. Dolstra, and A. Martín. 2003. "Identification of QTLs Associated With Yield and Its Components in *Miscanthus sinensis* Anderss." *Euphytica* 132, no. 3: 353–361. https://doi.org/10.1023/A:1025041926259.

Barnaud, C., and R. Muradian. 2024. "Ecosystem Services and Collective Action: New Commons, New Governance Challenges." *Ecosystem Services* 70: 101662. https://doi.org/10.1016/j.ecoser.2024.101662.

Beale, C. V., and S. P. Long. 1997. "Seasonal Dynamics of Nutrient Accumulation and Partitioning in the Perennial C4-Grasses *Miscanthus* × *Giganteus* and *Spartina cynosuroides*." *Biomass and Bioenergy* 12, no. 6: 419–428. https://doi.org/10.1016/S0961-9534(97)00016-0.

Belmokhtar, N., S. Arnoult, B. Chabbert, J.-P. Charpentier, and M. Brancourt-Hulmel. 2017. "Saccharification Performances of *Miscanthus* at the Pilot and Miniaturized Assay Scales: Genotype and Year Variabilities According to the Biomass Composition." *Frontiers in Plant Science* 8: 740. https://doi.org/10.3389/fpls.2017.00740.

Ben Fradj, N., S. Rozakis, M. Borzęcka, and M. Matyka. 2020. "*Miscanthus* in the European Bio-Economy: A Network Analysis." *Industrial Crops and Products* 148: 112281. https://doi.org/10.1016/j.indcrop.2020.112281.

Brancourt-Hulmel, M. 1999. "Crop Diagnosis and Probe Genotypes for Interpreting Genotype Environment Interaction in Winter Wheat Trials." *Theoretical and Applied Genetics* 99: 1018–1030.

Briones, M. J. I., A. Massey, D. M. O. Elias, et al. 2023. "Species Selection Determines Carbon Allocation and Turnover in *Miscanthus* Crops: Implications for Biomass Production and C Sequestration." *Science of the Total Environment* 887: 164003. https://doi.org/10.1016/j.scitotenv.2023.164003.

Byun, C., S. de Blois, and J. Brisson. 2013. "Plant Functional Group Identity and Diversity Determine Biotic Resistance to Invasion by an Exotic Grass." *Journal of Ecology* 101, no. 1: 128–139. https://doi.org/10.1111/1365-2745.12016.

Cadoux, S., F. Ferchaud, C. Demay, et al. 2014. "Implications of Productivity and Nutrient Requirements on Greenhouse Gas Balance of Annual and Perennial Bioenergy Crops." *GCB Bioenergy* 6, no. 4: 425–438. https://doi.org/10.1111/gcbb.12065.

Cadoux, S., A. B. Riche, N. E. Yates, and J.-M. Machet. 2012. "Nutrient Requirements of *Miscanthus* × *Giganteus*: Conclusions From a Review of Published Studies." *Biomass and Bioenergy* 38: 14–22. https://doi.org/10.1016/j.biombioe.2011.01.015.

Chapin, F. S. 1980. "The Mineral Nutrition of Wild Plants." *Annual Review of Ecology and Systematics* 11: 233–260.

Chen, C.-L., H. van der Schoot, S. Dehghan, et al. 2017. "Genetic Diversity of Salt Tolerance in *Miscanthus*." *Frontiers in Plant Science* 8: 187. https://doi.org/10.3389/fpls.2017.00187.

Cibin, R., E. Trybula, I. Chaubey, S. M. Brouder, and J. J. Volenec. 2016. "Watershed-Scale Impacts of Bioenergy Crops on Hydrology and Water Quality Using Improved SWAT Model." *GCB Bioenergy* 8, no. 4: 837–848. https://doi.org/10.1111/gcbb.12307.

Clark, L. V., M. S. Dwiyanti, K. G. Anzoua, et al. 2019. "Genome-Wide Association and Genomic Prediction for Biomass Yield in a Genetically Diverse *Miscanthus sinensis* Germplasm Panel Phenotyped at Five Locations in Asia and North America." *GCB Bioenergy* 11, no. 8: 988–1007. https://doi.org/10.1111/gcbb.12620.

Codina Gironès, V., S. Moret, E. Peduzzi, M. Nasato, and F. Maréchal. 2017. "Optimal Use of Biomass in Large-Scale Energy Systems: Insights for Energy Policy." *Energy* 137: 789–797. https://doi.org/10.1016/j.energy.2017.05.027.

De Vega, J. J., A. Teshome, M. Klaas, J. Grant, J. Finnan, and S. Barth. 2021. "Physiological and Transcriptional Response to Drought Stress Among Bioenergy Grass *Miscanthus* Species." *Biotechnology for Biofuels* 14, no. 1: 60. https://doi.org/10.1186/s13068-021-01915-z.

Dierking, R. M., D. J. Allen, S. M. Brouder, and J. J. Volenec. 2016. "Yield, Biomass Composition, and N Use Efficiency During Establishment of Four *Miscanthus* × *Giganteus* Genotypes as Influenced by N Management." *Biomass and Bioenergy* 91: 98–107. https://doi.org/10.1016/j.biombioe.2016.05.005.

Dierking, R. M., D. J. Allen, S. M. Cunningham, S. M. Brouder, and J. J. Volenec. 2017. "Nitrogen Reserve Pools in Two *Miscanthus* × *Giganteus* Genotypes Under Contrasting N Managements." *Frontiers in Plant Science* 8: 1618. https://doi.org/10.3389/fpls.2017.01618.

Farrell, A. D., J. C. Clifton-Brown, I. Lewandowski, and M. B. Jones. 2006. "Genotypic Variation in Cold Tolerance Influences the Yield of *Miscanthus*." *Annals of Applied Biology* 149, no. 3: 337–345. https://doi.org/10.1111/j.1744-7348.2006.00099.x.

Ferchaud, F., and B. Mary. 2016. "Drainage and Nitrate Leaching Assessed During 7 Years Under Perennial and Annual Bioenergy Crops." *Bioenergy Research* 9, no. 2: 656–670. https://doi.org/10.1007/s12155-015-9710-2.

Ferchaud, F., G. Vitte, J.-M. Machet, N. Beaudoin, M. Catterou, and B. Mary. 2016. "The Fate of Cumulative Applications of 15N-Labelled Fertiliser in Perennial and Annual Bioenergy Crops." *Agriculture, Ecosystems & Environment* 223: 76–86. https://doi.org/10.1016/j.agee.2016.02.030.

Ferrarini, A., F. Fornasier, P. Serra, F. Ferrari, M. Trevisan, and S. Amaducci. 2017. "Impacts of Willow and *Miscanthus* Bioenergy Buffers on Biogeochemical N Removal Processes Along the Soil–Groundwater Continuum." *GCB Bioenergy* 9, no. 1: 246–261. https://doi.org/10.1111/gcbb.12340.

Fry, E. L., S. A. Power, and P. Manning. 2014. "Trait-Based Classification and Manipulation of Plant Functional Groups for Biodiversity–Ecosystem Function Experiments." *Journal of Vegetation Science* 25, no. 1: 248–261. https://doi.org/10.1111/jvs.12068.

Głowacka, K., L. V. Clark, S. Adhikari, et al. 2015. "Genetic Variation in *Miscanthus* × *Giganteus* and the Importance of Estimating Genetic Distance Thresholds for Differentiating Clones." *GCB Bioenergy* 7, no. 2: 386–404. https://doi.org/10.1111/gcbb.12166.

Greef, J. M., M. Deuter, C. Jung, and J. Schondelmaier. 1997. "Genetic Diversity of European *Miscanthus* Species Revealed by AFLP Fingerprinting." *Genetic Resources and Crop Evolution* 44, no. 2: 185–195. https://doi.org/10.1023/A:1008693214629.

Heaton, E. A., F. G. Dohleman, A. F. Miguez, et al. 2010. "Chapter 3–*Miscanthus*: A Promising Biomass Crop." In *Advances in Botanical Research*, edited by J.-C. Kader and M. Delseny, vol. 56, 75–137. Academic Press. https://doi.org/10.1016/B978-0-12-381518-7.00003-0.

Heckman, R., C. Guilherme Pereira, M. Aspinwall, and T. Juenger. 2024. "Physiological Responses of C4 Perennial Bioenergy Grasses to Climate Change: Causes, Consequences, and Constraints." *Annual Review of Plant Biology* 75: 737–769. https://doi.org/10.1146/annurev-arplant-070623-093952.

Hou, W., R. Raverdy, K. Lourgant, et al. 2022. "QTL Detection for Flowering-Time Related Traits in *Miscanthus sinensis* Using a Staggered-Start Design." *Bioenergy Research* 15, no. 2: 718–733. https://doi.org/10.1007/s12155-021-10386-x.

Hromádko, L., V. Vranová, D. Techer, P. Laval-Gilly, K. Rejšek, and P. Formánek. 2010. "Composition of Root Exudates of *Miscanthus* × *Giganteus* Greef et Deu." *Acta Universitatis Agriculturae et Silviculturae Mendelianae Brunensis* 58: 71–76. https://doi.org/10.11118/actaun201058010071.

Husson, F., J. Josse, and J. Pages. 2010. *Principal Component Methods-Hierarchical Clustering-Partitional Clustering: Why Would We Need to Choose for Visualizing Data*, 17. Applied Mathematics Department.

Iqbal, S., M. Brancourt-Hulmel, and M. Zapater. 2025. "Phenotyping Data for 'Nitrogen Economy Strategies Define Distinct Functional Groups of Genotypes in a *Miscanthus sinensis* Progeny'." 10.57745/CEDLW2, Recherche Data Gouv, V1, UNF:6:q03yACXjVm396GREJSrH7g== [fileUNF].

IUSS Working Group WRB. 2022. "World Reference Base for Soil Resources." In *International Soil Classification System for Naming Soils and Creating Legends for Soil Maps*, 4th ed. International Union of Soil Sciences (IUSS).

Justes, E., B. Mary, J.-M. Meynard, J.-M. Machet, and L. Thelier-Huché. 1994. "Determination of a Critical Nitrogen Dilution Curve for Winter Wheat Crops." *Annals of Botany* 74, no. 4: 397–407.

Kumari, A., J. N. Njuguna, X. Zheng, J. Kromdijk, E. J. Sacks, and K. Glowacka. 2024. "Genetic Basis of Non-Photochemical Quenching and Photosystem II Efficiency Responses to Chilling in the Biomass Crop *Miscanthus*." *GCB Bioenergy* 17, no. 1: e70015. https://doi.org/10.1111/gcbb.70015.

Lenhart, K., T. Behrendt, S. Greiner, et al. 2019. "Nitrous Oxide Effluxes From Plants as a Potentially Important Source to the Atmosphere." *New Phytologist* 221, no. 3: 1398–1408. https://doi.org/10.1111/nph.15455.

Leroy, J. 2021. *Etude écophysiologique temporelle dela gestion des réserves carbonées et azotées par trois génotypes de miscanthus*. PhD thesis., 183. AgroParisTech. https://pastel.hal.science/tel-04223136v1.

Leroy, J., F. Ferchaud, C. Giauffret, et al. 2022. "*Miscanthus Sinensis* Is as Efficient as *Miscanthus*×*Giganteus* for Nitrogen Recycling in Spite of Smaller Nitrogen Fluxes." *Bioenergy Research* 15, no. 2: 686–702. https://doi.org/10.1007/s12155-022-10408-2.

Lesur, C., M. Bazot, F. Bio-Beri, B. Mary, M.-H. Jeuffroy, and C. Loyce. 2014. "Assessing Nitrate Leaching During the Three-First Years of *Miscanthus* × *Giganteus* From On-Farm Measurements and Modeling." *GCB Bioenergy* 6, no. 4: 439–449. https://doi.org/10.1111/gcbb.12066.

Lewin, E., J. Clifton Brown, E. Magenau, et al. 2024. "Yield Development and Nutrient Offtake in Contrasting *Miscanthus* Hybrids Under Green and Brown Harvest Regimes." *GCB Bioenergy* 16, no. 8: e13149. https://doi.org/10.1111/gcbb.13149.

Magenau, E., J. Clifton-Brown, D. Awty-Carroll, et al. 2022. "Site Impacts Nutrient Translocation Efficiency in Intraspecies and Interspecies *Miscanthus* Hybrids on Marginal Lands." *GCB Bioenergy* 14, no. 9: 1035–1054. https://doi.org/10.1111/gcbb.12985.

Muhammad, S., B. L. Sanden, B. D. Lampinen, et al. 2020. "Nutrient Storage in the Perennial Organs of Deciduous Trees and Remobilization in Spring—A Study in Almond (*Prunus dulcis*) (Mill.) D. A. Webb." *Frontiers in Plant Science* 11: 658. https://doi.org/10.3389/fpls.2020.00658.

Namoi, N., C. Jang, G. D. Behnke, J. W. Lee, W. Yang, and D. Lee. 2024. "Nitrogen Fertilization Effects on Aged *Miscanthus* × *Giganteus* Stands: Exploring Biomass Yield, Yield Components, and Biomass Prediction Using In-Season Morphological Traits." *GCB Bioenergy* 16, no. 5: e13139. https://doi.org/10.1111/gcbb.13139.

Neukirchen, D., M. Himken, J. Lammel, U. Czypionka-Krause, and H. W. Olfs. 1999. "Spatial and Temporal Distribution of the Root System and Root Nutrient Content of an Established *Miscanthus* Crop." *European Journal of Agronomy* 11, no. 3: 301–309. https://doi.org/10.1016/S1161-0301(99)00031-3.

Nie, G., L. Huang, X. Ma, et al. 2017. "Enriching Genomic Resources and Transcriptional Profile Analysis of *Miscanthus sinensis* Under Drought Stress Based on RNA Sequencing." *International Journal of Genomics* 2017, no. 1: 9184731. https://doi.org/10.1155/2017/9184731.

Nsanganwimana, F., K. S. Al Souki, C. Waterlot, et al. 2021. "Potentials of *Miscanthus* × *Giganteus* for Phytostabilization of Trace Element-Contaminated Soils: Ex Situ Experiment." *Ecotoxicology and Environmental Safety* 214: 112125. https://doi.org/10.1016/j.ecoenv.2021.112125.

Nsanganwimana, F., B. Pourrut, M. Mench, and F. Douay. 2014. "Suitability of *Miscanthus* Species for Managing Inorganic and Organic Contaminated Land and Restoring Ecosystem Services. A Review." *Journal of Environmental Management* 143: 123–134. https://doi.org/10.1016/j.jenvman.2014.04.027.

Olson, S. N., K. Ritter, J. Medley, T. Wilson, W. L. Rooney, and J. E. Mullet. 2013. "Energy Sorghum Hybrids: Functional Dynamics of High Nitrogen Use Efficiency." *Biomass and Bioenergy* 56: 307–316. https://doi.org/10.1016/j.biombioe.2013.04.028.

Pihlatie, M., P. Ambus, J. Rinne, K. Pilegaard, and T. Vesala. 2005. "Plant-Mediated Nitrous Oxide Emissions From Beech (*Fagus sylvatica*) Leaves." *New Phytologist* 168, no. 1: 93–98. https://doi.org/10.1111/j.1469-8137.2005.01542.x.

Ra, K., F. Shiotsu, J. Abe, and S. Morita. 2012. "Biomass Yield and Nitrogen Use Efficiency of Cellulosic Energy Crops for Ethanol Production." *Biomass and Bioenergy* 37: 330–334. https://doi.org/10.1016/j.biombioe.2011.12.047.

Schjoerring, J. K., and M. Mattsson. 2001. "Quantification of Ammonia Exchange Between Agricultural Cropland and the Atmosphere: Measurements Over Two Complete Growth Cycles of Oilseed Rape, Wheat, Barley and Pea." *Plant and Soil* 228, no. 1: 105–115. https://doi.org/10.1023/A:1004851001342.

Scordia, D., E. G. Papazoglou, D. Kotoula, et al. 2022. "Towards Identifying Industrial Crop Types and Associated Agronomies to Improve Biomass Production From Marginal Lands in Europe." *GCB Bioenergy* 14, no. 7: 710–734. https://doi.org/10.1111/gcbb.12935.

Smith, L. C. 2017. *Nitrogen Conservation in Perennial Grasses Managed for Bioenergy Production*. University of Wisconsin-Madison.

Stavridou, E., R. J. Webster, and P. R. H. Robson. 2019. "Novel *Miscanthus* Genotypes Selected for Different Drought Tolerance Phenotypes Show Enhanced Tolerance Across Combinations of Salinity and Drought Treatments." *Annals of Botany* 124, no. 4: 653–674. https://doi.org/10.1093/aob/mcz009.

Steinbach, D., M. Alaux, J. Amselem, et al. 2013. "GnpIS: An Information System to Integrate Genetic and Genomic Data From Plants and Fungi." *Database* 2013: 1–9. https://doi.org/10.1093/database/bat058.

Strullu, L., S. Cadoux, M. Preudhomme, M. H. Jeuffroy, and N. Beaudoin. 2011. "Biomass Production and Nitrogen Accumulation and Remobilisation by *Miscanthus*×*Giganteus* as Influenced by Nitrogen Stocks in Belowground Organs." *Field Crops Research* 121, no. 3: 381–391. https://doi.org/10.1016/j.fcr.2011.01.005.

Sun, Q., Q. Lin, Z.-L. Yi, Z.-R. Yang, and F.-S. Zhou. 2010. "A Taxonomic Revision of *Miscanthus* s.l. (Poaceae) From China." *Botanical Journal of the Linnean Society* 164, no. 2: 178–220. https://doi.org/10.1111/j.1095-8339.2010.01082.x.

Tavakoli-Hashjini, E., A. Piorr, K. Müller, and J. L. Vicente-Vicente. 2020. "Potential Bioenergy Production From *Miscanthus* × *Giganteus* in Brandenburg: Producing Bioenergy and Fostering Other Ecosystem Services While Ensuring Food Self-Sufficiency in the Berlin-Brandenburg Region." *Sustainability* 12, no. 18: 7731. https://www.mdpi.com/2071-1050/12/18/7731.

van der Cruijsen, K., M. Al Hassan, G. van Erven, et al. 2024. "Salt Stress Alters the Cell Wall Components and Structure in *Miscanthus sinensis* Stems." *Physiologia Plantarum* 176, no. 4: e14430. https://doi.org/10.1111/ppl.14430.

van der Weijde, T., L. M. Huxley, S. Hawkins, et al. 2017. "Impact of Drought Stress on Growth and Quality of *Miscanthus* for Biofuel Production." *GCB Bioenergy* 9, no. 4: 770–782. https://doi.org/10.1111/gcbb.12382.

Weik, J., J. Lask, E. Petig, et al. 2022. "Implications of Large-Scale *Miscanthus* Cultivation in Water Protection Areas: A Life Cycle Assessment With Model Coupling for Improved Policy Support." *GCB Bioenergy* 14, no. 11: 1162–1182. https://doi.org/10.1111/gcbb.12994.

Weng, T.-Y., T. Nakashima, A. Villanueva-Morales, J. R. Stewart, E. J. Sacks, and T. Yamada. 2022. "Assessment of Drought Tolerance of *Miscanthus* Genotypes Through Dry-Down Treatment and Fixed-Soil-Moisture-Content Techniques." *Agriculture* 12, no. 1: 6. https://www.mdpi.com/2077-0472/12/1/6.

Wichern, F., E. Eberhardt, J. Mayer, R. G. Joergensen, and T. Müller. 2008. "Nitrogen Rhizodeposition in Agricultural Crops: Methods, Estimates and Future Prospects." *Soil Biology and Biochemistry* 40, no. 1: 30–48. https://doi.org/10.1016/j.soilbio.2007.08.010.

Zapater, M., M. Catterou, B. Mary, et al. 2017. "A Single and Robust Critical Nitrogen Dilution Curve for *Miscanthus* × *Giganteus* and *Miscanthus sinensis*." *Bioenergy Research* 10, no. 1: 115–128. https://doi.org/10.1007/s12155-016-9781-8.

Zhao, H., B. Wang, J. He, et al. 2013. "Genetic Diversity and Population Structure of *Miscanthus sinensis* Germplasm in China." *PLoS One* 8, no. 10: e75672. https://doi.org/10.1371/journal.pone.0075672.

Zheng, C., Z. Yi, L. Xiao, et al. 2022. "The Performance of *Miscanthus* Hybrids in Saline-Alkaline Soil." *Frontiers in Plant Science* 13: 921824. https://doi.org/10.3389/fpls.2022.921824.

Zub, H. W., S. Arnoult, J. Younous, I. Lejeune-Hénaut, and M. Brancourt-Hulmel. 2012. "The Frost Tolerance of *Miscanthus* at the Juvenile Stage: Differences Between Clones Are Influenced by Leaf-Stage and Acclimation." *European Journal of Agronomy* 36, no. 1: 32–40. https://doi.org/10.1016/j.eja.2011.08.001.

# Chapter 2

***Chapter 2 objectives and methodology within the overall thesis framework.***

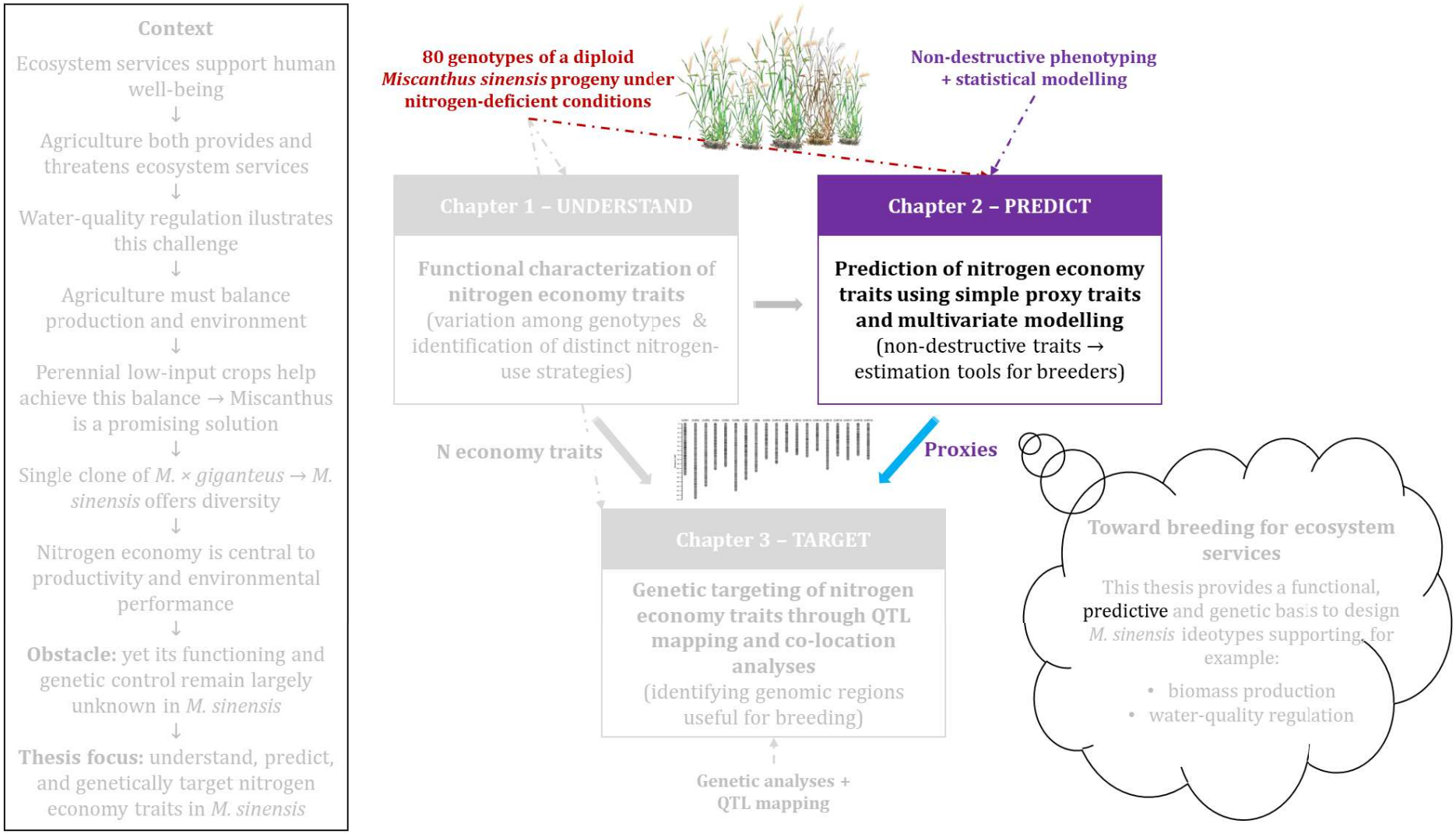

# Proxy Traits Help Breeders Predict Complex Nitrogen Economy Traits in a *Miscanthus sinensis* progeny

S Iqbal, M Zapater, S Monnot, M Brancourt-Hulmel

BioEcoAgro Joint Research Unit, INRAE, Univ de Liege, Univ Lille, Univ Picardie Jules Verne, Chaussée Brunehaut, Entrées- Mons, France.

**Keywords:** *Miscanthus sinensis*, Nitrogen economy, Proxy traits, Non-destructive phenotyping, Multivariate analysis, Partial Least Squares Regression

## Abstract

Improving the nitrogen economy of perennial bioenergy crops is key to enhancing ecosystem services, such as nutrient regulation and long-term soil fertility, without compromising biomass yield. In miscanthus, the nitrogen economy includes five components: nitrogen uptake, nitrogen losses, spring remobilization, and two types of autumn remobilization estimated *via* either the aboveground or the belowground methods. These components are difficult to quantify because they require nitrogen fluxes determination based on plant destructive measurements on both aboveground and belowground parts at several dates during the growing season. This study evaluated whether simple plant traits can predict all five components of the nitrogen economy in a segregant progeny of *M. sinensis*.

Thirty-five non-destructive morphological, phenological and physiological traits were measured as candidate proxies. Pairwise correlations were calculated to evaluate their potential as individual predictors, and a principal component analysis was used to characterize the multivariate structure and collinearity of the proxy set. Partial least squares regression models (PLS) were then developed to predict each nitrogen economy component using either all proxies or reduced predictor sets selected with the Variable Importance in Projection criterion (VIP).

Each proxy trait showed biologically interpretable relationships with each nitrogen economy component, although correlations were generally weak to moderate. Based on a repeated cross-validation procedure, PLS models improved predictive ability substantially. Across full and parsimonious models, prediction accuracies ranged from 0.62 to 0.74 for nitrogen uptake, 0.48 to 0.63 for autumn remobilization *(*aboveground method), 0.49 to 0.51 for autumn

remobilization (belowground method), 0.30 to 0.46 for spring remobilization and 0.24 to 0.39 for nitrogen losses. Parsimonious models that retained only strong predictors performed as well as the complete model, and in several cases even better, while relying on far fewer and simpler traits. For selection and counter selection in breeding, parsimonious models detected between seventy-five and ninety-five percent of the genotypes selected or discarded by the complete model.

These results demonstrate that nitrogen economy traits, previously measurable only destructively, can be approximated using a small set of non-destructive proxy traits, which offers higher throughput phenotyping for such complex traits. The approach provides a practical route for integrating nitrogen uptake and endogenous nitrogen recycling into breeding strategies for *M. sinensis* and offers clear potential for ecosystem service-oriented selection.

## 1. Introduction

Perennial crops grown for biomass production are increasingly recognized as a valuable resource for addressing the rising demand for biomass in the bioeconomy (Clifton-Brown et al., 2023). These authors reviewed that the cultivation and use of perennial biomass has markedly lower environmental impacts than annual crops, while offering a wider range of ecosystem services. To sustain these benefits, perennial crops must assimilate, recycle and allocate nitrogen efficiently in order to support growth, reproduction and long-term ecosystem functioning. Among perennial biomass crops, miscanthus stands out as particularly promising, combining high biomass productivity with the provision of multiple ecosystem services across diverse environments (Jørgensen, 2011; Kiesel et al., 2016; McCalmont et al., 2017; Tavakoli-Hashjini et al., 2020; Winberg et al., 2023).

The plant nitrogen economy, defined by the internal cycling of nitrogen and uptake of nitrogen from the soil together (Leroy et al., 2022), is central to sustaining productivity while reducing environmental impacts in miscanthus systems. Endogenous nitrogen fluxes include spring remobilization (SR), during which nitrogen stored in belowground parts (roots and rhizomes) is transferred to developing shoots at the start of the growing season, and autumn remobilization (AR), whereby nitrogen is withdrawn from senescing shoots and stored belowground for subsequent growth cycles (Strullu et al., 2011). Exogenous fluxes correspond to in-season nitrogen uptake from the soil. Together, these fluxes determine how much external

nitrogen is required to support biomass production and how much nitrogen is conserved within the plant between seasons (Strullu et al., 2011; Dierking et al., 2017; Leroy et al., 2022). Coordinated nitrogen recycling through spring and autumn remobilization maintains internal nitrogen availability for shoot development, while soil uptake supports continued growth with limited fertilizer input. In a segregant *M. sinensis* progeny, we previously showed that both endogenous and exogenous nitrogen fluxes were positively correlated with biomass yield, demonstrating that effective internal recycling combined with efficient uptake can sustain productivity (Iqbal et al., 2026). Such balanced nitrogen use reduces fertilizer requirements and minimizes nutrient export at winter harvest (Beale & Long, 1997), leading to lower nitrate leaching and nitrous oxide emissions compared with annual cropping systems (Cacho et al., 2018; Davis et al., 2019; Studt et al., 2021). These effects directly support regulating ecosystem services by protecting water quality and mitigating greenhouse-gas emissions (Lesur et al., 2014; Cibin et al., 2016; Weik et al., 2022). At the same time, the perennial growth habit and seasonal nitrogen remobilization of miscanthus promote soil carbon sequestration (Agostini et al., 2015; Zang et al., 2018) and contribute to long-term soil formation and fertility (Tavakoli-Hashjini et al., 2020). Through these interconnected mechanisms, nitrogen economy links plant productivity with ecosystem regulation and underpins multifunctional biomass cropping systems.

Despite its importance, quantifying nitrogen economy traits in miscanthus remains a major phenotyping challenge. Accurate estimation of endogenous fluxes such as SR and AR, as well as seasonal nitrogen uptake from the soil, requires repeated, date-specific measurements of nitrogen stocks in both aboveground and belowground plant compartments. These measurements rely on destructive harvests of shoots and labor-intensive excavation of rhizomes and roots at defined phenological stages, followed by analyses of changes in nitrogen pools to infer fluxes (Beale & Long, 1997; Himken et al., 1997; Strullu et al., 2011; Dierking et al., 2017). Although these approaches provide definitive estimates, they are time-consuming and unsuitable for large genetic populations or multi-environment breeding trials. Consequently, only a limited number of genotypes can be assessed destructively, restricting throughput, replication and experimental flexibility.

In parallel, numerous studies in miscanthus and other perennial grasses have demonstrated that simple, non-destructive traits can capture important aspects of plant performance at scale. Canopy height and phenological development have been repeatedly associated with biomass

yield, with early-season canopy height often emerging as a particularly informative indicator (Davey et al., 2017). Strong relationships have also been reported between aboveground biomass and stand volume, defined by the combination of plant height and circumference (Brancourt-Hulmel et al., 2021). Beyond manual measurements, remote-sensing approaches show that canopy structure and spectral indices can estimate biomass or moisture status (Miura et al., 2020; Hamada et al., 2021; Impollonia et al., 2022). In *Miscanthus* × *giganteus*, red-edge vegetation indices have successfully distinguished nitrogen fertilization treatments and improved yield prediction (Namoi et al., 2022). Collectively, these studies highlight the potential for simple, non-destructive traits to act as proxies for complex physiological processes.

However, while proxy traits have been widely used to estimate biomass and related performance attributes (Davey et al., 2017; Leroy, 2021), their capacity to predict core nitrogen economy traits in miscanthus remains largely unexplored. Existing studies have primarily focused on remobilization efficiencies, which describe the proportion of nitrogen transferred between plant compartments rather than the absolute quantities involved. For example, Leroy (2021) showed in three miscanthus genotypes that autumn remobilization efficiency was negatively correlated with the nitrogen content of aboveground tissues at the end of winter and that genotypes with a greater proportion of stems present in June exhibited more efficient nitrogen storage in rhizomes. Similarly, Yang and Udvardi (2018) reported a negative relationship between the duration from heading to harvest and nitrogen remobilization efficiency in perennial switchgrass. These findings demonstrate that simple phenological, structural or physiological traits can reflect variation in proportional nitrogen allocation within plants. Nevertheless, they do not address whether non-destructive traits can predict endogenous and exogenous nitrogen fluxes, which represent the actual quantities of nitrogen circulating through the plant-soil system. To date, no study has identified non-destructive traits capable of predicting these nitrogen fluxes across a segregant population, leaving nitrogen economy measurable only through plant destructive sampling.

This limitation creates a clear phenotyping gap that constrains both breeding and ecological evaluation of perennial biomass crops. A practical strategy to address such constraints is indirect selection through secondary traits, as proposed by Gallais (1984), whereby an economically important primary trait is improved using correlated secondary characters that are easier to measure or more heritable. In miscanthus, combining multiple morphological or

physiological traits has already been shown to substantially increase explanatory power compared with single-trait correlations for complex traits such as biomass yield (Robson et al., 2013; Slavov et al., 2014; Davey et al., 2017), suggesting that a multivariate proxy approach could be effective for nitrogen economy traits as well.

The optimal implementation of multi-trait indirect selection involves constructing a selection index, defined as a linear predictor that combines phenotypic values of secondary traits to estimate the genotypic value of a primary trait (Gallais, 1984). When many correlated secondary traits are involved, however, multicollinearity can limit the efficiency of classical approaches. Partial Least Squares (PLS) regression offers a robust solution in this context, as it derives latent variables that maximize covariance between predictors and response variables and is particularly well suited to situations where the number of predictors is large relative to the number of observations (Rougoor et al., 2000). Applications of PLS in animal and plant breeding have demonstrated its ability to model complex trait architectures while reducing multicollinearity and maintaining predictive power, including for milk yield in cattle (Rougoor et al., 2000) and baking quality in winter wheat using multiple biochemical and phenotypic predictors (Oury et al., 2010). Applied to nitrogen economy traits in perennial crops, this approach provides a framework for identifying non-destructive proxy traits that can predict endogenous and exogenous nitrogen fluxes at scales inaccessible to plant destructive sampling.

Within this framework, an important consideration is parsimony. In quantitative genetics, models that achieve high predictive performance with a limited number of parameters are preferred for practical implementation. For example, Brancourt-Hulmel et al. (1997) showed that in genotype-by-environment interaction analyses, optimal models were those that balanced efficiency with a minimal number of parameters. More recent work in PLS modelling has similarly demonstrated that variable reduction strategies, such as filtering based on Variable Importance in Projection (VIP) scores, can maintain or even improve predictive performance by eliminating noisy or weak predictors (Alenezi, 2021). Identifying reduced sets of informative proxy traits is therefore essential for developing phenotyping strategies that are both accurate and operationally feasible.

In this study, we address this phenotyping gap by establishing a proxy-based framework for predicting nitrogen economy traits in a segregant *Miscanthus sinensis* progeny. Our first objective was to identify and validate simple, non-destructive morphological, phenological and physiological traits that could serve as proxies for destructive nitrogen economy traits,

including spring remobilization, autumn remobilization and seasonal nitrogen uptake. Previous evidence showing that such traits can correlate with nitrogen remobilization efficiencies (Yang & Udvardi, 2018; Leroy, 2021) supports the hypothesis that certain easily measured indicators may show interpretable relationships with nitrogen economy traits and could therefore act as reliable proxies. Our second objective was to determine whether combining multiple proxy traits could better represent the complexity of nitrogen economy traits than any single trait alone. Given that individual traits often show only modest associations with complex physiological processes, we hypothesized that multivariate PLS models would provide more accurate predictions by integrating complementary information across correlated predictors. A further aim was to identify parsimonious predictor subsets using VIP criteria and to test whether reduced models could retain predictive performance while substantially decreasing model complexity. Finally, we evaluated how proxy-based prediction models could be applied in breeding contexts, particularly for counter-selection, by assessing whether simplified models could reliably identify inferior genotypes in a manner consistent with full models. Together, these objectives establish a non-destructive framework for assessing nitrogen economy traits in *Miscanthus sinensis*, enabling these previously inaccessible traits to be evaluated at scale and facilitating their integration into breeding strategies targeting ecosystem services.

## 2. Materials and Methods

### 2.1 Experimental site and trial design

The study was conducted based on the *Miscanthus sinensis* progeny trial established at the French National Research Institute for Agriculture, Food, and Environment (INRAE) in Estrées-Mons, northern France (49°87′ N, 3°01′ E). The site belongs to the experimental unit of GCIE, Grandes Cultures Innovation Environnement (doi: 10.15454/1.5572425838988464E12). The climate is classified as marine west coast (Cfb). Over the period 2017-2024, the experimental site was characterized by a mean annual temperature of 11.2°C and an average annual precipitation of 675 mm. During the 2023-2024 growing season considered in this study (February 2023 to February 2024), the mean temperature was 11.4°C and total precipitation reached 925 mm.

The soil at Estrées-Mons is a deep silt loam, classified as a Haplic Luvisol (IUSS Working Group WRB, 2022). The texture is approximately 16.5% clay, 72.7% silt and 7.8% fine sand,

with a near-neutral pH (7.9), a high cation exchange capacity (96.8 meq 100 $g^{-1}$) and a moderate organic carbon content (11.4 g $kg^{-1}$; C/N = 10.6). These physicochemical characteristics, determined in 2017, are considered representative of the site's baseline fertility. Soil mineral N concentrations were measured in the trial over the 0-150 cm depth in early spring. In March 2023, the mean soil mineral N stock was 20 kg N $ha^{-1}$ and increased to 29 kg N $ha^{-1}$ in March 2024. These levels were markedly lower than those recorded in a previously studied fertilized trial located at the same site, in which 120 kg N $ha^{-1}$ was applied as a urea-ammonium-nitrate solution in May, and soil mineral N concentrations measured in March or April over the 0-150 cm profile were 85, 85, 53 and 54 kg N $ha^{-1}$ in 2014, 2015, 2016 and 2017, respectively (Leroy et al., 2022). In our trial, during each plant sampling campaign, soil N concentrations were also measured in the 0-30 cm horizon, where most root activity occurs. Mean values were 8 kg N $ha^{-1}$ in March 2023, 11 kg N $ha^{-1}$ in July 2023, 12 kg N $ha^{-1}$ in September 2023 and 19 kg N $ha^{-1}$ in March 2024.

The trial comprised 127 *M. sinensis* genotypes derived from a diploid cross between *M. sinensis* 'Malepartus' (MAL) and 'Herman Mussel' (HER). Seeds resulting from this cross were germinated *in vitro* in 2014, transplanted to a greenhouse in 2015, and then transferred in the field at the INRAE GBFOr experimental unit of Orléans (Loiret, 47°49′ N, 1°54′ E) in 2016, where plants were clonally propagated by rhizome division in 2017. This progeny was established in 2018 at the INRAE GCIE experimental unit of Estrées-Mons in an incomplete block design with four blocks and a planting density of 1 plant $m^{-2}$. From establishment until the beginning of the present study, management primarily consisted of standard agronomic practices, including manual weed control, with no chemical inputs applied, and the plants were harvested each year in February. The trial was unfertilized and irrigated throughout the five years of cultivation in order to avoid water limitation. Recorded irrigation volumes in the progeny trial were 36, 926 and 393 $m^3$ in 2021, 2022 and 2023, respectively. Leaf litter and other plant residues senesced naturally in autumn and winter and were left on the soil surface.

The present study focused on a subset of 80 genotypes from the progeny trial, chosen to represent the range of variation in nitrogen fluxes and biomass production. Each genotype was represented by at least one replicate in each block. The nitrogen status of the trial was diagnosed using the nitrogen dilution curve developed for miscanthus (Zapater et al., 2017) to determine the nitrogen nutrition index (NNI) as in Laperche et al. (2008). The Malepartus parent (MAL) was used as a probe genotype, and its index was less than 1, indicating that the progeny trial

was nitrogen-deficient. The full methodological details of the determination of nitrogen status are provided in Iqbal et al. (2026).

## 2.2 Plant sampling

Plant sampling was carried out during four campaigns in order to characterize nitrogen quantities at key stages of the annual growth cycle, each corresponding to periods with distinct nitrogen stocks in the aboveground and belowground parts of the plants. Based on previous works (Leroy et al., 2022), the sampling dates were chosen to represent (i) winter dormancy; the maximum nitrogen quantity in belowground parts (date 0), (ii) the minimum nitrogen quantity in belowground parts after spring remobilization (date 1), (iii) the maximum nitrogen quantity in aboveground parts during active growth (date 2) and (iv) the end of the cycle after complete senescence (date 3). These dates were February 2023, July 2023, September 2023 and February 2024, respectively.

On each sampling date, both aboveground parts (AP: stems and leaves) and belowground parts (BP: rhizomes and associated roots) were collected. Aboveground parts were harvested at 7 cm above the soil surface, a commonly used cutting height in miscanthus plot trials (Cadoux et al., 2014; Scordia et al., 2022) and consistent with standard agricultural practices for mechanical harvesting. In this study, aboveground biomass included both the harvested portion and the basal stems remaining below the cutting height, which were collected during rhizome excavation to ensure complete accounting of aboveground biomass and to better reflect biomass and nitrogen dynamics. Belowground parts were excavated to a depth of approximately 30-40 cm, corresponding to the maximum rhizome depth. This destructive sampling ensured that nitrogen stocks were quantified in both compartments at each stage of the cycle.

Within the subset of 80 genotypes, 65 genotypes had at least four replicates each, allowing one plant per genotype to be sampled on each of the four dates. The remaining 15 genotypes had at least eight replicates each, permitting two plants per genotype to be sampled per date. This sampling framework ensured that spring remobilization, autumn remobilization, nitrogen uptake and nitrogen losses could be calculated reliably from changes in nitrogen quantities between the four sampling dates. For all analyses requiring nitrogen fluxes, biomass values were adjusted prior to calculation in order to reduce potential bias caused by plant-to-plant variability within genotypes, because sampling belowground biomass is destructive and the

same plants could not be reused at multiple dates. The correction procedure is described in detail in Iqbal et al. (2026).

## 2.3 Plant measurements and determination of biomass and nitrogen concentration

At each sampling date, the collected aboveground and belowground plant parts were used to determine biomass and nitrogen concentration. Immediately after harvest, the fresh weights of AP and BP were recorded. A representative subsample of each plant part was taken, weighed fresh, dried at 65 °C for 96 h until a constant weight had been reached and then weighed again to determine dry weight. The dry matter content was calculated as:

$$\text{Dry Matter Content} = \text{Dry weight of subsample} / \text{Fresh weight of subsample}$$

This dry matter content was then used to estimate the dry biomass of the entire sample:

$$\text{Dry Biomass} = \text{Fresh Weight of Entire Plant} \times \text{Dry Matter}$$

Biomass yield (t $ha^{-1}$) was subsequently determined based on dry biomass and the planting density.

Dried subsamples of AP and BP were analyzed for nitrogen concentration. For each compartment, nitrogen quantity was then calculated by combining dry biomass and nitrogen concentration as follows:

$$NA = WA \times [NA]$$

$$NB = WB \times [NB]$$

$$NT = NA + NB$$

where NA and NB represent the nitrogen quantities (kg N $ha^{-1}$) in aboveground and belowground compartments, respectively; WA and WB correspond to the dry matter quantities of each plant compartment (t $ha^{-1}$); and [NA] and [NB] are the corresponding nitrogen concentrations (g N $kg^{-1}$ DM). The nitrogen quantities obtained at the four sampling dates formed the basis for calculating the nitrogen economy traits examined in this study.

## 2.4 Quantification of nitrogen economy traits: N remobilization, uptake and losses

Nitrogen economy traits, including endogenous recycling of nitrogen within the plant (spring remobilization, SR; autumn remobilization, AR), exogenous nitrogen uptake from the soil and nitrogen losses, were quantified. All calculations followed the flux-based framework described in Iqbal et al. (2026) and were adapted from established methods (Strullu et al., 2011; Dierking et al., 2017; Leroy et al., 2022).

Spring remobilization (SR, kg N $ha^{-1}$), representing the nitrogen translocated from belowground storage organs to support new shoot growth in spring, was calculated following the method of Strullu et al. (2011) as:

$$SR = NB_0 - NB_1$$

where $NB_0$ was the nitrogen quantity in the belowground parts before spring regrowth ate date 0 (February 2023), and $NB_1$ was the nitrogen quantity after spring remobilization at date 1 (July 2023), during summer. The corresponding spring remobilization efficiency (SRE) was calculated relative to maximum aboveground nitrogen quantity measured at date 2 ($NA_2$):

$$SRE = (SR / NA_2) \times 100$$

Autumn remobilization (AR, kg N $ha^{-1}$), defined as the nitrogen withdrawn from senescing aboveground parts and stored in belowground parts before dormancy, was estimated using two complementary methods described by Dierking et al. (2017): *via* aboveground method (ARa), quantifying the decrease in aboveground nitrogen during senescence, and *via* belowground method (ARb), quantifying the increase in belowground nitrogen over the same period.

$$ARa = NA_2 - NA_3$$

where $NA_2$ was the nitrogen quantity in aboveground parts at the start of senescence at date 2 (September 2023), and $NA_3$ was the nitrogen quantity after full senescence at date 3 (February 2024).

$$ARb = NB_3 - NB_2$$

where $NB_3$ was the nitrogen quantity in belowground parts after full senescence (February 2024), and $NB_2$ was the nitrogen quantity in the belowground parts when aboveground nitrogen reached its maximum (September 2023). As for spring remobilization, the corresponding autumn remobilization efficiencies were calculated relative to the maximum aboveground nitrogen quantity and were coded as ARaE and ARbE, respectively.

Nitrogen uptake (N uptake, kg N $ha^{-1}$) represents the maximum nitrogen acquired from the soil during the growing season. It was calculated as:

$$N\ Uptake = NT_2 - NB_0$$

where $NT_2$ was the total nitrogen quantity of the whole plant at date 2 (September 2023), when aboveground biomass reached its peak nitrogen accumulation, and $NB_0$ was the nitrogen quantity in belowground parts before spring regrowth (February 2023). Similar to SRE, the corresponding nitrogen uptake efficiency was calculated relative to the maximum aboveground nitrogen quantity.

Nitrogen losses (N losses, kg N $ha^{-1}$) were calculated following the method of Leroy et al. (2022), considering the difference between total nitrogen at the peak of the growing season and after complete senescence:

$$N\ losses = NT_2 - NT_3$$

where $NT_2$ was the total nitrogen quantity at peak growth (September 2023), and $NT_3$ was the total nitrogen quantity at the end of the cycle (February 2024).

## 2.5 Phenotyping of proxy traits

Proxy traits related to plant size and architecture, canopy structure, phenology and growth dynamics, nitrogen status, nitrogen concentration and nitrogen pools were measured over the 2023 to 2024 growth cycle on the same plants used for nitrogen flux calculations. These traits were chosen because they are easy to measure and non-destructive during the season, making them suitable candidates for predicting nitrogen economy traits derived from plant destructive sampling. A schematic overview of the major aboveground and belowground plant compartments from which these traits were collected is provided in Figure 1.

Size and architecture traits included aboveground biomass, biomass partitioning between leaves and stems, stand volume and plant circumference. Aboveground biomass was obtained from the destructive harvests described previously. At the final harvest, the aboveground part was separated into subsamples of leaves and stems before drying, allowing the calculation of leaf and stem biomass separately. Circumference was measured after harvest by bunching the stems with a strap and measuring the plant circumference at fifty centimeters above the soil surface using a measuring tape. Stand volume was estimated by converting the bunched stem circumference at fifty centimeters into a cross sectional area representing the entire stem bundle of each plant and multiplying this area by canopy height. The use of bunched circumference avoided the need to count stems because the circumference already reflected the combined thickness of all stems. All size and architecture traits were measured during the destructive harvests conducted in February 2023 and February 2024.

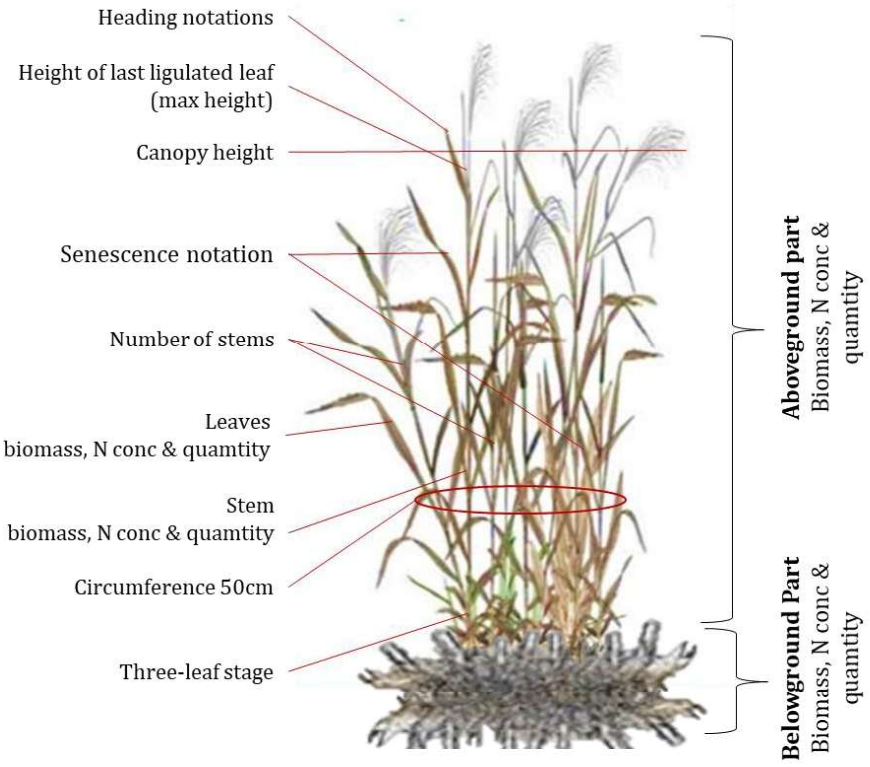


**Figure 1.** Illustration of *Miscanthus sinensis* showing the aboveground parts (stems and leaves) and belowground part (rhizome and associated roots), together with the main proxy traits measured for each compartment.

Canopy structure related traits included canopy height, maximum plant height and the number of stems. Canopy height was measured from the soil surface to the height at which most of the incident light was intercepted by the leaves using a measuring rod. Maximum height was measured from the soil surface to the base of the last ligulated leaf on the first cohort of stems.

The number of stems was determined by counting all stems with at least one ligulated leaf. Stem counts were performed in the field during the growing season and in the laboratory at the end of the cycle after the aboveground part had been harvested. All canopy structure traits were measured immediately before plant sampling in February 2023, July 2023, September 2023 and February 2024, with stem counts additionally performed in the field in June 2023 as well.

Phenology and growth dynamics related traits included emergence, the date of the three-leaf stage, senescence and life cycle duration. Emergence was recorded as the day when the first new bud (approximately 1 cm in size) was observed on the plant. The date of the three-leaf stage corresponded to the day when the first stem with three ligulated leaves was observed. This developmental stage was chosen by analogy with maize, another $C_4$ species (Cooper & MacDonald, 1970; Deleens et al., 1984; Nadeem et al., 2014). Senescence was scored visually several times per week from August to December and expressed as the proportion of aboveground parts that had senesced. The seasonal dynamics of senescence were modelled using a sigmoidal function:

$$\text{Senescence (\%)} = 100 / [1 + \exp (a / 25 * (x - b))]$$

where '*x*' represents the observation date expressed as day of year, '*a*' is a shape parameter controlling the slope of the senescence curve, and '*b*' corresponds to the inflection point (day of year at which 50% senescence is reached). The dates corresponding to 50% and 95% senescence were calculated as the DOY when 50% or 95% of the aboveground parts had turned brown and dried. Life cycle duration was calculated for each plant as the number of days between emergence and ninety-five percent senescence. All phenology and plant development traits were recorded through repeated field observations during the 2023 to 2024 growth cycle.

Nitrogen status was assessed using the nitrogen nutrition index (NNI). Proxy physiological traits were based on nitrogen concentration and nitrogen pools, as the product of biomass and nitrogen concentration for each considered compartment. Nitrogen concentration was analyzed for the aboveground and belowground compartments at each sampling date. At the final harvest in February 2024, nitrogen concentration was also measured separately in leaves and stems. During the growing season, nitrogen concentration in aboveground parts was obtained from a small subsample of stems. These subsamples were considered representative of the nitrogen concentration of the entire compartment without requiring full destructive sampling. For the belowground part, N concentration was determined from a small representative section of the

rhizome, after pre-grinding the entire rhizome. However, we first ensured that the nitrogen concentration in the PS was closely linked to the nitrogen concentration in small pieces (1cm) of rhizome associated with the stem (r = 0.8 to 0.94 depending on the year, data not shown), ensuring that the phenotyping was as non-destructive as possible.

Proxy traits based on nitrogen concentration included the nitrogen concentration of aboveground parts, leaves and stems in February 2024, the decline in aboveground nitrogen concentration between September 2023 and February 2024, the increase in belowground nitrogen concentration between July 2023 and February 2024, and the belowground nitrogen concentrations measured in July 2023 and February 2024. Proxy traits based on nitrogen pools included the nitrogen quantity in aboveground parts in February 2024 and the nitrogen quantities in leaves and stems in February 2024, calculated by combining dry biomass and nitrogen concentration for each compartment as described earlier.

## 2.6 Principal Component Analysis (PCA)

A principal component analysis (PCA) was performed to explore the multivariate structure and collinearity among the 35 non-destructive proxy traits collected on the 80 genotypes. Proxy traits were used as active variables, and the five nitrogen economy traits (SR, ARa, ARb, N uptake and N Losses) were included as supplementary quantitative variables. Trait values were centered and standardized. PCA was conducted using the PCA() function from the FactoMineR R package (version 4.3.2, R Core Team).

## 2.7 Partial Least Squares Regression (PLS1) modeling

Partial least squares regression (PLS1) models were developed to predict nitrogen economy traits (SR, ARa, ARb, N uptake and N Losses; response matrix **Y**) from the 35 proxy traits (predictor matrix **X**). Predictor and response variables were centered and standardized prior to modelling. PLS1 was selected due to its suitability for prediction in the presence of multicollinearity among predictors (Boulesteix & Strimmer, 2007).

Model training and evaluation were performed using a 5-fold cross-validation repeated 20 times and based on random split of genotypes between training and validation sets. For each repetition, the PLS1 model was trained using four folds and evaluated on the remaining fold, until all folds had been used as validation once. We selected the optimal number of latent

variables for each trait by minimizing the average Root Mean Squared Error of the validation set (RMSE_val). The smallest number of latent variables achieving the minimum RMSE_val was retained.

After selecting the optimal number of components, models were refitted and used to generate predicted values. Predicted values were obtained using the regression coefficients of the optimized model on the original scale to ensure that predictions remained interpretable in their original units. Prediction accuracy was quantified as the Pearson correlation between predicted and observed values in the validation set.

For each nitrogen-economy trait, predictive performance was summarized using several cross-validation statistics. The cross-validated square root of the coefficient of determination ($\sqrt{R^2}$_val) quantified how well the model explained variation in the validation set. The root mean squared error of the validation set (RMSE_val) expressed the average prediction error in the original units of each target trait (kg N $ha^{-1}$), while RMSE_cal represented the corresponding error in the calibration set. The standard error of RMSE_val (se_RMSE_val) reflected the variability of validation error across the 20 repeated cross-validation rounds. Two additional diagnostics were calculated: robustness difference, defined as the absolute difference between RMSE_cal and RMSE_val, and accuracy difference, defined as the absolute difference between $\sqrt{R^2}$_cal and $\sqrt{R^2}$_val. Smaller values for these two metrics indicate more stable model performance across calibration and validation sets. All statistics reported in Table 1 were computed using the optimal number of latent components selected for each PLS1 model. PLS1 models were fitted using the plsreg1() function from the plsdepot R package (version 0.1.17; Sanchez (2012)).

## 2.8 Selection of best predictors using VIP

We next used the optimized PLS models to obtain predicted values for each trait and to quantify the contribution of each predictor. Predictor importance was assessed using the Variable Importance in Projection (VIP) criterion, which summarizes the contribution of each predictor to the prediction of the response across all latent components and is widely used for variable selection in PLS regression (Farrés et al., 2015; Mahieu et al., 2023). A commonly used criterion is that predictors with VIP values greater than 1 are considered most relevant for explaining the response (Akarachantachote et al., 2014; Zheng et al., 2023). However, variables with VIP values between approximately 0.8 and 1 may still contribute meaningfully to model

prediction and should not be disregarded (Eriksson et al., 2001). Based on this literature, we interpreted VIP values of at least 1 as strong importance, values between 0.8 and 1 as moderate importance, and values below 0.8 as weak importance.

Using these thresholds, three models were constructed for each nitrogen economy trait. Model 1 represented the complete multivariate model and included all proxy traits. Model 2 and Model 3 represented parsimonious models, retaining predictors with VIP values of at least 0.8 and at least 1, respectively. For every model and every trait, we repeated the full PLS workflow independently. This included refitting the model with its specific predictor set, performing 5-fold cross-validation repeated 20 times, and selecting the optimal number of components for that predictor set. This ensured that each model was evaluated under conditions appropriate to its own reduced or full set of predictors.

For each model and each nitrogen economy trait, predicted values generated through cross-validation were compared with the corresponding observed values to quantify model performance in calibration and validation. This approach allowed assessment of whether multivariate PLS prediction could reliably approximate nitrogen economy traits and whether refinement of predictor sets based on VIP thresholds improved predictive ability.

## 2.9 Statistical analyses

All statistical analyses were conducted using R software (version 4.3.2, R Core Team). Pairwise relationships between proxy traits and nitrogen economy traits were quantified using Pearson correlation coefficients. Statistical significance was assessed at a threshold of $\alpha = 0.05$, with significance levels indicated as * for $p < 0.05$, ** for $p < 0.01$, *** for $p < 0.001$ and "NS" for non-significant results. Correlation analyses and associated p values were obtained using the cor.test function from the stats package.

Partial least squares regression (PLS1) models were fitted using the plsreg1 function from the plsdepot package (version 0.1.17). The cross-validation procedures, component selection and model reconstructions were carried out following the modelling framework described above. For each trait and model (Model 1, Model 2 and Model 3), predicted values were aggregated across all cross-validation folds and repetitions. Predictive accuracy between predicted and observed values was evaluated using the correlation between predicted and observed values in the calibration subsets and in the validation subsets. These correlations provided a direct

quantitative measure of predictive ability and allowed comparison of predictive performance between the full model and the two parsimonious models.

## 3. Results

### 3.1 Summer-to-autumn and winter-to-spring nitrogen dynamics formed distinct sources of variation and were each associated with biomass yield

Nitrogen economy traits formed two main component axes of variation when summarized by principal component analysis (PCA) based on SR, ARa, ARb, N uptake and N losses as active variables and biomass at the green (Biomass S) and brown (Biomass F) harvests as supplementary quantitative variables (Figure 2). These two first principal components together explained 72% of the total variance.

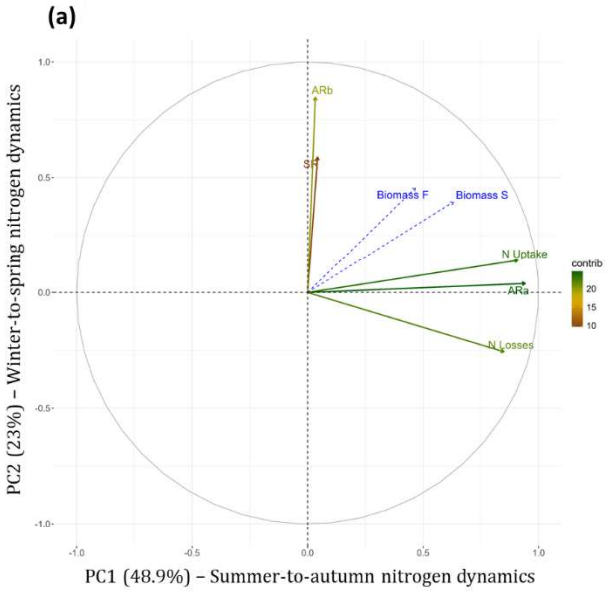


(b)

| Variable | PC1 Summer-to-autumn nitrogen dynamics (48.9%) | PC2 Winter-to-spring nitrogen dynamics (23%) |
|---|---|---|
| Spring remobilization | 0.1 % | 30.1 % |
| Autumn remobilization: ARa | 36.4 % | 0.1 % |
| Autumn remobilization: ARb | 0.1 % | 62.3 % |
| Nitrogen uptake | 33.9 % | 1.7 % |
| Nitrogen losses | 29.6 % | 5.7 % |

**Figure 2.** Principal component analysis of nitrogen economy traits and biomass yield. PCA biplot (plot a) constructed using SR, ARa, ARb, N Uptake and N Losses as active variables, with biomass yield at the green (Biomass S) and brown (Biomass F) harvests included as supplementary quantitative variables, and contribution of variables to the first two principal components (plot b). Trait abbreviations: SR = spring remobilization flux; ARa = autumn remobilization flux *via* aboveground method; ARb = autumn remobilization flux *via* belowground method; N Uptake = nitrogen uptake; N Losses = nitrogen losses; Biomass S = biomass in September 2023; Biomass F = biomass in February 2024.

The first principal component (PC1), interpreted as an axis of summer-to-autumn nitrogen dynamics, explained 48.9% of the variance and was driven mainly by N uptake, ARa and N losses. The second principal component (PC2), representing winter-to-spring nitrogen dynamics**,** explained 23% of the variance and was associated with SR and ARb (Figure 2b). Biomass at both harvests projected positively between the two axes, indicating that genotypes

with stronger summer-to-autumn nitrogen dynamics and greater winter-to-spring nitrogen dynamics tended to produce higher biomass yields (Figure 2a).

## 3.2 Each proxy trait showed weak to moderate pairwise correlations with nitrogen economy traits

Most significant correlations between nitrogen economy traits and candidate non-destructive proxy traits were weak to moderate in magnitude, but multiple proxy traits showed consistent correlations with each nitrogen flux (Figure 3).

**Spring remobilization (SR)**

Spring remobilization showed its strongest correlations with size and architecture related proxy traits. The highest correlations were observed for aboveground biomass (Feb23, r = 0.47; Feb24, r = 0.30) and stand volume (Feb23, r = 0.46; Feb24, r = 0.31). Among the traits measured in February, plant circumference at 50 cm (Feb23, r = 0.36; Feb24, r = 0.30) and nitrogen quantity in aboveground parts (Feb24, r = 0.32) also showed positive correlations with SR.

Several traits recorded during the season showed weaker but significant correlations with SR. Significant correlations included one negative correlation (r = -0.25) and positive correlations ranging from 0.23 to 0.47. They included canopy height (July23, r = 0.32; Sep23, r = 0.23), plant stem number (June23, r = 0.24; July23, r = 0.32) and nitrogen nutrition index defined for each genotype (July23, r = 0.37). The only negative correlation was observed for the decline in aboveground nitrogen concentration from September to February (r = -0.25).

**Nitrogen uptake**

Nitrogen uptake showed its strongest correlations with size and architecture related proxy traits as well. Aboveground biomass (Feb23, r = 0.51; Feb24, r = 0.63) and stand volume (Feb23, r = 0.50; Feb24, r = 0.60) showed the highest correlations. Among the traits measured in February, positive correlations were also observed for circumference at 50 cm (Feb23, r = 0.38; Feb24, r = 0.53), stem number (Feb23, r = 0.31; Feb24, r = 0.49), canopy height (Feb23, r = 0.38; Feb24, r = 0.33), stem biomass (Feb24, r = 0.40), and nitrogen quantity in aboveground parts (Feb24, r = 0.51) and stems (Feb24, r = 0.41).

Seasonal measurements also showed significant correlations with nitrogen uptake. Significant correlations ranged from -0.31 to -0.24 and from 0.23 to 0.63. These included stem number (June23, r = 0.52; July23, r = 0.34; Sep23, r = 0.38), canopy height (July23, r = 0.36; Sep23, r = 0.38), maximum height (July23, r = 0.30; Sep23, r = 0.37) and nitrogen nutrition index (July23, r = 0.51). Negative correlations were observed for the three-leaf stage (r = -0.31) and for belowground nitrogen concentration in July (r = -0.24).

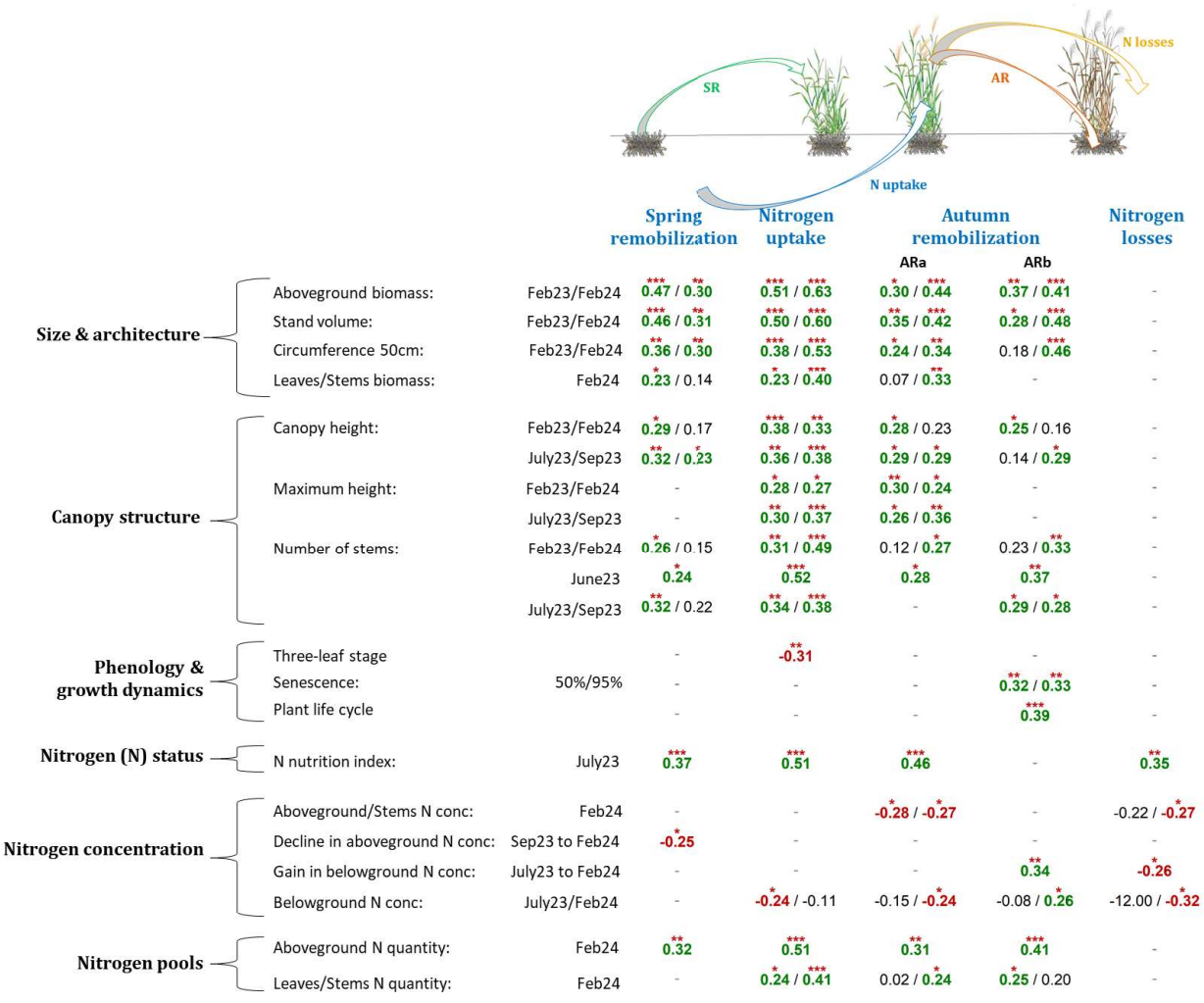


**Figure 3.** Pairwise correlation matrix between nitrogen economy traits (SR, ARa, ARb, N Uptake and N Losses) and candidate proxy traits, with Pearson correlation coefficients (r) and significance levels indicated (*** p < 0.001, ** p < 0.01, * p < 0.05). Green cells represent significant positive correlations and red cells represent significant negative correlations. For proxy traits measured at multiple dates, correlation values are presented in the same row (e.g. Feb23/Feb24). Variable coding for nitrogen economy traits follows Figure 2.

## Autumn remobilization *via* aboveground method (ARa)

For autumn remobilization measured with the aboveground parts, the strongest correlation was observed for nitrogen nutrition index (July23, r = 0.46). Among the proxy traits measured in February, positive correlations were found for aboveground biomass (Feb23, r = 0.30; Feb24,

r = 0.44), stand volume (Feb23, r = 0.35; Feb24, r = 0.42), circumference at 50 cm (Feb23, r = 0.24; Feb24, r = 0.34) and stem biomass (Feb24, r = 0.33). Nitrogen quantity in aboveground parts measured in February also correlated with ARa (Feb24, r = 0.31).

Seasonal traits that showed significant correlations with ARa ranged from -0.28 to -0.24 and from 0.24 to 0.46. They included canopy height (July23, r = 0.29; Sep23, r = 0.29), maximum height (July23, r = 0.26; Sep23, r = 0.36) and stem number (June23, r = 0.28). Negative correlations were observed for nitrogen concentration in aboveground parts (Feb24, r = -0.28), nitrogen concentration in stems (Feb24, r = -0.27) and belowground nitrogen concentration (Feb24, r = -0.24) at the February harvest.

**Autumn remobilization *via* belowground method (ARb)**

Significant correlations with autumn remobilization estimated *via* belowground method ranged from 0.25 to 0.48. ARb showed its strongest correlations with stand volume (Feb23, r = 0.28; Feb24, r = 0.48) and circumference at 50 cm (Feb24, r = 0.46). Among the traits measured in February, aboveground biomass (Feb23, r = 0.37; Feb24, r = 0.41), nitrogen quantity in aboveground parts (Feb24, r = 0.41), canopy height (Feb23, r = 0.25), stem number (Feb23, r = 0.33) and belowground nitrogen concentration (Feb24, r = 0.26) also showed positive correlations with ARb.

Several traits recorded during the season were correlated with ARb, including plant life cycle duration (r = 0.39), stem number (June23, r = 0.37), senescence timing (50%, r = 0.32; 95%, r = 0.33) and canopy height (Sep23, r = 0.29). Gain in belowground nitrogen concentration from July to February also showed a positive correlation with ARb (r = 0.34).

**Nitrogen losses**

Significant correlations with nitrogen losses were limited in magnitude and number. Significant correlations included negative correlations ranging from -0.32 to -0.26 and a single positive correlation (r = 0.35). Nitrogen nutrition index (July23, r = 0.35) showed a positive correlation with nitrogen losses. Negative correlations were observed for belowground nitrogen concentration measured in February (r = -0.32), for nitrogen concentration in stems (Feb24, r = -0.27), and for the gain in belowground nitrogen concentration from July to February (r = -0.26).

## 3.3 Proxy traits were strongly collinear in multivariate space

Using the 35 proxy traits as active variables and the five nitrogen economy traits as supplementary quantitative variables in a principal component analysis (PCA) (Figure 4), the first two principal components explained 54.1% of the total variance (PC1 = 31.7%; PC2 = 22.4%). In the variables plot, proxy traits describing plant size and architecture (aboveground biomass, stand volume, circumference at 50 cm, leaves biomass and stems biomass), canopy structure (canopy height, maximum height, and number of stems), phenology and growth

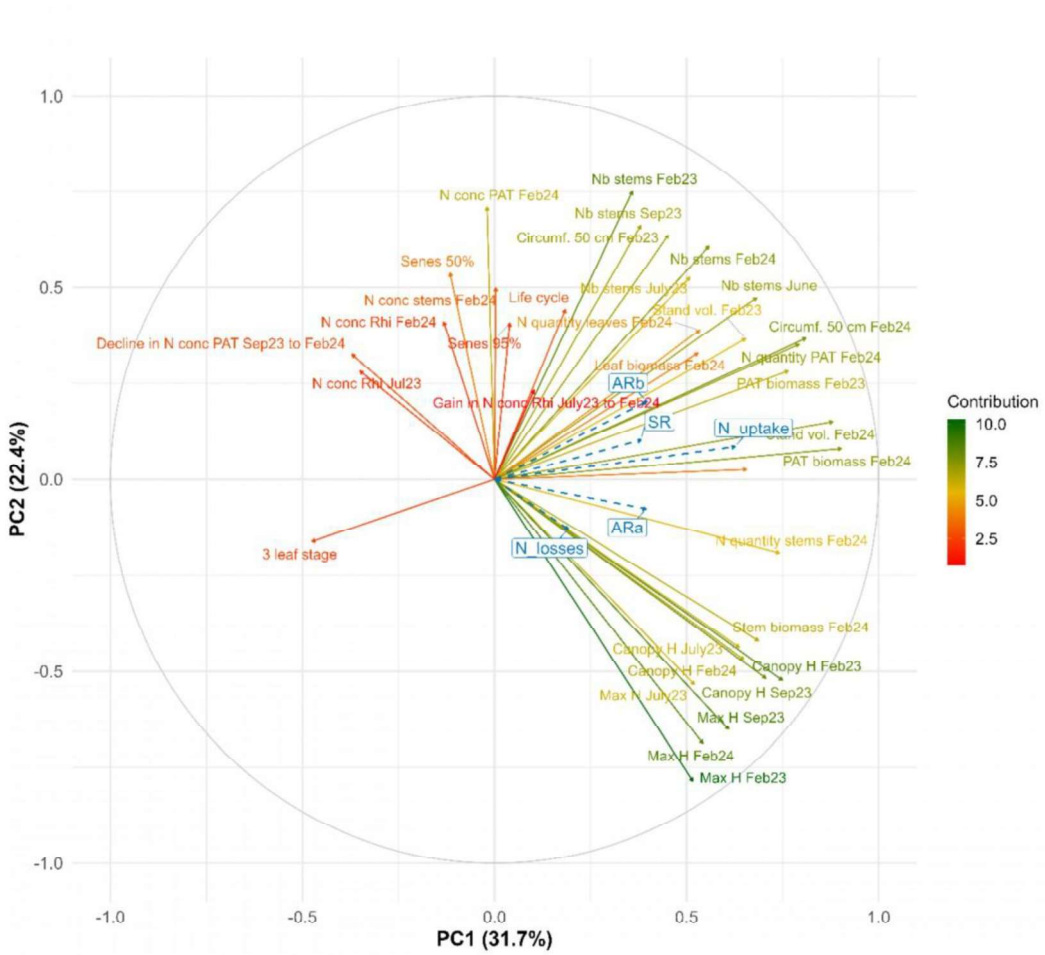


**Figure 4.** Principal component analysis of proxy traits and nitrogen economy traits. PCA biplot constructed using 35 proxy traits as active variables, with the five nitrogen economy traits (SR, ARa, ARb, N Uptake, N Losses) projected as supplementary quantitative variables. Variable coding follows the abbreviations section (page number XVIII).

dynamics (three-leaf stage, senescence timing at 50% and 95%, and plant life cycle), and nitrogen status (nitrogen nutrition index) generally projected in similar directions (Figure 4b).

This pattern indicates that proxy traits were highly collinear and captured overlapping sources of variation rather than independent trait dimensions.

When the nitrogen economy traits were projected as supplementary variables, nitrogen uptake, SR, ARa, ARb and nitrogen losses all fell within the main cloud of proxy traits (Figure 4). Each nitrogen economy trait mostly projected between these two components, indicating that each trait shared variance with several correlated proxies rather than with any single descriptor. This multivariate structure suggested that individual proxies were unlikely to capture nitrogen economy traits on their own and the use of partial least squares (PLS) regression was necessary to combine information across many correlated predictors.

## 3.4 Proxy-based PLS models predicted nitrogen economy traits with trait-specific accuracy

**Predictions for summer-to-autumn nitrogen dynamics**

Using univariate PLS1 models fitted with all 35 proxy traits as predictors, nitrogen uptake was predicted with the highest accuracy among nitrogen economy traits (Figure 5a). The correlation between observed and predicted values in the calibration dataset was $r_{(cal)} = 0.81$. In the validation dataset, prediction accuracy decreased to $r_{(val)} = 0.62$, showing that nitrogen uptake could be predicted with reasonable reliability from non-destructive traits. Cross-validation metrics supported this pattern ($\sqrt{R^2}\_cal = 0.79$; $\sqrt{R^2}\_val = 0.64$), with RMSE_val = 39.08 kg N $ha^{-1}$ (Table 1).

Autumn remobilization estimated *via* aboveground method (ARa) was predicted with intermediate accuracy (Figure 5b). Calibration performance was $r_{(cal)} = 0.74$, while prediction accuracy in validation was $r_{(val)} = 0.48$. Cross-validation statistics were consistent with these results ($\sqrt{R^2}\_cal = 0.71$; $\sqrt{R^2}\_val = 0.51$), with RMSE_val = 33.39 kg N $ha^{-1}$ (Table 1), indicating that ARa could be partly predicted from the proxy trait set.

Nitrogen losses showed the weakest predictive performance among traits describing summer-to-autumn nitrogen dynamics (Figure 5c). Calibration correlation reached $r_{(cal)} = 0.62$, but validation accuracy was low ($r_{(val)} = 0.24$). Cross-validation statistics similarly indicated

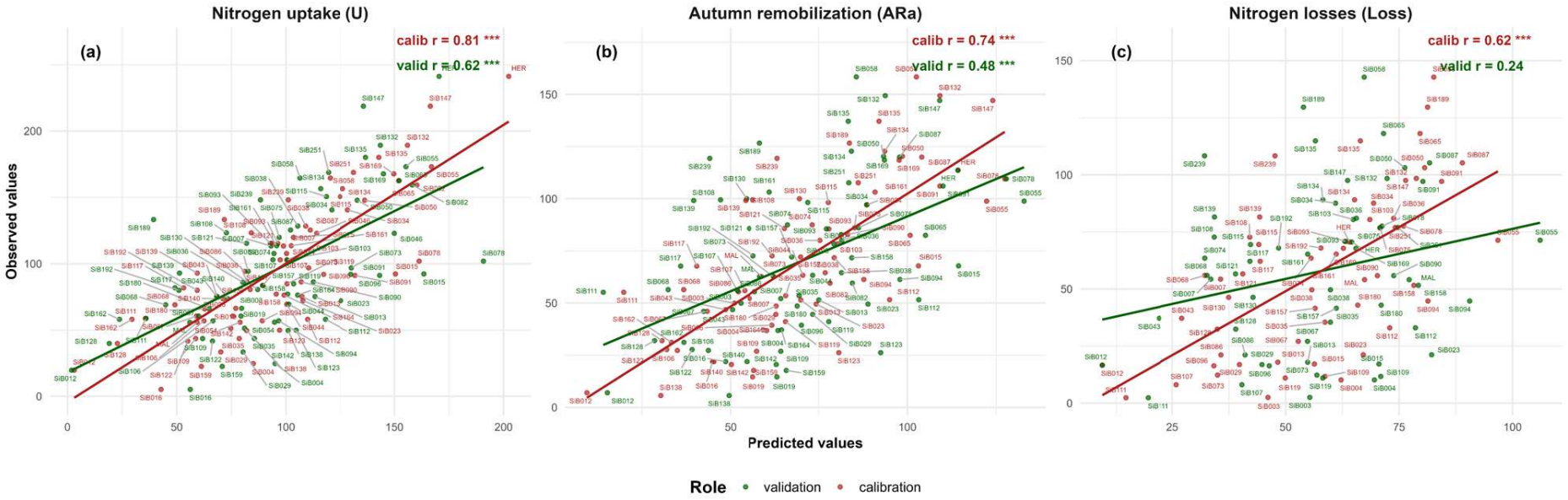


**Figure 5.** Prediction accuracy between observed and predicted values for traits describing summer-to-autumn nitrogen dynamics based on the full proxy-based PLS1 model (Model 1): nitrogen uptake (a), autumn remobilization estimated *via* aboveground method (ARa) (b), and nitrogen losses (c). Pearson correlation coefficients (r) and significance levels (*** $p < 0.001$, ** $p < 0.01$, * $p < 0.05$) are shown for both calibration (red) and validation (green) in each panel.

**Table 1.** Cross-validation statistics for the three proxy-based PLS1 models predicting nitrogen economy traits. Model 1 includes all 35 proxy traits as predictors; Model 2 includes proxy traits with VIP ≥ 0.8; and Model 3 includes proxy traits with VIP ≥ 1. For each nitrogen economy trait, the table reports the observed range, $\sqrt{R^2}$ values for calibration and validation, RMSE values for calibration and validation, the standard error of RMSE in validation, and robustness and accuracy differences.

| Variable | Range | Model | $\sqrt{R^2}$_cal | $\sqrt{R^2}$_val | RMSE_cal | RMSE_val | se_RMSE_val | Robustness diff | Accuracy diff |
|---|---|---|---|---|---|---|---|---|---|
| Spring remobilization | 0.2-84.9 | **1** | **0.62** | **0.41** | **12.5** | **15.8** | **0.3** | **0.21** | **0.03** |
| | | 2 | 0.63 | 0.49 | 12.3 | 14.8 | 0.3 | 0.16 | 0.1 |
| | | 3 | 0.61 | 0.53 | 12.5 | 14.2 | 0.3 | 0.1 | 0.07 |
| Nitrogen Uptake | 5.2-241.2 | **1** | **0.79** | **0.64** | **29.6** | **39.1** | **0.7** | **0.21** | **0.01** |
| | | 2 | 0.78 | 0.67 | 29.9 | 37.6 | 0.6 | 0.17 | 0.01 |
| | | 3 | 0.86 | 0.73 | 24.5 | 34.3 | 0.6 | 0.21 | 0 |
| Autumn remobilization: ARa | 5.6-158.4 | **1** | **0.71** | **0.51** | **25.5** | **33.4** | **0.5** | **0.25** | **0.03** |
| | | 2 | 0.87 | 0.61 | 17.8 | 32.1 | 0.6 | 0.38 | 0 |
| | | 3 | 0.71 | 0.59 | 25.4 | 30.3 | 0.4 | 0.15 | 0.01 |
| Autumn remobilization: ARb | 0.5-72.8 | **1** | **0.68** | **0.52** | **10.9** | **13.5** | **0.2** | **0.19** | **0.1** |
| | | 2 | 0.67 | 0.51 | 11.1 | 13.5 | 0.2 | 0.18 | 0.09 |
| | | 3 | 0.63 | 0.57 | 11.5 | 12.9 | 0.2 | 0.07 | 0.05 |
| Nitrogen Losses | 2.3-142.8 | **1** | **0.58** | **0.35** | **28.0** | **35.5** | **0.6** | **0.22** | **0.04** |
| | | 2 | 0.64 | 0.43 | 26.3 | 33.5 | 0.6 | 0.22 | 0.02 |
| | | 3 | 0.6 | 0.46 | 27.2 | 32.6 | 0.5 | 0.15 | 0.01 |

limited predictive ability ($\sqrt{R^2}$_cal = 0.58; $\sqrt{R^2}$_val = 0.35), with RMSE_val = 35.45 kg N ha$^{-1}$ (Table 1). Validation performance for nitrogen losses was not significant, suggesting that the proxy traits only weakly captured the variation in nitrogen losses.

**Predictions for winter-to-spring nitrogen dynamics**

Within traits describing winter-to-spring nitrogen dynamics, spring remobilization (SR) showed moderate predictability (Figure 6a). Calibration performance was $r_{(cal)}$ = 0.65, whereas validation accuracy decreased to $r_{(val)}$ = 0.30. Cross-validation statistics ($\sqrt{R^2}$_cal = 0.62; $\sqrt{R^2}$_val = 0.41) and RMSE_val = 15.78 kg N ha$^{-1}$ (Table 1) indicated that proxy traits captured a meaningful but limited fraction of the variation in SR.

In contrast, autumn remobilization estimated *via* belowground method (ARb) showed the highest predictability among winter-to-spring nitrogen dynamics traits (Figure 6b). The calibration correlation was $r_{(cal)}$ = 0.71 and validation accuracy was $r_{(val)}$ = 0.49. Cross-validation results confirmed moderate predictive performance ($\sqrt{R^2}$_cal = 0.68; $\sqrt{R^2}$_val = 0.52), with RMSE_val = 13.47 kg N ha$^{-1}$ (Table 1).

Across all traits, robustness values (0.19-0.25) and small accuracy differences (0.01-0.04) indicated stable model performance between calibration and validation sets, suggesting minimal overfitting and good generalization of the retained PLS components (Table 1).

## 3.5 Variable Importance in Projection (VIP) identified the most informative proxy traits

**Summer-to-autumn nitrogen dynamics**

Based on Variable Importance in Projection (VIP) scores, the strongest predictors of nitrogen uptake (VIP ≥ 1) included the seasonal decline in aboveground nitrogen concentration toward the end of the season, together with harvest-time indicators of plant size and nitrogen pools. These included aboveground biomass and stand volume in February, circumference at 50 cm, aboveground nitrogen quantity, stem biomass, and stem nitrogen quantity (Figure 7b). Additional strong contributors included nitrogen nutrition index, stem number measured both at harvest and during the growing season, and maximum canopy height during the season.

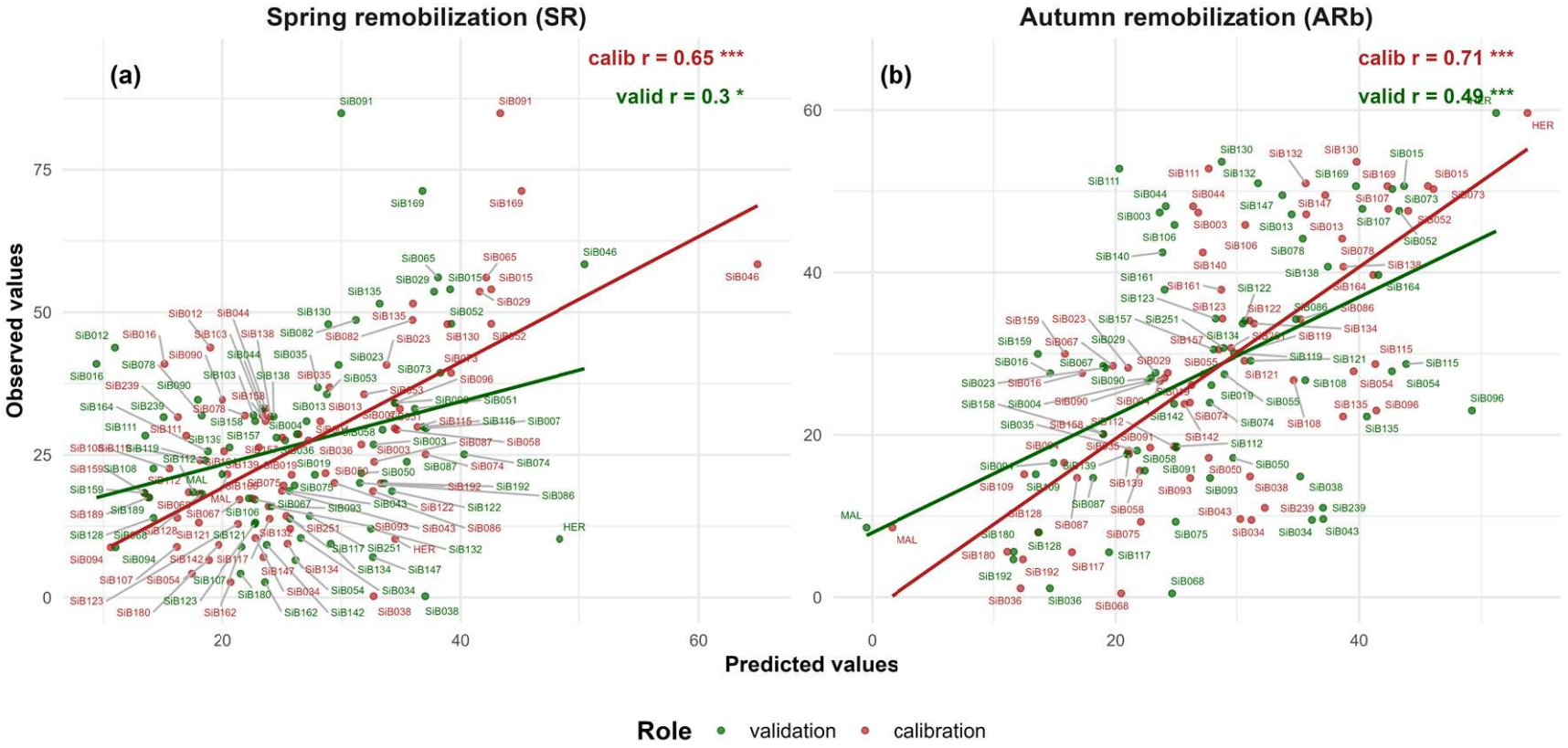


**Figure 6.** Prediction accuracy between observed and predicted values for traits describing winter-to-spring nitrogen dynamics based on the full proxy-based PLS1 model (Model 1): spring remobilization (SR) (a) and autumn remobilization estimated *via* belowground method (ARb) (b). Pearson correlation coefficients (r) and significance levels (*** $p < 0.001$, ** $p < 0.01$, * $p < 0.05$) are shown for both calibration (red) and validation (green) in each panel.

For autumn remobilization estimated *via* aboveground method (ARa), the strongest contributors included the seasonal decline in aboveground nitrogen concentration, nitrogen nutrition index, and harvest-time traits describing plant size and nitrogen status, including aboveground biomass, stand volume, canopy height, aboveground nitrogen concentration, stem nitrogen concentration, and belowground nitrogen concentration. The seasonal change in belowground nitrogen concentration, maximum height during the season, and stem number in September also showed strong VIP values (data not shown).

For nitrogen losses, the strongest predictors included the seasonal decline in aboveground nitrogen concentration, belowground nitrogen concentration at harvest, the seasonal gain in belowground nitrogen concentration, nitrogen nutrition index, and nitrogen concentrations in aboveground parts and stems at harvest. Canopy height at harvest and during the season, plant life cycle duration, and senescence timing (50%) also contributed strongly (data not shown).

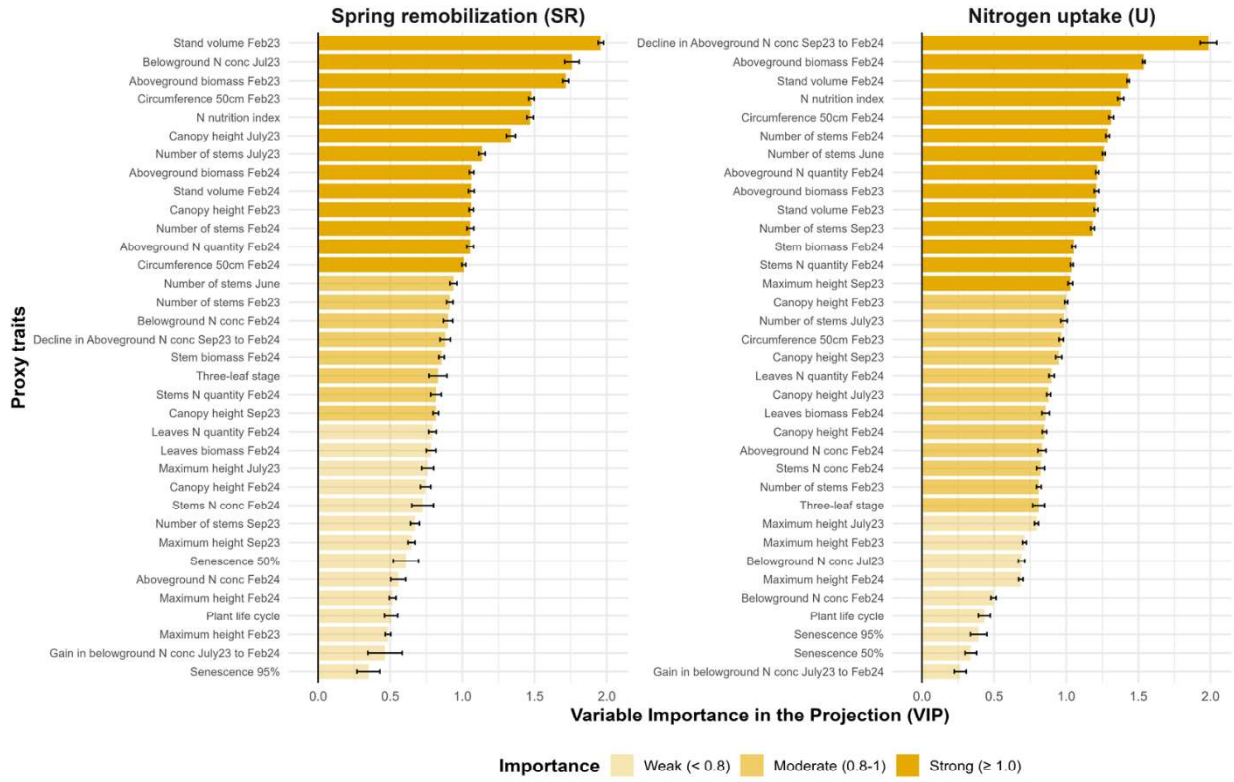


**Figure 7.** Variable Importance in Projection (VIP) profiles for the full proxy-based PLS1 model (Model 1), showing the contribution of each proxy trait to the prediction of spring remobilization (a) and nitrogen uptake (b). Bars represent mean VIP values across cross-validation iterations, and thin lines above each bar indicate associated standard deviations. Proxy traits with VIP values of at least 1 are considered as strong importance, values between 0.8 and 1 as moderate and values below 0.8 as weak importance. Trait abbreviations for proxy traits follow the abbreviations section (page number XVIII).

**Winter-to-spring nitrogen dynamics**

For spring remobilization (SR), the strongest predictors included stand volume and aboveground biomass in February, belowground nitrogen concentration in July, circumference at 50 cm, canopy height in February as well as during the season, stem number in February as well as during the season, aboveground nitrogen quantity in February, and nitrogen nutrition index (Figure 7a). Together, these traits reflected both canopy development and nitrogen pool size variation relevant to SR.

For autumn remobilization estimated *via* belowground method (ARb), the strongest contributors included the seasonal gain in belowground nitrogen concentration, stand volume and aboveground biomass at harvest, circumference at 50 cm, belowground nitrogen concentration at harvest, and aboveground and leaf nitrogen quantities at harvest. Additional strong predictors included stem number at harvest and during the growing season, plant life cycle duration, and senescence timing (50% and 95%) (data not shown).

## 3.6 Parsimonious models achieved predictive performance comparable to the full model

**Summer-to-autumn nitrogen dynamics**

Across traits linked to summer-to-autumn nitrogen dynamics, reducing the predictor set using VIP thresholds generally maintained or improved predictive performance while substantially decreasing model complexity.

Nitrogen uptake remained the most predictable trait across models. The validation correlation between observed and predicted values increased from r = 0.62 for Model 1 (n = 35 predictors) to r = 0.65 for Model 2 (n = 26), reaching r = 0.74 for the most parsimonious Model 3 (n = 15) (Figure 8). Cross-validated $\sqrt{R^2}\_val$ similarly increased from 0.64 (Model 1) to 0.67 (Model 2) and 0.73 (Model 3), while RMSE_val decreased from 39.1 to 37.6 and 34.3 kg N $ha^{-1}$, respectively (Table 1). These results indicate that nitrogen uptake could be predicted with high accuracy using a limited subset of informative proxy traits.

For autumn remobilization estimated *via* aboveground method (ARa), prediction accuracy was highest for the intermediate reduced model. Validation accuracy increased from r = 0.48 for Model 1 (n = 35) to r = 0.63 for Model 2 (n = 25), then declined slightly to r = 0.57 for Model

3 (n = 12) (Figure 8). Cross-validated √R²_val increased from 0.51 (Model 1) to 0.61 (Model 2), accompanied by a decrease in RMSE_val from 33.4 to 32.1 kg N ha$^{-1}$ (Table 1). These results show that ARa benefited from removing weak predictors, with Model 2 providing the best balance between predictive ability and parsimony.

Nitrogen losses showed consistently lower predictive performance than other nitrogen economy traits, although parsimony improved validation accuracy. The validation correlation between observed and predicted values increased from r = 0.24 in Model 1 (n = 35) to r = 0.36 in Model 2 (n = 19) and r = 0.39 in Model 3 (n = 10) (Figure 8). Cross-validated √R²_val increased from 0.35 (Model 1) to 0.43 (Model 2) and 0.46 (Model 3), with corresponding decreases in RMSE_val (Table 1). These results indicate that focusing on high-VIP predictors improved model performance for nitrogen losses, although this trait remained the most difficult to predict.

**Winter-to-spring nitrogen dynamics**

For traits associated with winter-to-spring nitrogen dynamics, reducing the predictor set consistently improved or maintained predictive performance while reducing the number of predictors.

For spring remobilization (SR), prediction accuracy increased progressively as the predictor set was reduced. Validation correlations increased from r = 0.30 for Model 1 (n = 35 predictors) to r = 0.42 for Model 2 (n = 21), reaching r = 0.46 for Model 3 (n = 13) (Figure 8). Cross-validated √R²_val increased from 0.41 (Model 1) to 0.49 (Model 2) and 0.53 (Model 3), while RMSE_val decreased from 15.8 to 14.8 and 14.2 kg N ha$^{-1}$, respectively (Table 1). These results indicate that SR could be predicted more effectively when models focused on the most informative proxy traits.

For autumn remobilization estimated *via* belowground method (ARb), prediction accuracy remained stable across models, with validation correlations ranging from r = 0.47 to r = 0.51 (Figure 8). The most parsimonious model (Model 3; n = 14 predictors) achieved the highest accuracy (r = 0.51), as well as the highest cross-validated √R²_val (0.57) and lowest RMSE_val (12.9 kg N ha$^{-1}$) (Table 1). These results demonstrate that ARb could be predicted effectively using a small number of high-VIP traits.

Across traits, robustness values (0.07-0.38) indicated that reduced predictor sets generally behaved consistently across calibration and validation datasets, while accuracy differences (0.00–0.10) suggested that parsimony often improved validation performance. Overall, these results demonstrate that VIP-based predictor reduction substantially decreased model complexity while retaining, and in several cases improving, predictive accuracy.

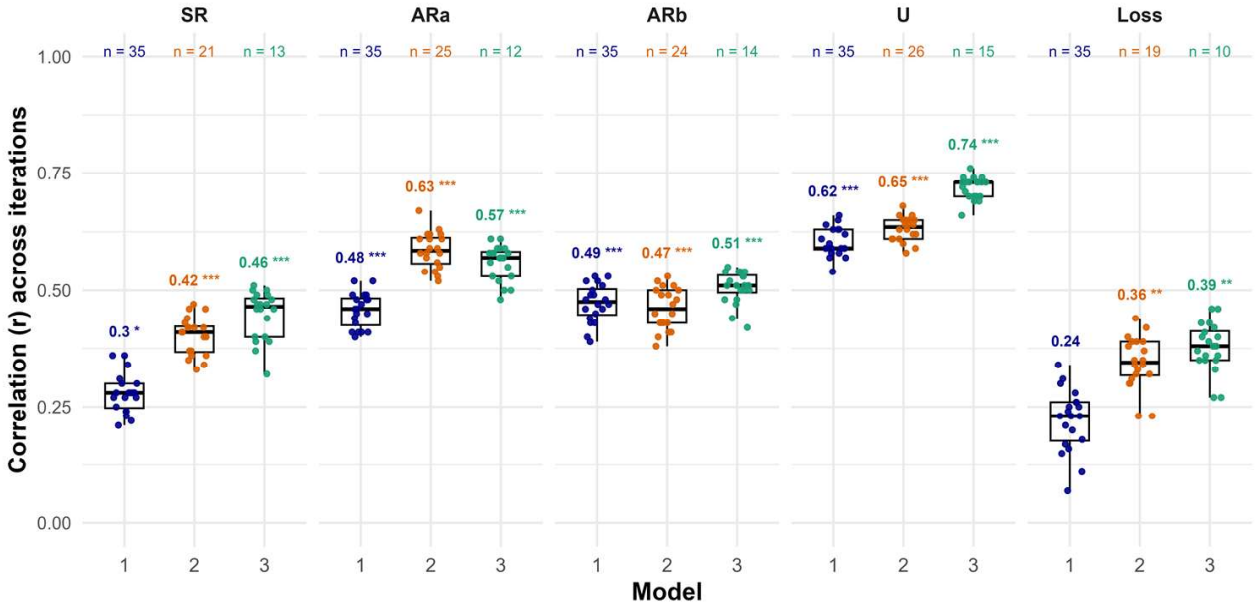


**Figure 8.** Predictive accuracy of Model 1, Model 2 and Model 3 for each nitrogen economy trait (SR, ARa, ARb, Nitrogen uptake(U) and Nitrogen losses). Boxplots show the distribution of Pearson correlation coefficients between predicted and observed values across cross-validation iterations. The number of predictors (n) included in each model is shown above each box. Model definitions: Model 1 includes all 35 proxy traits; Model 2 includes predictors with VIP ≥ 0.8; Model 3 includes predictors with VIP ≥ 1.0.

## 3.7 Parsimonious models gave selection outcomes similar to the full model

Across traits, parsimonious models were consistent with the complete model for selecting the top half of genotypes (Table 2). For every pair of models (M1-M2, M1-M3 and M2-M3), the percentage of genotypes that were common to both models within the top half and the bottom of the distribution was rather very high. For spring remobilization, overlap between models was very high, with 89-92% of the top-half genotypes shared among Model 1, Model 2 and Model 3. Consistency was also strong for autumn remobilization *via* belowground method (ARb), where 82-97% of top-half genotypes were common across model pairs. For autumn remobilization *via* aboveground method (ARa), overlaps in the top half ranged from 77% to 86%. Nitrogen uptake showed similarly high consistency between the full and parsimonious models (78-92%), and nitrogen losses displayed overlaps of 86-93% between model pairs.

These results indicate that parsimonious models identified largely the same high-performing genotypes as the complete predictor set.

Patterns were similar for counter-selection of the poorest-performing genotypes (bottom half of the distribution). For spring remobilization and ARb, consistency between models was again very high, with 82-97% of bottom-half genotypes shared between model pairs. For ARa, overlaps ranged from 74% to 83%, while for nitrogen uptake they ranged from 75% to 89%. Nitrogen losses showed 83-93% consistency between models for the bottom half of genotypes. Together, these results show that parsimonious proxy-based models produced selection and counter-selection outcomes that were broadly consistent with those from the complete model, supporting their potential use in breeding contexts where simplified and high throughput phenotyping is required.

**Table 2.** Agreement in genotype selection across proxy-based models for each nitrogen economy trait. For each trait, the table reports the percentage of genotypes that were commonly selected in the top half (high-performing) and bottom half (low-performing) when comparing Model 1 vs Model 2, Model 1 vs Model 3, and Model 2 vs Model 3. Model codes: M1 = full model (35 predictors), M2 = parsimonious model with VIP ≥ 0.8, M3 = parsimonious model with VIP ≥ 1.0.

| **Trait** | **Top half of genotypes** | | | **Bottom half of genotypes** | | |
|---|---|---|---|---|---|---|
| | **M1–M2** | **M1–M3** | **M2–M3** | **M1–M2** | **M1–M3** | **M2–M3** |
| Spring remobilization | 89% | 92% | 92% | 89% | 92% | 92% |
| Autumn remobilization: ARa | 77% | 86% | 86% | 74% | 83% | 83% |
| Autumn remobilization: ARb | 97% | 85% | 82% | 97% | 85% | 82% |
| Nitrogen Uptake | 92% | 83% | 78% | 89% | 81% | 75% |
| Nitrogen Losses | 90% | 86% | 93% | 86% | 83% | 93% |

## 4. Discussion

The results of this study demonstrate that simple, non-destructive traits can provide meaningful insight into the nitrogen economy of *Miscanthus sinensis*. First, we identified morphological, phenological and physiological proxy traits showing measurable and biologically interpretable relationships with nitrogen economy traits, supporting the hypothesis that individual non-destructive descriptors can already reflect variation in nitrogen economy. Second, we found that combining proxy traits in multivariate partial least squares (PLS) models better captured the complexity of nitrogen economy traits than any single trait, and that parsimonious models retained predictive performance while relying on fewer, more informative predictors. Third, we showed that these models can support breeding by producing consistent selection and counter-selection outcomes for nitrogen economy traits. Accordingly, this discussion focuses on (i) non-destructive proxy traits can predict nitrogen economy traits with PLS models showing rather good correlations and parsimony, (ii) some of the proxy traits correspond to expected ecophysiological traits, and (iii) how proxy-based multivariate and parsimonious prediction models can support breeding decisions and ecosystem service-oriented selection. Together, these findings show that nitrogen economy traits, previously accessible only through plant destructive flux measurements, can now be approximated at scale using simple, easy-to-measure proxy traits. These conclusions are supported by measurements on 80 segregant *M. sinensis* genotypes, providing a robust empirical basis for identifying reliable proxy-trait relationships.

### 4.1 Non-destructive proxy traits can predict nitrogen economy traits with PLS models showing rather good correlations and parsimony

The complete proxy-based models that used all 35 predictors showed that combining multiple non-destructive traits can predict nitrogen economy traits with trait specific accuracy. Prediction accuracy was highest for nitrogen uptake ($r_{(val)}$= 0.62). It was moderate for autumn remobilization estimated either *via* belowground method ($r_{(val)}$ = 0.49) or the aboveground method ($r_{(val)}$ = 0.48) as well as spring remobilization ($r_{(val)}$ = 0.30). Nitrogen losses were the most difficult to predict ($r_{(val)}$ = 0.24). These validation values show that multivariate combinations of simple morphological and phenological traits can recover a portion of variation in nitrogen economy traits. This pattern is consistent with evidence that prediction

accuracy decreases as the biological and computational complexity of the target trait increases, even when partial least squares regression is used to aggregate information across correlated predictors (Mehmood et al., 2020). The key point is that multivariate models aggregate information from many weak or moderate correlations into trait specific predictions that go beyond what any single proxy can provide.

Nitrogen economy traits are indeed intrinsically complex because they integrate several physiological processes that unfold over time. Their calculation requires combining information on nitrogen concentration and biomass from both the aboveground and belowground parts of the plant, often measured destructively at multiple sampling dates. As a result, each trait reflects not a single event but a sequence of nitrogen movements and storage dynamics across different plant parts and developmental stages, making them much harder to approximate than directly measured traits. Such a complexity was also found for the bread-baking quality of winter wheat and was successfully predicted by proxy traits based on indirect tests (Oury et al., 2010).

In many calibration studies using partial least squares regression to predict directly measured traits such as leaf nitrogen concentration, calibration accuracy is typically very high because the target reflects a single dominant dimension of variation. For example, VIS-NIR spectroscopy combined with PLSR achieved calibration $R^2$ values up to 0.83 for cotton leaf nitrogen concentration (Xiao et al., 2022), and hyperspectral models for cotton leaf nitrogen content reached calibration $R^2$ values ranging from 0.79 to 0.91 (Zhang et al., 2022). By contrast, the nitrogen economy traits studied here are composite quantities derived from destructive sampling of multiple plant parts at several dates. Against this background, calibration correlations ($r_{(}cal_{)}$) between observed and predicted values ranging from about 0.62 to 0.81 across traits (Figures 5 and 6; Table 1) indicate that the models captured a substantial part of the variation in these complex targets, even though the values are lower than those reported for simpler traits in some calibration studies. We also showed that the most parsimonious models based on the selection of the most important variables through high VIP (> 1) produced higher validation correlations and lower prediction errors than the complete model for most of the nitrogen economy traits. It was the case for nitrogen uptake, spring and autumn remobilizations, while nitrogen losses remained the most difficult trait to predict although the parsimonious models still improved validation accuracy compared with the complete model. From a modelling perspective, this behavior is expected and well documented

in PLS literature. Predictors with low VIP values contribute little to the covariance structure linking predictors and response and tend to introduce noise or overfitting when retained, whereas high-VIP predictors concentrate most of the informative signal (Chong & Jun, 2005; Mehmood et al., 2012). Removing weak variables therefore focuses the model on predictors that carry meaningful covariance with the nitrogen economy traits and can improve the stability and generalizability of the latent components, particularly in high-dimensional contexts (Alenezi, 2021). The robustness statistics for our parsimonious models, which showed closely aligned calibration and validation behavior and only small differences in accuracy, support this interpretation. In practical terms, these results show that parsimonious proxy-based models can retain predictive performance while relying on fewer, more informative traits, thereby reducing the number of measurements required for phenotyping.

## 4.2 Some of the proxy traits correspond to expected ecophysiological traits

**Summer-to-autumn nitrogen dynamics**

Across the summer-to-autumn nitrogen dynamics, several traits describing plant size and architecture, canopy structure and nitrogen status showed positive relationships with nitrogen uptake. Genotypes with larger and denser canopies, characterized by high aboveground biomass, greater stand volume, more stems and taller canopies, tended to acquire more nitrogen from the soil. These relationships are consistent with previous work showing that canopy height, stem density and architectural development in miscanthus strongly influence biomass accumulation and therefore nitrogen demand (Robson et al., 2013; Davey et al., 2017). Relationships with nitrogen nutrition index indicate that genotypes maintaining higher nitrogen status during the season also tended to have greater uptake. These patterns suggest that canopy development and plant size can provide meaningful indications of nitrogen acquisition potential.

Autumn remobilization *via* aboveground method shared some of these proxy traits but differed in others. Positive correlations with stand volume, aboveground biomass and stem number indicate that genotypes with larger canopies tend to withdraw more nitrogen from senescing shoots. Negative relationships with aboveground nitrogen concentration in February suggest that more complete withdrawal leads to lower nitrogen remaining in aboveground tissues at the end of winter, which aligns with the expectation that efficient autumn recycling reduces nitrogen concentrations in senesced biomass.

Nitrogen losses showed fewer significant relationships, which is consistent with the multiple diffuse processes that contribute to nitrogen loss from the plant (Leroy, 2021), including potential losses to the atmosphere. The positive relationship with nitrogen nutrition index suggests that genotypes with higher nitrogen status during the season can lose more nitrogen by the end of the cycle. Negative relationships with belowground nitrogen concentration in February and with the seasonal increase in belowground nitrogen concentration indicate that genotypes storing less belowground nitrogen tend to lose more. This interpretation is consistent with evidence from other plant systems showing that improving nitrogen recycling reduces nitrogen remaining in labile pools that are vulnerable to loss (Havé et al., 2017).

A specific phenological relationship emerged within this axis. Nitrogen uptake was negatively correlated with the timing of the three-leaf stage, although it showed no association with emergence. Because nitrogen uptake increased with larger and earlier developing canopies, it is plausible that genotypes reaching the three-leaf stage earlier had more time for canopy expansion and, in turn, more opportunity for nitrogen acquisition. The absence of a correlation with emergence indicates that this relationship is not explained simply by earlier spring growth but rather by subsequent developmental progression. While the underlying mechanism cannot be established from the present data, these patterns show that phenological traits can contribute to explaining variation in uptake.

**Winter-to-spring nitrogen dynamics**

Spring remobilization and autumn remobilization *via* belowground method formed a second axis linked to nitrogen storage and use of belowground nitrogen reserves. Several size and architecture traits measured in late winter, including stand volume, aboveground biomass and circumference at 50 cm, were positively correlated with spring remobilization. These associations align with the understanding that early season growth in perennial grasses relies on nitrogen stored in belowground organs (Dierking et al., 2017). Relationships with canopy height and stem number measured earlier in the season indicate that genotypes with more vigorous early shoot development tended to mobilize more nitrogen from belowground organs. The positive relationship with nitrogen nutrition index suggests that genotypes maintaining adequate nitrogen status during canopy development also tended to recycle more endogenous nitrogen in spring.

Autumn remobilization *via* belowground method showed correlations with belowground nitrogen concentration in February, the seasonal increase in belowground nitrogen concentration and senescence timing. These relationships indicate that genotypes that accumulated more nitrogen in rhizomes and roots over the season, and that senesced more gradually, tended to store more nitrogen *via* this pathway. Positive correlations with aboveground nitrogen quantity and stem number indicate that canopy size and nitrogen pools influenced the quantity of nitrogen eventually transferred to belowground organs.

The divergence between the proxy sets for autumn remobilization *via* aboveground and belowground methods is consistent with their biological definitions. Autumn remobilization *via* aboveground method captures the nitrogen withdrawn from shoots, whereas autumn remobilization *via* belowground method captures the nitrogen that actually reaches belowground organs. Since not all nitrogen withdrawn from shoots is stored, it is expected that the two traits exhibit different proxy relationships and that they are not correlated.

Previous studies have proposed non-destructive indicators of nitrogen remobilization efficiency, but these indicators describe the proportion of nitrogen transferred rather than the magnitude of nitrogen movement. In miscanthus, Leroy (2021) identified two efficiency-related relationships across three genotypes: individuals producing a larger proportion of their final stem number early in the season tended to exhibit higher efficiency of nitrogen storage in belowground organs, and nitrogen storage efficiency was negatively correlated with nitrogen content remaining in aboveground parts at the end of winter. In perennial switchgrass, Yang and Udvardi (2018) reported a negative correlation between heading date and nitrogen remobilization efficiency, showing that phenology can provide insight into recycling processes in other C4 grasses. These studies demonstrate that structural or phenological traits can signal aspects of nitrogen allocation or conservation, but they do not quantify the actual nitrogen fluxes entering or leaving aboveground and belowground pools. This distinction is relevant because fluxes capture the total amount of nitrogen acquired, stored or lost across the season.

The present study extends this earlier work by examining a segregant *M. sinensis* progeny and by evaluating a wider suite of proxy traits, linking these non-destructive traits to the quantitative magnitudes of nitrogen uptake, spring remobilization, autumn remobilization and nitrogen losses. In this sense, the study provides a broader and flux-oriented proxy framework for nitrogen economy in *M. sinensis*.

Taken together, these proxy relationships address the first objective and its hypothesis by showing that individual non-destructive traits carry biologically interpretable information about nitrogen uptake, endogenous nitrogen recycling and nitrogen losses. Summer-to-autumn nitrogen dynamics were most closely reflected by traits describing canopy size, architecture and nitrogen status, whereas winter-to-spring nitrogen dynamics were most closely reflected by traits describing structural biomass at harvest, early canopy expansion, nitrogen concentration in rhizomes and senescence timing. These findings confirm that non-destructive traits can act as meaningful indicators of nitrogen economy in *M. sinensis*, while the generally weak to moderate correlations also make clear that no single proxy can fully represent any nitrogen flux. This limitation motivated the second part of the study, which examined whether multivariate and parsimonious models could better capture the complexity of nitrogen economy traits.

## 4.3 Parsimonious proxy-based models are more reliable tools for indirect selection

We also assessed whether these models could support breeding decisions through consistent selection and counter-selection outcomes. The comparison of genotype rankings between the complete and parsimonious models (Table 2) showed that, for all nitrogen economy traits, between roughly three quarters and more than ninety percent of genotypes were shared in the top half or bottom half of the distribution. Agreement was particularly high for spring remobilization and autumn remobilization *via* belowground method, where both high-performing and low-performing genotypes were largely the same across models. Autumn remobilization *via* aboveground method and nitrogen uptake also showed strong overlaps, and even for nitrogen losses the simplified models identified broadly the same sets of genotypes as the full model. Because breeding decisions for complex traits typically focus on retaining or discarding groups of genotypes rather than relying on precise numerical predictions, these overlaps indicate that parsimonious models can yield selection and counter-selection outcomes that remain consistent with those obtained from the full predictor set. As such decisions rely on how models generalize rather than on calibration fit, the stability of validation outcomes across models is especially relevant for breeding applications.

Beyond their predictive performance, these models have relevance for ecosystem-service-oriented selection because nitrogen economy traits are directly relevant to functions that

influence nutrient retention and nutrient removal in cropping systems. Predictions for nitrogen uptake identify genotypes capable of acquiring and exporting substantial amounts of soil nitrogen when harvested at the green stage. Such genotypes are particularly relevant for the regulating service of water-quality improvement, because they can remove excess nitrogen from nutrient-enriched catchment areas (particularly in zones connected to groundwater flow and drainage networks such as ditches or streams) and thereby contribute to reducing nitrate accumulation. This application aligns with proposals to cultivate miscanthus in water-catchment regions to mitigate rising soil nitrate levels (Weik et al., 2022) and with evidence that miscanthus stands can reduce nitrate leaching (Cibin et al., 2016; Ferchaud & Mary, 2016; Ferrarini et al., 2017). In parallel, predictions for spring remobilization and autumn remobilization *via* belowground method highlight genotypes that rely more on endogenous nitrogen recycling and less on new nitrogen uptake. Such genotypes contribute to provisioning services (CICES 5.1, 2018), including soil-nitrogen conservation and the long-term maintenance of soil fertility, because stronger endogenous recycling leaves less nitrogen exposed to loss in aboveground parts at the end of the season. Together, these results show that proxy-based predictions can help identify *Miscanthus sinensis* genotypes that combine favorable nitrogen-economy profiles with potential contributions to both water-quality regulation and soil-resource conservation.

Taken together, the modelling, parsimony and selection results show that combining multiple non-destructive proxies in multivariate models makes it possible to predict complex nitrogen economy traits with trait-specific accuracy and that parsimonious versions of these models can retain, and sometimes improve, performance while relying on fewer predictors. These findings validate our hypotheses that multivariate PLS models would provide accurate predictions by integrating complementary proxy traits, that VIP-selected subsets would yield parsimonious models with performance comparable to the complete model, and that proxy-based prediction models would reliably identify both the best and poorest-performing genotypes. At the same time, the high consistency in selection and counter-selection outcomes between complete and parsimonious models indicates that simplified predictor sets are sufficient for supporting breeding decisions that aim to integrate nitrogen economy traits and their associated ecosystem services. Together, these findings demonstrate that nitrogen economy can be represented reliably through integrative proxy-based models, meeting the expectations set by our hypotheses for predictive accuracy, parsimony and selection consistency. Looking ahead, extending and validating these proxy-based models across genetic backgrounds, environments

and management conditions will be an important step towards fully integrating nitrogen economy into *Miscanthus sinensis* breeding strategies.

## 5. Conclusion and Perspectives

This study demonstrates that nitrogen economy in *Miscanthus sinensis*, previously accessible only through plant destructive and time-consuming flux measurements, can be reliably approximated using simple non-destructive proxy traits. Across eighty segregant genotypes, morphological, architectural, phenological and nitrogen status traits captured biologically interpretable variation in nitrogen uptake, spring remobilization, autumn remobilization and nitrogen losses. Multivariate PLS models, together with parsimonious VIP-based variants, confirmed our hypotheses by predicting these complex fluxes with trait-specific accuracy and by retaining performance even when predictor sets were reduced. Equally important, complete and parsimonious models produced consistent selection and counter-selection outcomes, demonstrating that simplified trait sets are sufficient to support breeding decisions that integrate nitrogen economy alongside biomass productivity.

From a breeding perspective, the proxy-based models developed here provide a practical toolbox for incorporating nitrogen economy into breeding pipelines without relying on plant destructive sampling. At the same time, several limitations point to future work. The models were developed and tested within a single progeny grown in one environment, and external validation across multiple genetic backgrounds, sites, years and management regimes will be necessary to ensure robustness and transferability. Expanding the proxy framework to include remote sensing traits, integrating these models with genomic prediction and testing their stability under contrasting nitrogen inputs represent promising next steps. Looking ahead, these combined strategies will help embed nitrogen economy into *Miscanthus sinensis* improvement pipelines and strengthen the crop’s contribution to sustainable biomass production and ecosystem service delivery.

## References

Agostini, F., Gregory, A. S., & Richter, G. M. (2015). Carbon sequestration by perennial energy crops: is the jury still out? *Bioenergy research*, *8*(3), 1057-1080.

Akarachantachote, N., Chadcham, S., & Saithanu, K. (2014). Cutoff threshold of variable importance in projection for variable selection. *Int J Pure Appl Math*, *94*(3), 307-322.

Alenezi, F. N. (2021). Majority scoring with backward elimination in PLS for high dimensional spectrum data. *Scientific Reports*, *11*(1), 16974.

Beale, C., & Long, S. (1997). Seasonal dynamics of nutrient accumulation and partitioning in the perennial C4-grasses *Miscanthus× giganteus* and *Spartina cynosuroides*. *Biomass and Bioenergy*, *12*(6), 419-428.

Boulesteix, A.-L., & Strimmer, K. (2007). Partial least squares: a versatile tool for the analysis of high-dimensional genomic data. *Briefings in bioinformatics*, *8*(1), 32-44.

Brancourt-Hulmel, M., Denis, J., & Biarnes-Dumoulin, V. (1997). Comparison of joint regression, AMMI model and factorial regression for efficiency and parsimony in plant breeding.

Brancourt-Hulmel, M., Raverdy, R., Girones, J., Arnoult, S., Mignot, E., Griveaux, Y., & Navard, P. (2021). Variability of stem solidness among miscanthus genotypes and its role on mechanical properties of polypropylene composites. *GCB Bioenergy*, *13*(9), 1576-1585.

Cacho, J., Negri, M., Zumpf, C., & Campbell, P. (2018). Introducing perennial biomass crops into agricultural landscapes to address water quality challenges and provide other environmental services. *Wiley Interdisciplinary Reviews: Energy and Environment*, *7*(2), e275.

Cadoux, S., Ferchaud, F., Demay, C., Boizard, H., Machet, J. M., Fourdinier, E., Preudhomme, M., Chabbert, B., Gosse, G., & Mary, B. (2014). Implications of productivity and nutrient requirements on greenhouse gas balance of annual and perennial bioenergy crops. *GCB Bioenergy*, *6*(4), 425-438.

Chong, I.-G., & Jun, C.-H. (2005). Performance of some variable selection methods when multicollinearity is present. *Chemometrics and intelligent laboratory systems*, *78*(1-2), 103-112.

Cibin, R., Trybula, E., Chaubey, I., Brouder, S. M., & Volenec, J. J. (2016). Watershed-scale impacts of bioenergy crops on hydrology and water quality using improved SWAT model. *Gcb Bioenergy*, *8*(4), 837-848.

Clifton-Brown, J., Hastings, A., von Cossel, M., Murphy-Bokern, D., McCalmont, J., Whitaker, J., Alexopoulou, E., Amaducci, S., Andronic, L., & Ashman, C. (2023). Perennial biomass cropping and use: Shaping the policy ecosystem in European countries. *GCB Bioenergy*, *15*(5), 538-558.

Cooper, C. S., & MacDonald, P. W. (1970). Energetics of early seedling growth in corn (Zea mays L.) 1. *Crop Science*, *10*(2), 136-139.

Davey, C. L., Robson, P., Hawkins, S., Farrar, K., Clifton-Brown, J. C., Donnison, I. S., & Slavov, G. T. (2017). Genetic relationships between spring emergence, canopy phenology, and biomass yield increase the accuracy of genomic prediction in Miscanthus. *Journal of Experimental Botany*, *68*(18), 5093-5102.

Davis, M. P., Groh, T. A., Jaynes, D. B., Parkin, T. B., & Isenhart, T. M. (2019). Nitrous oxide emissions from saturated riparian buffers: Are we trading a water quality problem for an air quality problem? *Journal of Environmental Quality*, *48*(2), 261-269.

Deleens, E., Gregory, N., & Bourdu, R. (1984). Transition between seed reserve use and photosynthetic supply during development of maize seedlings. *Plant Science Letters*, *37*(1-2), 35-39.

Dierking, R. M., Allen, D. J., Cunningham, S. M., Brouder, S. M., & Volenec, J. J. (2017). Nitrogen reserve pools in two *Miscanthus* × *giganteus* genotypes under contrasting N managements. *Frontiers in plant science*, *8*, 1618.

Eriksson L, Johansson E, Kettaneh-Wold N, Wold S (2001). Multi- and megavariate data analysis. Principles and applications. Umetrics Academy, Umea

Farrés, M., Platikanov, S., Tsakovski, S., & Tauler, R. (2015). Comparison of the variable importance in projection (VIP) and of the selectivity ratio (SR) methods for variable selection and interpretation. *Journal of Chemometrics*, *29*(10), 528-536.

Ferchaud, F., & Mary, B. (2016). Drainage and nitrate leaching assessed during 7 years under perennial and annual bioenergy crops. *BioEnergy Research*, *9*(2), 656-670.

Ferrarini, A., Fornasier, F., Serra, P., Ferrari, F., Trevisan, M., & Amaducci, S. (2017). Impacts of willow and miscanthus bioenergy buffers on biogeochemical N removal processes along the soil–groundwater continuum. *Gcb Bioenergy*, *9*(1), 246-261.

Gallais, A. (1984). Use of indirect selection in plant breeding. 10th Eucarpia Congress: Efficiency in Plant Breeding. Wageningen, the Netherlands,

Hamada, Y., Zumpf, C. R., Cacho, J. F., Lee, D., Lin, C.-H., Boe, A., Heaton, E., Mitchell, R., & Negri, M. C. (2021). Remote Sensing-Based Estimation of Advanced Perennial Grass Biomass Yields for Bioenergy. *Land*, *10*(11), 1221. https://www.mdpi.com/2073-445X/10/11/1221

Havé, M., Marmagne, A., Chardon, F., & Masclaux-Daubresse, C. (2017). Nitrogen remobilization during leaf senescence: lessons from Arabidopsis to crops. *Journal of experimental botany*, *68*(10), 2513-2529.

Himken, M., Lammel, J., Neukirchen, D., Czypionka-Krause, U., & Olfs, H.-W. (1997). Cultivation of Miscanthus under West European conditions: Seasonal changes in dry matter production, nutrient uptake and remobilization. *Plant and soil*, *189*(1), 117-126.

Impollonia, G., Croci, M., Martani, E., Ferrarini, A., Kam, J., Trindade, L. M., Clifton-Brown, J., & Amaducci, S. (2022). Moisture content estimation and senescence phenotyping of novel Miscanthus hybrids combining UAV-based remote sensing and machine learning. *GCB Bioenergy*, *14*(6), 639-656.

Iqbal, S., Brancourt-Hulmel, M., & Zapater, M. (2026). Nitrogen Economy Strategies Define Distinct Functional Groups of Genotypes in a *Miscanthus sinensis* Progeny. *GCB Bioenergy*, *18*(1), e70096. https://doi.org/https://doi.org/10.1111/gcbb.70096

Jørgensen, U. (2011). Benefits versus risks of growing biofuel crops: the case of Miscanthus. *Current Opinion in Environmental Sustainability*, *3*(1), 24-30. https://doi.org/https://doi.org/10.1016/j.cosust.2010.12.003

Kiesel, A., Wagner, M., & Lewandowski, I. (2016). Environmental performance of miscanthus, switchgrass and maize: Can C4 perennials increase the sustainability of biogas production? *Sustainability*, *9*(1), 5.

Laperche, A., Le Gouis, J., Hanocq, E., & Brancourt-Hulmel, M. (2008). Modelling nitrogen stress with probe genotypes to assess genetic parameters and genetic determinism of winter wheat tolerance to nitrogen constraint. *Euphytica*, *161*(1), 259-271.

Leroy, J. (2021). *Etude écophysiologique temporelle de la gestion des réserves carbonées et azotées par trois génotypes de miscanthus* AgroParisTech].

Leroy, J., Ferchaud, F., Giauffret, C., Mary, B., Fingar, L., Mignot, E., Arnoult, S., Lenoir, S., Martin, D., & Brancourt-Hulmel, M. (2022). *Miscanthus sinensis* is as efficient as *Miscanthus× giganteus* for nitrogen recycling in spite of smaller nitrogen fluxes. *Bioenergy Research*, *15*(2), 686-702.

Lesur, C., Bazot, M., Bio-Beri, F., Mary, B., Jeuffroy, M. H., & Loyce, C. (2014). Assessing nitrate leaching during the three-first years of *Miscanthus× giganteus* from on-farm measurements and modeling. *Gcb Bioenergy*, *6*(4), 439-449.

Mahieu, B., Qannari, E. M., & Jaillais, B. (2023). Extension and significance testing of variable importance in projection (VIP) indices in partial least squares regression and principal components analysis. *Chemometrics and Intelligent Laboratory Systems*, *242*, 104986.

McCalmont, J. P., Hastings, A., McNamara, N. P., Richter, G. M., Robson, P., Donnison, I. S., & Clifton-Brown, J. (2017). Environmental costs and benefits of growing Miscanthus for bioenergy in the UK. *Glob Change Biol Bioenergy*, *9*(3), 489-507. https://doi.org/10.1111/gcbb.12294

Mehmood, T., Liland, K. H., Snipen, L., & Sæbø, S. (2012). A review of variable selection methods in partial least squares regression. *Chemometrics and intelligent laboratory systems*, *118*, 62-69.

Mehmood, T., Sæbø, S., & Liland, K. H. (2020). Comparison of variable selection methods in partial least squares regression. *Journal of Chemometrics*, *34*(6), e3226.

Miura, N., Yamada, S., & Niwa, Y. (2020). Estimation of canopy height and biomass of *Miscanthus sinensis* in semi-natural grassland using time-series UAV data. *ISPRS Annals of the Photogrammetry, Remote Sensing and Spatial Information Sciences*, *3*, 497-503.

Nadeem, M., Mollier, A., Morel, C., Prud'Homme, L., Vives, A., & Pellerin, S. (2014). Remobilization of seed phosphorus reserves and their role in attaining phosphorus autotrophy in maize (Zea mays L.) seedlings. *Seed Science Research*, *24*(3), 187-194.

Namoi, N., Jang, C., Robins, Z., Lin, C.-H., Lim, S.-H., Voigt, T., & Lee, D. (2022). Aerial imagery can detect nitrogen fertilizer effects on biomass and stand health of *Miscanthus* × *giganteus*. *Remote Sensing*, *14*(6), 1435.

Oury, F.-X., Chiron, H., Faye, A., Gardet, O., Giraud, A., Heumez, E., Rolland, B., Rousset, M., Trottet, M., & Charmet, G. (2010). The prediction of bread wheat quality: joint use of the phenotypic information brought by technological tests and the genetic information brought by HMW and LMW glutenin subunits. *Euphytica*, *171*(1), 87-109.

Robson, P., Jensen, E., Hawkins, S., White, S. R., Kenobi, K., Clifton-Brown, J., Donnison, I., & Farrar, K. (2013). Accelerating the domestication of a bioenergy crop: identifying and modelling morphological targets for sustainable yield increase in Miscanthus. *Journal of Experimental Botany*, *64*(14), 4143-4155.

Rougoor, C., Sundaram, R., & Van Arendonk, J. (2000). The relation between breeding management and 305-day milk production, determined via principal components regression and partial least squares. *Livestock Production Science*, *66*(1), 71-83.

Sanchez, G. (2012). plsdepot: Partial least squares (PLS) data analysis methods. *R package version 0.1*, *17*.

Scordia, D., Papazoglou, E. G., Kotoula, D., Sanz, M., Ciria, C. S., Pérez, J., Maliarenko, O., Prysiazhniuk, O., von Cossel, M., & Greiner, B. E. (2022). Towards identifying industrial crop types and associated agronomies to improve biomass production from marginal lands in Europe. *GCB Bioenergy*, *14*(7), 710-734.

Slavov, G. T., Nipper, R., Robson, P., Farrar, K., Allison, G. G., Bosch, M., Clifton-Brown, J. C., Donnison, I. S., & Jensen, E. (2014). Genome-wide association studies and prediction of 17 traits related to phenology, biomass and cell wall composition in the energy grass *Miscanthus sinensis*. *New phytologist*, *201*(4), 1227-1239.

Strullu, L., Cadoux, S., Preudhomme, M., Jeuffroy, M. H., & Beaudoin, N. (2011). Biomass production and nitrogen accumulation and remobilisation by *Miscanthus*×*giganteus* as influenced by nitrogen stocks in belowground organs. *Field Crops Research*, *121*(3), 381-391. https://doi.org/https://doi.org/10.1016/j.fcr.2011.01.005

Studt, J. E., McDaniel, M. D., Tejera, M. D., VanLoocke, A., Howe, A., & Heaton, E. A. (2021). Soil net nitrogen mineralization and leaching under *Miscanthus* × *giganteus* and Zea mays. *Gcb Bioenergy*, *13*(9), 1545-1560.

Tavakoli-Hashjini, E., Piorr, A., Müller, K., & Vicente-Vicente, J. L. (2020). Potential bioenergy production from *Miscanthus*× *Giganteus* in Brandenburg: Producing bioenergy and fostering other ecosystem services while ensuring food self-sufficiency in the Berlin-Brandenburg region. *Sustainability*, *12*(18), 7731.

Weik, J., Lask, J., Petig, E., Seeger, S., Marting Vidaurre, N., Wagner, M., Weiler, M., Bahrs, E., Lewandowski, I., & Angenendt, E. (2022). Implications of large-scale miscanthus cultivation in water protection areas: A Life Cycle Assessment with model coupling for improved policy support. *Gcb Bioenergy*, *14*(11), 1162-1182.

Winberg, J., Smith, H. G., & Ekroos, J. (2023). Bioenergy crops, biodiversity and ecosystem services in temperate agricultural landscapes—A review of synergies and trade-offs. *GCB Bioenergy*, *15*(10), 1204-1220. https://doi.org/https://doi.org/10.1111/gcbb.13092

Xiao, Q., Wu, N., Tang, W., Zhang, C., Feng, L., Zhou, L., Shen, J., Zhang, Z., Gao, P., & He, Y. (2022). Visible and near-infrared spectroscopy and deep learning application for the qualitative and quantitative investigation of nitrogen status in cotton leaves. *Frontiers in Plant Science*, *13*, 1080745.

Yang, J., & Udvardi, M. (2018). Senescence and nitrogen use efficiency in perennial grasses for forage and biofuel production. *Journal of Experimental Botany*, *69*(4), 855-865.

Zang, H., Blagodatskaya, E., Wen, Y., Xu, X., Dyckmans, J., & Kuzyakov, Y. (2018). Carbon sequestration and turnover in soil under the energy crop Miscanthus: Repeated 13C natural abundance approach and literature synthesis. *GCB Bioenergy*, *10*(4), 262-271.

Zapater, M., Catterou, M., Mary, B., Ollier, M., Fingar, L., Mignot, E., Ferchaud, F., Strullu, L., Dubois, F., & Brancourt-Hulmel, M. (2017). A single and robust critical nitrogen dilution curve for *Miscanthus*× *giganteus* and *Miscanthus sinensis*. *Bioenergy research*, *10*(1), 115-128.

Zhang, Q., Lulu, M., Xiangyu, C., Jiao, L., Caixia, Y., Qiushuang, Y., Xin, L., & Zhang, Z. (2022). Estimation of nitrogen in cotton leaves using different hyperspectral region data. *Notulae Botanicae Horti Agrobotanici Cluj-Napoca*, *50*(1), 12595-12595.

Zheng, R., Chen, Z., Guan, Z., Zhao, C., Cui, H., & Shang, H. (2023). Variable importance for projection (VIP) scores for analyzing the contribution of risk factors in severe adverse events to Xiyanping injection. *Chinese Medicine*, *18*(1), 15.

# Chapter 3

***Chapter 3 objectives and methodology within the overall thesis framework.***

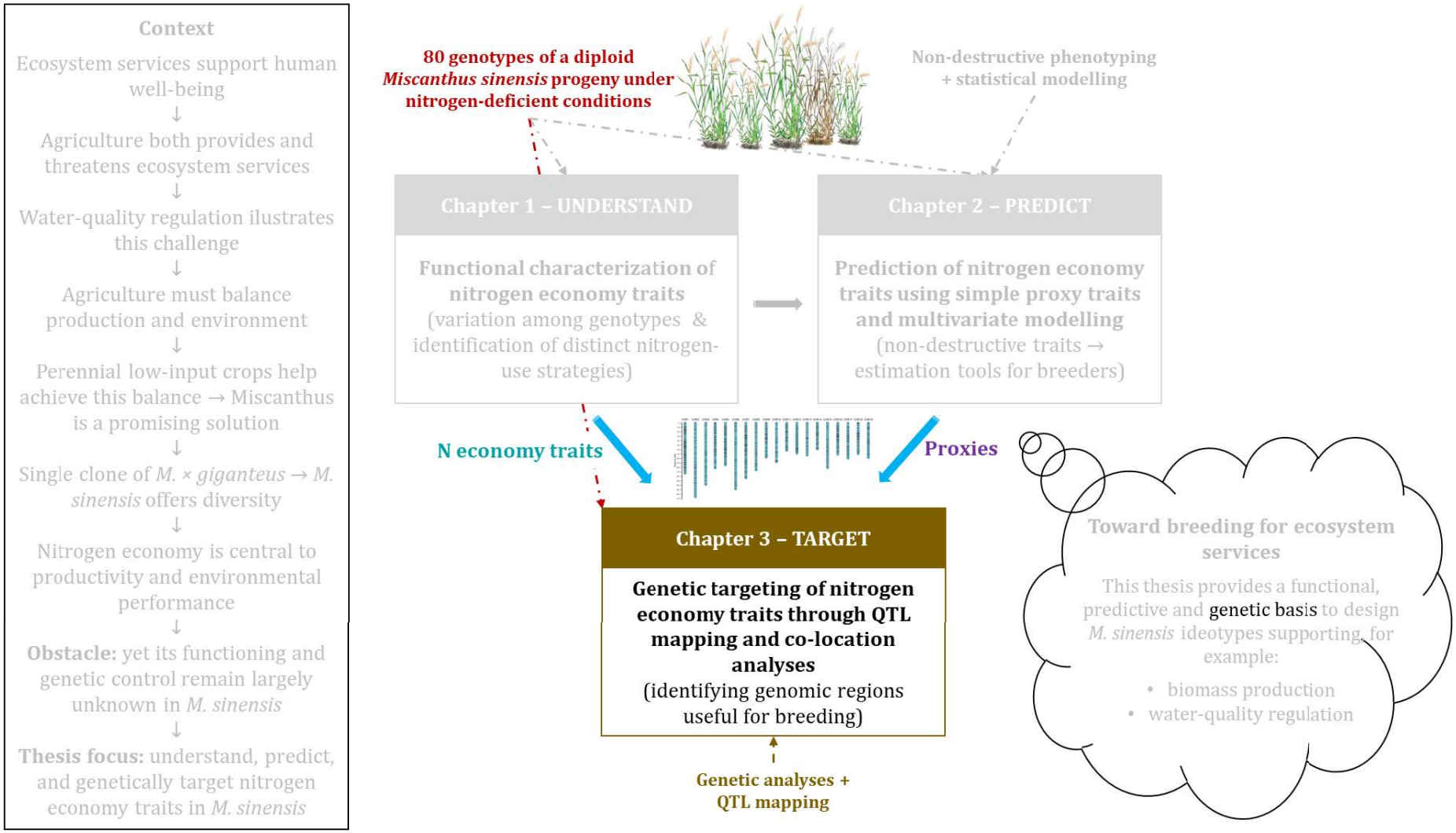

# QTL Mapping Identifies Genomic Regions for Nitrogen Economy Traits in a Full-sib *Miscanthus sinensis* Progeny

S Iqbal, K Lourgant, S Monnot, M Zapater and M Brancourt-Hulmel

BioEcoAgro Joint Research Unit, INRAE, Univ de Liege, Univ Lille, Univ Picardie Jules Verne, Chaussée Brunehaut, Entrées- Mons, France

**Keywords:** *Miscanthus sinensis*, Nitrogen economy, Quantitative trait loci (QTL) mapping, fullsibQTL, Perennial crop, Breeding

## Abstract

Sustainable bioenergy systems are increasingly expected to deliver ecosystem services alongside biomass production, making the nitrogen economy an important target for breeding perennial crops. In *Miscanthus sinensis*, nitrogen uptake, seasonal remobilization, and nitrogen losses jointly determine productivity under low nitrogen inputs while shaping environmental outcomes, yet their genetic control has remained largely unknown. The objective was to study their genetic control and evaluate their relevance for selection.

This study dissected the genetic architecture of nitrogen economy traits in a full-sib *M. sinensis* progeny using an integrated linkage map (19 linkage groups) and composite interval mapping adapted to outcrossing species. We mapped QTLs for spring remobilization (SR), autumn remobilization (ARa, ARb), nitrogen uptake, nitrogen losses, and nitrogen loss deviation, and tested whether phenotypic proxy-target relationships were genetically grounded *via* QTL co-location. We further evaluated breeding relevance through allelic effects and QTL pyramiding.

Across nitrogen economy traits, 19 QTLs were detected ($R^2$ = 8.8-37.1% per locus), with trait-specific genetic architectures and no systematic overlap of 2-LOD confidence intervals among uptake, remobilization, and losses. For proxy-based genetic tests, 26 have proxy traits yielded 85 proxy-trait QTLs ($R^2$ = 0.1-34.0%), while co-location with nitrogen economy QTLs was limited to two loci: one for nitrogen uptake and one for SR. This limited number of co-locations indicates that proxy-target relationships reflect shared genetic control at specific loci and coordinated physiological processes, rather than numerous co-locations across traits. Independent QTL sets for nitrogen uptake and SR supported selection toward specific

adaptation to contrasting ecosystem services. Finally, QTL pyramiding on nitrogen uptake and nitrogen loss deviation illustrated multilocus selection and counter-selection of genotypes with high uptake and contrasting loss profiles, showing how deviation-based traits can be used to address the undesirable positive link between uptake and losses.

This study provides the first QTL-based genetic dissection of nitrogen economy traits in *M. sinensis*, translating nitrogen acquisition, recycling, and losses into breeding-ready genetic targets for multifunctional miscanthus ideotypes. This provides a structured framework for opening new opportunities for breeding perennial biomass crops that support ecosystem services and resilient agricultural systems.

## 1. Introduction

The increasing demand for renewable energy is driving a shift toward land-use systems that deliver more than biomass production alone. Sustainable bioenergy crops are now expected to provide additional ecosystem services, including nutrient regulation, soil protection, and long-term system resilience, alongside productive capacity (Meehan et al., 2013). Perennial biomass crops are particularly well suited to this multifunctional role because their long-lived growth cycles stabilize resource use and reduce environmental disturbance relative to annual cropping systems, leading to reduced greenhouse gas emissions, lower negative environmental impacts, and improved ecosystem regulation (Whitaker et al., 2018).

In this context, perennial energy crops such as miscanthus have been shown to combine high biomass production with the maintenance of regulating ecosystem services, including carbon sequestration, improved water quality, and biodiversity support, when compared with annual crops (Tavakoli-Hashjini et al., 2020).

Miscanthus is a perennial C4 crop widely recognized for its lignocellulosic biomass production potential, with applications in bioenergy, bio-based materials, and related uses (Jones & Walsh, 2001; Heaton et al., 2004; Lewandowski et al., 2018). Commercial deployment has relied largely on a single sterile clone of *Miscanthus* × *giganteus*, which combines high biomass yields with low input requirements (Clifton-brown et al., 2004; Heaton et al., 2008; Brancourt-Hulmel & Höfte, 2022). However, this narrow genetic base limits genetic diversity, increasing susceptibility to pests and diseases (Greef et al., 1997; Zub & Brancourt-Hulmel, 2010), constrains adaptation across environments, particularly under cool climatic conditions (Jones

& Walsh, 2001; Zub et al., 2012), and restricts breeding progress by reducing phenotypic variability available for targeting different agronomic and end-use traits (Clifton-Brown et al., 2000). In contrast, *Miscanthus sinensis*, one of the parental species of *M.* × *giganteus*, exhibits extensive natural genetic diversity and phenotypic differentiation across its native range (Sun et al., 2010; Sacks et al., 2012; Zhao et al., 2013; Clark et al., 2014). This diversity makes *M. sinensis* a central resource for broadening the genetic base of miscanthus and for developing new cultivars with improved functional traits beyond biomass yield alone.

Nitrogen economy integrates nitrogen uptake, seasonal remobilization during spring and autumn, storage in belowground organs, and nitrogen losses, and plays a central role in how perennial plants sustain biomass production under low nitrogen inputs while limiting nitrogen export from the system (Beale & Long, 1997; Strullu et al., 2011; Leroy et al., 2022). Previous work in *Miscanthus sinensis* has demonstrated substantial variation in nitrogen economy traits and identified different genotype groups relying either on sustained nitrogen uptake or on endogenous nitrogen recycling, while maintaining comparable biomass production (Iqbal et al., 2026). These contrasted nitrogen use strategies are expected to underpin different ecosystem services, with more nitrogen-acquisitive genotypes contributing to regulating services such as nitrate removal and water quality protection, and more nitrogen-conservative genotypes supporting nutrient cycling, soil functioning, and long-term system stability.

Direct quantification of nitrogen economy traits requires plant destructive sampling and seasonally resolved measurements, limiting their routine use in breeding. To overcome this constraint, non-destructive proxy traits related to morphology, canopy structure, phenology, and nitrogen status have been shown to capture biologically meaningful variation in nitrogen economy and to predict components such as nitrogen uptake and remobilization (Chapter 2). While these proxy-based relationships are more or less robust at the phenotypic level, their underlying genetic basis remains unclear. Phenotypic associations between proxy traits and nitrogen economy traits may arise from shared genetic control, such as pleiotropy or tight linkage, or from coordinated physiological processes governed by distinct loci. Disentangling these alternatives requires explicit testing of whether proxy traits and nitrogen economy traits map to the same genomic regions.

In different grass species, nitrogen-related traits have been investigated using genetic approaches, showing that these processes can be linked to identifiable genomic regions. In sorghum, genome-wide analyses under contrasting nitrogen supply have identified multiple loci

associated with nitrogen use efficiency and related traits (Bollam et al., 2026). In switchgrass, genome-wide association analyses have similarly identified markers associated with nitrogen use and remobilization efficiency across diverse genetic backgrounds (Shrestha et al., 2022). Together, these studies indicate that nitrogen economy traits are genetically tractable in grasses, while also suggesting a complex, polygenic control. This context supports investigating whether similar genetic control underlies nitrogen uptake, remobilization, and losses in *Miscanthus sinensis*.

Genetic analyses in *Miscanthus sinensis* have so far focused primarily on aboveground biomass production, morphology, phenology, and flowering time. Across these traits, broad-sense heritability has generally been moderate to high, and QTL mapping studies have consistently revealed polygenic architectures involving numerous loci of small to moderate effect (Atienza et al., 2003; Slavov et al., 2014; Gifford et al., 2015; van der Weijde et al., 2017; Hou et al., 2022; Raverdy et al., 2022). These studies also demonstrate that QTL detection is sensitive to plant age and environmental conditions, with some loci showing stability across years or sites and others exhibiting strong context dependence (Dong et al., 2018; Hou et al., 2022; Raverdy et al., 2022). Despite these advances, belowground traits and nitrogen-related processes, including nitrogen uptake, seasonal remobilization, and losses, have not yet been investigated for heritability or QTL control in miscanthus. As a result, the genetic basis of the nitrogen economy remains largely unexplored, despite its central role in productivity and ecosystem service provision.

Quantitative trait locus mapping in full-sib populations provides a direct framework to address this gap by linking phenotypic variation to specific genomic regions in highly heterozygous, outcrossing species such as miscanthus (Wu et al., 2002; Margarido et al., 2007). Advances in SNP genotyping and integrated genetic map construction have enabled robust QTL detection for complex traits in *M. sinensis*, supporting the use of multilocus genetic information for selection strategies (Ma et al., 2012; Gazaffi et al., 2014). Beyond locus detection, QTL analyses allow estimation of allelic effects and evaluation of multilocus combinations, providing a foundation for selection approaches that extend beyond single-locus effects.

Against this background, the objective of this study was to translate nitrogen economy strategies in *Miscanthus sinensis* from phenotypic frameworks and proxy-based prediction into genetically defined targets that support selection. Specifically, we aimed to (i) identify genomic regions controlling nitrogen economy traits, including nitrogen uptake, seasonal remobilization

traits (SR, ARa, ARb), and nitrogen losses, hypothesizing that these traits are under polygenic control; (ii) test whether proxy-nitrogen economy relationships are genetically grounded through QTL co-location analyses; and (iii) evaluate the breeding relevance of detected loci by examining allelic effects and the potential for QTL pyramiding to support selection of targeted ideotypes.

To our knowledge, this study represents the first effort to dissect the genetic architecture of nitrogen economy traits in *Miscanthus sinensis* using QTL mapping at the progeny scale. By linking nitrogen acquisition, recycling, and losses to specific genomic regions and allelic effects, this work advances nitrogen economy from a functional concept to a breeding-ready genetic framework, enabling the development of multifunctional miscanthus ideotypes that combine sustained biomass production with ecosystem service delivery.

## 2. Materials and Methods

### 2.1 Plant material and field experiment

The study was conducted on a full-sib *Miscanthus sinensis* progeny derived from a controlled cross between the two parental genotypes ‘Malepartus’ (MAL) and ‘Herman Mussel’ (HER). The cross was performed in 2014 at the INRAE GCIE experimental unit of Estrées-Mons (doi: 10.15454/1.5572425838988464E12), after which seeds were germinated *in vitro*. Resulting seedlings were initially established under controlled conditions and subsequently established in the field at the INRAE GBFOr experimental unit of Orléans (Loiret, 47°49′ N, 1°54′ E) for clonal propagation by rhizome division to produce genetically identical replicates.

The progeny trial was established in 2018 at the INRAE GCIE experimental site of Estrées-Mons, northern France (49°87′ N, 3°01′ E), using an incomplete block design with four blocks and a planting density of 1 plant $m^{-2}$. A total of 127 progeny genotypes were initially planted. From this population, 80 genotypes were selected for detailed analysis of nitrogen economy traits. Genotypic data suitable for QTL analyses were available for 72 of these genotypes, which therefore constituted the mapping population. Each genotype was represented by at least one replicate per block.

The trial was managed under unfertilized conditions and irrigated to avoid water limitation. Plants were harvested annually in winter. Based on nitrogen nutrition index diagnosis using the

Malepartus parent as a probe genotype, the trial was characterized as nitrogen-deficient during the study period. The analyses presented here focus on the 2023-2024 growing cycle, during which nitrogen economy traits were quantified. Detailed descriptions of site characteristics, management practices, climatic conditions, and nitrogen status diagnosis are provided in Iqbal et al. (2026).

## 2.2 Nitrogen economy and proxy traits

Nitrogen economy traits were quantified to describe how *M. sinensis* genotypes acquire, redistribute, store, and lose nitrogen over the growing season. These traits included spring nitrogen remobilization (SR), autumn remobilization *via* aboveground method (ARa), autumn remobilization *via* belowground method (ARb), nitrogen uptake, and nitrogen losses. Together, these variables describe nitrogen fluxes among plant compartments across key phenological phases and constitute the nitrogen economy framework developed in Iqbal et al. (2026).

All plant sampling, nitrogen measurements, and calculations of nitrogen quantities, fluxes, and derived traits were performed following the protocols described in Iqbal et al. (2026). The present study directly uses these previously established trait values without modification.

In addition to nitrogen economy traits, a set of non-destructive proxy traits was measured to characterize plant size and architecture, canopy structure, phenology and growth dynamics, nitrogen status, nitrogen concentration, and nitrogen pools. These proxy traits were measured over the 2023-2024 growing cycle on the same plants used for nitrogen flux calculations. These proxy traits were identified and evaluated in Chapter 2 as potential predictors of plant destructive nitrogen economy traits. Variable Importance in Projection (VIP) scores derived from partial least squares analyses were used to select proxy traits with VIP > 1 for prediction of each nitrogen economy trait (Chapter 2).

Only these VIP-selected proxy traits were retained for genetic analyses and QTL co-location detections in the present study. Detailed descriptions of proxy trait measurements, statistical selection, and validation are provided in Chapter 2.

## 2.3 Calculation of nitrogen loss deviation

To identify genotypes combining high nitrogen uptake with contrasting nitrogen losses independently of the overall uptake-loss relationship, nitrogen loss deviation was calculated

following the approach proposed by Oury and Godin (2007) for grain protein deviation. Genotypic values of nitrogen losses were regressed against genotypic nitrogen uptake using a linear model fitted across all genotypes. For each genotype, nitrogen loss deviation was calculated as the standardized difference between observed nitrogen losses and the losses expected from the regression line at the same nitrogen uptake. This deviation quantifies nitrogen losses independently of uptake level, with negative values indicating genotypes exhibiting lower nitrogen losses than expected and positive values indicating higher losses than expected. While Oury and Godin (2007) applied this approach to a negative relationship between grain yield and protein concentration to identify genotypes exceeding expected protein levels, the present study applies the same deviation-based logic to a positive relationship between nitrogen uptake and nitrogen losses, in order to distinguish genotypes that decouple high uptake from high losses. Genotypes showing negative deviations would be desirable for an ecosystem service of water regulation.

## 2.4 Origin of genotypic data

Genotypic data were obtained using single-nucleotide polymorphism (SNP) markers generated by genotyping-by-sequencing. The initial variant call format (VCF) dataset comprised 39,112 SNPs**.** SNP discovery, filtering, and formatting followed the procedure described by Raverdy et al. (2022) for *Miscanthus sinensis*. Briefly, sequencing data were processed using established genotyping pipelines, and markers were filtered based on minor allele frequency and missing data thresholds prior to genetic map construction.

The resulting dataset comprised 35,026 SNP markers segregating according to expected full-sib segregation types for outcrossing populations (Wu et al., 2002). Three marker classes were retained: markers heterozygous in both parents (ab × ab), referred to as ‘Bridge’ (Bri) markers and segregating in a 1:2:1 ratio; markers heterozygous in Malepartus and homozygous in Herman Mussel (ab × aa), referred to as ‘Mal’ markers; and markers homozygous in Malepartus and heterozygous in Herman Mussel (aa × ab), referred to as ‘Her’ markers. The latter two marker types segregated in a 1:1 ratio. Marker nomenclature followed the classification of Wu et al. (2002), with Bri, Mal, and Her markers coded as B3.7, D1.10, and D2.15, respectively.

Following quality filtering, a total of 32,653 markers across 129 genotypes were retained for genetic map construction.

## 2.5 Genetic map construction

Genetic map construction followed the same methodological framework as described by Raverdy et al. (2022) for *M. sinensis*, using the OneMap R package (Margarido et al., 2007). Redundant markers were removed prior to map construction by collapsing markers with identical segregation patterns into bins, resulting in a reduced set of 8,462 representative markers used for downstream analyses. The remaining markers were tested for deviation from expected Mendelian segregation using chi-square tests with correction for multiple testing. Pairwise recombination fractions were estimated using two-point tests for outcrossing species (Wu et al., 2002).

Markers were grouped into linkage groups using only recombination information and correspondence with the *Miscanthus sinensis* reference genome (Mitros et al., 2020). The grouping was done using a maximum recombination fraction threshold of 0.35 and a validated LOD score suited to the data. This procedure resulted in 19 linkage groups, consistent with the base chromosome number of miscanthus (x = 19). Marker grouping was refined by retaining only markers consistent with their physical chromosome assignment, thereby ensuring correct linkage group composition. Segregation-distorted markers were retained during the grouping phase but removed prior to marker ordering and QTL detection, in accordance with the assumptions of the mapping model.

Marker ordering and genetic distance estimation were performed using multipoint approaches based on hidden Markov models implemented in OneMap and adapted for outcrossing species (Wu et al., 2002). Genetic distances were calculated using the Kosambi mapping function (Kosambi, 1943). The presence of genotyping errors was explicitly accounted for by specifying a genotyping error probability of 5 % in the hidden Markov model emission function, allowing uncertainty between observed and estimated genotypes to be considered, as implemented in OneMap (Taniguti et al., 2023).

The only difference relative to Raverdy et al. (2022) concerns marker ordering. Whereas Raverdy et al. ordered markers primarily according to their physical positions on the reference genome, marker ordering in the present study was performed based on the inference of the most likely genetic sequence using pairwise recombination fractions and multipoint likelihood comparisons. All other steps of map construction, filtering, grouping, and distance estimation were implemented identically.

The resulting integrated genetic map comprised 5,490 markers distributed across 19 linkage groups, spanning a total length of 1,813 cM, corresponding to an average marker density of approximately one marker every 0.33 cM.

## 2.6 Estimation of genotypic values and heritability

Genotypic values were estimated for each nitrogen economy trait and each proxy trait using linear mixed models fitted across the available replicate observations within the trial. When a trait was measured with replication at the plant level (*i.e.*, multiple observations per genotype), genotype was modelled as a random effect and genotypic best linear unbiased predictions (BLUPs) were extracted and used as genetic values for downstream analyses. For traits available only at the genotype level (*i.e.*, without within-genotype replication), no mixed-model aggregation was possible. In these cases, genotypic values corresponded to the observed genotype-level deviations from the population mean and were used directly in subsequent analyses. Replication was unbalanced across traits and genotypes, with the number of observations per genotype varying among traits and, for a given trait, among genotypes. Genotypic values derived either from mixed models or directly from genotype-level observations were subsequently used as phenotypic inputs for QTL mapping.

Broad-sense heritability ($H^2$) was estimated only for traits with within-genotype replication, based on variance components obtained from the mixed model. Heritability was calculated on a genotype-mean basis as:

$$H^2 = \sigma^2G / (\sigma^2G + \sigma^2E / \bar{r})$$

where $\sigma^2G$ is the genotypic variance, $\sigma^2E$ is the residual variance, and $\bar{r}$ is the mean number of observations per genotype for the trait considered. When a trait lacked within-genotype replication like nitrogen economy traits (SR, ARa, ARb, N uptake, N losses), heritability was not estimated. All analyses were performed in R (v4.5.1). Genotypic values and variance components were obtained using linear mixed models implemented in the lme4 package (v1.1-37).

## 2.7 QTL detection and characterization

QTL mapping was conducted using the integrated linkage map (19 linkage groups) together with genotypic values derived for each trait. As miscanthus is an outcrossing species, composite

interval mapping (CIM) adapted to full-sib progeny was implemented using the R package 'fullsibQTL' (Gazaffi et al., 2014; Gazaffi et al., 2020). The v0.0.9012 fullsibQTL version was used with the core functions create_fullsib(), cof_selection(), cim_scan(), cim_char(), r2_ls(), and get_segr(). This framework explicitly accounts for outcrossing segregation and estimates three genetic effects at each putative QTL position: two parental additive effects (parent P "Mal" additive effect and parent Q "Her" additive effect) and one dominance effect corresponding to the intra-locus interaction between parental alleles, based on multipoint QTL genotype probabilities along the linkage map.

For each trait, CIM scans were performed at 1-cM intervals across all linkage groups. Background genetic variation was controlled by selecting a limited set of marker cofactors within the fullsibQTL framework prior to genome scans. Genome-wide significance thresholds were determined using 1,000 phenotype permutations and a peak-based procedure following the algorithm of Chen and Storey (2006). In the present study, thresholds were derived from the distribution of the maximum (first) LOD peak obtained under permutation, and QTL were declared when observed LOD peaks exceeded the corresponding 5% genome-wide significance threshold. This conservative peak definition was chosen to prioritize robust and reproducible QTL signals for complex nitrogen economy traits, thereby minimizing false positives in subsequent QTL characterization and co-location analyses. QTL confidence intervals were defined using the 2-LOD drop-off criterion (Lander & Botstein, 1989). When multiple peaks occurred on the same linkage group, they were considered distinct QTL only when separated by a drop of at least 2 LOD units between adjacent peaks. For each detected QTL, parental additive effects, dominance effects, linkage phases, and the proportion of genotypic variance explained ($R^2$) were estimated within the CIM model. Co-location was assessed by comparing QTL positions within linkage groups using overlap of the 2-LOD confidence intervals derived for each trait. The full workflow used for QTL detection and post-scan characterization is summarized in Figure 1.

For each detected QTL, allelic states were inferred from the fullsibQTL model and coded numerically following the OneMap convention. Depending on the underlying segregation type and parental phase configuration, QTLs exhibited either two or three allelic states, coded as 1, 2, or 3. Across traits, two-state (1,2) or three-state (1,2,3) allelic configurations were observed for individual QTLs. These allelic state codes were subsequently used to visualize allelic effects and to define allelic combinations in multi-QTL analyses.

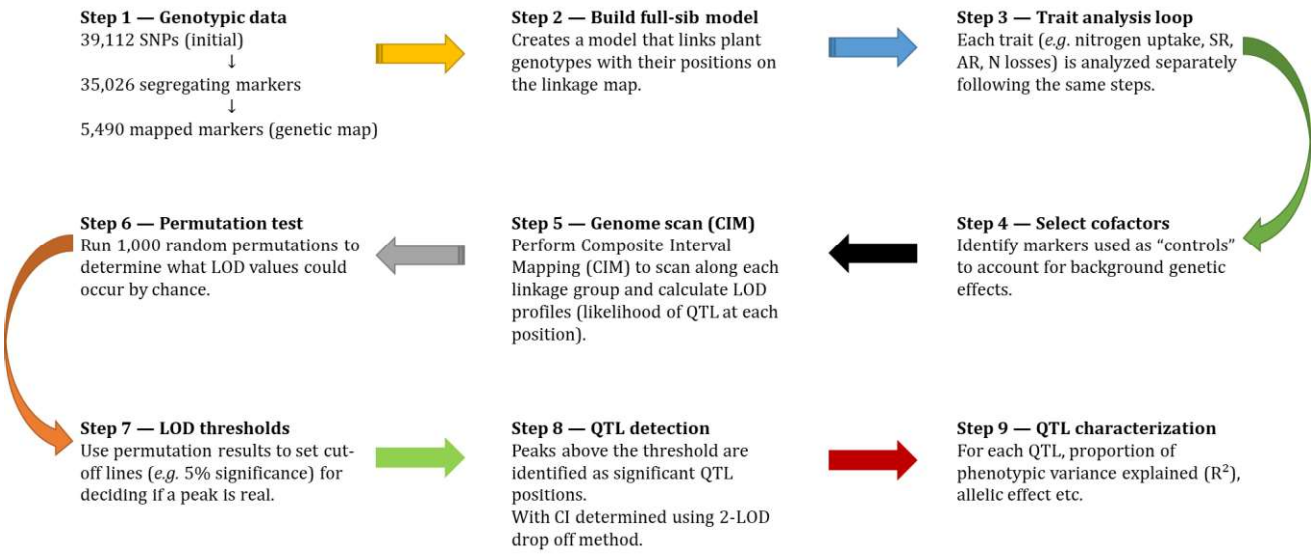


**Figure 1.** Schematic overview of the analytical workflow used for QTL detection and post-scan characterization in *Miscanthus sinensis*.

## 2.8 QTL pyramiding-based scoring of allelic classes for selection and counter-selection

Allelic classes defined by combinations of allelic states across the top three QTLs (qtl1-qtl2-qtl3) for nitrogen uptake and nitrogen loss deviation were used to assign selection and counter-selection scores (Table 1). For selection, allelic classes associated with higher nitrogen uptake were assigned priority scores, with a score of 2 given to classes showing the highest uptake values and a score of 1 given to secondary classes.

**Table 1.** Scoring scheme used to identify allelic classes for selection and counter-selection based on QTL pyramiding. Selection scores were assigned to allelic classes associated with high nitrogen uptake and negative nitrogen loss deviation, while counter-selection scores were assigned to allelic classes associated with high nitrogen uptake and positive nitrogen loss deviation. For each trait, allelic classes were ranked into two priority levels (score = 2 and score = 1) to account for multiple allelic classes meeting the selection or counter-selection criteria.

| Trait | Allelic classes at QTL | | | Selection score | Counter selection score |
|---|---|---|---|---|---|
| | qtl1 | qtl2 | qtl3 | | |
| N uptake | 1 | 1 | 1 | 0 | 0 |
| N uptake | 1 | 1 | 2 | 0 | 0 |
| N uptake | 1 | 2 | 1 | 1 | 0 |

| | | | | | |
|---|---|---|---|---|---|
| N uptake | 1 | 2 | 2 | 1 | 0 |
| N uptake | 2 | 1 | 1 | 0 | 0 |
| N uptake | 2 | 1 | 2 | 0 | 0 |
| N uptake | 2 | 2 | 1 | 0 | 0 |
| N uptake | 2 | 2 | 2 | 0 | 0 |
| N uptake | 3 | 1 | 1 | 0 | 0 |
| N uptake | 3 | 1 | 2 | 0 | 0 |
| N uptake | 3 | 2 | 1 | 2 | 1 |
| N uptake | 3 | 2 | 2 | 1 | 2 |
| N loss deviation | 1 | 1 | 2 | 2 | 0 |
| N loss deviation | 1 | 1 | 3 | 1 | 1 |
| N loss deviation | 1 | 2 | 1 | 0 | 0 |
| N loss deviation | 1 | 2 | 2 | 0 | 0 |
| N loss deviation | 1 | 2 | 3 | 0 | 0 |
| N loss deviation | 2 | 1 | 1 | 0 | 0 |
| N loss deviation | 2 | 1 | 2 | 0 | 0 |
| N loss deviation | 2 | 1 | 3 | 0 | 2 |
| N loss deviation | 2 | 2 | 1 | 1 | 0 |
| N loss deviation | 2 | 2 | 2 | 0 | 0 |
| N loss deviation | 2 | 2 | 3 | 0 | 0 |

Independently, allelic classes associated with negative nitrogen loss deviation were scored using the same scheme, with higher priority assigned to classes showing lower losses relative to uptake. For counter-selection, the same trait-specific scoring approach was applied to allelic classes associated with higher nitrogen uptake and positive nitrogen loss deviation. Scores were then summed across nitrogen uptake and nitrogen loss deviation to obtain combined selection and counter-selection scores ranging from 0 to 4. Genotypes were classified according to their combined scores and visualized in a bivariate space defined by nitrogen uptake and nitrogen losses (Figure 2).

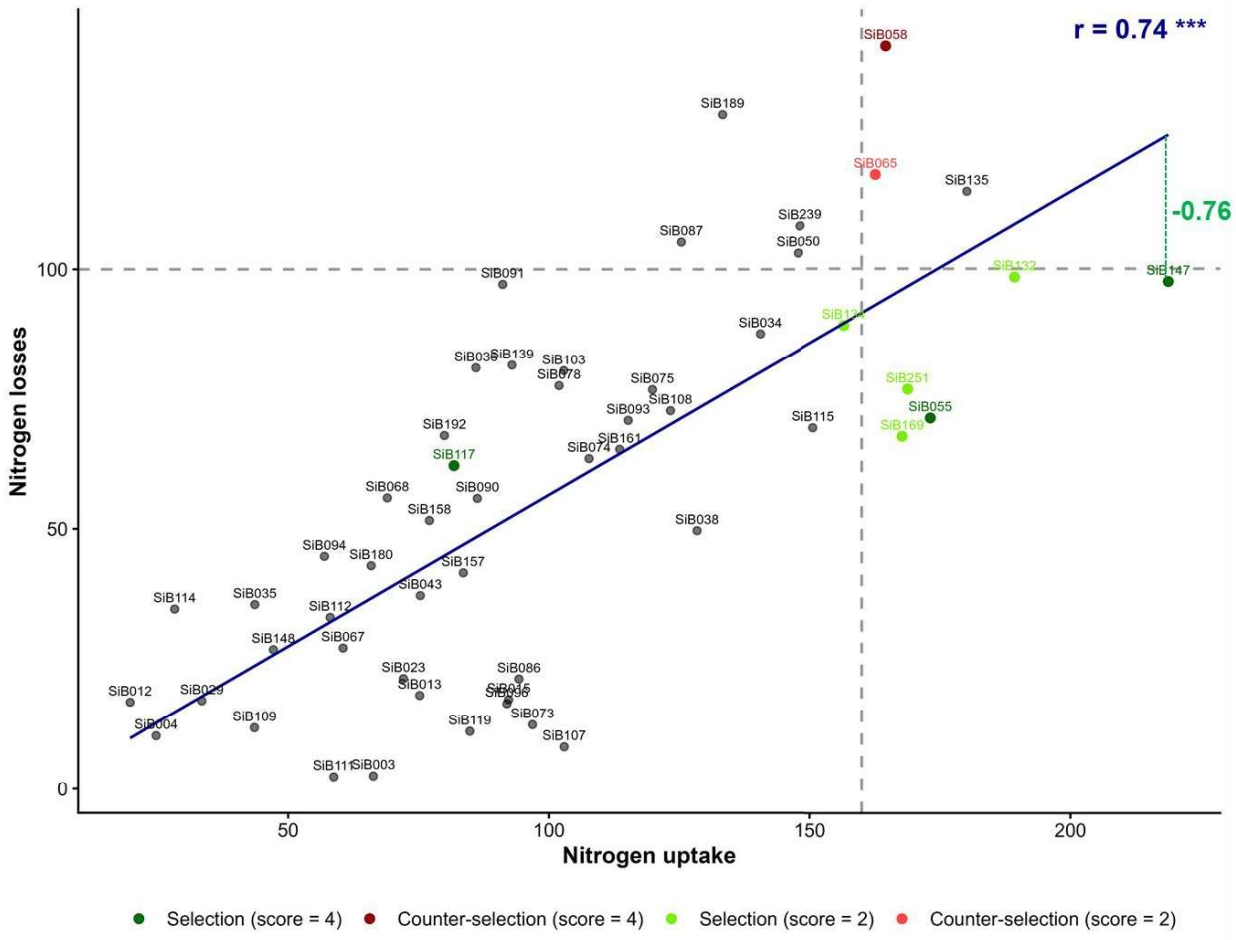


**Figure 2.** Relationship between nitrogen losses and nitrogen uptake across *Miscanthus sinensis* genotypes, illustrating selection and counter-selection based on QTL pyramiding. Nitrogen uptake (kg N ha$^{-1}$) is shown on the x-axis and nitrogen losses (kg N ha$^{-1}$) on the y-axis. The solid line represents the linear regression between nitrogen losses and nitrogen uptake, and the dashed lines indicate selection thresholds. Genotypes highlighted in green correspond to selected genotypes combining high nitrogen uptake with negative nitrogen loss deviation, while genotypes highlighted in red correspond to counter-selected genotypes combining high nitrogen uptake with non-desirable positive nitrogen loss deviation. Darker colors indicate genotypes with the highest combined scores (score = 4), and lighter colors indicate intermediate scores (score = 2). The dashed green line illustrates an example of nitrogen loss deviation for genotype SiB147 (-0.76), corresponding to its standardized vertical deviation from the regression line.

# 3. Results

## 3.1 Proxy traits showed a wide range of heritability from 0.12 to 0.93, with consistently higher values for canopy structure and phenology traits

Broad-sense heritability ($H^2$) of proxy traits ranged from 0.12 to 0.93 across traits (Figure 3), indicating substantial variation in genetic control among the evaluated proxies. Genotypic correlations among proxy traits, estimated from genotypic values, ranged from -0.22 to -0.52 for significant negative correlations and from 0.24 to 0.92 for significant positive correlations (data not shown).

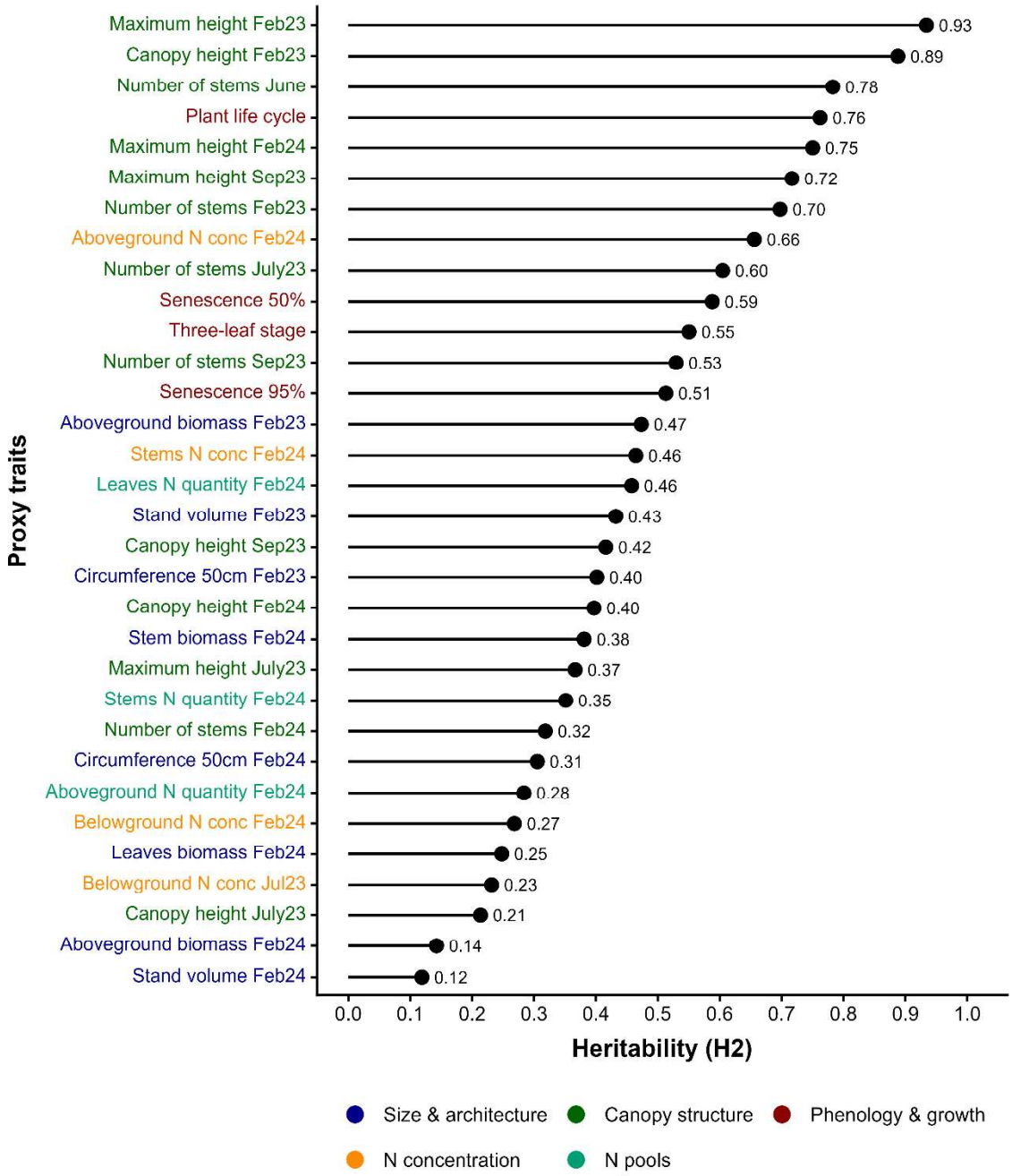


**Figure 3.** Broad-sense heritability ($H^2$) of proxy traits with within-genotype replication. Traits are colored by grouping into size and architecture, canopy structure, phenology and growth, nitrogen concentration, and nitrogen pools.

Heritability was generally higher for canopy structure and phenology-related traits. Maximum height measured in February 2023 showed the highest heritability ($H^2$ = 0.93), followed by canopy height in February 2023 ($H^2$ = 0.89). Several other canopy-related traits also exhibited high heritability, including number of stems measured in June ($H^2$ = 0.78) and maximum height measured in February 2024 ($H^2$ = 0.75) and September 2023 ($H^2$ = 0.72). Phenology and growth dynamics traits likewise showed moderate to high heritability, including plant life cycle ($H^2$ =

0.76), senescence timing ($H^2$ = 0.59 for 50% and 0.51 for 95%), and the three-leaf stage ($H^2$ = 0.55).

In contrast, size and architecture proxies showed lower heritability ($H^2$ = 0.12-0.47). Aboveground biomass measured in February 2023 showed moderate heritability ($H^2$ = 0.47), whereas values were lower for biomass measured in February 2024 ($H^2$ = 0.14) and for stand volume measured in February 2024 ($H^2$ = 0.12). Nitrogen-related proxy traits displayed intermediate heritability. Nitrogen concentration traits ranged from 0.23 to 0.66, with the highest value observed for aboveground nitrogen concentration in February 2024 ($H^2$ = 0.66). Nitrogen pool traits showed heritability values between 0.28 and 0.46, including leaves nitrogen quantity ($H^2$ = 0.46), stems nitrogen quantity ($H^2$ = 0.35), and aboveground nitrogen quantity ($H^2$ = 0.28).

## 3.2 Summer-to-autumn nitrogen dynamics were associated with 11 QTLs distributed across 9 linkage groups

For summer-to-autumn nitrogen dynamics, corresponding to the nitrogen dynamics from aboveground to belowground parts of the plant, a total of 11 QTLs were detected across nitrogen uptake, ARa, nitrogen losses, and nitrogen loss deviation (Table 2, Figure 4). These QTLs were distributed across multiple linkage groups, with individual loci explaining between 13.0% and 37.1% of the phenotypic variance, which corresponded to a rather high percentage.

For nitrogen uptake, four QTLs were detected on linkage groups 1, 5, 16, and 18 (Figure 4; Table 2). Individual QTLs explained between 13.0% and 24.3% of the phenotypic variance, with the largest effect detected on LG 18 (N uptake-qtl1; $R^2$ = 24.3%). Across the four detected QTLs, the global ($R^2$) proportion of phenotypic variance explained for nitrogen uptake was 64.0%. Additive allelic effects ranged from -15.95 to -0.08 for the Mal parent and from -19.54 to 18.72 for the Her parent, while dominance effects ranged from -22.56 to 1.11 (Table 2).

For autumn nitrogen remobilization *via* aboveground method (ARa), three QTLs were detected on linkage groups 11 and 18 (Figure 4, Table 2). Individual QTL effects ranged from 17.7% to 21.5% of the phenotypic variance. Two QTLs were detected on LG 11 (ARa-qtl1 and ARa-qtl3), while a third one was detected on LG 18 (ARa-qtl2). Across the three detected QTLs, the global $R^2$ for ARa was 56.7%. Additive allelic effects ranged from -9.43 to 41.03 for the Mal

parent and from -92.63 to 39.26 for the Her parent, while dominance effects ranged from -11.83 to 85.33 (Table 2).

For nitrogen losses, a single QTL was detected on linkage group 17 (N losses-qtl1), explaining 25.4% of the phenotypic variance (Figure 4, Table 2). This QTL was associated with additive effects of -2.35 for the Mal parent and -14.33 for the Her parent, and a dominance effect of 14.20 (Table 2). No additional QTLs exceeding the significance threshold were detected for this trait. In contrast, for nitrogen loss deviation, a quantification of nitrogen losses independently of nitrogen uptake level, three QTLs were detected on linkage groups 2, 4, and 6 (Table 2). Individual loci explained between 14.5% and 37.1% of the phenotypic variance, with the largest effect detected on LG 2 (N losses dev-qtl1; $R^2$ = 37.1%). Across the three detected QTLs, the global $R^2$ for nitrogen loss deviation was 54.1%. Additive allelic effects ranged from -0.21 to 0.30 for the Mal parent and from -0.27 to 0.37 for the Her parent, while dominance effects were always negative and ranged from -0.52 to -0.29 (Table 2).

No overlap of 2-LOD confidence intervals was observed between QTLs for nitrogen uptake, ARa, and nitrogen losses (Figure 4).

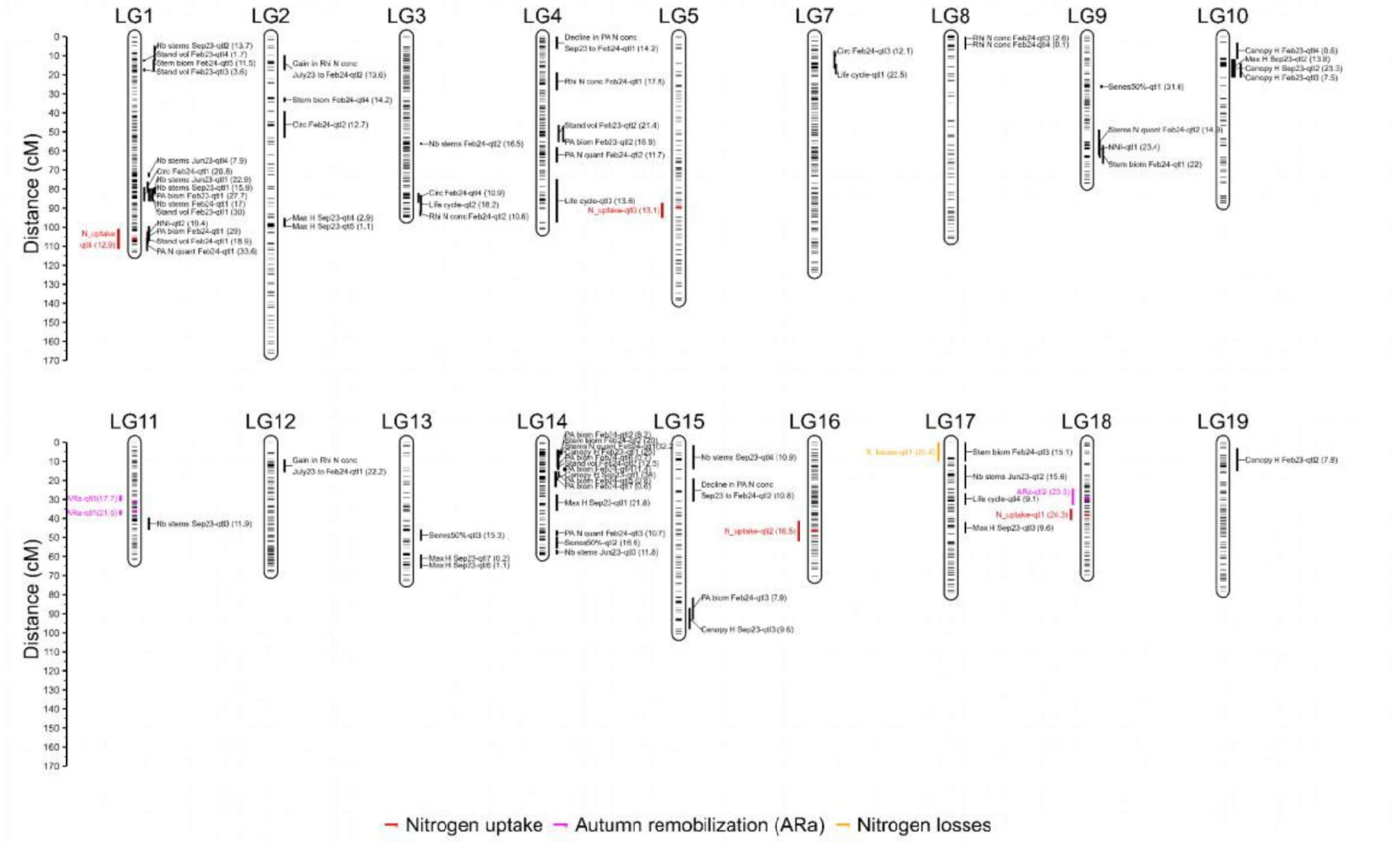


**Figure 4.** Integrated genetic map showing QTLs for summer-to-autumn nitrogen dynamics, including nitrogen uptake (red), autumn nitrogen remobilization *via* aboveground method (ARa; purple), and nitrogen losses (orange), together with their strong proxy traits (VIP > 1). QTL positions are shown on the linkage groups with 2-LOD confidence intervals. Values in brackets indicate the proportion of phenotypic variance explained ($R^2$) by each QTL.

**Table 2.** Summary statistics of QTLs identified at 5% genome-wide significance threshold for nitrogen economy traits in *Miscanthus sinensis*. For each detected QTL, the table reports the trait, QTL identifier, proportion of phenotypic variance explained ($R^2$, %), linkage group (LG), peak marker, peak position (cM), 2-LOD confidence interval (CI, cM), and -log10(p-value) of the QTL peak. Additive effects from the Malepartus parent (alpha 'Mal') and the Herman Mussel parent (alpha 'Her') are given with their corresponding hypothesis LOD tests (LOD H1 and LOD H2). The dominance effect arising from the interaction between parental alleles (delta 'Mal × Her') is given with its corresponding hypothesis LOD test (LOD H3).

| Trait | qtl-ID | $R^2$, % | LG | Peak marker | Peak Pos cM | CI cM | -log10(pval) | alpha 'Mal' | LOD H1 | alpha 'Her' | LOD H2 | delta 'Mal × Her' | LOD H3 |
|---|---|---|---|---|---|---|---|---|---|---|---|---|---|
| Nitrogen uptake | N uptake-qtl1 | 24.3 | 18 | BriMISSI18M70926026 | 38.2 | 34.9-41.0 | 10.91 | -5.79 | 0.85 | 18.72 | 6.63 | -22.56 | 8.29 |
| Nitrogen uptake | N uptake-qtl2 | 16.5 | 16 | HerMISSI16M68880180 | 46.6 | 41.2-51.9 | 7.31 | -15.95 | 4.55 | -12.28 | 3.62 | -3.33 | 0.29 |
| Nitrogen uptake | N uptake-qtl3 | 13.1 | 5 | MalMISSI05M85992784 | 89.7 | 87.1-95.2 | 8.36 | -0.08 | 0.00 | 6.31 | 0.97 | -20.68 | 8.42 |
| Nitrogen uptake | N uptake-qtl4 | 13.0 | 1 | HerMISSI01M148379278 | 106.2 | 100.9-111.6 | 6.88 | -8.09 | 1.66 | -19.54 | 6.92 | 1.11 | 0.03 |
| Autumn remobilization (ARa) | ARa-qtl1 | 21.5 | 11 | HerMISSI11M67940542 | 36.2 | 35.7-38.3 | 8.46 | 28.60 | 1.98 | 39.26 | 6.16 | -5.31 | 0.16 |
| Autumn remobilization (ARa) | ARa-qtl2 | 20.3 | 18 | BriMISSI18M54695263 | 29.5 | 24.3-33.0 | 6.47 | -9.43 | 3.22 | 6.02 | 1.47 | -11.83 | 4.57 |
| Autumn remobilization (ARa) | ARa-qtl3 | 17.7 | 11 | MalMISSI11M59709403 | 31.0 | 27.9-31.0 | 8.29 | 41.03 | 0.82 | -92.63 | 2.18 | 85.33 | 1.97 |
| Nitrogen losses | N losses-qtl1 | 25.4 | 17 | BriMISSI17M84815285 | 8.5 | 0.0-10.2 | 8.95 | -2.35 | 0.19 | -14.33 | 5.04 | 14.20 | 4.90 |
| Nitrogen loss deviation | N losses dev-qtl1 | 37.1 | 2 | MalMISSI02M2153274 | 164.6 | 160.0-166.0 | 7.77 | -0.01 | 0.00 | 0.37 | 4.46 | -0.49 | 5.64 |
| Nitrogen loss deviation | N losses dev-qtl2 | 14.7 | 6 | MalMISSI06M109407592 | 131.2 | 129.6-133.2 | 7.04 | 0.30 | 3.20 | -0.27 | 2.69 | -0.29 | 2.63 |
| Nitrogen loss deviation | N losses dev-qtl3 | 14.5 | 4 | BriMISSI04M1493000 | 100.7 | 97.8-101.1 | 7.37 | -0.21 | 2.02 | 0.03 | 0.04 | -0.52 | 7.47 |
| Spring remobilization | SR-qtl1 | 25.2 | 3 | BriMISSI03M106716136 | 6.9 | 5.3-9.2 | 11.19 | 3.59 | 2.52 | 7.99 | 10.17 | 2.40 | 1.11 |
| Spring remobilization | SR-qtl2 | 22.2 | 12 | BriMISSI12M59686597 | 52.2 | 49.8-54.3 | 10.34 | 0.96 | 0.19 | 7.64 | 8.99 | 2.12 | 0.94 |
| Spring remobilization | SR-qtl3 | 12.9 | 13 | BriMISSI13M62731557 | 64.2 | 62.9-69.9 | 8.12 | -5.20 | 4.06 | 6.50 | 6.66 | -1.00 | 0.14 |
| Spring remobilization | SR-qtl4 | 8.8 | 4 | BriMISSI04M72118100 | 52.9 | 50.0-56.8 | 6.49 | 5.89 | 5.36 | 1.58 | 0.38 | -1.90 | 0.58 |
| Autumn remobilization (ARb) | ARb-qtl1 | 24.9 | 1 | BriMISSI01M115469235 | 67.9 | 66.7-70.2 | 12.05 | -5.37 | 4.77 | -1.84 | 0.78 | 8.62 | 11.15 |
| Autumn remobilization (ARb) | ARb-qtl2 | 14.3 | 10 | BriMISSI10M49976691 | 43.9 | 40.7-44.1 | 11.47 | 4.87 | 5.63 | -7.29 | 8.41 | 3.24 | 1.97 |
| Autumn remobilization (ARb) | ARb-qtl3 | 9.0 | 8 | HerMISSI08M8843399 | 95.9 | 94.7-101.9 | 8.80 | -5.99 | 7.15 | -1.75 | 0.81 | -4.60 | 4.69 |
| Autumn remobilization (ARb) | ARb-qtl4 | 9.0 | 16 | HerMISSI16M11961850 | 12.4 | 7.1-16.9 | 7.87 | -0.22 | 0.01 | -2.91 | 1.55 | 6.25 | 7.46 |

## 3.3 Winter-to-spring nitrogen dynamics were associated with 8 QTLs distributed across 8 linkage groups

For winter-to-spring nitrogen dynamics, corresponding to nitrogen dynamics from belowground to aboveground parts of the plant, a total of 8 QTLs were detected across spring remobilization (SR) and ARb (Table 2, Figure 5). These QTLs were distributed across multiple linkage groups, with individual loci explaining between 8.8% and 25.2% of the phenotypic variance.

For spring nitrogen remobilization (SR), four QTLs were detected on linkage groups 3, 4, 12, and 13 (Figure 5; Table 2). Individual QTLs explained between 8.8% and 25.2% of the phenotypic variance, with the largest effect detected on LG 3 (SR-qtl1, $R^2$ = 25.2%). Across the four detected QTLs, the global ($R^2$) proportion of phenotypic variance explained for SR was 64.6%. Additive allelic effects ranged from -5.20 to 5.89 for the Mal parent and from 1.58 to 7.99 for the Her parent, while dominance effects ranged from -1.90 to 2.40 (Table 2).

For autumn nitrogen remobilization *via* belowground method (ARb), four QTLs were detected on linkage groups 1, 8, 10, and 16 (Figure 5, Table 2). Individual QTL effects ranged from 9.0% to 24.9% of the phenotypic variance, with the largest effect detected on LG 1 (ARb-qtl1, $R^2$ = 24.9%). Across the four detected QTLs, the global $R^2$ for ARb was 55.0%. Additive allelic effects ranged from -5.99 to 4.87 for the Mal parent and from -7.29 to -1.75 for the Her parent, while dominance effects ranged from -4.60 to 8.62 (Table 2).

Similarly, no overlap of 2-LOD confidence intervals was observed between QTLs for SR and ARb as well (Figure 5).

## 3.4 Co-location between nitrogen economy QTLs and proxy QTLs was limited to nitrogen uptake and spring remobilization

Shared genomic regions between nitrogen economy traits and their proxy traits were rarely detected. Among all nitrogen economy traits, co-location was detected for only two traits: nitrogen uptake (Figure 4) and spring remobilization (Figure 5). In both cases, co-location was restricted to a single locus, corresponding to one QTL per trait. No co-location was detected for ARa, ARb, and nitrogen losses.

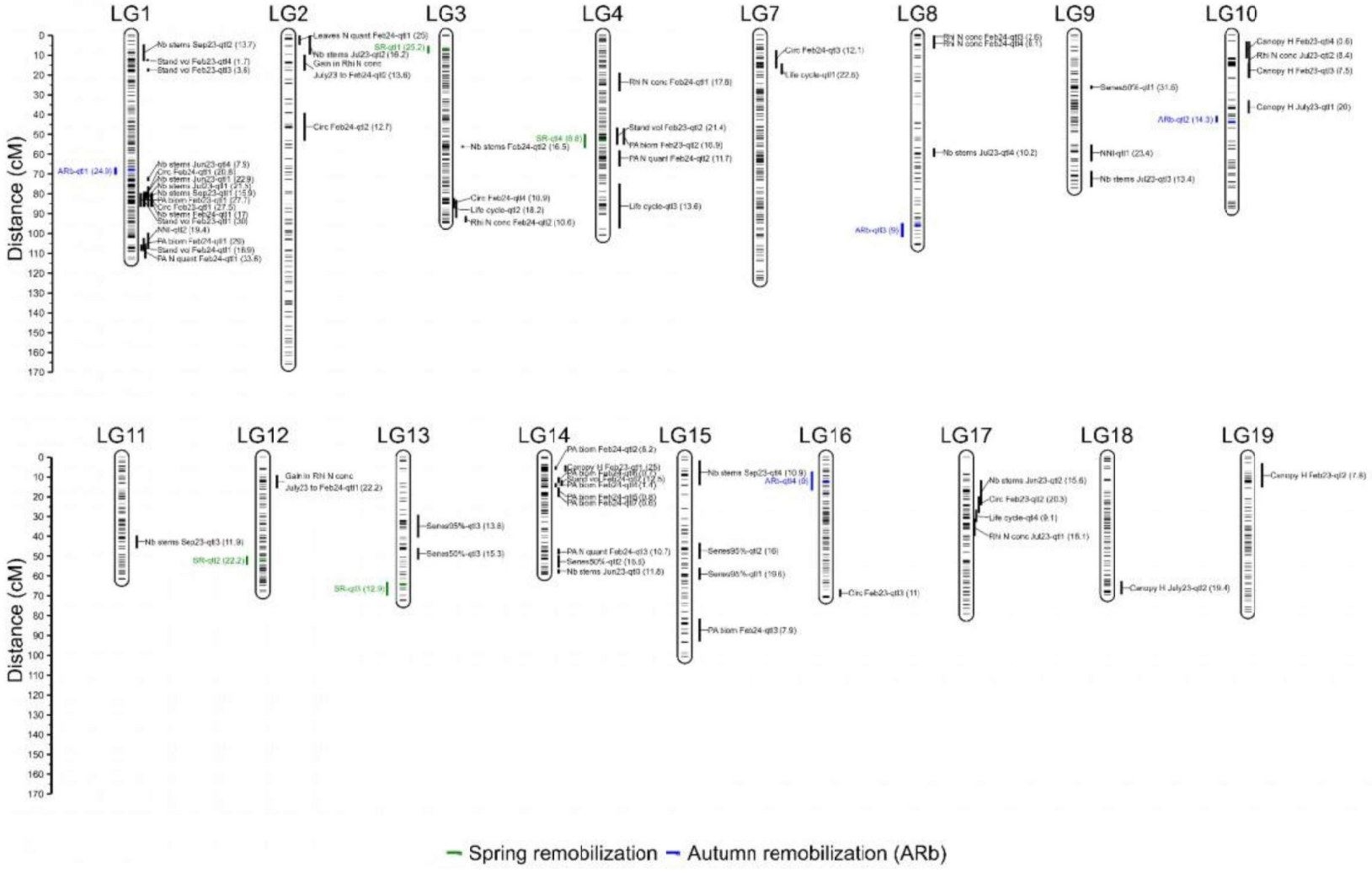


**Figure 5.** Integrated genetic map showing QTLs for winter-to-spring nitrogen dynamics, including spring nitrogen remobilization (SR, green) and autumn nitrogen remobilization *via* belowground method (ARb, blue), together with their strong proxy traits (VIP > 1). QTL positions are shown on the linkage groups with 2-LOD confidence intervals. Values in brackets indicate the proportion of phenotypic variance explained ($R^2$) by each QTL.

Across the five nitrogen economy traits, the corresponding set of 26 proxy traits, some of which were shared among multiple nitrogen economy traits, yielded a total of 85 proxy-trait QTLs that individually explained between 0.1% and 34.0% of the phenotypic variance (Supplementary Table 1). For spring remobilization, the corresponding set of 13 proxy traits yielded 41 QTLs. For ARa and ARb, the 12 and 14 corresponding proxy traits yielded 39 and 45 QTLs, respectively. For nitrogen uptake, the set of 15 proxy traits yielded 54 QTLs. For nitrogen losses, the 10 proxy traits provided 25 QTLs (Supplementary Table 1).

For nitrogen uptake, co-location was detected at one locus on linkage group 1. The N uptake-qtl4 co-located with QTLs for aboveground biomass in February 2024, Nitrogen Nutrition Index, aboveground nitrogen quantity in February 2024, and stand volume in February 2024 (Figure 4). In each case, the confidence interval of the proxy QTL overlapped with that of N uptake-qtl4.

For spring remobilization, co-location was detected at one locus on linkage group 4. The SR-qtl4 co-located with QTLs for aboveground biomass in February 2023 and stand volume in February 2023 (Figure 5). In both cases, the confidence intervals of the proxy QTLs overlapped with that of SR-qtl4.

## 3.5 Pyramiding allelic states at the top three QTLs separated genotypes into distinct nitrogen uptake, remobilization, and loss phenotypes

Allelic states at the best QTL (*i.e.* QTL explaining the highest phenotypic variance for each trait, also referred to as qtl1) differed among nitrogen economy traits; however, substantial genotypic variation was observed within each allelic state, with broader dispersion for some traits than others (Figure 6). For nitrogen uptake, allelic state 3 was associated with the highest mean value (132 kg N $ha^{-1}$), followed by allelic state 1 (93 kg N $ha^{-1}$), whereas allelic state 2 showed lower mean values (77 kg N $ha^{-1}$). Spring remobilization differentiated among all three allelic states, with allelic states 2 and 1 showing similar mean values (32 and 31 kg N $ha^{-1}$, respectively) and allelic state 3 associated with lower values (18 kg N $ha^{-1}$). For ARa, allelic state 2 showed higher mean values (90 kg N $ha^{-1}$) than allelic state 1 (57 kg N $ha^{-1}$), while for ARb, allelic state 2 was associated with higher mean values (35 kg N $ha^{-1}$) compared with allelic states 1 and 3 (22 and 21 kg N $ha^{-1}$, respectively). Nitrogen losses showed more limited differentiation among allelic states, with similar mean values for allelic states 3 and 1 (both 63 kg N $ha^{-1}$) and lower mean values for allelic state 2 (53 kg N $ha^{-1}$). Nitrogen loss deviation

(Figure 6b) differed slightly between allelic states, with allelic state 2 associated with higher mean value (0.2) compared with allelic state 1 (-0.1).

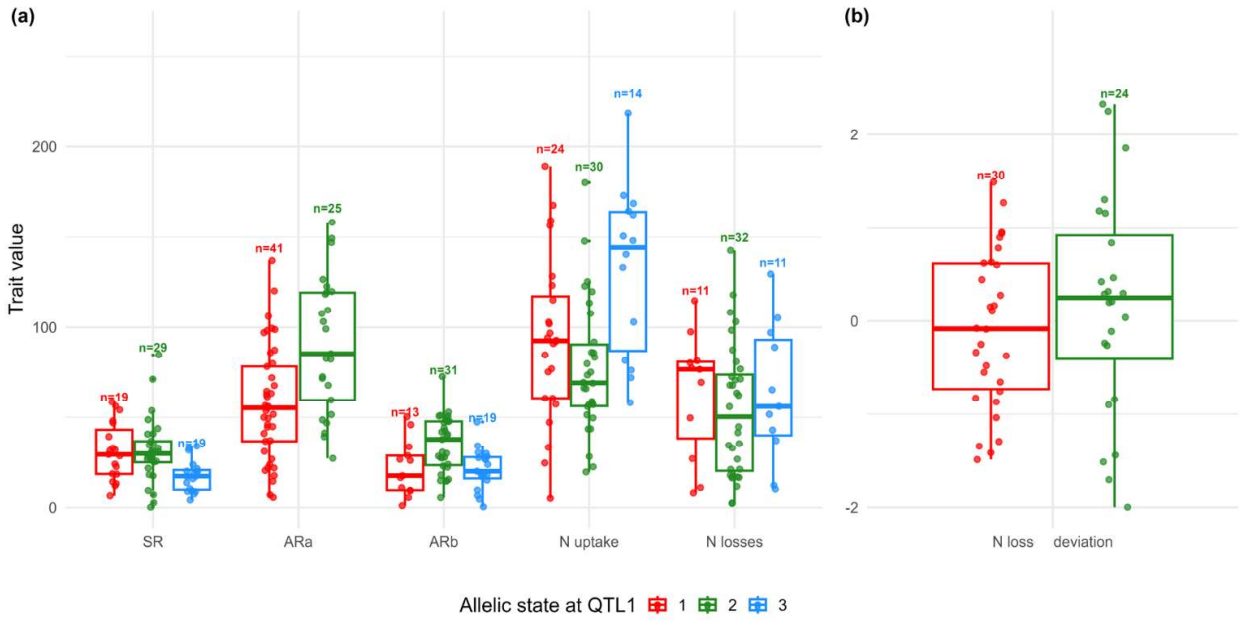


**Figure 6.** Allelic state effects at the best QTL for each nitrogen economy trait in *Miscanthus sinensis*. Nitrogen uptake, spring remobilization (SR), autumn remobilization *via* aboveground method (ARa), autumn remobilization *via* belowground method (ARb), and nitrogen losses are shown in panel (a), with trait values expressed in kg N ha$^{-1}$. Nitrogen loss deviation is shown in panel (b) and is unitless. Color indicates allelic state at the best QTL (qtl1). The '*n*' indicates the number of genotypes per allelic state at the best QTL for each trait.

Pyramiding allelic states across top three QTLs separated genotypes into relatively distinct phenotypes for each nitrogen economy trait (Figure 7). Allelic classes were defined by the combination of allelic states across the top three QTLs, reported in the order qtl1-qtl2-qtl3. For nitrogen uptake, higher mean values were observed for allelic classes such as 3-2-1 (159 kg N ha$^{-1}$), whereas lower mean values were associated with allelic classes such as 2-1-1 (49 kg N ha$^{-1}$). For spring remobilization, the allelic class 1-3-3 showed higher mean values (56 kg N ha$^{-1}$), while allelic classes such as 3-3-2 showed lower mean values (9). For ARa, higher mean values were observed for allelic classes such as 2-3-1 (144 kg N ha$^{-1}$), whereas lower mean values were associated with allelic classes such as 1-2-1 (29 kg N ha$^{-1}$). For ARb, the allelic class 2-1-1 was associated with higher mean values (43 kg N ha$^{-1}$), while allelic classes such as 1-3-1 showed lower mean values (6 kg N ha$^{-1}$). Interestingly for nitrogen losses deviation, positive mean values (2.3) were observed for allelic classes such as 2-1-3, whereas negative mean values (-0.8) were associated with allelic classes such as 1-2-2.

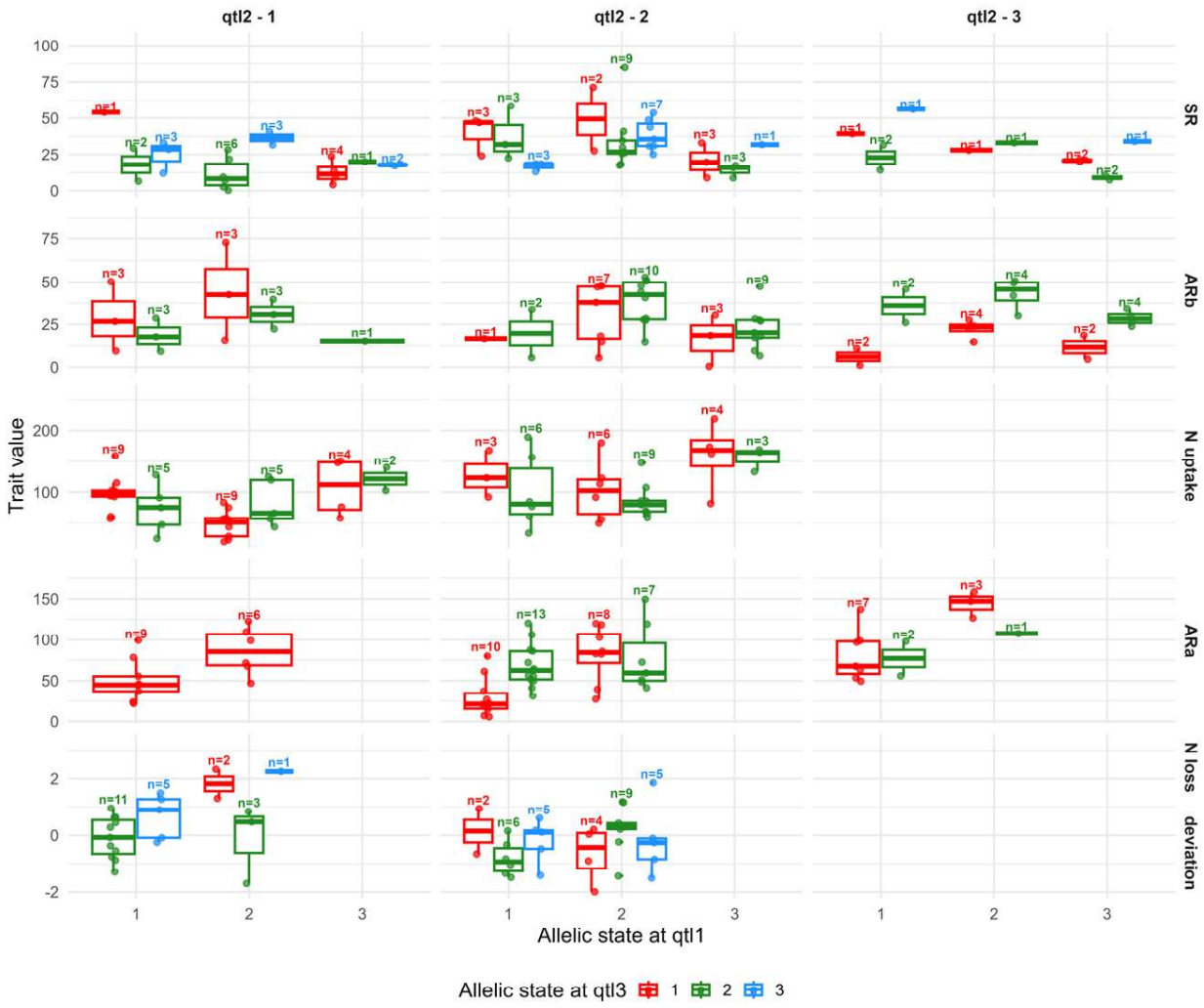


**Figure 7.** QTL pyramiding effects on nitrogen economy traits in *Miscanthus sinensis*. Trait values for nitrogen economy traits are shown for combinations of allelic states across the top three QTLs (qtl1, qtl2, and qtl3). Allelic classes are defined by the combination of allelic states at qtl1 (x-axis), qtl2 (facet columns), and qtl3 (color). Trait values are expressed in kg N $ha^{-1}$ for nitrogen uptake, SR, ARa, and ARb. The '*n*' above boxplots indicates the number of genotypes per allelic class. For example, the bottom-left green boxplot for nitrogen loss deviation corresponds to allelic class 1-1-2, indicating allelic state 1 at qtl1, allelic state 1 at qtl2, and allelic state 2 at qtl3.

## 3.6 QTL pyramiding allowed selection and counter-selection of genotypes with contrasting nitrogen losses at high nitrogen uptake performance

QTL pyramiding enabled the selection and counter-selection of genotypes combining high nitrogen uptake with contrasting nitrogen loss deviation (Figure 2). Genotypes achieving the highest combined selection score (score = 4, Table 1), *i.e.* showing the highest nitrogen uptake values and lowest nitrogen loss deviations, were clearly separated in phenotypic space. SiB147 and SiB055 combined high nitrogen uptake with negative nitrogen loss deviation and were positioned below the regression line relating nitrogen losses to nitrogen uptake. A third

genotype, SiB117, also achieved a selection score of 4 but was positioned above the regression line, corresponding to higher nitrogen losses relative to uptake, and was therefore identified and selected on the plot as a false positive.

Genotypes with an intermediate selection score (score = 2, Table 1), including SiB132, SiB251, and SiB169, showed high nitrogen uptake with moderately negative nitrogen loss deviation and clustered below the regression line. One additional genotype, SiB134, also achieved a score of 2 as it performed rather well for nitrogen uptake but was neutral for nitrogen losses relative to uptake.

Counter-selection identified genotypes combining high nitrogen uptake with positive nitrogen loss deviation. SiB058, which achieved the highest counter-selection score (score = 4), showed high nitrogen uptake and strongly positive nitrogen loss deviation and was positioned well above the regression line. SiB065, with a counter-selection score of 2, also exhibited elevated nitrogen loss relative to uptake and occupied a similar region of the phenotypic space. Across both selection and counter-selection groups, all identified genotypes were located in the high nitrogen uptake range, while differing consistently in the direction and magnitude of nitrogen loss deviation (Figure 2).

## 4. Discussion

The results of this study demonstrate that nitrogen economy traits in *Miscanthus sinensis*, despite their physiological complexity, can be translated into genetically defined targets relevant for selection. We identified genetic control underlying nitrogen uptake, seasonal nitrogen remobilization, and nitrogen losses, showing that these traits are associated with multiple QTLs exhibiting trait-specific genetic architectures. We further showed that relationships between nitrogen economy traits and non-destructive proxy traits are only partially supported by shared genetic control, indicating that proxy-target relationships arise from a combination of genetic linkage and coordinated physiological processes rather than from co-localization alone. Finally, combining allelic information in the form of QTL pyramiding across QTLs allowed multilocus genetic frameworks to support selection strategies, including the exploration of trade-off and contrasting nitrogen use profiles.

The discussion therefore focuses on three main points: first, how QTLs for nitrogen uptake and spring remobilization support selection toward specific ecosystem services; second, how QTL

pyramiding on nitrogen uptake and nitrogen loss deviation enabled breaking the strong link between uptake and losses; and third, the conditions under which QTLs for complex nitrogen economy traits are detected and the implications for their validation across environments.

## 4.1 QTLs identified for nitrogen uptake and spring remobilization enable selection for specific adaptation to ecosystem services

Nitrogen uptake and spring nitrogen remobilization are suitable targets for selection toward specific adaptation to ecosystem services in *Miscanthus sinensis*, as in this study we identified four distinct QTLs for each trait, explaining 13.0-24.3% and 8.8-25.2% of the phenotypic variance, respectively. No co-location was detected between QTLs controlling nitrogen uptake and those controlling spring remobilization, indicating genetically independent control and enabling their separate use in marker-assisted selection schemes aimed at distinct ecosystem service outcomes, where independent loci can be combined to improve selection precision (Bernardo, 2008).

In breeding theory, such genetic independence underpins specific adaptation, where selection is directed toward defined functions rather than broad performance across environments (Gallais, 1992). Within a nitrogen economy framework, nitrogen uptake and spring remobilization correspond to contrasting nitrogen use strategies, with uptake reflecting an acquisitive strategy based on soil nitrogen acquisition and remobilization reflecting a conservative strategy relying on internal nitrogen recycling. Both strategies can sustain biomass production (Iqbal et al., 2026), but they underpin different ecosystem services and therefore represent distinct targets for specific adaptation.

In this study, we identified multiple, independent QTLs controlling nitrogen uptake, providing a genetic basis for improving selection precision through multi-locus selection rather than reliance on single-QTL effects. This enables the targeted selection of acquisitive-type genotypes associated with regulating ecosystem services related to water quality protection, as perennial miscanthus systems have been shown to reduce nitrate leaching (Lesur et al., 2014; Ferchaud & Mary, 2016) leading to a reduced transfer to groundwater when deployed in water catchment areas, buffer zones, or marginal lands (Ferrarini et al., 2017).

Similarly, we detected distinct QTLs controlling spring remobilization, enabling targeted selection of conservative-type genotypes that support provisioning ecosystem services linked

to nutrient cycling, soil functioning, and system stability (CICES 5.1, 2018). By relying more strongly on internal nitrogen recycling, such genotypes reduce dependence on external nitrogen inputs and contribute to the long-term resilience of nutrient dynamics in perennial biomass systems (McCalmont et al., 2017; Tavakoli-Hashjini et al., 2020).

Together, the identification of genetically independent QTLs for nitrogen uptake and spring remobilization provides a clear genetic basis for selection toward specific adaptation to ecosystem services, rather than the general adaptation expected from a single genotype performing broadly across contexts (Gallais, 1992). This trait-based genetic framework supports the breeding of *Miscanthus sinensis* genotypes tailored to specific ecosystem services, while recognizing that the persistence of these QTL effects across environments and years will ultimately determine their value for selection.

## 4.2 QTL pyramiding on nitrogen uptake and nitrogen loss deviation enabled breaking the strong link between uptake and losses

In this study, we identified three QTLs controlling nitrogen loss deviation in *Miscanthus sinensis* (Table 2), revealing genetically controlled variation in nitrogen losses relative to nitrogen uptake. This result is particularly relevant given the positive phenotypic correlation between nitrogen uptake and nitrogen losses reported in *M. sinensis* (Iqbal et al., 2026), and provides a genetic basis for disentangling this unfavorable positive link. To target the ecosystem service of water regulation, genotypes with high nitrogen uptake are desirable, while high nitrogen losses counteract such good performance and are undesirable traits. Therefore, the nitrogen loss deviation helps to identify genotypes that deviate favorably from the relationship between nitrogen losses and nitrogen uptake. The use of deviation-based traits is well established in crop breeding as a means to break unfavorable trait associations, most notably through grain protein deviation in wheat, where standardized residuals from the yield-protein relationship have been used to identify genotypes combining high yield with elevated protein content (Oury & Godin, 2007). Importantly, subsequent multi-environment studies have shown that such deviation traits are not merely statistical constructs but can be genetically mapped, with associated genomic regions proposed as selectable targets within breeding programs (Mini et al., 2023). Together, these parallels support the use of nitrogen loss deviation as a biologically meaningful and genetically tractable trait to distinguish genotypes with high nitrogen uptake combined with lower nitrogen losses when targeting the water regulation ecosystem service.

Here, both nitrogen uptake and nitrogen loss deviation showed polygenic control with substantial phenotypic overlap among allelic classes at individual loci, indicating that effective selection requires QTL pyramiding to integrate allelic information across multiple loci. An approach consistent with marker-assisted selection for complex traits in which pyramiding favorable alleles across QTLs improves selection outcomes, as demonstrated in rice through stable performance of multi-QTL classes across generations (Kumar et al., 2018) and in maize through accumulation of favorable haplotypes at major yield QTLs (Wang et al., 2025), and as formalized in quantitative breeding theory (Bernardo, 2008).

The multilocus, multi-trait framework also revealed a limited number of false positives, where genotypes matched the allelic selection criteria but did not express the expected nitrogen uptake and nitrogen loss deviation combination. Such outcomes are an expected feature of marker-assisted selection for complex traits, where recombination, background genetic variation, and environmental sensitivity weaken the correspondence between marker profiles and phenotypic performance (Bernardo, 2008). Marker information therefore improves selection efficiency without guaranteeing phenotypic outcomes, making phenotypic validation an essential complement to genetic selection (Platten et al., 2019).

Within this context, the identification of both selected and counter-selected genotypes shows how QTL pyramiding on nitrogen uptake and nitrogen loss deviation can be used to explore contrasting nitrogen use profiles while maintaining transparency about the probabilistic nature of selection for complex traits.

## 4.3 QTLs were found for complex nitrogen economy traits under a specific condition and require a future validation across conditions and environments

In this study, we identified multiple QTLs controlling nitrogen uptake, seasonal remobilization, and nitrogen losses in *Miscanthus sinensis*, with loci explaining 8.8 to 37.1% of phenotypic variance. These effect sizes are characteristic of complex, integrative traits and are comparable to those reported for other quantitatively controlled traits in *M. sinensis*, such as flowering-time related traits, for which individual QTLs explained 2.7 to 30.7% of phenotypic variation (Hou et al., 2022).

We identified these QTLs within a defined experimental context, namely a single biparental population evaluated at one site over one experimental period. Previous work in *M. sinensis* shows that QTL detection for complex traits depends on multiple factors, including trait-specific sensitivity to climatic conditions, plant age, and their interactions. For example, multi-environment studies have shown that some biomass production QTLs show a relatively higher degree of consistency, with 40% to 60% remaining stable across environments, whereas only about 30% of biomass composition QTLs maintain similar consistency (Raverdy et al., 2022). In addition, climatic contrast has been shown to exert a stronger influence on QTL detection than plant age alone, indicating that environmental context can shape the expression of genetic effects for complex traits (Hou et al., 2022). Similar context-dependent patterns of QTL detection have been reported in miscanthus and other perennial crops across sites and years (Atienza et al., 2003; Ge et al., 2019).

A broader literature in grasses suggests that future miscanthu*s* genotypic studies should move beyond single-population, single-environment analyses. In sorghum, genome-wide analyses have shown that nitrogen use efficiency traits are associated with multiple loci under variable nitrogen supply (Bollam et al., 2026). In switchgrass, association mapping has demonstrated that nitrogen use and remobilization traits are controlled by multiple genomic regions across diverse genetic backgrounds (Shrestha et al., 2022). Complementary genomic studies in sugarcane have further identified genes involved in nitrogen uptake and transport, highlighting the molecular basis of nitrogen acquisition processes (Wang et al., 2019). Taken together, these studies indicate that the next step for miscanthus is to validate QTLs across environments and years, test their stability in additional genetic backgrounds, and progressively connect QTL regions with physiological mechanisms.

Within this broader context, the QTLs identified here define genetically meaningful loci underlying nitrogen economy traits as expressed under the studied conditions. These loci provide a first genetic framework that can be used to guide such validation efforts and to refine trait-specific marker sets. Triploid backgrounds will be of particular interest for obtaining sterile non-invasive varieties.

## 5. Conclusions and Perspectives

This study demonstrates that nitrogen economy traits in *Miscanthus sinensis*, despite their physiological complexity, can be genetically dissected and translated into targets relevant for

selection. By identifying QTLs controlling nitrogen uptake, seasonal nitrogen remobilization, and nitrogen losses, we showed that these key components of nitrogen economy are determined by several genomic regions and associated with distinct genetic architectures, establishing a novel genetic framework linking nitrogen acquisition, recycling, and loss to selection-oriented traits in perennial biomass crops.

This work highlights how genetic independence among nitrogen economy traits enables selection toward specific functional objectives. Independent QTLs for nitrogen uptake and spring remobilization support trait-based selection strategies aligned with contrasting ecosystem services, while the identification of nitrogen loss deviation as a genetically controlled trait shows how deviation-based approaches can be used to address the non-desirable positive link between nitrogen uptake and nitrogen losses. The multilocus perspective adopted here further illustrates the value of QTL pyramiding for complex traits, where single-locus effects alone are insufficient to robustly separate phenotypes. By combining allelic information across loci, selection decisions can be structured while explicitly acknowledging the probabilistic nature of genotype-phenotype relationships, reinforcing the need to integrate genetic information with phenotypic validation when targeting complex physiological traits.

From a forward-looking perspective, the QTLs identified in this study provide a foundation for future work aimed at refining and validating genetic control of nitrogen economy traits across environments, years, and genetic backgrounds. Increasing the number of repetitions per genotype, together with multi-environment and multi-year testing, will be essential to improve trait estimation, distinguish stable loci from context-dependent ones, and refine marker sets for breeding applications. In addition, the genetic regions identified here offer entry points for exploring the biological mechanisms underlying nitrogen economy through candidate gene analyses and functional validation of genes.

Overall, this study advances the genetic understanding of nitrogen economy in *Miscanthus sinensis* and provides a structured framework for integrating complex nitrogen traits into selection strategies. By linking nitrogen acquisition, recycling, and loss to defined genetic loci, this work opens new opportunities for breeding perennial biomass crops that support ecosystem services and resilient agricultural systems.

## References

Atienza, S. G., Satovic, Z., Petersen, K. K., Dolstra, O., & Martin, A. (2003). Identification of QTLs associated with yield and its components in *Miscanthus sinensis* Anderss. *Euphytica*, *132*(3), 353-361.

Beale, C., & Long, S. (1997). Seasonal dynamics of nutrient accumulation and partitioning in the perennial C4-grasses *Miscanthus* × *giganteus* and Spartina cynosuroides. *Biomass and Bioenergy*, *12*(6), 419-428.

Bernardo, R. (2008). Molecular Markers and Selection for Complex Traits in Plants: Learning from the Last 20 Years. *Crop Science*, *48*(5), 1649-1664. https://doi.org/https://doi.org/10.2135/cropsci2008.03.0131

Bollam, S., Rayaprolu, L., Romana, K. K., Ruperao, P., Selvanayagam, S., Vemula, A. K., Adapala, G., Valluri, V. K., Bajaj, P., Rathore, A., Odeny, D. A., Srivastava, R. K., Deshpande, S. P., & Gupta, R. (2026). Genome-wide association study and RNA sequencing identify candidate genes regulating nitrogen use efficiency and associated traits in sorghum (*Sorghum bicolor* (L.) Moench). *Food and Energy Security, 15*(1), e70174. https://doi.org/10.1002/fes3.70174

Brancourt-Hulmel, M., & Höfte, H. (2022). Biomass for the Future: Miscanthus and Sorghum for New End-Uses in France. *BioEnergy Research*, *15*(2), 669-671.

Chen, L., & Storey, J. D. (2006). Relaxed significance criteria for linkage analysis. *Genetics*, *173*(4), 2371-2381.

Clark, L. V., Brummer, J. E., Głowacka, K., Hall, M. C., Heo, K., Peng, J., Yamada, T., Yoo, J. H., Yu, C. Y., & Zhao, H. (2014). A footprint of past climate change on the diversity and population structure of *Miscanthus sinensis*. *Annals of Botany*, *114*(1), 97-107.

Clifton-Brown, J., Neilson, B., Lewandowski, I., & Jones, M. (2000). The modelled productivity of *Miscanthus* × *giganteus* (GREEF et DEU) in Ireland. *Industrial Crops and Products*, *12*(2), 97-109.

Clifton-brown, J. C., Stampfl, P. F., & Jones, M. B. (2004). Miscanthus biomass production for energy in Europe and its potential contribution to decreasing fossil fuel carbon emissions. *Global change biology*, *10*(4), 509-518.

Dong, H., Liu, S., Clark, L. V., Sharma, S., Gifford, J. M., Juvik, J. A., Lipka, A. E., & Sacks, E. J. (2018). Genetic mapping of biomass yield in three interconnected Miscanthus populations. *GCB Bioenergy*, *10*(3), 165-185.

Ferchaud, F., & Mary, B. (2016). Drainage and nitrate leaching assessed during 7 years under perennial and annual bioenergy crops. *BioEnergy Research*, *9*(2), 656-670.

Ferrarini, A., Fornasier, F., Serra, P., Ferrari, F., Trevisan, M., & Amaducci, S. (2017). Impacts of willow and miscanthus bioenergy buffers on biogeochemical N removal processes along the soil–groundwater continuum. *Gcb Bioenergy*, *9*(1), 246-261.

Gallais, A. (1992). Adaptation et adaptabilite en amelioration des plantes. *Selectionneur Francais*.

Gazaffi, R., Amadeu, R. R., Mollinari, M., Rosa, J. R., Taniguti, C. H., Margarido, G. R., & Garcia, A. A. (2020). fullsibQTL: an R package for QTL mapping in biparental populations of outcrossing species. *BioRxiv*, 2020.2012. 2004.412262.

Gazaffi, R., Margarido, G. R., Pastina, M. M., Mollinari, M., & Garcia, A. A. F. (2014). A model for quantitative trait loci mapping, linkage phase, and segregation pattern estimation for a full-sib progeny. *Tree Genetics & Genomes*, *10*(4), 791-801.

Ge, C., Ai, X., Jia, S., Yang, Y., Che, L., Yi, Z., & Chen, C. (2019). Interspecific genetic maps in *Miscanthus floridulus* and *M. sacchariflorus* accelerate detection of QTLs associated with plant height and inflorescence. *Molecular Genetics and Genomics*, *294*(1), 35-45. https://doi.org/10.1007/s00438-018-1486-6

Gifford, J. M., Chae, W. B., Swaminathan, K., Moose, S. P., & Juvik, J. A. (2015). Mapping the genome of *Miscanthus sinensis* for QTL associated with biomass productivity. *GCB Bioenergy*, *7*(4), 797-810.

Greef, J. M., Deuter, M., Jung, C., & Schondelmaier, J. (1997). Genetic diversity of European Miscanthus species revealed by AFLP fingerprinting. *Genetic Resources and Crop Evolution*, *44*(2), 185-195.

Heaton, E. A., Dohleman, F. G., & Long, S. P. (2008). Meeting US biofuel goals with less land: the potential of Miscanthus. *Global change biology*, *14*(9), 2000-2014.

Heaton, E. A., Long, S. P., Voigt, T. B., Jones, M. B., & Clifton-Brown, J. (2004). Miscanthus for renewable energy generation: European Union experience and projections for Illinois. *Mitigation and Adaptation Strategies for Global Change*, *9*(4), 433-451.

Hou, W., Raverdy, R., Lourgant, K., Mignot, E., Arnoult, S., Giauffret, C., & Brancourt-Hulmel, M. (2022). QTL Detection for Flowering-Time Related Traits in *Miscanthus sinensis* Using a Staggered-Start Design. *BioEnergy Research*, *15*(2), 718-733.

Iqbal, S., Brancourt-Hulmel, M., & Zapater, M. (2026). Nitrogen Economy Strategies Define Distinct Functional Groups of Genotypes in a *Miscanthus sinensis* Progeny. *GCB Bioenergy*, *18*(1), e70096. https://doi.org/https://doi.org/10.1111/gcbb.70096

Jones, M. B., & Walsh, M. (2001). *Miscanthus for energy and fibre*. Earthscan.

KOSAMBI, D. D. (1943). THE ESTIMATION OF MAP DISTANCES FROM RECOMBINATION VALUES. *Annals of Eugenics*, *12*(1), 172-175. https://doi.org/https://doi.org/10.1111/j.1469-1809.1943.tb02321.x

Kumar, A., Sandhu, N., Dixit, S., Yadav, S., Swamy, B., & Shamsudin, N. A. A. (2018). Marker-assisted selection strategy to pyramid two or more QTLs for quantitative trait-grain yield under drought. *Rice*, *11*(1), 35.

Lander, E. S., & Botstein, D. (1989). Mapping mendelian factors underlying quantitative traits using RFLP linkage maps. *Genetics*, *121*(1), 185-199.

Leroy, J., Ferchaud, F., Giauffret, C., Mary, B., Fingar, L., Mignot, E., Arnoult, S., Lenoir, S., Martin, D., Brancourt-Hulmel, M., & Zapater, M. (2022). *Miscanthus Sinensis* is as Efficient as *Miscanthus* × *Giganteus* for Nitrogen Recycling in spite of Smaller Nitrogen Fluxes. *BioEnergy Research*, *15*(2), 686-702. https://doi.org/10.1007/s12155-022-10408-2

Lesur, C., Bazot, M., Bio-Beri, F., Mary, B., Jeuffroy, M. H., & Loyce, C. (2014). Assessing nitrate leaching during the three-first years of *Miscanthus*× *giganteus* from on-farm measurements and modeling. *Gcb Bioenergy*, *6*(4), 439-449.

Lewandowski, I., Clifton-Brown, J., Kiesel, A., Hastings, A., & Iqbal, Y. (2018). Miscanthus. In *Perennial grasses for bioenergy and bioproducts* (pp. 35-59). Elsevier.

Ma, X.-F., Jensen, E., Alexandrov, N., Troukhan, M., Zhang, L., Thomas-Jones, S., Farrar, K., Clifton-Brown, J., Donnison, I., & Swaller, T. (2012). High resolution genetic mapping by genome sequencing reveals genome duplication and tetraploid genetic structure of the diploid *Miscanthus sinensis*. *PloS one*, *7*(3), e33821.

Margarido, G. R., Souza, A. P., & Garcia, A. A. (2007). OneMap: software for genetic mapping in outcrossing species. *Hereditas*, *144*(3), 78-79.

McCalmont, J. P., Hastings, A., McNamara, N. P., Richter, G. M., Robson, P., Donnison, I. S., & Clifton-Brown, J. (2017). Environmental costs and benefits of growing Miscanthus for bioenergy in the UK. *Glob Change Biol Bioenergy*, *9*(3), 489-507. https://doi.org/10.1111/gcbb.12294

Meehan, T. D., Gratton, C., Diehl, E., Hunt, N. D., Mooney, D. F., Ventura, S. J., Barham, B. L., & Jackson, R. D. (2013). Ecosystem-service tradeoffs associated with switching from annual to perennial energy crops in riparian zones of the US Midwest. *PloS one*, *8*(11), e80093.

Mini, A., Touzy, G., Beauchêne, K., Cohan, J.-P., Heumez, E., Oury, F.-X., Rincent, R., Lafarge, S., Le Gouis, J., & Consortium, B. (2023). Genetic regions determine tolerance to nitrogen deficiency in European elite bread wheats grown under contrasting nitrogen stress scenarios. *Theoretical and Applied Genetics*, *136*(11), 218.

Oury, F.-X., & Godin, C. (2007). Yield and grain protein concentration in bread wheat: how to use the negative relationship between the two characters to identify favourable genotypes? *Euphytica*, *157*(1), 45-57.

Platten, J. D., Cobb, J. N., & Zantua, R. E. (2019). Criteria for evaluating molecular markers: Comprehensive quality metrics to improve marker-assisted selection. *PloS one*, *14*(1), e0210529.

Raverdy, R., Lourgant, K., Mignot, E., Arnoult, S., Bodineau, G., Griveau, Y., Taniguti, C. H., & Brancourt-Hulmel, M. (2022). Linkage mapping of biomass production and

composition traits in a *Miscanthus sinensis* population. *BioEnergy Research*, *15*(2), 755-776.

Sacks, E. J., Juvik, J. A., Lin, Q., Stewart, J. R., & Yamada, T. (2012). The gene pool of Miscanthus species and its improvement. In *Genomics of the Saccharinae* (pp. 73-101). Springer.

Shrestha, V., Chhetri, H. B., Kainer, D., Xu, Y., Hamilton, L., Piasecki, C., Wolfe, B., Wang, X., Saha, M., Jacobson, D., Millwood, R. J., Mazarei, M., & Stewart, C. N., Jr. (2022). The genetic architecture of nitrogen use efficiency in switchgrass (*Panicum virgatum* L.). *Frontiers in Plant Science, 13*, 893610. https://doi.org/10.3389/fpls.2022.893610

Slavov, G. T., Nipper, R., Robson, P., Farrar, K., Allison, G. G., Bosch, M., Clifton-Brown, J. C., Donnison, I. S., & Jensen, E. (2014). Genome-wide association studies and prediction of 17 traits related to phenology, biomass and cell wall composition in the energy grass *Miscanthus sinensis*. *New phytologist*, *201*(4), 1227-1239.

Strullu, L., Cadoux, S., Preudhomme, M., Jeuffroy, M.-H., & Beaudoin, N. (2011). Biomass production and nitrogen accumulation and remobilisation by *Miscanthus* × *giganteus* as influenced by nitrogen stocks in belowground organs. *Field Crops Research*, *121*(3), 381-391.

Sun, Q., Lin, Q., Yi, Z.-L., Yang, Z.-R., & Zhou, F.-S. (2010). A taxonomic revision of Miscanthus sl (Poaceae) from China. *Botanical Journal of the Linnean Society*, *164*(2), 178-220.

Taniguti, C. H., Taniguti, L. M., Amadeu, R. R., Lau, J., Gesteira, G. d. S., Oliveira, T. d. P., Ferreira, G. C., Pereira, G. d. S., Byrne, D., & Mollinari, M. (2023). Developing best practices for genotyping-by-sequencing analysis in the construction of linkage maps. *GigaScience*, *12*, giad092.

Tavakoli-Hashjini, E., Piorr, A., Müller, K., & Vicente-Vicente, J. L. (2020). Potential bioenergy production from *Miscanthus* × *Giganteus* in Brandenburg: Producing bioenergy and fostering other ecosystem services while ensuring food self-sufficiency in the Berlin-Brandenburg region. *Sustainability*, *12*(18), 7731.

van der Weijde, T., Dolstra, O., Visser, R. G., & Trindade, L. M. (2017). Stability of cell wall composition and saccharification efficiency in Miscanthus across diverse environments. *Frontiers in plant science*, *7*, 2004.

Wang, X., Zhang, R., Sun, X., Wang, T., Li, J., Chen, D., Wang, J., Li, C., Wang, S., & Li, Z. (2025). Pyramiding of favorable haplotypes of major QTLs for yield-related traits to improve maize (Zea mays L.) productivity. *Agriculture Communications*, *3*(2), 100083.

Wang, J., Li, Y., Zhu, F., Ming, R., & Chen, L.-Q. (2019). Genome-wide analysis of nitrate transporter (NRT/NPF) family in sugarcane *Saccharum spontaneum* L. *Tropical Plant Biology, 12*(3), 133–149. https://doi.org/10.1007/s12042-019-09220-8

Whitaker, J., Field, J., Bernacchi, C., Cerri, C., Ceulemans, R., Davies, C., DeLucia, E., Donnison, I., McCalmont, J., & Paustian, K. (2018). Consensus, uncertainties and challenges for perennial bioenergy crops and land use. GCB Bioenergy 10: 150–164. In.

Wu, R., Ma, C.-X., Painter, I., & Zeng, Z.-B. (2002). Simultaneous maximum likelihood estimation of linkage and linkage phases in outcrossing species. *Theoretical population biology*, *61*(3), 349-363.

Zhao, H., Wang, B., He, J., Yang, J., Pan, L., Sun, D., & Peng, J. (2013). Genetic diversity and population structure of *Miscanthus sinensis* germplasm in China. *PLoS One*, *8*(10), e75672.

Zub, H., Arnoult, S., Younous, J., Lejeune-Henaut, I., & Brancourt-Hulmel, M. (2012). The frost tolerance of Miscanthus at the juvenile stage: differences between clones are influenced by leaf-stage and acclimation. *European Journal of Agronomy*, *36*(1), 32-40.

Zub, H. W., & Brancourt-Hulmel, M. (2010). Agronomic and physiological performances of different species of Miscanthus, a major energy crop. A review. *Agronomy for Sustainable Development*, *30*(2), 201-214. https://doi.org/10.1051/agro/2009034

# General Discussion & Perspectives

# 1. Introduction

Miscanthus is increasingly recognized as a strategic perennial biomass crop capable of contributing simultaneously to renewable energy supply, agricultural sustainability, and ecosystem service provision (Tavakoli-Hashjini et al., 2020; Weik et al., 2022). Beyond its high productivity and efficient resource use, a key attribute of miscanthus systems lies in their capacity to recycle nitrogen internally, thereby reducing dependence on external inputs and contributing to lower nitrate leaching risk (Beale & Long, 1997; Strullu et al., 2011; Leroy et al., 2022). However, despite the well-documented importance of nitrogen-use processes in perennial grasses (Li et al., 2024), the internal functioning, variability, and genetic control of nitrogen economy traits have remained largely unresolved in *Miscanthus sinensis*.

Within this broader context, understanding how nitrogen economy traits vary within *M. sinensis* is a necessary step toward developing cultivars that maintain high biomass production while supporting ecosystem services such as water-quality regulation, nutrient cycling, and long-term soil functioning. Previous studies demonstrated that *M. sinensis* possesses substantial intra-specific genetic diversity and strong adaptive potential (Sun et al., 2010; Zhao et al., 2013), but the extent to which this diversity translates into contrasting nitrogen-use strategies and structured functional behavior has not yet been explored. Likewise, although nitrogen recycling had been described at the whole-plant scale, its organization into coordinated processes and its genetic determinism had not been characterized prior to this work.

This thesis addressed these knowledge gaps through three complementary approaches applied to the same segregant *M. sinensis* progeny. First, nitrogen uptake, seasonal remobilization, nitrogen losses and their efficiencies were quantified under nitrogen-deficient field conditions to characterize inter-genotypic diversity and identify coherent nitrogen-use strategies. Second, non-destructive proxy traits were evaluated individually and in multivariate models to establish a predictive framework capable of estimating nitrogen economy traits without plant destructive sampling. Third, QTL mapping was used to dissect the genetic architecture of nitrogen economy traits and to test whether proxy-target relationships are supported by shared genomic control. Together, these approaches make it possible to move from the description of nitrogen fluxes, to their prediction, and ultimately to their genetic targeting in breeding.

The general discussion builds on the main findings of the three chapters and considers what they mean for nitrogen functioning, breeding, and ecosystem services in *M. sinensis*. It revisits

several key questions that emerge when results are viewed collectively rather than separately: why such large phenotypic diversity exists in nitrogen economy traits, how nitrogen limitation reveals contrasting genotypic capacity to maintain nitrogen status under low soil nitrogen availability, how nitrogen losses shape internal nitrogen recycling and the coordination between aboveground withdrawal and belowground storage, to what extent proxy-target relationships reflect shared genetic control, and how nitrogen economy traits can provide a basis for specific adaptation and prospects for general adaptation. These elements are then synthesized in the overall conclusion and perspectives to show how nitrogen economy traits can be progressively integrated into future *M. sinensis* breeding programs.

## 2. Extensive diversity in nitrogen-economy traits reflects high heterozygosity, strong recombination, transgressive segregation, and partly independent genetic control

The *M. sinensis* diploid biparental progeny exhibited exceptionally wide phenotypic diversity in nitrogen-economy traits, including nitrogen uptake, spring and autumn remobilizations, and their efficiencies, as shown in Table 1 (Chapter 1). Raverdy et al. (2022) further demonstrated that *M. sinensis* is highly heterogeneous at the species level, documenting both strong heterozygosity and extensive phenotypic variation across multiple traits. More broadly, studies conducted across the native range of the genus have also highlighted substantial genetic diversity in miscanthus (Sun et al., 2010; Sacks et al., 2012; Zhao et al., 2013; Clark et al., 2014). Together with our results, these findings confirm that this species harbors substantial evolutionary and breeding potential not only for biomass production but also for nitrogen-economy traits.

Several genetic mechanisms contribute to this strong segregation. First, the two parents themselves were highly distinct and belonged to contrasting functional groups concerning nitrogen economy: HER clustered in the acquisitive group 1, whereas MAL clustered in the deficient group 3, clearly reflecting opposite nitrogen-use strategies (Iqbal et al., 2026). Second, miscanthus is a naturally outcrossing genus characterized by self-incompatibility and high heterozygosity (Jiang et al., 2017), a feature also reflected in *M. sinensis*. In diploid full-sib miscanthus populations, up to four alleles may segregate per locus, generating highly variable progeny; this has been clearly documented in miscanthus breeding populations by Raverdy et al. (2022). Third, we observed evidence of high meiotic recombination in several progeny

genotypes, with frequent switches between parental homologs along chromosomes, indicating numerous crossover events (Figure 1). Figure 1 provides an illustrative example for a single genotype of the progeny on Chromosome 1. Across eukaryotes, meiotic recombination varies widely in both frequency and chromosomal distribution, and this variation is heritable and contributes to phenotypic diversification (Stapley et al., 2017). In maize, Pan et al. (2016) demonstrated that both intergenic and intragenic recombination events are strongly associated with phenotypic variation across complex agronomic traits, illustrating how recombination can reorganize functional diversity. A similar principle applies here: strong recombination in a genetically rich background increases the likelihood of generating different nitrogen-use strategies.

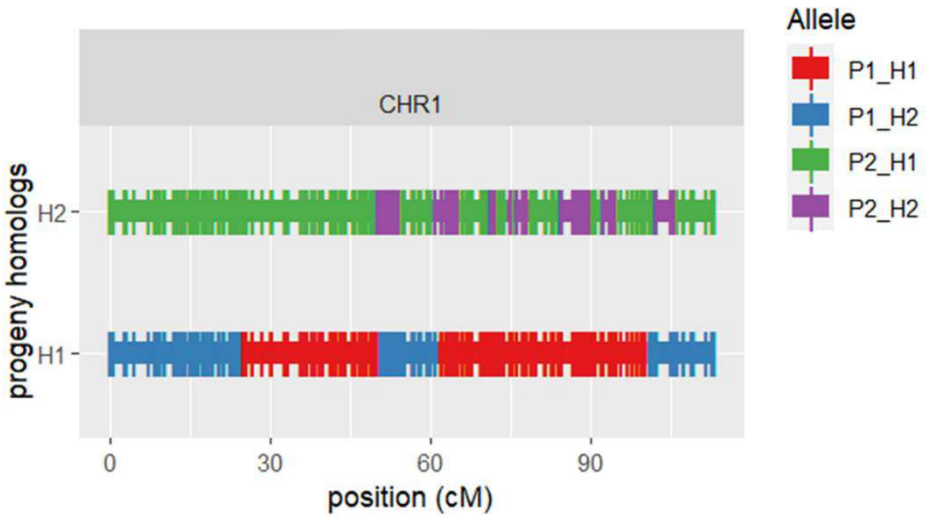


**Figure 1.** Example of crossover events in a genotype of the SiB *Miscanthus sinensis* progeny on Chromosome 1 (from Kristelle Lourgant). The plot shows the inheritance of parental homologs along Chromosome 1 for one progeny genotype. P1_H1 and P1_H2 represent the two homologs from Parent 1, while P2_H1 and P2_H2 represent the two homologs from Parent 2. The x-axis indicates genetic position (cM), and the y-axis distinguishes the two homologs of the progeny genotype (H1 and H2).

Transgressive segregation is another important source of diversity. In quantitative genetics, transgressive segregation arises when parents carry contrasting alleles that, when combined in the progeny, generate phenotypes exceeding parental limits. This mechanism has been repeatedly documented in major crops and linked to the dispersion and recombination of advantageous alleles (Mackay et al., 2021). Comparable patterns have also been reported in miscanthus breeding materials, where hybrid populations commonly display wider phenotypic ranges than their parents, providing opportunities to select superior individuals (Hou & Yi, 2023). Raverdy et al. (2022) also reported clear occurrences of transgressive segregation for biomass production and composition traits in *M. sinensis*, further supporting our interpretation.

Our results are fully consistent with this framework, since many nitrogen-economy traits showed progeny values beyond parental limits.

Finally, Chapter 3 showed that nitrogen uptake and nitrogen remobilization were associated with distinct QTL regions, indicating that these traits are at least partly controlled by independent genetic determinants. Such partial independence increases the number of possible phenotypic combinations because contrasting "uptake" and "recycling" alleles can recombine freely. Under nitrogen-limited conditions, this genetic independence becomes particularly visible, as genotypes rely on whichever nitrogen-use strategy (acquisitive *vs* conservative) their genotype supports most strongly.

Taken together, the very large diversity observed in nitrogen-economy traits in this diploid biparental *M. sinensis* population is therefore not experimental variability but reflects a real biological potential of the species. It results from its inherent heterozygosity and self-incompatibility, strong recombination generating novel allele combinations, transgressive segregation, and partly independent genetic control of nitrogen uptake and remobilization. The studied population illustrates that *M. sinensis* offers a rich genetic resource for breeding contrasted nitrogen-use ideotypes and supports the feasibility of selecting genotypes tailored to different nitrogen-economy strategies.

## 3. Nitrogen limitation revealed contrasting genotypic capacity to maintain nitrogen status under low soil nitrogen availability

This diversity in nitrogen economy became particularly informative under the nitrogen-limited conditions of our experiment. Mean soil mineral nitrogen measured in March 2023 and March 2024 was 20 and 29 kg N $ha^{-1}$, respectively, to a depth of 150 cm. These values are lower than those reported under comparable unfertilized miscanthus stands at the same location. Specifically, Strullu et al. (2011) reported soil mineral nitrogen contents of 51 ± 15 and 32 ± 15 kg N $ha^{-1}$ (0–150 cm) in *Miscanthus* × *giganteus* stands aged three and four years, respectively, while Ferchaud and Mary (2016) reported a mean value of 38 kg N $ha^{-1}$ (0-150 cm) across stands aged three to ten years. In the study of Strullu et al. (2011), miscanthus stands exhibited nitrogen deficiency in August, as indicated by mean nitrogen nutrition index (NNI) values below 1 in both 2008 and 2009 (data not shown).

In our study, nitrogen limitation was diagnosed by the probe genotype MAL (Chapter 1). However, despite low soil nitrogen availability, both nitrogen-deficient and non-deficient genotypes coexisted within the segregant *M. sinensis* progeny. This coexistence highlights intrinsic genotypic differences in nitrogen requirements and/or nitrogen acquisition capacity. Some genotypes maintained sufficient nitrogen status, with aboveground nitrogen concentration meeting the threshold required to maximize aboveground biomass production under low N availability. This may reflect a greater capacity to capture nitrogen from the soil, potentially supported by root-system traits that enhance soil exploration (*e.g.*, more extensive or deeper rooting). Such mechanisms have been highlighted for improving nitrate acquisition in maize, particularly under leaching conditions (Lynch, 2013). Alternatively, it may indicate that certain genotypes require less nitrogen to maximize biomass production, suggesting that their nitrogen demand is intrinsically lower under the same limiting conditions.

Consistently, the functional classification showed that acquisitive genotypes were mostly non-N-deficient (~ 71% of this group), whereas conservative genotypes more frequently exhibited nitrogen deficiency (>50% of this group) (Figure 8, Chapter 1). Together, these results indicate that nitrogen limitation revealed strong genotypic variability in nitrogen status within the progeny, even under uniformly low soil nitrogen availability. Testing whether these genotypic differences persist under nitrogen-sufficient conditions will be an important next step to determine whether they primarily reflect inherent nitrogen demand, nitrogen acquisition capacity, or both.

## 4. Reducing nitrogen losses revealed a coordinated internal nitrogen transfer between autumn withdrawal and belowground storage

In our study, nitrogen uptake was strongly and positively correlated with nitrogen losses (r = 0.70; Figure 7, Chapter 1), and no significant relationship was initially detected between autumn remobilization estimated from aboveground withdrawal (ARa) and belowground nitrogen storage (ARb). This indicated that although substantial quantities of nitrogen were withdrawn from aboveground parts during senescence, they were not systematically recovered belowground. This interpretation is consistent with previous miscanthus studies showing that nitrogen cycling during the autumn-winter period is accompanied by substantial unrecovered nitrogen. In *Miscanthus* × *giganteus*, Beale and Long (1997) and Himken et al. (1997) first reported large seasonal decreases in whole-plant nitrogen content between late summer and

winter, while Strullu et al. (2011) confirmed that only part of the nitrogen removed from aboveground tissues was subsequently detected belowground. More recently, Leroy et al. (2022) quantified nitrogen losses of 42-56% between September and February in *M.* × *giganteus* and *M. sinensis*, which is consistent with our results showing substantial nitrogen losses during the same period (2%-67% of September whole-plant nitrogen; Iqbal et al. (2026)), only partly attributable to leaf abscission. Together, these studies demonstrate that nitrogen losses are an intrinsic and quantitatively important component of perennial nitrogen recycling, rather than a negligible residual fraction.

To further clarify the role of nitrogen losses in structuring nitrogen economy relationships, we used nitrogen loss deviation to evaluate losses largely independently from nitrogen uptake by reducing the dominant uptake-loss trend. In practice, this involved excluding all genotypes positioned above the uptake-loss regression line, that is, those exhibiting higher-than-expected nitrogen losses relative to their uptake. When these genotypes were removed, a clearer internal structure of the nitrogen economy emerged. In particular, ARa and ARb became significantly positively correlated ($r = 0.50$; Figure 2), whereas no relationship existed when all genotypes were considered. This demonstrates that nitrogen losses are one of the primary reasons why high ARa does not always translate into high ARb. In genotypes exhibiting lower-than-expected losses, nitrogen withdrawn during autumn senescence is more efficiently transferred and conserved belowground, revealing an underlying coordination between autumn withdrawal and belowground storage once the confounding influence of high-lost nitrogen is reduced. Leroy et al. (2022) already suggested that nitrogen losses explain why ARb is systematically lower than ARa; our results go a step further by showing that, once losses are accounted for, the internal nitrogen economy reveals a more coherent structure.

Even after removing genotypes with high nitrogen losses, no significant relationship was observed between ARb and spring remobilization (SR) (Figure 2). This indicates that the quantity of nitrogen stored belowground at the end of winter does not fully determine the amount subsequently remobilized during spring regrowth. A plausible explanation is that winter processes modify both the size and accessibility of nitrogen reserves, through biochemical stabilization in storage compounds, transformations between molecular forms, additional nitrogen losses, and possible changes in plant structure such as increases in rhizome biomass or nitrogen reallocation to newly formed roots between autumn and late winter. These processes are increasingly recognized as key regulators of how perennial grasses control the contribution

of stored nitrogen to spring regrowth (Li et al., 2024). The absence of a relationship between ARb and SR in our study may therefore reflect the combined influence of these winter transformations and losses, which merit explicit quantification in future work.

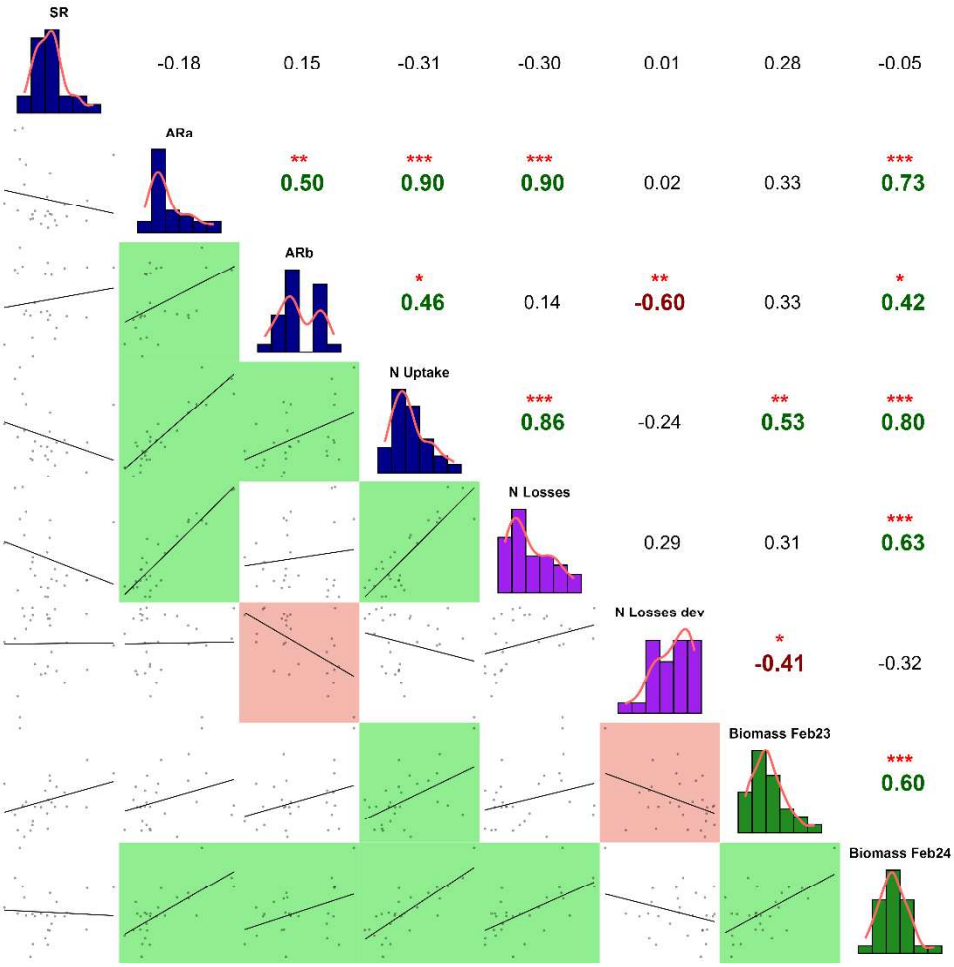


**Figure 2:** Pairwise correlation matrix and scatterplots for nitrogen- related traits and aboveground biomass yield in *Miscanthus sinensis* progeny excluding all genotypes showing positive nitrogen loss deviations. Pearson correlation coefficients (r) are shown in the upper triangle, with significance levels indicated as follows: *** for $p < 0.001$, ** for $p < 0.01$, * for $p < 0.05$, and non- significant correlations ($p \geq 0.1$). Trait abbreviations are given in the abbreviation table.

Overall, these results show that nitrogen losses are not only outcomes of nitrogen economy but also key factors structuring it. Accounting for losses revealed a previously hidden coordination between autumn withdrawal and belowground storage, indicating that high-loss genotypes can mask the internal organization of nitrogen transfers. In this context, reducing nitrogen losses is expected to increase nitrogen retained in belowground organs, potentially supporting rhizome and root development and strengthening plant functions such as frost resistance and soil exploration capacity. In parallel, perennial bioenergy systems such as miscanthus have been shown to contribute to lower nitrate concentrations in drainage water and buffer zones (Ferchaud & Mary, 2016; Ferrarini et al., 2017). Within this framework, genotypes combining

high nitrogen uptake with low loss deviation appear promising for supporting water-quality regulation. Conversely, genotypes that return more nitrogen to soil pools through residues and rhizodeposition may contribute to nutrient cycling, while efficient spring remobilization remains essential to sustain biomass production without excessive depletion of soil nitrogen resources.

## 5. QTL co-location occurs only where proxy-nitrogen trait relationships are strongest

Co-location between proxy traits and nitrogen economy traits was detected only for nitrogen uptake (Figure 3, Chapter 3) and spring remobilization (Figure 4, Chapter 3). For nitrogen uptake, co-location occurred with aboveground biomass in February 2024, stand volume in February 2024, nitrogen nutrition index, and aboveground nitrogen quantity in February 2024, and these proxies were also those showing the strongest correlations with uptake ($r = 0.51$-$0.65$; Table 1). For spring remobilization, co-location involved aboveground biomass in February 2023 and stand volume in February 2023, which likewise showed the highest correlations with this trait ($r = 0.42$-$0.45$; Table 1). The fact that co-location systematically occurred with the proxies most strongly associated with the corresponding nitrogen economy traits indicates that these overlaps most likely reflect genuine shared genetic regulation rather than statistical coincidence. Similar interpretations have been reported in miscanthus flowering studies, where co-located QTLs for multiple correlated phenological traits were attributed to shared genetic control of developmentally linked processes (Hou et al., 2022; Park et al., 2024).

The limited number of co-locations is therefore biologically meaningful, highlighting that shared genomic regulation occurs only where traits are most closely related. In perennial grasses, co-location generally occurs when traits are both biologically related and genetically or developmentally coordinated, while many other traits are controlled by distinct loci. In Napier grass, co-located QTLs for highly correlated biomass and water-use traits were interpreted either as the result of tight linkage between adjacent loci or as pleiotropic genomic regions influencing multiple traits simultaneously (Muktar et al., 2022). In miscanthus, QTL clusters combining related traits have also been repeatedly documented, with co-locations arising from pleiotropy, linked genes, strong genetic correlations, and the presence of major regulatory genes within shared genomic intervals (Hou et al., 2022; Raverdy et al., 2022; Park

et al., 2024). Our results align well with this framework, since co-location appeared precisely where proxy and target traits exhibited the strongest phenotypic consistency.

By contrast, the absence of co-location for ARa, ARb and nitrogen losses is consistent with previous evidence showing that trait-specific QTLs are common in miscanthus and that many physiological traits map to distinct genomic regions. QTL studies in miscanthus have demonstrated that genetic control depends strongly on trait type, developmental timing and environment, resulting in mixtures of shared and independent QTLs across traits (Raverdy et al., 2022). This supports the idea that proxies can remain highly relevant even when they do not systematically share overlapping QTLs with nitrogen economy traits, because they may act as integrative indicators of plant functioning rather than simple genetic substitutes.

**Table 1.** Pairwise correlation matrix between nitrogen uptake, spring remobilization, and their co-located proxy traits in *Miscanthus sinensis* progeny. Pearson correlation coefficients (r) are presented, with significance levels indicated as *** for $p < 0.001$. Proxies shown correspond only to those traits for which QTL co-location with nitrogen uptake or spring remobilization was detected.

| Proxy traits | Nitrogen uptake | Proxy traits | Spring remobilization |
|---|---|---|---|
| Aboveground biomass Feb24 | 0.65*** | Aboveground biomass Feb23 | 0.45*** |
| Stand volume Feb24 | 0.60*** | Stand volume Feb23 | 0.42*** |
| Nitrogen nutrition index | 0.51*** | | |
| Aboveground N quantity Feb24 | 0.55*** | | |

Overall, these results show that proxy-target relationships are genetically supported precisely where phenotypic relationships are strongest, while in other cases proxies continue to provide biologically meaningful information even without explicit QTL overlap. Co-located regions for nitrogen uptake and spring remobilization therefore represent robust genomic targets, since they are supported simultaneously by phenotypic association and shared QTL intervals. At the same time, the absence of widespread co-location highlights that nitrogen economy traits are genetically complex and trait-specific in *Miscanthus sinensis*. Proxy traits constitute useful

tools for phenotyping and selection, even when they reflect partly distinct components of the underlying genetic architecture.

## 6. Nitrogen economy traits as a basis for specific adaptation and prospects for general adaptation

Specific adaptation in *Miscanthus sinensis* emerges strongly from this work because the contrasting nitrogen-use strategies themselves were identified and characterized in this thesis: nitrogen uptake and spring remobilization represent distinct acquisitive *versus* conservative strategies (Chapter 1) that are under independent genetic control (Chapter 3). As demonstrated in Chapter 3, independent QTLs were detected for nitrogen uptake and for spring remobilization, with no co-location between them, confirming that these traits can be selected separately to target distinct ecosystem service objectives. Nitrogen uptake reflects an acquisitive strategy based on soil nitrogen acquisition, whereas spring remobilization represents a conservative strategy relying on internal nitrogen recycling. Both strategies are compatible with sustained biomass production (Iqbal et al., 2026), but they differ in their potential environmental implications. Perennial bioenergy systems such as miscanthus have been shown to contribute to reduced nitrate concentrations in drainage water and landscape buffer functions (Ferchaud & Mary, 2016; Ferrarini et al., 2017), suggesting that genotypes with stronger acquisition capacity may be particularly relevant when nitrate capture at the system level is targeted. Conversely, strong internal recycling supports nutrient conservation, soil functioning and long-term system stability (McCalmont et al., 2017; Tavakoli-Hashjini et al., 2020). In the framework defined by Gallais (1992), these findings provide a clear genetic basis for specific adaptation, where genotypes are aligned with well-defined ecosystem service objectives.

Beyond specific adaptation, our results also point to a possible route toward more general adaptation based on nitrogen economy traits. Since nitrogen uptake and spring remobilization were demonstrated to be genetically independent and associated with distinct genomic regions, it is, in principle, possible through breeding to combine favorable alleles for both traits within the same genetic background. Such genotypes would be expected to couple a strong capacity to acquire soil nitrogen with an efficient ability to recycle internal nitrogen, offering the prospect of genotypes that could function effectively across a broader range of nitrogen contexts. A key outcome of this study is that the genetic architecture of nitrogen economy traits

indicates that combining high uptake and strong remobilization within the same genotype is, in principle, achievable through breeding.

Whether genotypes expressing both high uptake and strong remobilization will perform better than more specialized acquisitive or conservative ideotypes will ultimately depend on environmental conditions and management objectives. In practice, any genotype envisaged for broader adaptation in miscanthus will also need to integrate favorable nitrogen economy traits with other essential agronomic attributes, such as multi-year yield stability and tolerance to climatic stresses, which are known to be central to the long-term performance of perennial bioenergy crops (McCalmont et al., 2017). Nitrogen economy traits therefore define one important axis along which broader general adaptation could be explored, while their agronomic relevance will need to be evaluated in conjunction with these additional performance criteria.

## 7. General conclusion

This thesis shows that nitrogen economy traits in *Miscanthus sinensis* can be characterized, predicted, and genetically targeted in ways directly useful for breeding genotypes contributing to biomass production and other ecosystem services. Starting from the well-known benefits of nitrogen recycling in perennial grasses for reducing fertilizer needs and nitrate leaching, we first demonstrated that key nitrogen economy traits, namely nitrogen uptake, seasonal remobilization, nitrogen losses and their efficiencies, are not marginal side variables but central, highly variable components of how *M. sinensis* progeny function under nitrogen-deficient conditions. The existence of strong diversity in these traits in the studied population highlights that *M. sinensis* harbors substantial potential for tailoring nitrogen economy strategies to contrasting environmental and management goals.

A major outcome is that this diversity follows coherent nitrogen-use strategies rather than random variation. Across the progeny, we identified acquisitive nitrogen profiles relying more strongly on external uptake and conservative profiles relying more strongly on internal recycling, and showed that both strategies can sustain high biomass production when nitrogen is limiting. Nitrogen economy traits therefore provide a functional axis along which genotypes differ in how they acquire, recycle and retain nitrogen, while still supporting the primary breeding objective of biomass yield. This functional structuring of nitrogen use is the biological foundation on which the rest of the thesis builds.

The second key contribution is that nitrogen economy traits, which were previously accessible only through plant destructive and time-consuming flux measurements, can now be approached using scalable tools. Simple non-destructive traits capturing plant morphology, architecture, phenology and nitrogen status were shown to predict nitrogen uptake, spring and autumn remobilizations, and nitrogen losses with rather interpretable accuracy in multivariate and parsimonious proxy-based PLS models. In parallel, QTL analyses revealed that nitrogen uptake, seasonal remobilization and nitrogen losses are each controlled by several genomic regions with trait-specific architectures, and that some proxy-target relationships are supported by shared QTL. Together, these results provide a realistic pipeline for practical use: proxies enable large-scale estimation of nitrogen economy traits, QTLs and allelic information support selection within diploid progeny, and their combination allows nitrogen-economy ideotypes to be defined and targeted using explicit phenotypic and genetic information.

Finally, this thesis shows how nitrogen economy traits can be mobilized to design ideotypes aligned with ecosystem service objectives. Independent genetic control of nitrogen uptake and spring remobilization enables specific adaptation: acquisitive ideotypes combining high uptake with controlled losses, *i.e.* low nitrogen loss deviation, are relevant where nitrate capture and water-quality regulation are targeted, whereas conservative ideotypes relying more strongly on endogenous recycling can contribute to nutrient conservation, soil functioning and system stability. At the same time, our results suggest that ideotypes combining strong acquisition capacity with efficient internal recycling could also be envisaged in future breeding efforts, although their practical advantage over specialized ideotypes remains to be demonstrated and will depend on environmental and management contexts. In practice, deploying such ideotypes at the scale of agricultural systems will require translating selected diploid genotypes into agronomically usable, sterile triploid cultivars and evaluating their performance in landscape configurations where biomass production and ecosystem services are assessed together.

Overall, this thesis moves nitrogen economy traits from a conceptual notion to an operational breeding axis in *M. sinensis*. It delivers a coherent functional, predictive and genetic framework showing that nitrogen uptake, recycling and losses can be measured, modelled and selected upon. This provides the scientific basis needed to develop miscanthus ideotypes that maintain biomass production while contributing to water regulation, nutrient cycling and the long-term resilience of agroecosystems, and it sets the stage for the future work that will validate and deploy these strategies in multi-environment, system-level contexts.

## 8. Perspectives and future research

This thesis represents the first integrated effort to characterize nitrogen economy traits, develop proxy-based prediction tools, and dissect their genetic control within a segregant *Miscanthus sinensis* progeny. The findings should, however, be interpreted within clear boundary conditions that define the scope of inference. The study focused on 80 diploid genotypes belonging to a single genetic background derived from a biparental cross, and therefore reflects patterns expressed at given genetic background and ploidy levels. All measurements were conducted at a single experimental site under nitrogen-deficient but well-watered conditions, and nitrogen economy trait estimations relied on one year of observations. These characteristics define the environmental and genetic frame within which the results are obtained, while also highlighting the substantial experimental effort required to phenotype nitrogen economy traits at this scale in the field and establishing a strong empirical foundation for extending this work.

The immediate next step is validation of both the relationships identified and the nitrogen economy strategies inferred. The functional groups described in this thesis now need to be tested for stability across years, sites, climates and management regimes to determine whether acquisitive and conservative nitrogen strategies remain consistent under environmental variability. Increasing replication at the plant and genotype levels will strengthen trait estimation and improve the signal-to-noise ratio in nitrogen flux measurements. Multi-environment and multi-year trials are therefore essential to distinguish stable nitrogen behavior from context-dependent responses. Equally important will be testing nitrogen strategies under contrasting nitrogen availability, from deficiency to moderate and fertilized systems, and under different water regimes, to understand whether nitrogen uptake strategies remain robust and whether recycling-based functioning is maintained or altered when resource supply changes.

On the genetic side, the QTLs identified here represent starting points rather than endpoints. They now need to be validated across multiple environments, plant ages and genetic backgrounds to distinguish stable loci from those that are environmentally contingent. Moving from QTLs to underlying genes is a key step, through candidate gene mining, fine mapping and functional validation. Integration with transcriptomic resources, including RNA-seq initiatives such as the transcriptomic analysis of autumn nitrogen remobilization during senescence in *M. sinensis*, will help connect genomic regions to biological pathways controlling nitrogen acquisition and recycling. In parallel, advancing from QTL-based to genomic selection

frameworks will allow nitrogen economy traits to be incorporated into predictive breeding pipelines. Combining genomic information with phenomics, non-destructive proxies and modelling approaches will progressively build a more efficient, integrated selection architecture for nitrogen-related performance.

Finally, the longer-term perspective concerns deployment. Translating nitrogen economy traits into operational varieties requires transferring the relevant traits from diploid materials into tetraploid backgrounds and then building sterile triploid ideotypes suitable for commercial cultivation. Opportunities also exist to pyramid favorable alleles and complementary nitrogen strategies across diverse genetic backgrounds to enhance resilience and broaden adaptive potential. Ultimately, these ideotypes must be evaluated not only for plant performance but also for ecosystem service delivery in real agricultural contexts. Field- and landscape-scale assessments will be needed to quantify contributions to nitrate capture, nutrient cycling stability and system resilience. This implies a shift from evaluating plant performance to assessing how nitrogen economy traits contribute to the functioning of agricultural systems over time.

Together, these perspectives define a clear research pathway: from validation, to mechanistic insight, to genetic refinement, and finally to deployment. Building on the foundations laid in this thesis, future work can transform nitrogen economy traits from experimentally demonstrated possibilities into operational tools for breeding *Miscanthus sinensis* cultivars that sustain biomass production while actively supporting environmental objectives.

## References:

Beale, C., & Long, S. (1997). Seasonal dynamics of nutrient accumulation and partitioning in the perennial C4-grasses *Miscanthus× giganteus* and *Spartina cynosuroides*. *Biomass and Bioenergy*, *12*(6), 419-428.

Clark, L. V., Brummer, J. E., Głowacka, K., Hall, M. C., Heo, K., Peng, J., Yamada, T., Yoo, J. H., Yu, C. Y., & Zhao, H. (2014). A footprint of past climate change on the diversity and population structure of *Miscanthus sinensis*. *Annals of Botany*, *114*(1), 97-107.

Ferchaud, F., & Mary, B. (2016). Drainage and nitrate leaching assessed during 7 years under perennial and annual bioenergy crops. *BioEnergy Research*, *9*(2), 656-670.

Ferrarini, A., Fornasier, F., Serra, P., Ferrari, F., Trevisan, M., & Amaducci, S. (2017). Impacts of willow and miscanthus bioenergy buffers on biogeochemical N removal processes along the soil–groundwater continuum. *Gcb Bioenergy*, *9*(1), 246-261.

Gallais, A. (1992). Adaptation et adaptabilite en amelioration des plantes. *Selectionneur Francais*.

Himken, M., Lammel, J., Neukirchen, D., Czypionka-Krause, U., & Olfs, H.-W. (1997). Cultivation of Miscanthus under West European conditions: Seasonal changes in dry matter production, nutrient uptake and remobilization. *Plant and soil*, *189*(1), 117-126.

Hou, W., Raverdy, R., Lourgant, K., Mignot, E., Arnoult, S., Giauffret, C., & Brancourt-Hulmel, M. (2022). QTL Detection for Flowering-Time Related Traits in *Miscanthus sinensis* Using a Staggered-Start Design. *BioEnergy Research*, *15*(2), 718-733.

Hou, W., & Yi, Z. (2023). Heterosis for biomass yield and quality traits in a reciprocal cross population between *Miscanthus sinensis* and *Miscanthus lutarioriparius*. *Industrial Crops and Products*, *205*, 117451.

Iqbal, S., Brancourt-Hulmel, M., & Zapater, M. (2026). Nitrogen Economy Strategies Define Distinct Functional Groups of Genotypes in a *Miscanthus sinensis* Progeny. *GCB Bioenergy*, *18*(1), e70096. https://doi.org/https://doi.org/10.1111/gcbb.70096

Jiang, J., Guan, Y., McCormick, S., Juvik, J., Lubberstedt, T., & Fei, S. z. (2017). Gametophytic self-incompatibility is operative in *Miscanthus sinensis* (Poaceae) and is affected by pistil age. *Crop Science*, *57*(4), 1948-1956.

Leroy, J., Ferchaud, F., Giauffret, C., Mary, B., Fingar, L., Mignot, E., Arnoult, S., Lenoir, S., Martin, D., & Brancourt-Hulmel, M. (2022). *Miscanthus sinensis* is as efficient as *Miscanthus× giganteus* for nitrogen recycling in spite of smaller nitrogen fluxes. *Bioenergy Research*, *15*(2), 686-702.

Li, D., Wang, J., Chen, R., Chen, J., Zong, J., Li, L., Hao, D., & Guo, H. (2024). Nitrogen acquisition, assimilation, and seasonal cycling in perennial grasses. *Plant Science*, *342*, 112054.

Lynch, J. P. (2013). Steep, cheap and deep: an ideotype to optimize water and N acquisition by maize root systems. *Annals of botany*, *112*(2), 347-357.

Mackay, I. J., Cockram, J., Howell, P., & Powell, W. (2021). Understanding the classics: the unifying concepts of transgressive segregation, inbreeding depression and heterosis and their central relevance for crop breeding. *Plant Biotechnology Journal*, *19*(1), 26-34.

McCalmont, J. P., Hastings, A., McNamara, N. P., Richter, G. M., Robson, P., Donnison, I. S., & Clifton-Brown, J. (2017). Environmental costs and benefits of growing Miscanthus for bioenergy in the UK. *Glob Change Biol Bioenergy*, *9*(3), 489-507. https://doi.org/10.1111/gcbb.12294

Muktar, M. S., Habte, E., Teshome, A., Assefa, Y., Negawo, A. T., Lee, K.-W., Zhang, J., & Jones, C. S. (2022). Insights into the genetic architecture of complex traits in Napier grass (*Cenchrus purpureus*) and QTL regions governing forage biomass yield, water use efficiency and feed quality traits. *Frontiers in plant science*, *12*, 678862.

Pan, Q., Li, L., Yang, X., Tong, H., Xu, S., Li, Z., Li, W., Muehlbauer, G. J., Li, J., & Yan, J. (2016). Genome-wide recombination dynamics are associated with phenotypic variation in maize. *New Phytologist*, *210*(3), 1083-1094.

Park, Y.-H., Yook, M.-J., Lim, S.-H., & Kim, D.-S. (2024). Detection of QTLs controlling flowering in a cross-pollinated F1 population of *Miscanthus sinensis*. *Industrial Crops and Products*, *213*, 118357.

Raverdy, R., Lourgant, K., Mignot, E., Arnoult, S., Bodineau, G., Griveau, Y., Taniguti, C. H., & Brancourt-Hulmel, M. (2022). Linkage mapping of biomass production and composition traits in a *Miscanthus sinensis* population. *BioEnergy Research*, *15*(2), 755-776.

Sacks, E. J., Juvik, J. A., Lin, Q., Stewart, J. R., & Yamada, T. (2012). The gene pool of Miscanthus species and its improvement. In *Genomics of the Saccharinae* (pp. 73-101). Springer.

Stapley, J., Feulner, P. G., Johnston, S. E., Santure, A. W., & Smadja, C. M. (2017). Variation in recombination frequency and distribution across eukaryotes: patterns and processes. *Philosophical Transactions of the Royal Society B: Biological Sciences*, *372*(1736), 20160455.

Strullu, L., Cadoux, S., Preudhomme, M., Jeuffroy, M.-H., & Beaudoin, N. (2011). Biomass production and nitrogen accumulation and remobilisation by *Miscanthus* × *giganteus* as influenced by nitrogen stocks in belowground organs. *Field Crops Research*, *121*(3), 381-391.

Sun, Q., Lin, Q., Yi, Z.-L., Yang, Z.-R., & Zhou, F.-S. (2010). A taxonomic revision of Miscanthus sl (Poaceae) from China. *Botanical Journal of the Linnean Society*, *164*(2), 178-220.

Tavakoli-Hashjini, E., Piorr, A., Müller, K., & Vicente-Vicente, J. L. (2020). Potential bioenergy production from *Miscanthus*× *Giganteus* in Brandenburg: Producing bioenergy and fostering other ecosystem services while ensuring food self-sufficiency in the Berlin-Brandenburg region. *Sustainability*, *12*(18), 7731.

Weik, J., Lask, J., Petig, E., Seeger, S., Marting Vidaurre, N., Wagner, M., Weiler, M., Bahrs, E., Lewandowski, I., & Angenendt, E. (2022). Implications of large-scale miscanthus cultivation in water protection areas: A Life Cycle Assessment with model coupling for improved policy support. *Gcb Bioenergy*, *14*(11), 1162-1182.

Zhao, H., Wang, B., He, J., Yang, J., Pan, L., Sun, D., & Peng, J. (2013). Genetic Diversity and Population Structure of *Miscanthus sinensis* Germplasm in China. *PLOS ONE*, *8*(10), e75672. https://doi.org/10.1371/journal.pone.0075672

# Nitrogen economy towards ecosystem services: plant key traits and QTL detection in *Miscanthus sinensis*

**Key-words**: Ecosystem services, Nitrogen economy, Genetic variability, *Miscanthus sinensis*, Proxy traits, Quantitative Trait Loci (QTL) mapping.

## A simplified thesis summary for the general public

Agriculture must produce biomass while limiting its environmental impact, especially on water quality affected by nitrogen excess in the soil. Miscanthus can meet this challenge as it combines productivity with low fertilizer needs, supported by internal nitrogen recycling. This thesis studied nitrogen functioning in a *Miscanthus sinensis* progeny grown under low-nitrogen field conditions. While sustaining productivity, it showed that genotypes differ strongly in how they acquire, recycle, and retain nitrogen, following different strategies. Some genotypes rely on nitrogen uptake from the soil, which can support water-quality regulation by nitrate removal, while others rely on internal recycling, which can support crop-system resilience. It also showed that these complex traits can be predicted using simple proxy measurements and identified genetic regions controlling them, providing tools to breed miscanthus varieties that support both biomass production and environmental benefits.

# Gestion de l'azote en vue de services écosystémiques : traits majeurs de la plante et détection de QTL chez *Miscanthus sinensis*

**Mots-clés :** Services écosystémiques, gestion de l'azote, variabilité génétique, *Miscanthus sinensis*, caractères proxys, cartographie de régions chromosomiques (QTL).

## Résumé de thèse vulgarisé pour le grand public

L'agriculture doit produire de la biomasse tout en limitant ses impacts environnementaux, notamment sur la qualité de l'eau affectée par l'excès d'azote dans les sols. Le miscanthus offre un fort potentiel en associant productivité et faibles besoins en fertilisation grâce au recyclage interne de l'azote. Cette thèse a étudié le fonctionnement azoté au champ d'une descendance de *Miscanthus sinensis* en conditions azotées déficientes. Elle montre que les génotypes, tout en maintenant la productivité, adoptent deux stratégies : certains captent l'azote du sol, favorisant la régulation des nitrates en excès, tandis que d'autres misent sur le recyclage interne, renforçant la résilience des systèmes de culture. Ces caractères complexes peuvent en outre être prédits par des mesures indirectes simples et les régions génomiques les contrôlant peuvent être identifiées, fournissant ainsi des outils pour sélectionner des variétés qui favorisent à la fois productivité et bénéfices environnementaux.